2011

Development of a physiologically-relevant in vitro system to study exhaled bioaerosols

Rania Ahmad Azzam Hamed
University of Iowa

DEVELOPMENT OF A PHYSIOLOGICALLY-RELEVANT IN VITRO SYSTEM TO STUDY EXHALED BIOAEROSOLS

by

Rania Ahmad Azzam Hamed

An Abstract

Of a thesis submitted in partial fulfillment
of the requirements for the Doctor of
Philosophy degree in Pharmacy
in the Graduate College of
The University of Iowa

July 2011

Thesis Supervisor: Assistant Professor Jennifer Fiegel

ABSTRACT

Airborne infectious diseases remain a major global health threat. The primary vector for their transmission is coarse and fine droplets, known as bioaerosols, exhaled from infected individuals during natural respiratory maneuvers, such as breathing, coughing and sneezing. Unfortunately, our current knowledge of the mechanisms by which these exhaled bioaerosols are formed in the lungs is in its infancy. In particular, progress in this field has been hindered by the complex structure of the respiratory fluid and the resulting lack of understanding of the biophysical properties of the fluid.

In this thesis, a series of *in vitro* mimetics of conducting airway mucus were developed to enable in depth studies of mucus properties and bioaerosol formation from mucus-like surfaces. These mucus mimetics overcome major limitations of currently available models by matching the primary chemical composition and key physical properties of the mimetic to that of native tracheal mucus. Three mimetics were chosen to facilitate the study of highly viscoelastic (diseased) mucus and non-diseased mucus under low shear conditions, such as breathing, or high shear conditions, such as cough.

To study bioaerosol formation *in vitro*, an enhanced simulated cough machine (SCM) was developed to generate bioaerosols from mucus mimetic surfaces during cough. By controlling the temperature and relative humidity within the SCM, the detectability of bioaerosols generated from the mimetic surfaces was improved due to limited aerosol drying. The size distribution of the bioaerosols was multimodal, with four to five modes being observed for all surfaces probed. While varying the composition of surfactant at the air-mucus interface had a significant impact on surface viscoelastic properties, the size distribution of bioaerosols generated from these surfaces did not differ significantly. However, the ability to generate bioaerosols from different surfaces was highly dependent on surface properties of the mimetic, with highly viscoelastic surfaces generating bioaerosols in only half the experiments. This research will enhance our

knowledge of bioaerosol formation in the respiratory tract and ultimately guide the development of alternative strategies to suppress bioaerosol formation.

Abstract Approved: _____
Thesis Supervisor

_____
Title and Department

_____
Date

DEVELOPMENT OF A PHYSIOLOGICALLY-RELEVANT IN VITRO SYSTEM TO STUDY EXHALED BIOAEROSOLS

by

Rania Ahmad Azzam Hamed

A thesis submitted in partial fulfillment
of the requirements for the Doctor of
Philosophy degree in Pharmacy
in the Graduate College of
The University of Iowa

July 2011

Thesis Supervisor: Assistant Professor Jennifer Fiegel

Graduate College
The University of Iowa
Iowa City, Iowa

CERTIFICATE OF APPROVAL

_____

PH.D. THESIS

_____

This is to certify that the Ph.D. thesis of

Rania Ahmad Azzam Hamed

has been approved by the Examining Committee
for the thesis requirement for the Doctor of Philosophy
degree in Pharmacy at the July 2011 graduation.

Thesis Committee: _____
Jennifer Fiegel, Thesis Supervisor

_____
Douglas R Flanagan

_____
Maureen D Donovan

_____
Aliasger K Salem

_____
Thomas M Peters

To my beloved parents, Azzam Hamed and Bahia Nazer, and my brothers, Raed, Rami and Fadi for their continuous support and patience

ACKNOWLEDGMENTS

I would like to thank my advisor Dr. Jennifer Fiegel for her unconditional support and help from the initial to the final level. This work would not have been possible without her. I have gained tremendous knowledge and experience from interacting with her and being part of her research group. I also would like to thank my committee members, Drs. Douglas Flanagan, Maureen Donovan, Aliasger Salem and Thomas Peters. Special thanks to Drs. Douglas Flanagan and Thomas Peters for their input on this work.

I am grateful to all members in my laboratory (Dr. Timothy Brenza, Mai Tu, Amir Farnoud, Stacy Ross, Emily Thomas and Buffy Stohs) for their help, fun time and scientific discussions. I have learned a lot from the intellectual exchanges and laboratory meetings we had, in addition to the interesting conversations about life and science. I am also greatly thankful for the undergraduate students, Laura Northrup, Alexander Benson and Kyle Merrill, who helped me in this work and gave me the opportunity to guide them. In addition, I would like to thank my colleague Mohammed Saleh who helped me in analyzing the results of the bioaerosol study. His effort is appreciated.

I express my love and heartfelt gratitude to my parents, despite being thousands of miles away; their love, understanding, patience and support were essential throughout this challenging process. I am heartily thankful to my brothers Raed, Rami and Fadi who supported me, believed in me and provided me with strength throughout these years. Finally, I would like to show my gratitude to all my friends with whom I shared an enjoyable time during these years.

ABSTRACT

Airborne infectious diseases remain a major global health threat. The primary vector for their transmission is coarse and fine droplets, known as bioaerosols, exhaled from infected individuals during natural respiratory maneuvers, such as breathing, coughing and sneezing. Unfortunately, our current knowledge of the mechanisms by which these exhaled bioaerosols are formed in the lungs is in its infancy. In particular, progress in this field has been hindered by the complex structure of the respiratory fluid and the resulting lack of understanding of the biophysical properties of the fluid.

In this thesis, a series of *in vitro* mimetics of conducting airway mucus were developed to enable in depth studies of mucus properties and bioaerosol formation from mucus-like surfaces. These mucus mimetics overcome major limitations of currently available models by matching the primary chemical composition and key physical properties of the mimetic to that of native tracheal mucus. Three mimetics were chosen to facilitate the study of highly viscoelastic (diseased) mucus and non-diseased mucus under low shear conditions, such as breathing, or high shear conditions, such as cough.

To study bioaerosol formation *in vitro*, an enhanced simulated cough machine (SCM) was developed to generate bioaerosols from mucus mimetic surfaces during cough. By controlling the temperature and relative humidity within the SCM, the detectability of bioaerosols generated from the mimetic surfaces was improved due to limited aerosol drying. The size distribution of the bioaerosols was multimodal, with four to five modes being observed for all surfaces probed. While varying the composition of surfactant at the air-mucus interface had a significant impact on surface viscoelastic properties, the size distribution of bioaerosols generated from these surfaces did not differ significantly. However, the ability to generate bioaerosols from different surfaces was highly dependent on surface properties of the mimetic, with highly viscoelastic surfaces generating bioaerosols in only half the experiments. This research will enhance our

knowledge of bioaerosol formation in the respiratory tract and ultimately guide the development of alternative strategies to suppress bioaerosol formation.

TABLE OF CONTENTS

LIST OF TABLES

LIST OF FIGURES

CHAPTER 1

INTRODUCTION

1.1. Respiratory Tract Structure

The respiratory tract is divided into three regions: head airways or nasopharyngeal region, lung airways or tracheobronchial region, and pulmonary or alveolar region (Figure 1-1). The nasopharyngeal region consists of the nose, mouth, pharynx and larynx. This region is the principle site where inhaled air is warmed and humidified before it enters the lungs. The tracheobronchial region constitutes the conducting zone of the airways. It resembles an inverted tree, which originates from the trachea and ends at the terminal bronchioles. The trachea of the airways bifurcates to form two main bronchi. These two main bronchi divide into smaller bronchi which form lung lobes, three lobes on the right side and two lobes on the left side. These lobes undergo further divisions to form bronchioles. The alveolar region, where gas exchange takes place, continues beyond the terminal bronchioles and includes respiratory bronchioles and alveolar ducts and terminates in the alveolar sacs.[1, 2] A proposed airway model, developed based on anatomical and morphological aspects of the normal human respiratory tract, is described by 24 airway generations; with the trachea as generation 0 and the alveolar sacs as generation 23 (Figure 1-2).[2]

Throughout the lung, the structure and composition of the fluid lining the respiratory tract vary at different generations. The mucosal epithelia of large conducting airways are coated with a continuous fluid layer known as airway lining fluid (ALF) (Figure 1-3). The primary functions of the ALF are to protect the underlying lung tissues by trapping and clearing inhaled foreign material and to hydrate the epithelial cells on the mucosal surface. The thickness of fluid lining the tracheobronchial region decreases with each successive generation into the respiratory tract. It has been reported that in non-pathological conditions the depth varies between 10 and 30 μm in the trachea and

between 2 and 5 μm in the bronchi.[3, 4] While actual measurements of the *in-vivo* depth of the airway fluids is difficult to obtain, the tracheobronchial fluid in excised human airways has been measured between 7 and 55 μm, illustrating a variation between subjects.[5, 6] The mucus gel layer extends from the trachea to terminal bronchioles (approximately airway generation 15).[7]

ALF is composed of two primary layers: a low viscosity aqueous periciliary fluid (sol layer) adjacent to the lung tissues, which enables free ciliary movement and a mucus gel layer which lies atop the periciliary layer and alters viscoelastic properties to the airway fluid.[8] The sol layer contains a Newtonian fluid composed of water and soluble proteins[9] with 0.25-μm diameter cilia, 5-50 μm in length, which varies according to position and function.[7, 10] The cilia move in the periciliary fluid, the depth of which is a little less than the ciliary length, so that the overlying mucus is penetrated the ciliary tips during the effective ciliary movement.[11]

The mucus gel layer is a cross-linked network. It is composed of approximately 93-97% (w/w) water and 3-7% (w/w) solids. The solids content include 1% (w/w) proteins and 1-5% (w/w) glycoproteins (mucins), 0.5-1% (w/w) lipids, and 0.70-1.40% (w/w) ions.[12-14] The extended network of the mucus gel layer is attributed to a number of covalent and non-covalent bonds. The intra-molecular disulfide bridges covalently link glycoprotein subunits forming an extended mucin polymer. In addition, these long mucin chains physically entangle with each other and contribute to the gel network. The non-covalent linkages such as hydrogen bonds, ionic interactions, and Van der Waals forces are also occurring in a mucus gel. The sugar units of the oligosaccharide side chains, which comprise 80% of mucin weight, form hydrogen bonds with the neighboring units of mucin chains. The ionic interactions between positively charged amino acids in mucin chains and the negatively charged sugar units (sialic acid and sulfated sugar residues) resulted in a more extended network. Van der Waals forces also form between neighboring oligosaccharide moieties. These covalent and non-covalent linkages cross-

link the high molecular weight glycoproteins (mucins) giving mucus an extended gel network which enhances the viscoelastic properties of mucus secretions (Figure 1-4).[15-17]

The lower levels of the respiratory tract, pulmonary or alveolar region, are covered by a lining layer of pulmonary surfactant secreted from type II pneumocytes and adsorbed onto an aqueous subphase.[18, 19] The alveolar fluid has a thickness of 0.2 μm.[20] It is composed of a complex mixture of 90 wt% lipids and 10 wt% proteins. The lipids are composed of 93-96% phospholipids and 4-7% neutral lipid. The pulmonary surfactant proteins are (SP-A, B, C and D). The main function of the alveolar surfactant is to reduce the surface tension at the air-alveolar interface to near zero to prevent the collapse of the lung during expiration.[21]

1.2. Physical Properties of Tracheal Mucus

Tracheal mucus is a viscoelastic material exhibiting both solid-like (elastic) and liquid-like (viscous) behavior due to its cross-linked nature. The viscoelastic properties of mucus have been extensively studied by bulk rheology.[22-25, 25] In these studies, the solid-like behavior is characterized by the elastic or storage modulus G' which measures the ability of mucus to stretch and return to its original shape, whereas the liquid-like behavior is characterized by the viscous or loss modulus G" which measures the resistance of mucus to flow.[26]

Typical values of the bulk rheological properties of native, non-diseased tracheal mucus obtained from human subjects and dogs were reported in several studies (Table 1-1).[22-25] Different techniques were used to obtain mucus *in-vivo* such as endotracheal tube, bronchoscopy brush and tracheal pouch. The complex modulus G*, where $G^* = \sqrt{[(G')^2 + (G'')^2]}$ and tan δ, where δ is the phase angle shift between stress applied and strain resulted, have been reported at frequencies of 1 rad/sec and 100 rad/sec. A frequency of 1 rad/sec corresponds to ciliary activity, whereas, 100 rad/sec corresponds to a cough frequency.[27] Data showed great variability in mucus bulk rheology, where G*

were in the range of 5.01-34.67 Pa at 1 rad/sec and 11.48-81.28 Pa at 100 rad/sec. Tan δ values were between 0.21-0.57 at 1 rad/sec (showing the dominance of the elastic behavior of mucus at low frequencies) and 0.61-1.21 at 100 rad/sec (showing no clear dominance in elastic or viscous behavior at high frequencies). Based on these available data G', G" and δ were calculated (Table 1-1). G' and G" at 1 rad/sec were in the range of 4.88-32.2 Pa and 1.12-12.60 Pa, respectively, (showing that G' dominated G" at low frequencies). At 100 rad/sec, G' and G" were between 9.67-51.96 Pa and 7.70-62.65 Pa, respectively, (showing that G' dominated G" at high frequencies, and that G' and G" values at 100 rad/sec are larger than those at 1 rad/sec). The phase angle shift (δ) also varied considerably ranging between11.86-29.62° at 1 rad/sec (showing G' dominated G" at low frequencies) and 31.38-50.43° at 100 rad/sec (showing no clear dominance in elastic or viscous behavior at high frequencies).

Although the bulk rheology of mucus has been extensively studies, the bulk rheological properties of native, non-diseased tracheal mucus vary significantly.[25] The wide variation observed in the viscoelastic properties of tracheal mucus can be attributed to: 1) contamination of mucus with saliva, 2) inhomogeneity in mucus sample, 3) variation in mucus samples obtained from the same subject and from one subject to another, 4) small quantities of native mucus obtained from healthy human airways, 5) alteration in the rheological properties of mucus sample if not measured freshly (i.e. storage method may alter the rheological properties of the mucus sample), 6) complex nature of the mucus itself , and 7) variation in the measurement techniques.[7, 28]

1.3. Surface Tension of Tracheal Mucus

The surface tension at the air-mucus interface of the trachea and first and second generation bronchi of large animals (horses and sheep) and rodents (rats and guinea pigs) has been measured *in-vivo* and reported to be between 31.4-34.0 mN/m.[29-32] This relatively low surface tension suggests that the large conducting airways of the

respiratory tract are covered with a surface active material capable of lowering the surface tension.[29-32] Light and transmission electron micrographs have corroborated the presence of a surfactant film by demonstrating a continuous osmiophilic film at the air-mucus interface (Figure 1-5).[31, 33, 34] This surfactant film is critically important for normal function of the tracheobronchial tree. It decreases the surface tension of the interface to facilitate mucociliary and cough clearance,[35] aids the penetration of foreign materials (pathogens, environmental contaminants and therapeutics) into the gel phase for clearance,[30, 36] and reduces evaporation of the subphase.[37]

Lipids, a major component of the tracheobronchial secretions, contribute about 1% of respiratory mucus components. They are mainly concentrated in the gel phase of the ALF, particularly associated with mucus glycoproteins (mucins).[38] Lipids in the tracheal secretions contribute to the bulk rheological properties of the tracheobronchial secretions by reducing the viscosity and elasticity of mucus making it more fluid.[38] In addition, surface-active lipids likely play an active role in lowering the surface tension at the air-mucus interface below that achievable by proteins alone and influence the surface properties of the large conducting airways.[36]

The exact chemical composition of lipids in the tracheal secretions is still not known and is subject to controversy. In normal individuals, lipids are comprised of phospholipids, neutral lipids and glycolipids, and that neutral lipids represent the major lipid component in normal tracheobronchial secretions.[13, 39-41] Slomiany *et al.*[13] demonstrated that neutral lipids, phospholipids and glycolipids represent 5%, 2.75% and 4.75% of the total dry weight of the tracheobronchial secretions, respectively. Neutral lipids such as cholesterol, free fatty acids, cholesterol esters and triacylglycerols accounted for1.87%, 2.39%, 0.39% and 0.37%, respectively, of the total dry weight. Phospholipids such as phosphatidylcholine, lysophosphatidylcholine, sphingomyelin and phosphatidylethanolamine accounted for 0.89%, 0.81%, 0.43% and 0.34%, respectively, of the total dry weight. Finally, glycolipids such as glycosphingolipids and

glyceroglucolipids accounted for 1.19% and 0.62%, respectively, of the total dry weight. In contrast, Bhaskar *et al*.[39, 41] have demonstrated, qualitatively and quantitatively, that neutral lipids and phospholipids were the only lipid components identified in both normal human and normal canine tracheal secretions with no glycolipids. In another study,[40] identifying the lipid composition in the *in-vitro* secretions of human and canine tracheal explants has shown a wide range of lipids (neutral lipids, phospholipids and glycolipids) was detected and that neutral lipids and phospholipids were predominant whereas the presence of glycolipids may be the result of the stimulation of the tissue due to excision. In spite of these differences, it is generally accepted that phosphatidylcholine represents the major phospholipid and that dipalmitoylphosphatidylcholine (DPPC) is the major phosphatidylcholine species.[42-44]

It has been shown that phospholipid composition and proportions in tracheal aspirates are similar to that recovered from bronchoalveolar lavage (BAL) fluid,[42, 45] implying that alveolar surfactants may reach the trachea during normal breathing and ciliary transport, or by spatial distribution due to surface tension gradient (Marangoni flows) which spreads surfactants from areas of high surfactant concentration (low surface tension) to areas of low surfactant concentration (high surface tension).[46] In addition, it has been shown that airway epithelial cells (bronchiolar epithelium and Clara cells) and airway secretory cells (submucosal glands) synthesize, store and secrete their own lipids.[33, 38, 45, 47] However, surfactant composition in the tracheal secretions was markedly different from those of the underlying airway mucosa, showing that secretion by the airway epithelium alone could not account for the levels of surfactants in the large conducting airways.[48] Furthermore, the breakdown of macrophages, degradation of phospholipids and neutral lipids by enzymatic activity, bacterial secretion and transudation of tissue fluid may be considered another minor source of lipids in the tracheal secretions.[47]

1.4. Existing Model Systems of Tracheal Mucus

Several model systems of tracheal mucus have been used to study the physical properties of mucus secretions,[22, 24] mucociliary and cough clearance,[49] and bioaerosol formation in the lungs.[15, 50] These existing model systems can be divided into two categories:

1) Synthetic gels: Viscoelastic gels of locust bean gum,[15, 50] gum tragacanth,[51] guar gum,[52] scleroglucan,[52] Polyox water-soluble resin,[53] carrageenan,[50] pig gastric mucins[16] and mayonnaise[54] have been used as mucus simulants. The viscoelastic gels were prepared by mixing each of these polymeric materials, excluding mayonnaise, in aqueous solutions. To induce cross-links to the polysaccharide gels of locust bean gum, guar gum and gum tragacanth, specific concentration of the cross-linking agent sodium borate was added to enhance their viscoelastic property.[15, 50-52] In these models, the viscoelastic properties of gels increased by increasing the concentration of the polymeric material in mucus simulant formulation or increasing the concentration of the cross-linking agent. Therefore, by manipulating these two factors the bulk viscoelastic properties of mucus simulants was matched to that of native tracheal mucus. However, the chemical composition, component concentration and surface properties of these gels do not model tracheal mucus.
2) *In-vivo* secretions: Patients with chronic airway diseases such as cystic fibrosis (CF) and chronic obstructive pulmonary disorder (COPD) produce large quantities of mucus, enabling the direct removal of those secretions via hypertonic saline induction or by expectoration.[55] These secretions are often contaminated by oral bacteria and saliva which alter the physical properties of tracheal mucus. On the other hand, secretions from subjects with no lung disease are scanty, making their collection difficult, if not impossible.

However, several techniques have been used to obtain normal tracheobronchial mucus using one of these techniques:

I. Scraping the tracheal mucosa immediately following tracheostomy of anesthetized dogs.[56]

II. Scraping the mucus layer from endotracheal tubes removed from patients undergoing elective surgery but did not have evidence of respiratory diseases.[23]

III. Placing a cytology brush, using bronchoscope, on the tracheal epithelium of intubated healthy dogs or healthy subjects and allowing mucus to collect on the brush by normal mucociliary flow for a period of 10-20 minute in healthy dogs or 20-30 sec in healthy subjects, then mucus was removed from the brush by gentle scraping.[22, 56]

IV. Placing a tracheal pouch in canine to allow repeated collection of normal mucus. In this technique, milliliter quantities were aspirated using a sterile syringe.[57]

These techniques were hampered by the small quantities of mucus obtained, which were generally between 1 and 5 µL in volume.[22, 23, 56] These quantities are insufficient for extensive analysis by the existing rheological techniques. In addition, large variation was observed in the rheological properties of secretions obtained using these techniques, which was attributed to evaporation from the mucus surface or stress induced by the collection procedure which may alter the physical properties of tracheal mucus.

Therefore, the currently available models of tracheal mucus (synthetic gels and *in-vivo* secretions) are limited in their usefulness for studying the surface rheology of tracheal mucus and bioaerosol formation from the surfaces of the ALF of the large conducting airways. Synthetic gels lack key physicochemical properties of native tracheal mucus such as chemical composition, component concentrations and surface tension,

which are critical to our understanding of mucus function. On the other hand, the difficulty in collecting sufficient normal human mucus, inaccessibility of human secretions, large inter-subject and intra-subject variability in mucus bulk viscoelastic properties, and alteration in the physical properties of tracheal mucus in diseased states limit the use of the *in-vivo* secretions model.

1.5. Bioaerosol Formation in the Lungs

Airborne infectious diseases, such as influenza, tuberculosis, severe acute respiratory syndrome (SARS) and whooping cough, remain a major global health threat.[15] The major vector for the transmission of airborne infectious diseases is coarse and fine droplets exhaled from infected individuals and spread to healthy person. These droplets carried in exhaled breath are known as bioaerosols.[15, 50, 58, 59] Two potential regions have been identified as the source of bioaerosol formation in the respiratory tract.[60]

The primary theory for bioaerosol droplet formation in the lungs suggests that the passage of air during inhalation and exhalation over the ALF destabilizes the ALF surface due to shear forces. This leads to wave-like formation at the surface and breakup into droplets which may contain lung fluid components and trapped pathogens. These droplets become entrained within the airstream and are then exhaled (Figure 1-6).[7, 58, 62] Recent studies indicate that bioaerosol droplets originate from the surfaces of the ALF of the large conducting airways during coughing, sneezing, talking and normal breathing, and that coughing and sneezing produce the highest concentration of droplets per maneuver.[50, 58, 59, 61] Critical air speed of 5-30 m/sec is necessary to initiate wave disturbances on mucus surface, which is easily achieved through normal respiratory maneuvers.[8] During cough, the air velocity may reach up to 280 m/sec.[62]

To better understand how mucus physicochemical properties affect bioaerosol formation, Vasudevan and Lange[63] used mathematical modeling to study perturbation to

lung mucus. The typical fluid properties for the mucus layer were: viscosity (μ) of 10-1500 m/kg·sec, density (ρ) of 1000-1500 kg/m^3, and elasticity (G') of 0.1-150 kg/m·sec^2. In this model, a relationship between the instability of the mucus layer by perturbations (manifested as waves or droplets) due to cough, manifested by waves or droplets, and the properties of a viscoelastic fluid was studied. Two approaches were suggested to suppress the aerosolization of bioaerosols: 1) complete suppression of droplet formation or 2) enlargement of droplet size such that they quickly settle out of the exhaled air. In their mathematical model elasticity should be increased and viscosity decreased for complete suppression of droplet formation. In making the fluid more elastic, the fluid becomes more resistant to breakup. However, if larger droplets were desired, bulk elasticity should be decreased and viscosity should be increased. Vasudevan and Lange[64] used this same model of mucus layer with surface tension of 10-200 N/m of human trachea to study the effect of surface tension on perturbations using a viscoelastic system with air-mucus interface. Their model demonstrated that increasing the surface tension makes the interface more resistant to perturbations and breakup, which could suppress droplet formation. However, to enlarge the droplets such that they settle out of an airstream quickly, a decrease in surface tension would be desired. These models provide a good starting point for understanding the role of mucus physicochemical properties on bioaerosol formation.

A secondary model for bioaerosol formation suggests that these exhaled droplets form through the reopening of closed peripheral airways since the concentration of exhaled droplets decreased after holding breath.[60]A proposed model by Johnson *et al.*[60] known as bronchiole fluid film burst (BFFB) is based on exhaled droplets forming in the lower bronchioles during the inhalation phase of normal breathing. Briefly, in normal breathing and during exhalation, the bronchiolar wall fully contracted. Therefore, the fluid lining the surface of the bronchiole forms a continuous fluid layer over the interior surface of the fully contracted bronchioles. This fluid layer contains surfactant which

prevents the fully contracted bronchiole from collapse. In the fully contracted bronchiole, liquid film can completely block the airway. During inhalation, the expansion or reopening of the closed bronchioles will reduce the fluid blockage to a thin membrane. The film breakage will lead to production of droplet aerosols.

1.5.1 In-Vivo Data of Bioaerosol Formation

Table 1-2 illustrates a summary for bioaerosol size distributions and average concentrations produced during various expiratory maneuvers from healthy individuals and anesthetized bull calves reported in recent studies. In early studies, the mouths and throats of subjects were coated with dye. Stained expiratory droplets were collected onto a glass slide. The size of these droplets generated during different expiratory maneuvers such as normal breathing, sneezing, coughing and speaking was determined using light microscopy.[65, 66] An early study by Duguid, who measured droplets size generated by sneezing, coughing and speaking demonstrated that most droplets (95%) were between 2-100 μm and that the most common diameter lies between 4 and 8 μm.[65] In another early study by Loudon and Roberts,[66] the size and number of particles emitted during coughing and talking inside an air-tight box were determined. The size of stained particles was varied between 2.9 to >1471 μm. They found that particles >10 μm were deposited on a paper placed on the box floor after 30 minutes. However, particles <10 μm were recovered by a Millipore filter implying that they remained suspended in air for 30 minutes. In addition, it was demonstrated that droplets generated during talking were larger than those generated during coughing, and that talking produced more droplets than coughing. In these studies,[65, 66] the authors agreed that mouth is the site of origin of bioaerosols and those droplets <1 μm were difficult to recognize by microscope.

In more recent studies,[58, 59, 67-70] the size of exhaled droplets was determined using more sensitive sampling instruments, where droplets in the submicron size range were measured (Table 1-2). Fairchild and Stamper [67] determined the size of particles in

exhaled breath using laser aerosol spectrometry, which counts particles in 15 size ranges from 0.1 to 3.0 μm diameter. They found that the majority of droplets were <0.3 μm and less than 2% of the droplets were >1 μm in diameter. Papineni and Rosenthal [59] determined the size and number of droplets generated during four respiratory maneuvers (mouth and nose breathing, coughing and talking). Two techniques were used in this study: 1) the optical particle counter (OPC) with a lower diameter detection limit of 0.3 μm, and 2) an electron microscopy used to size and count particles collected on a glass slide. They demonstrated that the size of most droplets generated during the four respiratory maneuvers was <1 μm in diameter and no diameter >2.5 μm was reported. They also found that coughing produced the highest number of droplets per maneuver, followed by mouth breathing, then the nose breathing. In these recent studies, and due to the higher sensitivity of the instruments, the majority of the droplets were in the sub-micron size.

Significant inter-subject variability has been observed for each maneuver in various studies. A recent study by Edwards *et al.* [58] showed that the primary population of bioaerosols exhaled from 11 healthy human subjects during normal breathing was <1 μm in diameter. The inter-subject variability observed in the expired particle numbers revealed the existence of two distinct groups: super-producers (individuals who produce >500 droplets per liter of air) and low producers (individuals who produce <500 droplets per liter of air) over a six hour measurement period during normal breathing. The significant variation in exhaled bioaerosols between normal healthy individuals of low producers and high producers was attributed to the inter-subject variability in mucus physicochemical properties such as bulk viscoelastic properties, surface tension and surface viscoelastic properties.

Yang *et al.*[68] determined the size distributions for dried droplet nuclei and initial (original) droplets generated during coughing using an aerodynamic particle sizer. The dried droplet nuclei were mixed with low relative humidity (35%); whereas, initial

droplets were coughed into a sampling bag that has a higher relative humidity (95% RH) than surrounding air. The size distribution for the dried droplet nuclei was between 0.58-5.42 μm, and 82% of droplets were between 0.74-2.12 μm. However, the size distribution for initial coughed droplets was multimodal showing three peaks at 1, 2 and 8 μm. This study demonstrated the effect of RH on the size of exhaled bioaerosols, where droplets formed at low RH (droplet nuclei) where smaller than coughed droplets formed at higher RH.

In a very recent study by Chao *et al.*,[69] the size distributions for droplets generated during coughing and speaking (subjects counted from 1-100) was measured using interferometric Mie imaging technique, with a lower size detection limit of about 2 μm. This technique enables measuring the original size of droplet in close proximity to the mouth. It has been shown that the geometric mean diameter for coughed droplets was 13.5 μm and that for speaking droplets was 16.0 μm. The geometric mean diameter for speaking droplets was larger than that for coughing droplets, similar to what has been reported by Loudon and Roberts.[66] This suggests that the higher air velocity during coughing promotes smaller droplets compared to the lower air velocity during speaking.

In a comprehensive study by Morawska *et al.*[70], the size distribution of droplets generated during different respiratory activities was measured. Multimodal distribution was observed, where for all respiratory activities the majority of particles were of diameters below 0.8 μm and a second mode was at 1.8 μm. Speech produced additional particles in modes near 3.5 and 5 μm. This study was in agreement with Yang *et al.*[68], demonstrating that bioaerosols exhibited multimodal size distribution.

1.5.2 In-Vitro Data of Bioaerosol Formation

Bioaerosols were also generated *in-vitro* from mucus simulant surfaces using a simulated cough machine (SCM) (Table 1-3).[15, 58] The SCM passes high velocity stream of air over the mucus simulant surface to simulate air flow during a cough. Droplets were

generated from the mucus simulant surface. The size and concentration of bioaerosols produced from the mucus surfaces were quantified using optical particle counter and optical particle sizer. In these studies,[15, 58] the effect of the physical properties (bulk and surface rheology and surface tension) of mucus simulants on bioaerosol formation and particle size distribution was studied. Zayas *et al.*[15] used a mucus simulant of locust bean gum (LBG) cross-linked with sodium borate. Mucus simulants of varying degrees of viscoelastic properties were used to generate aerosols using a SCM. It was found that increasing the bulk viscoelastic properties of the mucus simulant, by increasing the volume of the cross-linking agent (sodium borate), reduces the number of fine aerosols striking a target placed 40 cm from the SCM and increases the number of large droplets which did not reach the target but deposited on paper immediately below the exit of the SCM. In another study, [58] bioaerosol droplets were generated *in-vitro* from a mucus simulant surface (2% LBG cross-linked with sodium borate) using a SCM. It has been shown that the size of droplets, measured using optical particle counter (OPC), was in the submicron range (~ 320 nm). Although the OPC provides more information on the size range of particles, the sampling rate of OPC is still a major limitation. Because droplets are susceptible to evaporation during measurement, a method with rapid sampling rate is necessary to report the original (initial) droplet size. Delivering normal saline onto the mucus simulant surface reduced the number of droplets and those formed were of larger size compared to those formed in the absence of normal saline. In contrast, the delivery of a surfactant mixture of 7% DPPC and 3% 1-palmitoyl-2-oleoyl-sn-glycero-3-phosphoglycerol (POPG) onto the mucus simulant surface reduces the size of droplets relative to saline delivery. In a second series of experiments,[50] Watanabe *et al.* found that $CaCl_2$ solution (1.29%) produce significant reduction in the number of droplets generated from the mucus simulant surface.[50] The reduction in droplet number following the delivery of normal saline and $CaCl_2$ solutions into the mucus simulant surface was attributed to increasing the surface elasticity of mucus simulant and consequently

reducing the ability of mucus simulant surface to breakup into small droplets. These studies show that bioaerosol formation can be altered by changing the physicochemical properties of the airway lining fluid.

Although the size distribution and concentration of exhaled bioaerosols have been studied previously in both *in vivo* and *in vitro* experiments, there are a variety of limitations to these studies. The effect of temperature and %RH on droplet size was not taken into consideration at the point of formation within the SCM or at the point of exit into the surrounding environment. In most cases, droplets exited into a lower temperature and %RH environment than that of the human trachea. This would have lead to droplet evaporation and shrinkage before the droplets reached the measuring instrument. Therefore, the reported droplet size was not indicative of their initial size upon formation. In addition, different measuring techniques were used to study the size distribution of bioaerosols. Large discrepancies would be expected in the reported size distributions as each technique has its own limits of detection. Discrepancy in the size distribution of exhaled bioaerosols was also observed *in vivo* between healthy individuals, which has been attributed to inter-subject variability. The source of this variability has not been identified, although differences due to the physical properties of an individual's lung fluid or the physical structure of an individual's lung tree could be expected. In previous *in-vitro* bioaerosol studies, while the effect of surface viscoelastic properties on bioaerosol formation were probed, surface tension was not specifically studied. Since only the bulk viscoelastic properties of lung mucus were modeled, the effect of surfactant at the surface of the lung fluids on bioaerosol formation remains unstudied. It is expected that surface viscoelastic properties and surface tension will affect bioaerosol formation. The surface tension of the mucus layer was mathematically modeled to predict its effect on bioaerosol formation. However, a high surface tension range (100 to 2000 mN/m) was used compared to that of tracheal surface tension (~ 32 mN/m). Thus, more accurate matching

of the surface properties of mucus is necessary to better understand the mechanism of bioaerosol formation.

1.6. Objectives

Our current knowledge of how bioaerosols are formed from the conducting airways in the lungs is in its infancy. The complex structure and biophysical properties of the airway lining fluid (ALF) have made both experimental and mathematical modeling challenging. Current experimental methods to study the formation of bioaerosols generated from the ALF have been limited by their lack of physiological relevance, as mucus simulants commonly used in *in-vitro* studies do not have both the same physical and chemical properties of native mucus. In addition, current existing models of tracheal mucus have significant limitations that the synthetic gels lack the key physicochemical properties of native tracheal mucus such as chemical composition, component concentrations and surface tension. In addition, the large variability in the rheological properties of normal and diseased *in-vivo* secretions, limit the use of these models. These limitations highlight the need for a better *in-vitro* model of tracheal mucus to study the surface rheology of surfactants adsorbed at the air-mucus interface of the large conducting airways and elucidate the mechanism of bioaerosol formation from tracheal surfaces. Therefore, the research presented in this thesis aims to develop a more physiologically relevant model system to study bioaerosol formation *in-vitro*. The objectives and specific aims of this research are explained as follows:

Objective 1: To develop a more physiologically relevant *in-vitro* model mimetic of native, non-diseased tracheal mucus.

Specific Aim 1.1: To match the chemical composition and concentration to the primary components in native mucus.

Specific Aim 1.2: To match key physical properties, specifically the bulk viscoelastic properties and surface tension, to that of native mucus.

Objective 2: To probe the surface rheology of the conductive airway surfactants, where the underlying subphase is a viscoelastic, non-Newtonian mucus gel.

Specific Aim 2.1: To study the surface rheology of the primary surface-active component, (dipalmitoylphosphatidylcholine, DPPC), adsorbed at the air-mimetic interface of the *in-vitro* model mucus mimetic.

Specific Aim 2.2: To study the surface rheology of the exogenous surfactant, Infasurf®, adsorbed at the air-mucus interface of the *in-vitro* model mucus mimetic.

Specific Aim 2.3: To investigate the effect of subphase viscoelastic properties on the surface rheology of DPPC and Infasurf® films.

Objective 3: To develop an enhanced simulated cough machine (SCM) with features that better mimic the conditions of the trachea.

Specific Aim 3.1: To condition the SCM for lung temperature and humidity.

Specific Aim 3.2: To limit the occurrence of edge effects during simulated cough.

Objective 4: To determine key parameters that control the size distribution of bioaerosols generated from an *in-vitro* model mucus mimetic surface.

Specific Aim 4.1: To correlate the effect of bulk viscoelastic properties of the *in-vitro* model mimetic to bioaerosol size distribution.

Specific Aim 4.2: To correlate the effect of surface tension of the *in-vitro* model mimetic on bioaerosol size distribution.

Specific Aim 4.3: To correlate the effect of surface rheology of the *in-vitro* model mucus mimetic on bioaerosol size distribution.

Specific Aim 4.4: To probe the mechanism of action of calcium chloride, a known bioaerosol suppressant.

Table 1-1: Typical values of the bulk viscoelastic properties of native non-diseased tracheal mucus in human subjects and dogs.[22-25, 25]

Bulk viscoelastic property	**Typical values of native tracheal mucus**
G' (1rad/sec)	4.9-32.2 Pa
G" (1rad/sec)	1.1-12.6 Pa
G' (100 rad/sec)	9.7-52.0 Pa
G" (100 rad/sec)	7.7-62.7 Pa
tan δ (1 rad/sec)	0.2-0.6
δ (1 rad/sec)	11.9-29.6°
tan δ (100 rad/sec)	0.6-1.2
δ (100 rad/sec)	31.4-50.4°
G* (1 rad/sec)	5.0-34.7 Pa
G* (100 rad/sec)	11.5-81.3 Pa

†The bulk shear storage modulus G', bulk shear loss modulus G" and phase angle shift (δ) between applied stress and resulted strain, were calculated based on available data of tan δ and the bulk complex modulus G*, where $G^* = \sqrt{[(G')^2 + (G'')^2]}$.

Table 1-2: Size distributions and average concentrations of bioaerosols produced during different expiratory maneuvers reported in recent studies.

Subjects	**Expiratory maneuvers**	**Bioaerosol size distribution**	**Bioaerosol concentration**	**Bioaerosol measurement technique**
Healthy human volunteers (n=5) [59] Age: 20-40 years	Nose and mouth breathing, coughing, talking	0.3-8 µm (~ 85% of droplets are < 1 µm). Multimodal peaking at 0.6 µm and 1-1.5 µm.	Inter-subject variability Inter-mode variability Droplet concentration: 1/liter-280/liter Highest droplet concentration: coughing mode. Lowest droplet concentration: nose breathing mode.	Optical particle counter (OPC, Climet CI7300); lower diameter detection limit of 0.3 µm. Sampling rate: 7 L/min Analytical transmission electron microscopy (AEM)
Healthy human volunteers (n=11) [58]	Normal mouth breathing Delivery of isotonic saline for 6 min Delivery of isotonic saline and lung surfactants	<1 µm 72% diminution of bioaerosols in high producers for ~ 6 hrs and opposite trend observed in low producers. Amplify bioaerosol particle production in high and low producers	Inter-subject variability ranging from 1 particle/L to > 10,000 particles/L. High producers: Expiring > 500 particles/L over 6-hr period. Low producers: Expiring < 500 particles/L over 6-hr period.	Optical particle counter (OPC, Climet, Ultimate 100).
Anesthetized bull calves (n=7) [71]	Normal breathing Delivery of isotonic saline for 6 min	Not reported > 50% diminution of bioaerosols for 120 min compared to pre-treatment	Inter-subject variability (high producers and low producers)	Optical particle counter (OPC, Climet)
Healthy volunteers (n=11) [69]	Coughing and speaking (counting 1-100)	Coughing: Geometric mean: 13.5 µm Speaking: Geometric mean: 16.0 µm	Per cough: 947-2085 droplets During speaking: 112-6720 droplets	Interferometric Mie Imaging. Lower size detected is ~ 2 µm. Aerodynamic particle sizer

Table 1-3 continued

Subjects	Expiratory maneuvers	Bioaerosol size distribution	Bioaerosol concentration	Bioaerosol measurement technique
Healthy human volunteers (n=54) [68] 3 age groups: 10-12, 20-30, and 30-50 years 27 males and 27 females	Coughing	Droplet nuclei: 0.58-5.42 µm (82% between 0.74-2.12 µm). Coughed droplets: 0.62-15.9 µm with multimodal peaking at 1, 2, and 8 µm. No significant variation among the 3 age groups in average droplet size.	10-12 years: Male:1089±594 droplet/cm^3, female: 881±358 droplet/cm^3 20-30 years: Male: 1323±685 droplet/cm^3. Female: 896±442 droplet/cm^3 30-50 years: Male: 2355±663 droplet/cm^3. Female:2066±612 droplet/cm^3	Aerodynamic particle sizer (APS, Model 3310A, TSI Inc.) Scanning mobility particle sizer (SMPS, Model 3934, TSI Inc.)
5 male subjects with a positive-pressure full face air-liner respirator supplied by clean air (< 0.01 particles/cm^3). [67]	Normal breathing, talking, deep breathing, walking, stepping up and stepping down, and coughing once or twice per minute	Majority of particles had diameter < 0.3 µm, < 2% of particles had diameter >1 µm.	Particle conc.: < 0.1 to ~ 4 particles/cm^3. Marked variation in particle conc. during various activities. Lowest conc. during normal breathing. Highest conc. during step-ups.	Laser aerosol spectrometer counted particles in 15 size ranges from 0.1 µm to 3.0 µm. (Company and model of the particle counter were not mentioned).
Healthy volunteers (n=15) [70]	Breathing, coughing, speaking	Multimodal peaking at ≤ 0.8 µm and 1.8 µm for all activities additional peak:3.5- 5 µm for speaking only	Coughing: 0.64/cm^3 Mouth breathing: 0.092/cm^3 Nose breathing: 0.05/cm^3 Speaking: 0.307/cm^3	Aerodynamic particle sizer (APS)
Healthy volunteers (n=17) [60]	Normal breathing, varied breath-holding periods, and contrasting inhalation and exhalation rates	Majority of droplets: < 2 µm.	Normal breathing: 0.2/cm^3 Inhaling normal breathing: 1.1/ cm^3 Rapid inhalation: 2.6/ cm^3	Aerodynamic particle sizer (APS)

Table 1-4: Bioaerosols generated *in-vitro* from mucus simulant surfaces using a SCM reported in recent studies.

Mucus simulant	**Treatment of mucus simulant**	**Results**	**Bioaerosol measurement technique**
LBG-borax [58]	No treatment Delivery of normal saline for 6 min Delivery of surfactants (DPPC and POPG)/normal saline	≈ 320 nm Diminution of droplets count Increase droplet size Droplet size is smaller relative to that formed in saline delivery; conc. higher	Sympatec, HELOS/KF laser-diffraction particle sizer.
LBG-borax [15]	Increase bulk viscoelasticity of LBG by increasing the volume of borax	Diminution of droplets count Increase droplet size	Target: bulls eye-type (circles within circles) with paper sheets placed to lateral sides, on top, and below the target
LBG-borax [50]	Delivery of normal saline and $CaCl_2$ Delivery of Tween 80 and sodium dodecyl sulfate (SDS) solutions in isotonic saline Delivery of Tween 80 and SDS solutions	Significant diminution in droplets count Significant diminution in droplets count No significant diminution in droplets count Median aerosol particle size ~200 nm	Optical particle counter (OPC, Climet)

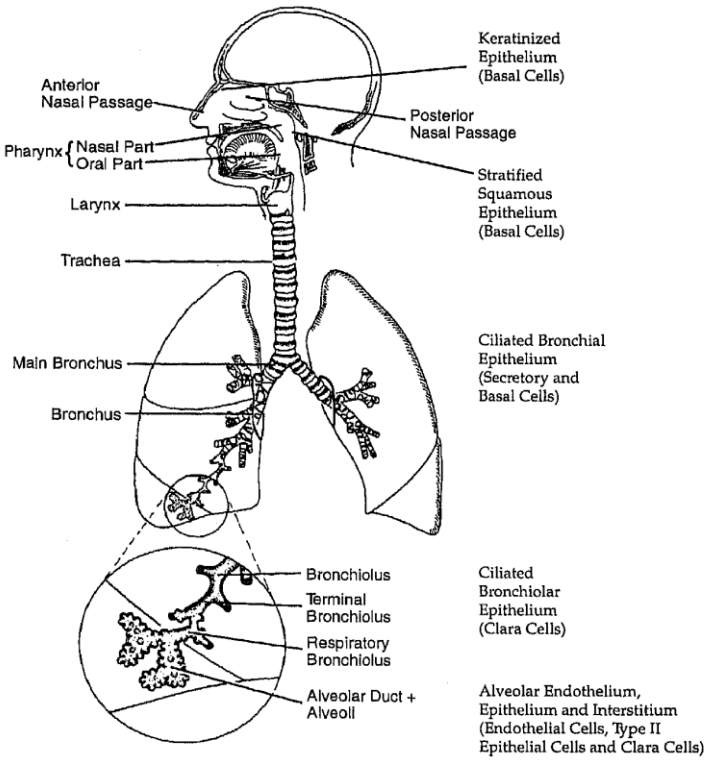

Figure 1-1: Anatomical and morphological overview of the human respiratory tract regions. (From reference 10, reproduced by permission).

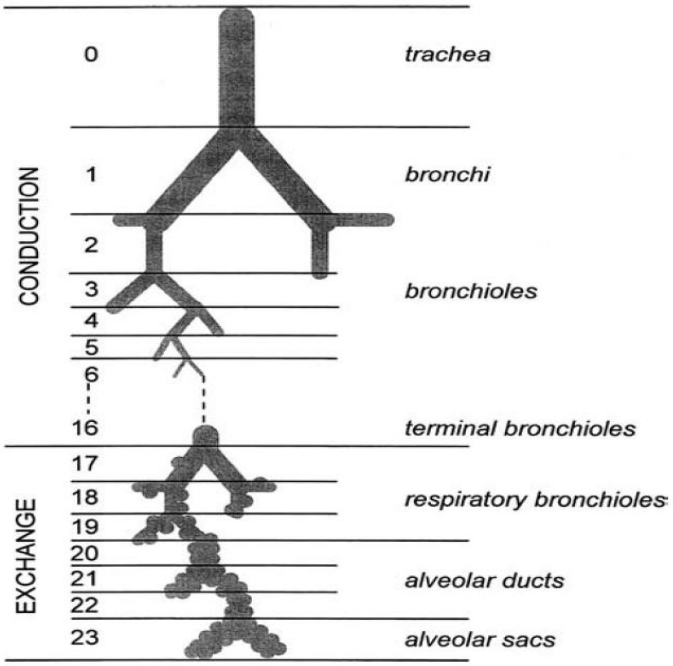

Figure 1-2: Classic human lung model as described by Weibel. The model proposed the existence of 24 airway generations (each generation groups airways of similar size) with the trachea as generation 0, bronchi as generation 1, bronchioles to terminal bronchioles (bronchioles not associated with alveoli) as generations 2 to16, respiratory bronchioles (bronchioles associated with alveoli protruding from their walls) as generations 17 to19, alveolar ducts as generations 20 to 22, and the alveolar sacs as generation 23. The conducting zone extends from the trachea to the terminal bronchioles and the gas exchange zone extends from the respiratory bronchioles to the alveolar sacs. (From Reference 2, reproduced by permission)

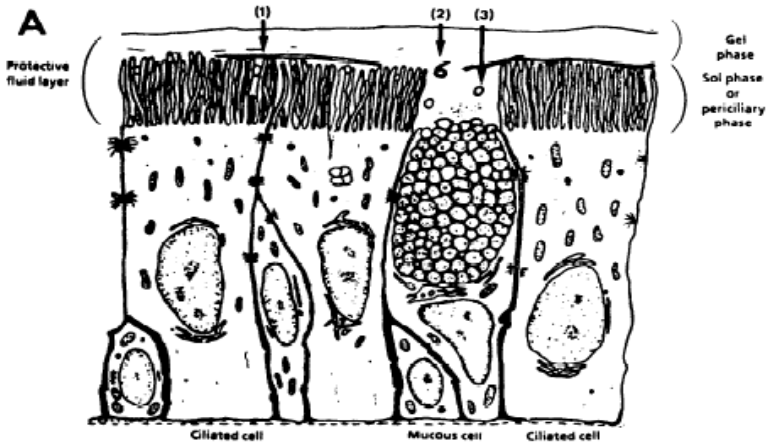

Figure 1-3: Gel phase and sol (or periciliary) phase of the protective airway fluid layer lining the tracheobronchial mucosa. Osmiophilic structures composed of phospholipids are observed as mono- or bilayers (l), lamellar structures (2) and vesicles (3). (From reference 72, used with permission).

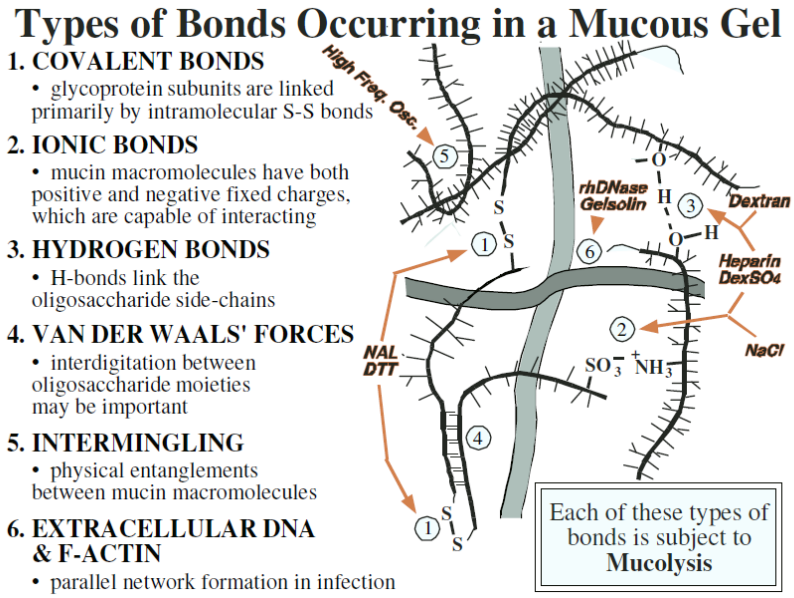

Figure 1-4: High molecular weight glycoproteins (mucins) cross-linked by covalent bonds (disulfide bridges) and non-covalent bonds (hydrogen binds, ionic interactions and Van der Waals forces). (From reference 15, reproduced by permission).

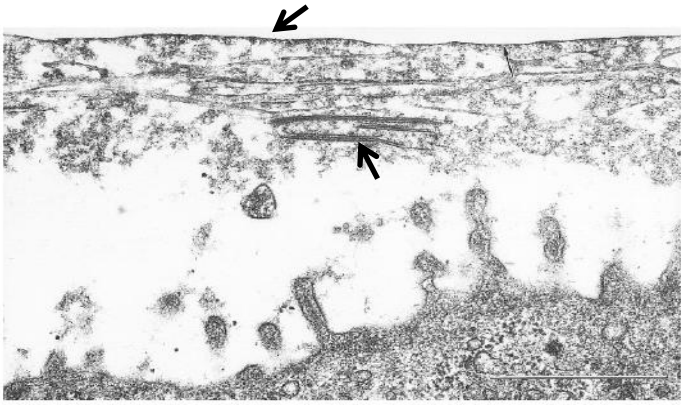

Figure 1-5: Lipid monolayer at the surface of rat tracheal mucus and lipid sheets within rat tracheal mucus indicated by arrows. (From reference 34, used with permission).

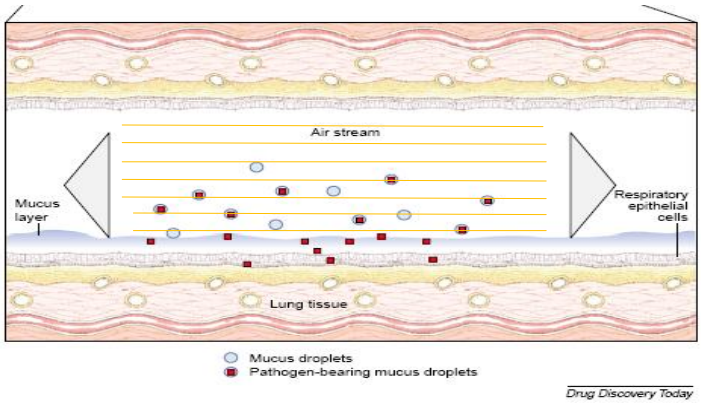

Figure 1-6: The principle theory for bioaerosols formation in the trachea. Droplets are formed due to the shearing of ALF surface via airstreams during inhalation and exhalation. (From reference 8, adapted by permission).

CHAPTER 2

IN-VITRO MODEL MIMETIC OF TRACHEAL MUCUS

2.1. Introduction

Although the currently existing models of tracheal mucus have shown great improvements in understanding the function of airway secretions, these models have several drawbacks. Synthetic viscoelastic gels have been used to understand the relationship between the bulk rheological properties of the tracheal secretions and ciliary and cough clearance.[15, 49, 73] However, these synthetic gels lack key chemical and physical properties (i.e. bulk chemical composition, bulk viscoelastic properties and surface tension). *In-vivo* tracheal secretions have been used to determine the chemical composition and physical properties (bulk rheology and surface tension) of tracheal secretions in normal and diseased states.[12, 22, 23, 74] However, airway secretions in healthy individuals are severely limited in quantity. These drawbacks have limited our ability to study how mucus properties alter its function.

A significant body of literature has developed to characterize the composition of pulmonary mucus. Human airway mucus contains approximately 93-97% (w/w) water and 3-7% (w/w) solids, of which the solids content is about 1% (w/w) proteins and 1-5% (w/w) glycoproteins, 0.5-1% (w/w) lipids and 0.70-1.4% (w/w) minerals.[12-14] Mucins, high molecular weight macromolecules ($1.8x10^6$ to $4.4x10^7$ Da) composed of oligosaccharide side chains *O*-glycosidically linked to a peptide core, are essential in maintaining the rheological properties of mucus.[14] Respiratory tract glycoproteins have been shown to be similar in composition to other mammalian epithelial glycoproteins.[75] Many types of serum proteins have been identified in the tracheobronchial secretions, including immunoglobulins (IgG, IgA, IgM), albumin, fibrinogen, lysozyme, lactoferrin and other components.[76] Albumin is the major serum protein component in the secretions.[76] Previous studies of the ion content in human airway secretions have reported

ion concentrations of 165 ± 42 mmol/1000 g sodium, 13.2 ± 5.4 mmol/1000 g potassium, 162 ± 60 mmol/1000 g chloride, 3.1 ± 1.0 mmol/1000 g calcium, and 27 ± 16 mmol/1000 g phosphorous, leading to an osmolarity of 359 ± 56 mOsmol/L.[77] The pH of human airway mucus has been reported between 5.4-8.2.[14] Phospholipids represent the second major lipid component, after neutral lipids, in normal tracheal secretions.[13, 39, 40] Of the phospholipid classes (phosphatidylcholine, phosphatidylglycerol, phosphatidylinositol, phosphatidylethanolamine, lysophosphatidylcholine and sphingomyelin), phosphatidyl-choline comprises the most abundant phospholipid.[13, 42-44]

The tracheal mucus is a viscoelastic gel layer, which exhibited both elastic and viscous properties.[15-17] The surface tension at the air-mucus interface is reported to be between 31.4-34.0 mN/m.[29-32] Tracheal mucus is chemically composed of 93-97% (w/w) water, and 3-7 % (w/w) solids (proteins, glycoproteins, lipids and minerals).[12-14] While the composition and some key properties of human mucus are fairly well established, few studies have been conducted to develop a mucus simulant that contains these properties. This chapter will focus on the development of a more physiologically relevant *in-vitro* model of the mucus lining the trachea. In this model, the chemical composition, component concentration, and physical properties (bulk viscoelasticity and surface tension) of the *in-vitro* model mucus mimetic have been matched to that of native tracheal mucus. Specifically, a series of mucus mimetics have been developed utilizing components (glycoproteins, proteins, lipids, ions and water) at concentrations similar to that found natively in tracheal mucus. The *in-vitro* model mucus mimetic was cross-linked using a bi-functional cross-linking agent to alter the viscoelastic properties to mucus mimetic. The surface tension of the *in-vitro* model mucus mimetic was matched to that of the native mucus. The cross-linking mechanism of the *in-vitro* model mucus mimetic was then investigated using the Fourier transform-infrared (FT-IR) spectroscopy.

2.2. Materials and Methods

2.2.1. Materials

Pig gastric mucin (PGM)-type III, n-hexane (99.0% purity) and glutaraldehyde (G7651, 50% w/w solution) were purchased from Sigma-Aldrich, Inc. (St. Louis, MO), bovine serum albumin (fraction V, lyophilized powder) from Spectrum (Gardena, CA) and 1, 2-dipalmitoyl-sn-glycero-3-phosphocholine (DPPC) from Genzyme Pharmaceuticals (Cambridge, MA). Glutaraldehyde (GA, 50% w/w solution), and methanol (99.9% purity) were purchased from Fisher Scientific (Fair Lawn, NJ). Purified water (18 MΩ cm) was used in all experiments obtained from a NANOpure Infinity Ultrapure Water System, Barnstead International (Northbrook, IL). All other chemical reagents: sodium chloride (NaCl), calcium chloride ($CaCl_2$), sodium phosphate monobasic (NaH_2PO_4**.** H_2O), sodium phosphate dibasic (Na_2HPO_4), potassium bromide (KBr), and sodium borohydride ($NaBH_4$) were of analytical grade and used without further purification.

2.2.2. Preparation of Mucin Solutions

The effect of increasing the concentration of pig gastric mucin (PGM)-Type III in solution on the viscoelastic properties of the solution was tested. In these studies, DPPC was dispersed with the other components (PGM-type III, albumin, ions and water) in the bulk. Initially, a series of mucin solutions was developed with increasing concentrations of PGM-type III (2%, 3%, 4% and 6%, w/v), 1% (w/v) ions (Na^+, Ca^{+2}, P^{+5} and Cl^-) in buffer at pH 7.4, 1% (w/v) protein (albumin), 1% (w/v) DPPC (added to the bulk), and 91-95 ml water. To prepare 30 ml of the mimetic, 5 ml of buffer (154 mM NaCl, 3 mM $CaCl_2$, 15 mM NaH_2PO_4/Na_2HPO_4; pH 7.4) was added to 0.3 g DPPC in an amber glass bottle and stirred for about 2 hours using a magnetic stirrer. Then, 0.3 g albumin, PGM-type III (0.6 g, 0.9 g, 1.2 g and 1.8 g to prepare 2%, 3%, 4% and 6% (w/v) mucin solutions, respectively), buffer (154 mM NaCl, 3 mM $CaCl_2$, 15 mM

NaH_2PO_4/Na_2HPO_4; pH 7.4) of 23.8 ml, 23.5 ml, 23.2 and 22.6 ml to prepare 2%,3%, 4% and 6% (w/v) mucin solutions, respectively, were added to the amber glass bottle. Ingredients were mixed at 4°C on a tube rotator (Glas-Col, IN) for at least 6 days to mix the sample. Table 2-1 illustrates a description for the composition of mucin solutions (2%, 3%, 4% and 6%, w/v).

2.2.3. Altering and Controlling Bulk Viscoelastic Properties to Mucus Mimetic

A mucus mimetic formulation composed of 4% (w/v) PGM-type III, 1% (w/v) ions (Na^+, Ca^{+2}, P^{+5} and Cl^-), 1% (w/v) proteins (albumin), 0.17% (w/v) DPPC (added to mimetic surface) and 94 ml water was used for the further studies. To prepare 30 ml of the mimetic, 0.3 g albumin, 1.2 g PGM-type III and 28.2 ml buffer (154 mM NaCl, 3 mM $CaCl_2$, 15 mM NaH_2PO_4/Na_2HPO_4; pH 7.4) were added to an amber glass bottle. Ingredients were mixed at 4°C on a tube rotator (Glas-Col, IN) for at least 6 days to mix the sample. The bi-functional cross-linking agent, glutaraldehyde (GA) (Figure 2-1), was used to induce cross-linking to mucus mimetic and consequently alter mimetic bulk viscoelastic properties. The bulk viscoelastic properties of the mucus mimetic were controlled by altering GA concentrations (5, 10, 15, 20, 25 and 50%, w/w) added to mucus mimetic formulations and/or cross-linking time (1 day, 2 days and 3 days). Cross-linking of the mucus mimetic was achieved by adding a specific volume and concentration of GA solution and mixing using a tube rotator (Glas-Col, IN) for a specified cross-linking time at 4°C.

2.2.4. Reformulation of the *In-Vitro* Model Mucus Mimetic

The *in-vitro* model mucus mimetic formulation was composed of 4% (w/v) PGM-type III, 1% (w/v) ions (Na^+, Ca^{+2}, P^{+5} and Cl^-), 1% proteins (albumin), 0.17% (w/v) DPPC, and 94 ml water. To prepare 30 ml of the mimetic, 0.3 g albumin, 1.2 g PGM-type III and 28.2 ml buffer (154 mM NaCl, 3 mM $CaCl_2$, 15 mM NaH_2PO_4/Na_2HPO_4; pH 7.4)

were added to an amber glass bottle. Ingredients were mixed at 4°C on a tube rotator (Glas-Col, IN) for 24 hours to mix the sample. Cross-linking of the mucus mimetic was achieved by adding specific volume and concentration of GA solution and mixing manually for 5 minutes at room temperature. The mucus mimetic was kept stationary at room temperature (~ 22°C) for 24 hours.

2.2.5. Bulk Rheology of Mucus Mimetic

The bulk viscoelastic properties of the mucus mimetic were determined using a controlled-stress cone and plate rheometer (RheoStress 1, Haake®; 60 mm diameter, 4° cone angle). The cone-plate rheometer was connected to a temperature control system (Haake® F3-CH refrigerated circulator) to maintain temperature at 23°C. The gap between the cone and plate was adjusted to 0.138 mm for all measurements. A solvent trap was used to cover the sample during analysis to minimize sample dehydration during testing. For each experiment, 5 ml of mimetic was loaded onto the lower plate, spread evenly over the entire surface area of the plate and allowed to relax and equilibrate at 23°C for 60 seconds. The upper cone was lowered into position, excess sample was removed from the edges of the cone and plate, and then the measurement was made. The bulk shear storage (or elastic) modulus G' and the bulk shear loss (or viscous) modulus G" were determined using RheoWin® Data Pro Manager (v.2.96). The strain-dependence of G' and G" over a strain range of 0.01 to 1.1 and at a constant frequency (ω) of 2 rad/sec was determined to verify the linear viscoelastic region (LVR). Within the linear viscoelastic region, the viscoelastic shear moduli (G' and G") remain constant and are independent of strain. Thus, G' and G" are directly related to the molecular structure of the sample and not to the applied strain. On the basis of this test, a value of an applied strain of 0.1 was chosen and used in subsequent frequency-dependent experiments. G' and G" were determined as a function of frequency over a range of 0.5 to 105 rad/sec. Bulk viscoelastic properties were determined for at least three independent samples.

2.2.6. Investigating GA Cross-linking Mechanism of Mucus Mimetic Using FT-IT Spectroscopy

Samples of native albumin, native PGM-type III, 1% (w/v) albumin cross-linked using 50% GA (w/w), 4% (w/v) PGM-type III cross-linked using 50% GA (w/w), uncross-linked mucus mimetic, mucus mimetic cross-linked using 50% GA (w/w), and mucus mimetic cross-linked using 50% GA (w/w) and then reduced using ($NaBH_4$) were pelletized with KBr powder and characterized by FT-IR spectroscopy. To prepare 30 ml of 1% (w/v) albumin, 0.3 g of albumin and 29.7 ml buffer (154 mM NaCl, 3 mM $CaCl_2$, 15 mM NaH_2PO_4/Na_2HPO_4, pH 7.4) were added to an amber glass bottle and mixed at 4°C on a tube rotator (Glas-Col, IN) for 24 hours to mix the sample. To prepare 30 ml of 4% (w/v) PGM-type III,1.2 g of PGM-type III and 28.8 ml buffer (154 mM NaCl, 3 mM $CaCl_2$, 15 mM NaH_2PO_4/Na_2HPO_4, pH 7.4) were added to an amber glass bottle and mixed at 4°C on a tube rotator (Glas-Col, IN) for 24 hours to mix the sample. To prepare 30 ml of mucus mimetic, 0.3 g albumin, 1.2 g PGM-type III and 28.5 ml buffer (154 mM NaCl, 3 mM $CaCl_2$, 15 mM NaH_2PO_4/Na_2HPO_4, pH 7.4) were added to an amber glass bottle. Ingredients were mixed at 4°C on a tube rotator (Glas-Col, IN) for 24 hours to mix the sample. Samples of 1% (w/v) albumin, 4% (w/v) PGM-type III and mucus mimetic were cross-linked by adding 0.5 ml-50% GA (w/w) to each sample. GA was mixed manually for 5 minutes at room temperature, and kept at room temperature for 24 hours. In the cross-linked and reduced mucus mimetic, the cross-linked mucus mimetic was immersed in a freshly prepared 1.2 mg/ml of $NaBH_4$ in phosphate buffer (15 mM NaH_2PO_4/Na_2HPO_4, pH 7.4) for 2 hours. Samples of the cross-linked albumin, cross-linked PGM-type III, uncross-linked mucus mimetic, cross-linked mucus mimetic, and cross-linked/reduced mucus mimetic were frozen at -80°C for 4 hours and lyophilized in a Labconco FreeZone 4.5 liter freeze dry system (chamber pressure of less than 0.02 mbar and collector temperature of less than -50°C). Finally, KBr pellets were prepared by mixing 15 mg of each sample with 250 mg of dry KBr (KBr was dried in an oven before

use). The mixture was ground in a mortar with a pestle to a fine powder and loaded into a pellet die set. The die set was aligned in a Carver Laboratory Press (model # C) and compressed to ~ 15,000 PSI. Pellets were left under pressure at least 10 minutes and then removed gently from the die set. Pellets were stored in a desiccator.

FT-IR measurements were carried out at room temperature on a Nicolet Nexus 670 FT-IR spectrometer. All spectra were taken with a resolution of 4 cm^{-1} and 32 scans in the 4000-1000 cm^{-1} range. Omnic 6.1 software (Thermo Nicolet Instruments Corp.) was used to analyze the different sample spectra. An air spectrum was obtained as a reference and was then subtracted from the sample by the instrument-controlled computer. At least three KBr pellets were prepared for each sample.

2.2.7. Control Experiments for the Spreading Solvent (n-hexane:methanol 95:5 v/v)

To ensure that the spreading solvent (n-hexane:methanol 95:5 v/v) is not surface active and has the ability to efficiently spread DPPC at the air-liquid interface, three control experiments were conducted as described in Table 2-2. In all these experiments, a Langmuir-Blodgett (LB) Teflon coated trough (KSV Instruments, Finland) with a working area of 78 cm x 7.5 cm was placed on a vibration isolation table inside a home-built environmental chamber (Figure 2-2). The LB trough was equipped with a double barrier system and a Wilhelmy plate (KSV Instruments, Finland) attached to a microbalance to record the surface pressure or surface tension. Before each experiment, the LB trough and barriers were thoroughly cleaned with ethanol and de-ionized water, and the surface was aspirated by a tube connected to a vacuum-aspirator. A liquid subphase composed of 150 mM NaCl and 1.5 mM $CaCl_2$, chosen in accordance with the chemical composition of alveolar fluid, was used.[18] To ensure cleanliness of the surface, a zero reading of the surface pressure (Π) on complete compression of the interface was obtained. Surface pressure (Π) is defined as $\Pi = \gamma_o - \gamma$, where γ is the surface tension of the

surfactant covered the interface and γ_o is the surface tension for a clean air-liquid interface. A volume of 250 ml of the liquid subphase was poured into the LB trough mounted on a temperature regulated base plate and the temperature was maintained at 37 ± 0.5°C by an external circulating water bath. The subphase was allowed to equilibrate for 30 minutes at 37 ± 0.5°C [this temperature was used by Yu *et al.*[78] to study the surface activity of DPPC using the spreading solvent (n-hexane:methanol 95:5 v/v), and the initial surface tension was reported. The 20 mm x 10 mm Wilhelmy platinum plate was dipped into the subphase and the surface tension was reported. In the first and second control experiments, an amount of 180 µL of the spreading solvent (n-hexane:methanol 95:5 v/v) was spread at the air-liquid interface using a micro-syringe, (180 µL is equivalent to the amount of 1 mg/ml DPPC required to lower the surface tension of the liquid subphase to ~ 32 mN/m). After spreading, 10 minutes were allowed for solvent to evaporate.

In the first control experiment, the surface tension for the air-liquid interface after the addition of the spreading solvent (n-hexane:methanol 95:5 v/v) was reported. In the second experiment, the surface pressure-surface area isotherm for three successive compression-expansion cycles for the air-liquid interface after the addition of the spreading solvent (n-hexane:methanol 95:5 v/v) was recorded. A 77.4% area reduction of the maximum surface area, at a speed of 61.04 mm/min, was performed.

In the third control experiment, an amount of 180 µL of 1 mg/ml DPPC in n-hexane:methanol (95:5 v/v) was spread at the air-liquid interface using a micro-syringe to lower the surface tension to ~ 32 mN/m. The mean molecular area of DPPC was 30$Å^2$/ molecule. Three successive compression-expansion cycles, of a 33.0% area reduction of the maximum surface area at a speed of 61.04 mm/min was performed. Minimum and maximum surface tensions for each compression-expansion cycle were reported. All control experiments were performed at least three times.

2.2.8. Measurement and Modification of the Surface Tension

DPPC was dissolved in the spreading solvent (n-hexane:methanol 95:5 v/v) and was added onto water or mimetic surfaces using a micro-syringe to achieve a surface tension of ~ 32 mN/m. Ten minutes were allowed to elapse for the solvent to evaporate. The surface tension measurements of the water and mucus mimetic before and after spreading DPPC at the air-water and air-mimetic interface were determined using two methods: Wilhelmy plate balance (KSV Instruments, Finland) and a detachment method using the du Noüy ring (Sigma 70, KSV Instruments, Finland). In the Wilhelmy plate method, a platinum plate (20 mm x 10 mm) attached by a thread to a force transducer was dipped into ~ 10 ml of mucus mimetic sample in a round Pyrex petri-dish (5.0 cm diameter x 1.5 cm depth). The plate was hung on a balance and oriented perpendicular to the interface. The force experienced by the balance as the plate interacts with the interface was measured and used to calculate the surface tension using the following equation:

$$\gamma = F / (2 L \cdot \cos \theta)$$

where γ is the surface tension of the interface, F is the force exerted by the plate when it is brought in contact with the interface, L is the perimeter of the plate, and θ is the contact angle made between the interface and the plate. The force (F) is measured by the balance, the contact angle (θ) is assumed to be zero, and the perimeter (L) is known by the manufacturer. The surface tension is calculated using the KSV software.

In the detachment method, a platinum iridium du Noüy ring (circumference 5.910 cm, R/r 52.94) was attached to the balance. A sample of ~ 10 ml volume of mucus mimetic was placed in a round Pyrex dish (50 mm diameter) inside a thermostated vessel used for controlling the temperature of the sample (~ 22°C). The ring was allowed to come into contact with the sample at a speed up of 20 mm/min and a wetting depth of 6.0 mm. The force required to completely separate the ring from the sample was directly

measured by a transducer connected to the ring. The surface tension is calculated using the following equation: $\gamma = F/(4\pi R)$,[79] where F is the detachment force for the meniscus and $(4\pi \cdot R)$ is the periphery of the surface detached.

Before conducting surface tension measurements, the Wilhelmy plate and du Noüy ring were flamed before use to remove surface contaminants. To ensure cleanliness of the Wilhelmy plate and du Noüy ring, the surface tension of Nanopure water of ~ 72.8 mN/m at 20°C was verified before each measurement. At least three surface tension measurements were conducted for each sample.

2.2.9. Statistical Analysis

A paired t-test was performed to compare the surface tension of the air-liquid interface before and after addition of a spreading solvent. Levels of significance were accepted at the $p<0.05$ level. Statistical analyses were performed using Minitab 15 software.

2.3. Results and Discussion

2.3.1. Chemical Composition of Mucus Mimetic

The synthetic mucus mimetic developed in this study was composed of 4% (w/v) PGM-type III, 1% (w/v) albumin, 154 mM NaCl, 3 mM $CaCl_2$, buffer (15 mM $NaHPO_4/Na_2HPO_4$, pH 7.4), and 94 ml water. DPPC (0.17% w/v) was spread on the surface of the mucus mimetic to lower the surface tension to ~ 32 mN/m. Table 2-3 illustrates a comparison between the chemical composition of the *in-vitro* model mucus mimetic and native tracheal mucus.

The components used to formulate the mucus mimetic were chosen based on their abundance in native mucus and their similarity to components found natively in lungs. Pig gastric mucin (PGM-Type III) with 0.5-1.5% sialic acid was utilized in these studies as the glycoprotein source, due to availability and similarity to sialic acid content in

native respiratory mucus.[80, 81] Bovine serum albumin was used at a concentration of 1% in the mimetic. Dipalmitoylphosphatidylcholine (DPPC) was chosen to reduce the surface tension of the mucus mimetic as it represents ~ 50% of the PC molecular species in the tracheal secretions.[42, 44]

Although our *in-vitro* model mimetic of tracheal mucus is more complex in composition compared to the other existing models, matching the chemical composition and component concentrations of the *in-vitro* model mimetic to those of native tracheal mucus is critically important since the physical properties (bulk viscoelasticity and surface tension) of tracheal mucus are determined by composition.[82] Therefore, changes in mucus chemical composition and component concentrations may alter the physical properties of tracheal secretions.

2.3.2. Bulk Rheology of Mucin Solutions

The first attempt that was used to alter the viscoelastic moduli of the mucus mimetic was to gradually increase mucin concentration. Table 2-4 represents the bulk viscoelastic properties of mucin solutions containing 2%, 3%, 4% and 6% (w/v) PGM-type III at 1 rad/sec and 100 rad/sec; where G' is the bulk shear storage modulus, G" is the bulk shear loss modulus, δ is the phase angle shift between applied stress and resulting strain, and G* is the bulk complex modulus. G' and G" at 1 rad/sec and 100 rad/sec were measured using the cone and plate rheometer. Other rheological properties (tan δ, δ, and G*) were calculated based on available data of G' and G"; where $\tan \delta = (G''/G')$, $\delta = \tan^{-1} \delta$, and $G^* = \sqrt{[(G')^2 + (G'')^2]}$.

Figures 2-3 to 2-6 illustrate the frequency-dependence of G' and G" for mucin solutions containing 2%, 3%, 4% and 6% (w/v) PGM-type III, respectively. At low PGM-type III concentrations (2% and 3%, w/v), both G' and G" increased with frequency and exhibited very low values at 1 rad/sec. For the mucin solution of 2% (w/v) PGM-type III, G' and G" at 1 rad/sec were 0.11 ± 0.09 and 0.10 ± 0.09 (n=3),

respectively (Figure 2-3). However, for the mucin solution of 3% (w/v) PGM-type III, G' and G" at 1 rad/sec were 0.08 ± 0.06 (n=3) and 0.29 ± 0.33 (n=3), respectively (Figure 2-4). In addition, large variation in the bulk rheological measurements was observed at these concentrations.

At higher PGM-type III concentrations (4% and 6%, w/v) (Figures 2-5 and 2-6), no significant increase was observed for G' at 1 rad/sec [0.08 ± 0.04 Pa (n=4) at 4% (w/v) PGM-type III to 0.15 ± 0.06 Pa (n=6) at 6% (w/v) PGM-type]. However, G" at 1 rad/sec gradually increased from 0.11 ± 0.04 Pa (n=4) at 4% (w/v) PGM-type III to 0.27 ± 0.09 Pa (n=6) at 6% (w/v) PGM-type III. This indicates that at a frequency of 1 rad/sec the mimetics behaved as a viscous solution, with a more liquid-like response where G" dominated G'. This same observation has been reported by Madsen *et al.*[83] who found that 15% (w/w) mucin solutions, prepared from the commercially available pig gastric mucin from Sigma, did not form a gel but instead gave viscous solutions where G" dominated G' when investigated at a frequency range of 0.63-15.9 rad/sec.

Based on the typical values of G' and G" of tracheal mucus reported in Chapter 1 (Table 1-1), the aim was to match the bulk viscoelastic properties of this mucus mimetic to that of native, non-diseased tracheal mucus with a value of G' ranges between 9-12 Pa and a value of G" between 1.5-3 Pa at 1 rad/sec. Therefore, it was obvious that even by increasing mucin concentration in the mucus mimetic formulations to a value of 6% (w/v), the typical values of bulk viscoelastic properties of native, non-diseased tracheal mucus could not be achieved. This observation was supported by a study of Kocevar and coworkers[16] who had found that even at concentrations of 60% (w/w) of porcine gastric mucin, values of bulk viscoelastic properties similar to natural mucus could not be attained, limiting the use of pig gastric mucin as an *in-vitro* model mucus system. The inability of PGM-type III to form a gel, where G' dominated G", may be related to the structural damage to the commercial mucin products that occurs during the isolation, purification and freeze drying processes of the commercial mucin preparation.[83]

2.3.3. Altering and Controlling the Bulk Viscoelastic Properties of Mucus Mimetic

The structural material responsible for the viscoelastic properties of tracheal mucus is the high molecular weight glycoproteins (mucins).[84] Natively, glycoproteins in the tracheal mucus are cross-linked by covalent bonds (disulfide bridges) and non-covalent bonds (hydrogen bonds, electrostatic interactions, and Van der Waals forces), giving mucus an extended gel network. In addition, other components such as albumin interact with glycoproteins and influence the rheological properties of mucus.[76]

In these studies, the bi-functional agent glutaraldehyde (GA) was used to induce cross-linking to the mucin chains. The strategy of using a cross-linking agent, particularly GA, has been used by other researchers to induce additional cross-linking to bovine cervical mucus, achieving large changes in the elasticity of mucus.[85] In addition, GA has been widely used for protein conjugation.[86] This strategy enables precise control over the viscoelastic properties of the mimetic via tailoring of GA concentration and/or cross-linking time.

2.3.3.1. Bulk Rheology of Mimetic as a Function of GA Concentration

The bulk viscoelastic properties of the mucus mimetic were controlled by altering the GA concentration added to the formulation. Figures 2-7 and 2-8 illustrate the frequency-dependence of G' and G", respectively, of mucus mimetic formulations cross-linked using various concentrations of GA solutions (5, 10, 15, 20, and 25%, w/w) for 3 days. Data showed that mimetics cross-linked using 5% (w/w) and 10% (w/w) GA solutions exhibited approximately equivalent values of G' and G". However, by increasing GA concentration from 15% (w/w) to 25% (w/w), both G' and G" increased with increasing GA concentration. For mimetics cross-linked using 5%, 10% and 15% (w/w) GA solutions, both G' and G" increased with increasing frequency. However, this

trend appears to be less significant at higher GA concentrations (20% and 25% w/w) where plateau regions (i.e. region where G' and G" are independent of frequency) was observed over a wide frequency range and extended from the lowest frequencies. This plateau region is typically seen in the rheological behavior of entangled polymer solutions and respiratory mucus [84] which indicates the formation of extremely stable and strongly cross-linked gel network.[16, 87]

2.3.3.2. Bulk Rheology of Mucus Mimetic as a Function of Cross-linking Time

The bulk viscoelastic properties of the mucus mimetic were controlled by varying the duration of GA cross-linking. Figures 2-9 and 2-10 illustrate the frequency-dependence of G' and G" of mucus mimetic formulations cross-linked for various cross-linking times (1, 3, 6 and 9 days). In Figure 2-9, G' of mucus mimetic cross-linked for only 1 day exhibited a plateau region over a frequency range of 0.5 up to 75 rad/sec. Beyond that frequency range, a reduction in G' was observed which suggests a break down in the cross-links of mimetic at high frequencies. On the other hand, G' of mucus mimetics cross-linked for 3, 6 and 9 days exhibited broad plateau regions, where G' were independent of frequency, over the entire frequency range (0.5-105 rad/sec). The appearance of the plateau regions suggests the formation of gel networks cross-linked using a high concentration of GA solution (25% w/w) for long cross-linking times (3, 6 and 9 days). G' of the cross-linked mucus mimetic increased with increasing the duration of the cross-linking process. However, it is noted that the G' values of mucus mimetics cross-linked for 6 and 9 days were approximately equivalent which indicates that the cross-linking was completed after 6 days.

Similar trends were observed for G" (Figure 2-10), where G" increased with increasing the duration of the cross-linking process at 1, 3 and 6 days and G" values of mucus mimetics cross-linked for 6 and 9 days were approximately equivalent.

It is observed that G’ is larger than G” at all frequencies. This effect of GA on the rheological properties of mucus was reported earlier by Gelman and Meyer[85] who found that GA increases the elasticity of bovine cervical mucus, but has relatively little effect on mucus viscosity. The researchers indicated that this increase in mucus elasticity was due to the formation of additional intermolecular links by the cross-linking agent GA via the ε -amino groups on the protein moiety of the glycoprotein chains, probably by the formation of covalent bonds (Schiff bases) between the amino groups of mucin chains and the aldehyde groups of GA.

2.3.4. Classification of Mucus Mimetics According to Bulk Viscoelastic Properties

Mucus mimetic formulations were classified into 3 categories based on the values of the bulk viscous and elastic moduli (G’ and G”). Mucus mimetic 1 exhibited extremely low bulk viscoelastic properties at low frequency (G'=0.3 and G"=0.4 Pa at 1 rad/sec) and relatively high bulk viscoelastic properties at high frequency (G'=20.7 and G'=9.8 at 100 rad/sec). The high frequency values matched that of native mucus, though the low frequency values were significantly lower than all reported values for native mucus (Table 2-5). Therefore, mimetic 1 was chosen to represent native mucus during respiratory maneuvers that produce high shear, such as coughing. Mucus mimetic 2 exhibited G’ and G” values at 1 rad/sec within the range of minimum reported values for native mucus (G'=10.7 and G"=2.4 Pa), but lower G' and G" values at 100 rad/sec due to network breakdown at high shear (G'=6.7 and G"=7.5 Pa). Mimetic 2 was chosen to mimic average bulk viscoelastic conditions of mucus from healthy individuals during respiratory maneuvers that produce low shear, such as normal breathing. Mucus mimetic 3 exhibited higher G' and G" values at 1 rad/sec than the other two mimetics (G'=19.1 and G"=3.5 Pa). However, mimetic 3 exhibited lower G' and G" at 100 rad/sec (G'=8.8 and G"=5.2) due to network breakdown, similar to that observed for mimetic 2. Mimetic

3 mimics mucus with relatively high bulk viscoelastic properties during low shear maneuvers. None of the mimetics were able to achieve values of G' and G" at 1 rad/sec that matched the high end of reported values for native mucus (25.2-33.5 Pa; Table 2-5), even at high GA concentration. The three mimetics were obtained by tailoring GA cross-linking process (i.e. altering GA concentration and/or duration of GA cross-linking). Mimetics 1, 2 and 3 were cross-linked with 0.5 ml-15% (w/w) GA solution and mixed for 24 hours, 0.5 ml-25% (w/w) GA solution and mixed for 3 days, and 1.0 ml-50% (w/w) GA solution and mixed for 3 days, respectively.

Mucus mimetic 1 was chosen for further the surface rheological studies and bioaerosol formation, since it exhibited low bulk viscoelastic properties and more liquid-like behavior at low frequency (1 rad/sec), which enabled surfactant spreading onto the surface, and exhibited properties that matched native tracheal mucus at high frequency (100 rad/sec), which matched properties during high shear event such as coughing.

2.3.5. Linear Viscoelastic Region of Mucus Mimetics

To ensure that the observed viscoelastic behavior of a material is only related to its molecular structure and not to applied stress, rheological measurements should be conducted in regions where the viscoelastic shear modulus is independent of strain, the linear viscoelastic region (LVR). Within LVR, the material response is independent of the magnitude of the deformation and the material structure is maintained intact. In the dynamic oscillation test, the levels of applied strain are increased at a constant frequency. The point at which the viscoelastic modulus (either G’ or G”) deviates by more than 10% from a constant (plateau) value indicates departure from LVR and is known as the critical strain.

Figure 2-11 illustrates the oscillation strain sweep study of the mucus mimetic 1 conducted over a range of 0.03 to 1.1 and at fixed frequency of 2 rad/sec. The LVR for the mucus mimetic occurred over a strain range of 0.03 to 0.12 where the observed

viscoelastic properties were independent of the applied strain. Beyond a critical strain of 0.12, G' and G" strongly decreased with deformation and the network was disrupted. Figure 2-12 illustrates the oscillation strain sweep study of mucus mimetic 2 conducted over a range of 0.01 to 1.1 and at fixed frequency of 2 rad/sec. The LVR for the mucus mimetic 2 occurred over a strain range of 0.01 to 1.1. The LVR for the mucus mimetic 2 extended over a longer range and exhibited a higher critical strain value compared to that of mucus mimetic 1. This observation is related to the mucus mimetic 2 forming a significantly stronger cross-linked network.[88] Figure 2-13 illustrates the oscillation strain sweep study of mucus mimetic 3 conducted over a range of 0.01 to 1.1 and at fixed frequency of 2 rad/sec. The LVR for the mucus mimetic 3 occurred over a strain range of 0.025 to 0.4 where G' and G" were independent of the applied strain. The mucus mimetic 3 exhibited longer range and higher critical strain value compared to that of mucus mimetic 1. Again, this is attributed to the mucus mimetic 3 forming a stronger cross-linked network. Based on these tests, a value of an applied strain of 0.1 was chosen and used in subsequent frequency-dependent experiments.

2.3.6. Frequency-Dependence of Bulk Viscoelastic Properties of Mucus Mimetic

Figure 2-14 represents the frequency-dependence of G' and G" of the mucus mimetic 1, cross-linked using 0.5 ml-15% (w/w) GA solution for 24 hours over a frequency range of 0.5-105 rad/sec. Both moduli increased with increasing frequency, indicating that G' and G" were frequency-dependent over this region. The mucus mimetic exhibited G'=0.3 ± 0.08 Pa and G"=0.38 ± 0.10 Pa (n=13) at 1 rad/sec. Three distinct regions in bulk rheological behavior were observed. At low frequencies (0.5-10 rad/sec), G" was slightly higher than G' which indicates that mimetic exhibited more viscous behavior. In region II, at a frequency range (10-50 rad/sec), values of G' and G" were approximately equivalent. In region III, at high frequencies (50-105 rad/sec),

mimetic exhibited elastic behavior where G' dominated G". The bulk rheological behavior observed for the mucus mimetic is typical for a temporary network where the structure is partially cross-linked or entangled and thus cannot reach the plateau region.

The mucus mimetic 2, cross-linked using 0.5 ml-25% (w/w) GA solution for 3 days, exhibited G'=10.68 ± 1.30 Pa (n=6) and G"=2.34 ± 0.14 Pa (n=6), at 1 rad/sec (Figure 2-15). Investigating the bulk rheological behavior of the mucus mimetic indicates that G' exhibited a broad plateau region extended out from the lowest frequencies up to higher frequencies (0.5-70 rad/sec). This indicates that the mucus mimetic exhibited a cross-linked gel network over this frequency range. However, beyond a frequency of 70 rad/sec, G' decreased with increasing frequency, which may suggest that the fully entangled network started to fall apart at high frequencies.

The mucus mimetic 3 cross-linked with 1.0 ml-50% (w/w) GA solution for 3 days exhibited G'=19.08 ± 2.59 Pa (n=5) and G"=3.54 ± 0.30 Pa (n=5), at 1 rad/sec (Figure 2-16). G' exhibited a broader plateau region which extends over a larger frequency range (0.5-80 rad/sec) compared to that observed in the mucus mimetic 2 (0.5-70 rad/sec), which indicates that the gel network of the mucus mimetic 3 was more cross-linked compared to that of the mucus mimetic 2. Beyond a frequency of 80 rad/sec, G' decreased as a function of frequency which suggests that the gel network started to fall apart at high frequencies. Table 2-6 summarizes the bulk viscoelastic properties of the three mimetics at frequencies of 1 rad/sec and 100 rad/sec.

2.3.7. Reformulation of Mucus Mimetic

Although GA was able to enhance the bulk viscoelastic properties of the *in-vitro* model mucus mimetic by introducing cross-links to mimetic throughout the study, a large variability and inconsistency in mimetic bulk viscoelastic properties was observed between mucin lots. Therefore, the *in-vitro* model mucus mimetic was reformulated to limit the observed variability.

An alteration in the bulk rheological properties of the *in-vitro* model mucus mimetic was observed (i.e. a more liquid-like property was visually noted for the mucus mimetic 1) while conducting bioaerosol studies. This change can be seen in Figures 2-17A and 2-17B, which compare the bulk viscoelastic properties of two separate mucus mimetics cross-linked using 0.5 ml-15% GA solution. G' values for the two mimetics were statistically the same. However, a variation in the G" values between the two mimetics was observed, where the typical mucus mimetic exhibited higher G" values compared to the cross-linked *in-vitro* model mucus mimetic particularly at a frequency range of 4 to 30 rad/sec.

Potential reasons for this alteration were considered, including the type of GA used for cross-linking, components of mucus mimetic and mucus mimetic method of preparation. Therefore, the effect of each factor on the bulk viscoelastic properties of the mucus mimetic were investigated, including: 1) GA concentration, 2) materials involved in altering viscoelastic properties to mucus mimetic [PGM-type III and albumin], 3) GA type, 4) preparation method and 5) cross-linking process of *in-vitro* model mucus mimetic.

Initially, to investigate the effect of GA concentration on the cross-linking process, a high concentration of GA solution (50% w/w) was used. The high concentration of GA solution was expected to increase the bulk viscoelastic properties of the mucus mimetic. Figure 2-18 illustrates the frequency-dependence of G' and G" for the mucus mimetic cross-linked using 0.5 ml-50% (w/w) GA solution for 24 hours. Both G' and G" exhibited lower values compared to the mucus mimetics 2 and 3 cross-linked using high concentrations of GA solutions (25% and 50% w/w). This suggests that cross-linking within the mucus mimetic was hindered even at high GA concentration.

To investigate the effect of albumin on altering the bulk viscoelastic properties of mucus mimetic by GA cross-linking, a mucin solution containing 4% (w/v) PGM-type III only (cross-linked PGM) [i.e. no albumin was added to the formulation] was prepared

and cross-linked using 0.5 ml-25% (w/w) GA solution for 3 days. Figure 2-19 represents the frequency-dependence of G' and G" for this formulation, where G' and G" at 1 rad/sec exhibited values of 0.12 ± 0.01 Pa and 0.27 ± 0.03 Pa (n=5), respectively. However, when the mucus mimetic composed of 4% (w/v) PGM-type III and 1% (w/v) albumin was cross-linked using 0.5 ml-25% (w/w) GA solution for 3 days, a mucus mimetic of bulk viscoelastic properties similar to that of mucus mimetic 2, which exhibited G' of 10.68 ± 1.30 Pa and 6.70 ± 2.71 Pa at 1 and 100 rad/sec, and G" of 2.34 ± 0.14 Pa and 7.5 ± 1.95 Pa at 1 and 100 rad/sec, was obtained (Figure 2-15). In addition, G' dominated G", indicating a more elastic mimetic. However, the cross-linked PGM (Figure 2-19) exhibited lower frequency-dependence values of G' and G" compared to that of mucus mimetic 2. The significant increase in the bulk viscoelastic properties of mucus mimetic containing 1% albumin, suggested that albumin contributes in the cross-linking process via GA. Albumin is a lysine rich molecule.[89] The ε-amino groups in the lysine residues are the most reactive end group of the amino acids with GA.[90] Lysine residues in albumin are exposed on the surface because of the polarity of the amine group and thus are more accessible to GA. Therefore, the ε-amino groups likely react with GA forming covalent and irreversible cross-linking. The formation of these cross-links leads to an increase in elasticity, where bulk shear storage modulus G' is proportional to the number of cross-links.

To investigate the effect of albumin concentration on the cross-linking process of the mucus mimetic, mucus mimetic formulation of varying albumin concentrations (0%, 1%, 1.25% or 1.5% w/v) were prepared. It was expected that increasing albumin concentration will enhance the bulk viscoelastic properties of the cross-linked mucus mimetic. Figures 2-20A and 2-20B represent the frequency-dependence of G' and G" for mucus mimetics containing 0%, 1%, 1.25% or 1.5% (w/v) albumin. Table 2-7 illustrates G' and G" at 1 rad/sec for the mucus mimetic formulations. Both G' and G" increased with increasing albumin concentration. However, G' and G" values of the mucus mimetic

formulation containing 1% (w/v) albumin were lower than those reported for the typical mucus mimetic, which contains 1% (w/v) albumin (Table 2-6), suggesting that albumin was not significantly cross-linked by GA solution.

Commercially available GA may contain GA polymers as impurities, which can affect the cross-linking process. A purified GA has a purification index (PI) of <0.5 (Sigma, product information sheet). PI is defined as A_{235}/ A_{280}, where A_{235} is the UV absorbance at 235 nm assigned for □-□ * for C=C bond ofα-β-unsaturated aldehydic oligomers (impurity), and A_{280} is the UV absorbance at 280 nm assigned for n-□ * for C=O of the aldehyde group in pure monomeric GA. To determine whether the purity of GA significantly impacted the cross-linking process of the mucus mimetics, two types of GA were investigated: GA with PI of 2.54 and 0.30. Figures 2-21A and 2-21B illustrate the frequency-dependence of G' and G" of mucus mimetic cross-linked for 24 hours using 0.5 ml-15% (w/w) of GA solution of the two purification indexes 0.30 and 2.54. Both mimetics exhibited equivalent rheological properties. Although higher values of G' and G" were expected for mimetic cross-linked using the more purified GA (PI=0.3), it has been shown that GA polymerization is also important in bridging larger gaps between two reaction sites[91] and consequently enhancing elasticity. Therefore, even with the use of the more purified GA, the cross-linking process of the mucus mimetic was not taking place.

Finally, the method of mucus mimetic preparation was altered to determine its impact on the cross-linking process. Therefore, mucus mimetic was prepared by mixing the mimetic components for 24 hrs, and then mix GA solution manually for 5 min. The cross-linking process was taken place at room temperature (~ 23°C). Specifically, the effects of longer mixing time and higher temperature were investigated. Longer mixing times may enhance the physical entanglement between mucins and albumin, thereby decreasing the ability of the molecules to rearrange during cross-linking and limiting the ability of the endgroups to meet and react. Longer mixing time for GA solution may

enhance intra-molecular cross-linking, thereby limiting the number of endgroups available for cross-linking. Finally, a higher cross-linking temperature should speed up the reaction time and may enhance GA cross-linking.[92] Therefore, mimetic was prepared using the following modifications: ingredients were mixed for 24 hours instead of 7 days. GA was mixed manually for 5 minutes rather than for 24 hours using a tube rotator and the cross-linking process took place at room temperature (~ 22°C) rather than at 4°C. Figures 2-22 illustrates the frequency-dependence of G' and G" for mucus mimetic, prepared using the modified method mentioned above. Both G' and G" achieve higher values compared to those reported in Figure 2-18. These results demonstrated that by: 1) reducing the mixing time of the mimetic components, 2) decreasing the mixing of GA solution, and 3) increasing the cross-linking temperature, the mucus mimetic was cross-linked. High values of G' and G" were obtained. This modified method can be used as an alternative method for mimetic preparation, if the GA cross-linking process of mucus mimetic cannot be obtained at 4°C. This method was used in further bioaerosol study.

2.3.8. Investigating the Mechanism of Mucus Mimetic Cross-linking Using GA

The FT-IR method has been widely used to investigate the GA cross-linking mechanism of proteins, such as albumin [93] and gelatin,[94] polyaminosaccharides such as, hyaluronic acid (HA) [95] and chitosan,[96] and glycoproteins, such as pig gastric mucins.[97] In these studies, FT-IR spectroscopy was conducted before and after the cross-linking reaction to investigate the structural modifications in molecules and to detect the new chemical bonds formed during the cross-linking reaction.

The mucus mimetic is composed of two main components, PGM-type III and albumin, which can be involved in the cross-linking process. PGM-type III is a large macromolecule of polysaccharides O-glycosidically bonded to a protein core[98] and albumin is a globular protein composed of 604 peptide units.[99]

Figure 2-23A shows the FT-IR spectrum of native albumin. The characteristic peaks of albumin appeared at 3308 cm^{-1} corresponding to O-H and N-H stretching (stretching vibrations of H atoms covalently bound to O and N atoms and at the same time hydrogen bonded to other atoms), and 2959 cm^{-1} corresponding to C-H stretching. The strong peaks at 1656 and 1540 cm^{-1} are attributed to amides I and II, where amide I corresponding to C=O stretching vibrations and amide II corresponding to C-N stretching coupled with N-H bending vibrations. The spectrum of native albumin (Figure 2-23A) agrees with that reported by Feng *et al.*[100] for equivalent material. In the cross-linking of albumin with 50% (w/w) GA solution (Figure 2-23B), it is expected that the most important interaction between albumin and GA is the one formed by the imine groups (Figure 2-24).[97] GA reacts rapidly with the amine groups at around neutral pH, where unprotonated amine groups of lysine and hydroxylysine residues are very reactive nucleophiles.[89, 101] The imine group (C=N) in IR spectroscopy appears at a peak of variable intensity in the range of 1640-1690 cm^{-1}.[102] This peak was hidden by the strong peak observed at 1654 cm^{-1} which corresponds to the C=O stretching of amide groups and therefore was difficult to evaluate.

In the spectrum of native PGM-type III (Figure 2-25A), the following peaks were observed: peak at 3390 cm^{-1} corresponds to the O-H stretching of primary and secondary aliphatic alcohol, and the N-H stretching of the amine groups; peak at 2921 cm^{-1} corresponds to C-H stretching of aliphatic bonds; peak at 1654 cm^{-1} corresponds to C=O stretching of amide groups; peak at 1549 cm^{-1} corresponds to C-N stretching coupled with N-H bending vibrations of amide groups; and peak at 1049 cm^{-1} corresponds to C-O stretching of primary and secondary alcohols. The spectra of native PGM-type III (Figure 2-25A) agree with those that were reported by Capra *et al.*[97] for equivalent material. Figure 2-25B shows FT-IR spectrum of PGM-type III cross-linked using 50% (w/w) GA solution. In the cross-linking reaction of PGM-type III with GA, it is expected that the most important interaction between PGM-type III and GA is the one formed by the imine

groups of the mucin chains (Figure 2-24).[97] The imine group (C=N) in IR spectroscopy appears at a peak of variable intensity in the range of 1640-1690 cm^{-1}.[102] This peak was hidden by the strong peak observed at 1654 cm^{-1} which corresponds to the C=O stretching of amide groups and therefore was difficult to evaluate.

FT-IR spectroscopy was used to investigate the structural changes of mucus mimetic cross-linked with 50% (w/w) GA solution. The cross-linked mucus mimetic was then reduced and the molecular structure of the two mimetics was compared, the imine bonds in the reduced mimetic should not appear in the FT-IR spectra. Figures 2-26A, 2-26B and 2-26C illustrate the FT-IR spectra of the uncross-linked mucus mimetic, mucus mimetic cross-linked with 50% (w/w) GA solution for 24 hours, and mucus mimetic cross-linked with 50% (w/w) GA solution and then reduced using 1.2 mg/ml of $NaBH_4$ in phosphate buffer (15 mM NaH_2PO_4/Na_2HPO_4, pH 7.4), respectively. No appreciable spectroscopic differences were observed in the FT-IR spectra between uncross-linked mucus mimetic and cross-linked mucus mimetic, where the imine group band in the range of 1640-1690 cm^{-1} was not detected. This is because the peak of C=O stretching of amide groups of native albumin and native PGM-type III appear at the same position of the imine group band. In addition, no change was seen in the FT-IR spectra between the cross-linked mucus mimetic, and cross-linked and then reduced mucus mimetic. This is because the imine group was not observed in the FT-IR spectrum of the cross-linked mimetic. Therefore, FT-IR spectroscopy was unable to distinctly identify the new bonds formed during the cross-linking process of mucus mimetic by GA.

The inability of FT-IR spectroscopy to identify new bonds after GA cross-linking has been reported by Tomihata *et al.*,[95] where FT-IR spectroscopy was performed on uncross-linked hyaluronic acid (HA) films and HA films cross-linked with GA. It has been shown that no difference was seen in the FT-IR spectra between the uncross-linked and cross-linked HA films. This observation was attributed to the resemblance of the chemical structure of HA molecule to those of the acetals formed between the hydroxyl

groups of HA and the aldehyde groups of GA at acidic pH. On the other hand, FT-IR spectroscopy was used to investigate the structural changes of chitosan-glycine beads, which can be used for controlled released drug delivery systems, cross-linked with GA.[96] A significant new peak at 1631 cm^{-1} was detected in the cross-linked chitosan-glycine beads' spectra which corresponds to the imine groups (C=N) as a result of the Schiff base reaction between the amine groups in chitosan and aldehydic groups in GA.

Proton (^{1}H)-NMR could be used as an alternative method to investigate the mechanism of mucus mimetic cross-linking using GA, where the imine proton peak increases and the aldehyde single peak decreases gradually.[103] One complication to this approach may be that application of NMR for macromolecules larger than 20 kDa can be hampered by poor resolution.[104]

2.3.9. Surface Tension of Mucin Solution

The surface tension of uncross-linked mucus [composed of 4% (w/v) PGM-type III, 1% (w/v) ions, 1% (w/v) albumin, 1% (w/v) DPPC (dispersed in the bulk), and 94 ml water] obtained using the Wilhelmy plate balance was 49.45 ± 3.54 mN/m (n=4). This surface tension was significantly higher than the surface tension at the air-mucus interface of the large conducting airways (~ 32 mN/m). Therefore, to achieve a surface tension of ~ 32 mN/m, studies were conducted to test DPPC spreading onto the air-mimetic interface. Adding a higher quantity of DPPC to the bulk cannot achieve lowering in the surface tension, since it would be difficult for DPPC molecule to partition to the mimetic surface due to its viscous properties.

2.3.9.1. Spreading Solvent for Surfactant DPPC

The surface activity of the spreading solvent (n-hexane:methanol 95:5 v/v) at the air-water interface was determined by a series of experiments (Table 2-2). In the first experiment, the surface tension of the air-water interface before and after spreading (n-hexane:methanol 95:5 v/v) was determined (Table 2-8). The surface tension of the clean

air-water interface was 71.80 ± 0.32 mN/m (n=6). After the addition of spreading solvent to the air-water interface, the surface tension of the interface showed no significant change (71.90 ± 0.32 mN/m, n=6) ($p>0.05$). Therefore, the spreading solvent exhibited no surface activity.

In the second experiment, the surface activity of the spreading solvent (n-hexane:methanol 95:5 v/v) was determined during compression-expansion cycles on water subphase. It was important to study the surface activity of the spreading solvent during the compression-expansion cycles because the surface pressure-surface area isotherm for mucus mimetic covered with DPCP was studied (Chapter 3). Table 2-9 illustrates $\gamma_{subphase}$ (the surface tension of the clean air-liquid interface), γ^* (initial surface tension of the air-water interface after the addition of the spreading solvent and before initiating the compression-expansion cycles), and γ_{min} and γ_{max} (the minimum and maximum surface tensions of the air-water interface with the spreading solvent for each compression-expansion cycle). No significant difference was observed between $\gamma_{subphase}$ and γ^* ($p>0.05$). Furthermore, the air-liquid interface with the spreading solvent exhibited no change in γ_{min} and γ_{max} compared to $\gamma_{subphase}$ during the three compression-expansion cycles, ($p>0.05$). Figure 2-27 represents the surface pressure-surface area isotherm of the compression-expansion cycles conducted on the air-water interface with the spreading solvent for one of the three experiments reported in Table 2-9. Maximum surface pressure did not exceed 0.4 mN/m upon compression during the three cycles, indicating that the spreading solvent is not surface active.

Orbulescu *et al.*[105] have shown that spreading solvents such as chloroform, toluene, and benzene were not significantly surface active, when the maximum changes in surface pressure upon the compression of the pure solvent spread on the water subphase at 20 ± 0.5°C were less than 0.5 mN/m. Our data were in good agreement with Orbulescu *et al.*, where maximum changes in surface pressure upon the compression of

the spreading solvent (n-hexane:methanol 95:5 v/v) on the air-liquid interface were less than 0.4 mN/m.

To ensure that the spreading solvent n-hexane:methanol (95:5 v/v) has the ability to efficiently spread DPPC at the air-liquid interface, γ_{min} and γ_{max} were measured during three compression-expansion cycles. Table 2-10 summarizes the surface properties of the air-liquid interface before and after the addition of DPPC. A surface area reduction of ~ 33.0% of the interface was able to achieve γ_{min} of 1.82 ± 0.60 mN/m, upon compression during the third cycle. However, lower γ_{min} values were achieved upon compression during the first and second cycles, 0.7 ± 0.0 and 1.21 ± 0.29 mN/m, respectively. These results were in good agreement with Yu *et al.*[78] who performed six successive cycles of compression-expansion of DPPC monolayer spread onto an air-liquid interface using a similar subphase (150 mM NaCl and 1.5 mM $CaCl_2$ in water). They found that a 33.3% reduction in interface surface area at 37°C was able to lower the surface tension from ~ 30 mN/m (initial surface tension) to ~ 3 mN/m.

2.3.9.2. Altering the Surface Tension of Mucus Mimetics

Spreading of surfactant droplets onto viscoelastic surfaces is a dynamic process that is driven by the Marangoni effect, a convective flow that pushes surfactant from areas of high surfactant concentration (low surface tension) to area of low surfactant concentration (high surface tension).[46] The surface tension of the mucus mimetic before spreading DPPC, measured using the Wilhelmy plate balance, was 53.25 ± 1.22 mN/m (n=9) (Table 2-11). This surface tension is in good agreement with the reported surface tension of bovine mucin solutions, proteins, and polysaccharides (which all have surface tensions between 45 and 60 mN/m).[29, 106] The surface tension of the mucus mimetic was lowered to 30.16 ± 2.38 (n=4) by spreading DPPC solution (0.17%, w/v) onto the air-mimetic interface (Table 2-11). For the typical mucus mimetic, we observed good

spreading of the surfactant over the entire interface via fluorescence microscopy which will be discussed in detail in Chapter 3.

The surface tension of the typical mucus mimetic was also evaluated using the detachment method using du Noüy ring. The du Noüy ring method has been used in previous studies to measure the surface tension of native mucus samples obtained from CF patients.[107,108] As shown in Table 2-11, the du Noüy ring method gave higher surface tension values for the mucus mimetic before and after spreading DPPC compared to those obtained by the Wilhelmy plate balance, 56.36 ± 0.37 mN/m and 48.23 mN/m, respectively. This may be related to the fact that the detachment of the du Noüy ring was not consistent. In addition, a disruption may occur in the DPPC monolayer during ring detachment leading to inaccurate surface tension measurements.

In the du Noüy ring method, a basic surface tension (γ_{basic}) is measured, where $\gamma_{basic} = F/(4\pi \cdot R)$,[79] where F is the detachment force for the meniscus and $4\pi \cdot R$ is the periphery of the surface detached. However, an empirical correction factor (*f*) is applied for surface tension determination using du Noüy ring, which accounts for the fact that the film slips on the surface of the ring prior to detaching. This factor depends on two dimensionless ratios (R^3/V and R/r), where R is radius of the ring, r is the radius of the ring wire, and V is the volume of the meniscus. Therefore, the corrected surface tension is $\gamma_{corrected} = \gamma_{basic} \cdot f$.[79] The correction factor (*f*) was developed based on Newtonian liquids such as water, glycerol and other liquids.[109] Therefore, the surface tension measurements were likely less reliable as the mucus mimetic samples were non-Newtonian.

To further investigate the applicability of the two methods (Wilhelmy plate balance and du Noüy ring), the surface tension of an air-water interface before and after the addition of DPPC were measured. DPPC [11 µL of 1 mg/ml in hexane:methanol (95:5 v/v)] was spread at an air-water interface to get an equilibrium surface tension of ~ 33 mN/m with an area of coverage of 30 $Å^2$/molecule. The surface tension measurements

of DPPC spread at an air-water interface measured using the du Noüy ring were higher than those measured with the Wilhelmy plate balance (51.57 ± 1.41 mN/m and 33.72 ± 1.08 mN/m, respectively, Table 2-12).

The surface tension for the mucus mimetics 2 and 3 was difficult to measure using the Wilhelmy plate balance due to their high elastic (gel-like) property (both mucus mimetics 2 and 3 exhibited substantial high G' values). Therefore, the du Noüy ring method was explored to determine the surface tension of these complex and highly cross-linked systems. The surface tensions of the mimetics 2 and 3, measured using the du Noüy ring method, were 76.83 ± 5.83 mN/m (n=3) and 95.04 ± 7.78 mN/m (n=3), respectively (Table 2-13). These high surface tension values for the mucus mimetics may be due to a high force of separation required to remove the ring from the mimetic surface. This method has been previously used by Deneuville *et al.*[107] and Albers *et al.*[108] to measure the surface tension of cystic fibrotic mucus where surface tension values of 80.9 ± 23.6 mN/m (n=27) and 81.1 ± 14.4 mN/m (n=18) were reported. The surface tension values of mimetics 2 and 3 were in good agreement with those of CF mucus. The surface tension of the mimetics 2 and 3, and CF mucus were relatively close to each other, as both exhibited high bulk viscoelastic properties, however, these extremely high surface tension values are still questionable.

2.4. Conclusions

A more physiologically relevant *in-vitro* model mimetic of tracheal mucus was developed by matching the chemical composition, and the key physical properties (bulk viscoelasticity and surface tension) of the mimetic to that of native tracheal mucus. A series of mucus mimetic formulations (mimetics 1, 2 and 3), of different bulk viscoelastic properties, were developed via tailoring of the GA concentration and/or cross-linking time. The wide range of the bulk viscoelastic properties of the three mimetics provide an insight on the rheological behavior of the tracheal mucus during normal breathing (i.e. of

low frequency behavior) and cough maneuver (of high frequency behavior). Matching the surface tension at the air-mimetic interface was of critical important to study the surface rheological behavior of the large conducting airways, thereby understanding the mechanism of bioaerosol formation. Therefore, mucus mimetic 1 which exhibited more liquid-like behavior at low frequencies and more solid-like behavior at high frequencies, was used in the further surface rheological studies and bioaerosol formation.

Table 2-1: Chemical composition of mucin solutions (2%, 3%, 4% and 6%, w/v).

Mucin solutions (w/v)	**PGM-type III (g)**	**Albumin (g)**	**DPPC (g)**	**Buffer containing 1% ionic salts (ml)**
2%	0.6	0.3	0.3	28.8
3%	0.9	0.3	0.3	28.5
4%	1.2	0.3	0.3	28.2
6%	1.6	0.3	0.3	27.6

Table 2-2: Description of the three control experiments for the spreading solvent (n-hexane:methanol 95:5)

Control experiment	**Description of the experiment**
1	Surface activity of the spreading solvent (n-hexane:methanol 95:5 v/v) at the air-liquid interface with no compression-expansion cycles.
2	Surface activity of the spreading solvent (n-hexane:methanol 95:5 v/v) at the air-liquid interface during three compression-expansion cycles.
3	Three compression expansion cycles for DPPC at an air-liquid interface using the spreading solvent (n-hexane:methanol 95:5 v/v).

Table 2-3**:** Comparison between the chemical composition of the *in-vitro* model mucus mimetic and native tracheal mucus.

***In-Vitro* Model Mucus Mimetic**	**Native Tracheal Mucus**
1% (w/v) bovine serum albumin	0.7-1.3% (w/w) proteins[12 ,76, 110]
4% (w/v) PGM-type III	1-5% (w/w) glycoproteins[12 ,76, 110]
0.17% (w/v) DPPC (on surface)	0.5-1.1% (w/w) lipids[12, 13 ,76, 110]
1% (w/v) ions in buffer: 154 mM Na^{+}, 3 mM Ca^{+2}, 30 mM P^{+5} and 160 mM Cl^{-})	0.70-1.4% (w/w) ionic salts[12]
94 ml water	93-97% (w/w) water[12 ,76, 110]

Table 2-4: Average bulk viscoelastic properties at 1 rad/sec and 100 rad/sec for mucin solutions containing 2%, 3%, 4% and 6% (w/v) PGM-type III.

	Mucin Solution			
Bulk viscoelastic property	**2% (w/v)**	**3% (w/v)**	**4% (w/v)**	**6% (w/v)**
G’ (1 rad/sec) Pa	0.1	0.1	0.1	0.2
G” (1 rad/sec) Pa	0.1	0.3	0.1	0.3
G’ (100 rad/sec) Pa	18.9	20.3	15.3	11.4
G” (100 rad/sec) Pa	13.4	29.7	11.9	10.2
tan δ (1rad/sec)	0.9	3.6	1.4	1.8
δ (1 rad/sec)	42.3°	74.6°	54.0°	61.0°
tan δ (100 rad/sec)	0.7	1.5	0.8	0.9
δ (100 rad/sec)	35.4°	55.7°	37.8°	41.7°
G* (1 rad/sec) Pa	0.2	0.3	0.1	0.3
G* (100 rad/sec) Pa	23.1	36.0	19.4	15.3

Table 2-5: Range of minimum and maximum reported bulk rheological properties of native tracheal mucus[22-25] at 1 rad/sec and 100 rad/sec.

Bulk rheological property	**Minimum reported value**	**Maximum reported value**
G’ (1 rad/sec)	4.5-11.1, average 7.8 Pa	25.2-33.5, average 29.3 Pa
G” (1 rad/sec)	0.9-3.2, average 2.0 Pa	8.7-11.6, average 10.1 Pa
G’ (100 rad/sec)	10.2-22.6, average 16.4 Pa	47.3-52.3, average 49.8 Pa
G” (100 rad/sec)	5.3-19.2, average 12.2 Pa	46.3-64.2, average 55.2Pa
tan δ (1rad/sec)	0.2-0.3, average 0.3	0.4
δ (1 rad/sec)	11.3°-16.2°, average 13.7°	19.3°
tan δ (100 rad/sec)	0.5-0.9, average 0.7	1.0-1.2, average 1.1
δ (100 rad/sec)	27.5°-40.4°, average 34.6°	44.4°-50.9°, average 47.7°
G* (1 rad/sec)	4.5-11.6, average 8.1 Pa	26.6-35.5, average 31.1 Pa
G* (100 rad/sec)	11.5-29.7, average 20.6 Pa	66.2-82.8, average 74.4 Pa

Table 2-6: Bulk viscoelastic properties of the three mucus mimetics at frequencies of 1 rad/sec and 100 rad/sec. Data are represented as the mean ± SD.

***In-vitro* model mucus mimetic**	**G' at 1 rad/sec (Pa)**	**G" at 1 rad/sec (Pa)**	**G' at 100 rad/sec (Pa)**	**G" at 100 rad/sec (Pa)**
Mucus mimetic 1 (n=11)	0.3 ± 0.1	0.4 ± 0.1	20.7 ± 5.9	9.8 ± 2.0
Mucus mimetic 2 (n=6)	10.7 ± 1.3	2.4 ± 0.1	6.7 ± 2.7	7.5 ± 2.0
Mucus mimetic 3 (n=5)	19.1 ± 2.6	3.5 ± 0.3	8.8 ± 0.9	5.2 ± 0.9

Table 2-7: The bulk shear storage modulus G' and bulk shear loss modulus G" for mucus mimetic formulations, at 1 rad/sec, composed of 4% (w/v) PGM-type III and different concentrations of albumin (0%, 1%, 1.25% and 1.5%, w/v), cross-linked with 0.5 ml-15% (w/w) GA for 24 hours; data are represented as the mean ± SD (n=3).

Albumin bovine concentration (w/v)	**G' (1 rad/sec) Pa**	**G" (1 rad/sec) Pa**
0% albumin	0.0 ± 0.0	0.0 ± 0.0
1% albumin	0.2 ± 0.1	0.2 ± 0.1
1.25% albumin	0.2 ± 0.0	0.3 ± 0.0
1.5% albumin	0.3 ± 0.0	0.3 ± 0.0

Table 2-8: Surface activity of the spreading solvent (n-hexane:methanol 95:5) at the air-water interface without compression-expansion cycles; data are represented as the mean ± SD (n=6).

Air-liquid interface	**Surface tension (mN/m)**
Air-liquid interface before spreading (n-hexane:methanol 95:5 v/v)	71.8 ± 0.3
Air-liquid interface after spreading(n-hexane:methanol 95:5 v/v)	71.9 ± 0.3

Table 2-9: Minimum and maximum surface tensions monitored during the three successive compression-expansion cycles of the spreading solvent (n-hexane:methanol 95:5 v/v) at the air-liquid interface.

Run #	**$\gamma_{Subphase}$ (mN/m)**	**γ^* (mN/m)**	**Cycle 1 γ (mN/m)**	**Cycle 2 γ (mN/m)**	**Cycle 3 γ (mN/m)**
1	71.7	71.9	‡γ_{min} 71.7 †γ_{max} 71.9	γ_{min} 71.6 γ_{max} 71.9	γ_{min} 71.56 γ_{max} 71.92
2	71.3	71.7	γ_{min} 71.7 γ_{max} 71.8	γ_{min} 71.7 γ_{max} 71.9	γ_{min} 71.80 γ_{max} 71.91
3	71.9	72.0	γ_{min} 71.9 γ_{max} 72.0	γ_{min} 71.9 γ_{max} 72.0	γ_{min} 71.87 γ_{max} 72.00
Mean± SD	71.6±0.3	71.9 0.1	γ_{min} 71.8±0.1 γ_{max} 71.9±0.1	γ_{min} 71.7 ± 0.1 γ_{max} 71.9 ± 0.1	γ_{min} 71.7 ± 0.2 γ_{max} 71.9 ± 0.1

γ^* is the initial surface tension at the air-liquid interface after the addition of the spreading solvent and allowing 10 minutes for spreading solvent to evaporate.

‡γ_{min} is the minimum surface tension monitored upon compression.

†γ_{max} is the maximum surface tension monitored upon expansion.

Table 2-10: Minimum and maximum surface tensions monitored during the three successive compression-expansion cycles of DPPC spread at the air-liquid interface using the spreading solvent (n-hexane:methanol 95:5 v/v).

Run #	**$\gamma_{Subphase}$ (mN/m)**	**Volume (µL)**	**γ^* (mN/m)**	**Cycle 1 γ (mN/m)**	**Cycle 2 γ (mN/m)**	**Cycle 3 γ (mN/m)**
1	72.4	187	31.62	‡γ_{min} 0.7 †γ_{max} 26.6	γ_{min} 1.2 γ_{max} 33.5	γ_{min} 1.9 γ_{max} 36.5
2	72.4	182	32.34	γ_{min} 0.7 γ_{max} 26.9	γ_{min} 1.5 γ_{max} 29.2	γ_{min} 2.4 γ_{max} 33.9
3	72.7	190	32.15	γ_{min} 0.7 γ_{max} 29.3	γ_{min} 0.9 γ_{max} 31.3	γ_{min} 1.2 γ_{max} 33.9
Mean± SD	72.5±0.2	186.3±4.0	32.0±0.4	γ_{min} 0.7±0.0 γ_{max} 27.6±1.4	γ_{min}1.2±0.3 γ_{max} 31.3±2.1	γ_{min}1.8±0.6 γ_{max}34.8±1.5

γ^* is the initial surface tension at the air-liquid interface after spreading DPPC at the air-liquid interface and allowing 10 minutes for spreading solvent to evaporate.

‡γ_{min} is the minimum surface tension monitored upon compression.

†γ_{max} is the maximum surface tension monitored upon expansion.

Table 2-11: Surface tension of the typical mucus mimetic before and after spreading DPPC onto mimetic surface measured using the Wilhelmy plate balance and du Noüy ring method; data are represented as the mean ± SD.

Mucus Mimetic Formulation	**Wilhelmy plate balance Surface Tension (mN/m)**	**Du Noüy ring Surface Tension (mN/m)**
Typical mucus mimetic	53.3 ± 1.2 (n= 9)	56.4 ± 0.4 (n=3)
Typical mucus mimetic covered with DPPC	30.2 ± 2.4 (n=4)	48.2 (n=1)

Table 2-12: Surface tension of water before and after the addition of 11 µL of 1.02 mg/ml DPPC in n-hexane:methanol (95:5 v/v) measured using the Wilhelmy plate balance and du Noüy ring method; data are represented as the mean ± SD.

Interface	**Wilhelmy plate balance Surface Tension (mN/m)**	**Du Noüy ring Surface Tension (mN/m)**
Pure water interface	72.8 ± 1.0 (n=3)	71.4 ± 0.2 (n= 3)
DPPC spread at air-water interface	33.7 ± 1.1 (n=3)	51.6 ± 1.4 (n=3)

Table 2-13: Surface tension of mucus mimetics 2 and 3 measured using the du Noüy ring method; data are represented as the mean ± SD (n=3).

Mucus Mimetic Formulation	**Surface Tension (mN/m)**
Mucus mimetic 2	76.8 ± 5.8
Mucus mimetic 3	95.0 ± 7.8

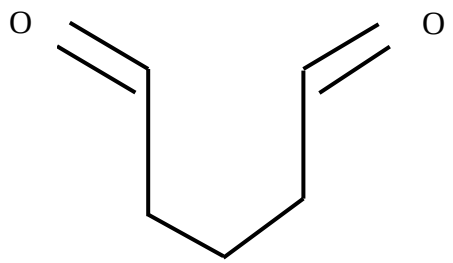

Figure 2-1: Chemical structure of glutaraldehyde (GA).

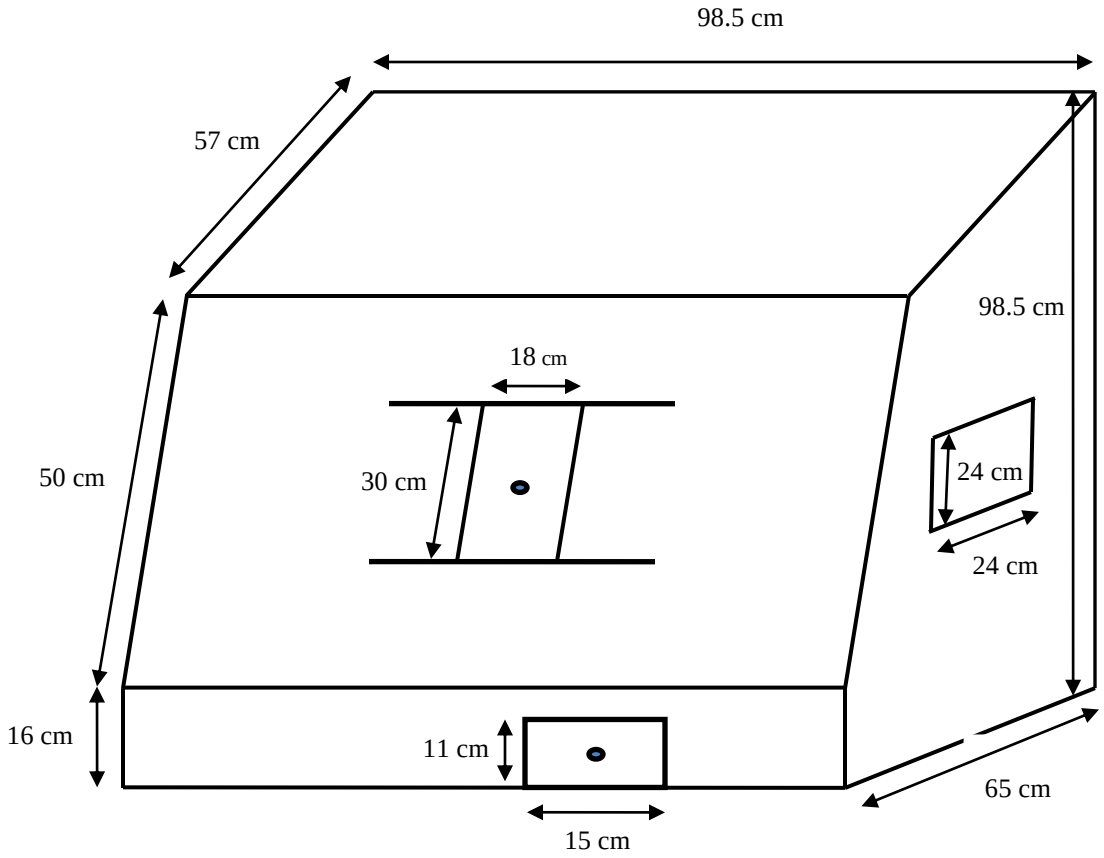

Figure 2-2: Sketch for the enclosure system with its dimensions.

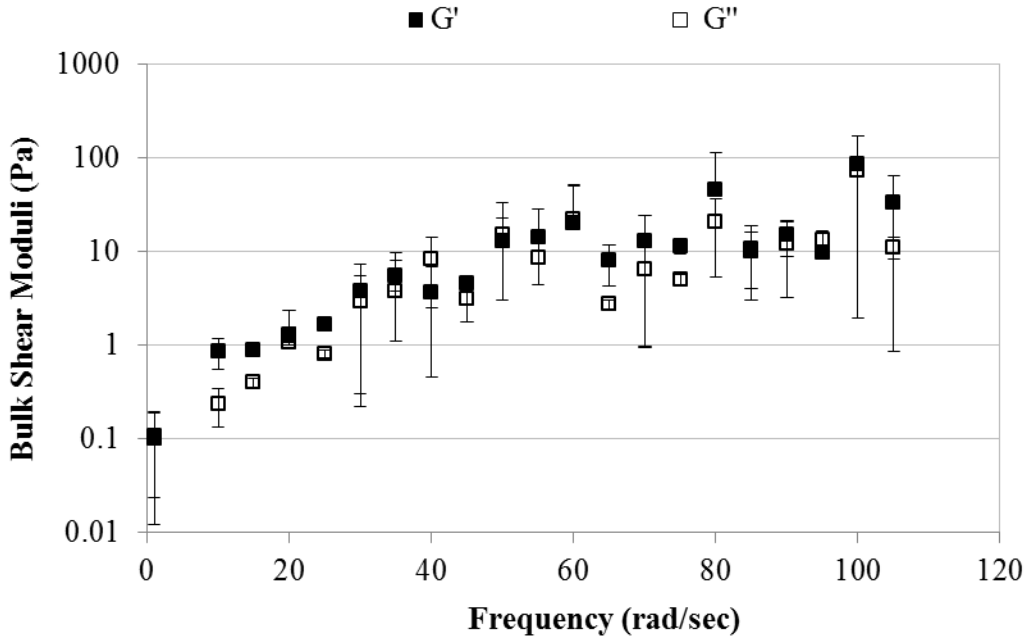

Figure 2-3: Frequency-dependence of bulk shear storage modulus G' and bulk shear loss modulus G" for mucin solution of 2% (w/v) PGM-type III. Data are represented as the mean ± SD (n=3).

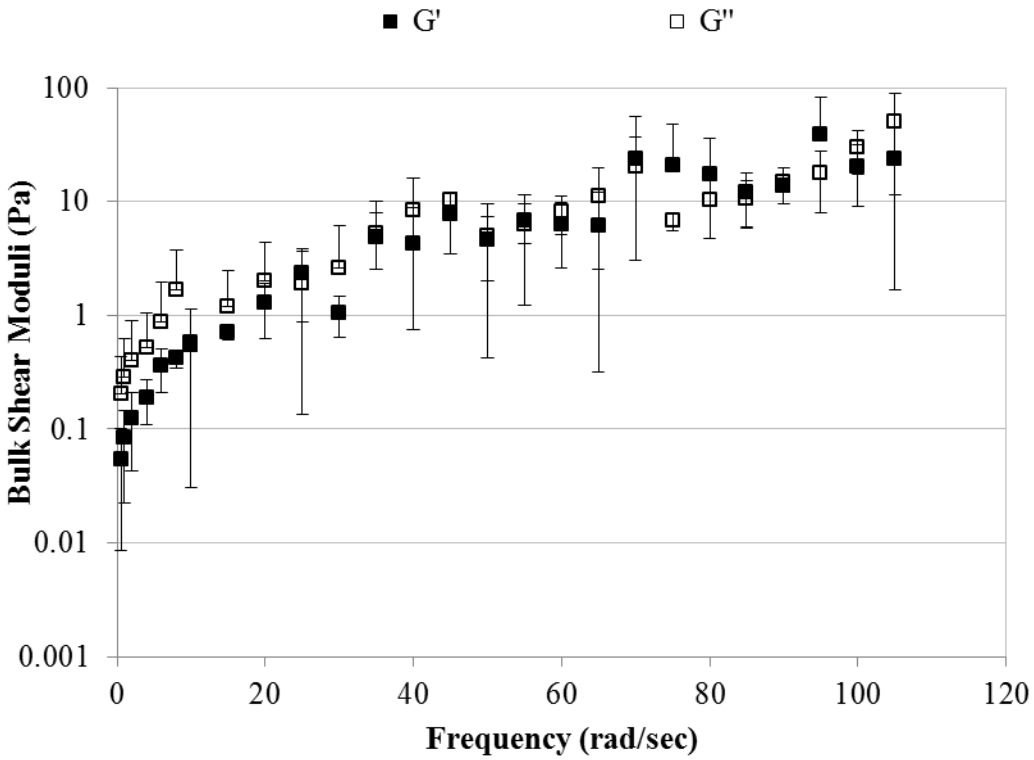

Figure 2-4: Frequency-dependence of bulk shear storage modulus G' and bulk shear loss modulus G" for mucin solution of 3% (w/v) PGM-type III. Data are represented as the mean ± SD (n=3).

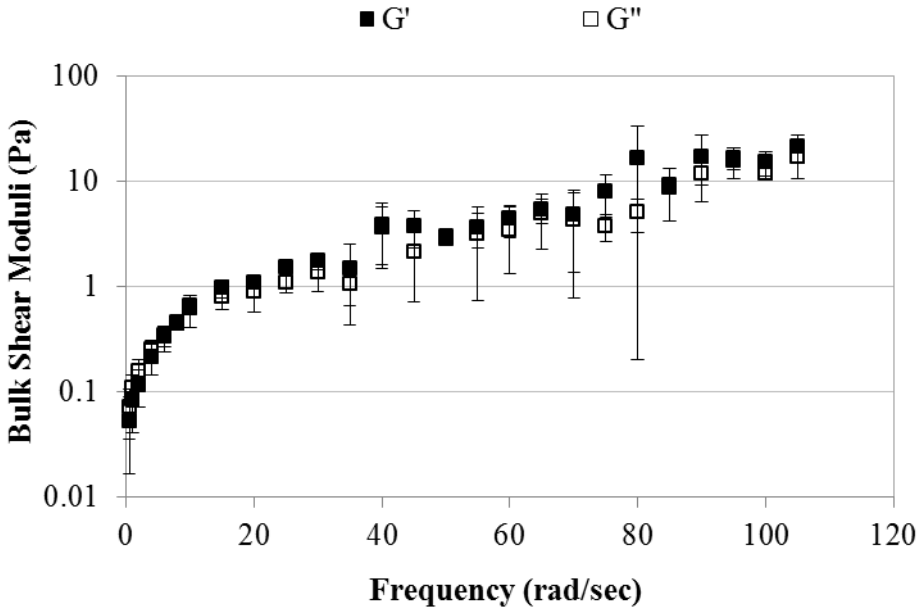

Figure 2-5: Frequency-dependence of bulk shear storage modulus G' and bulk shear loss modulus G" for mucin solution of 4% (w/v) PGM-type III. Data are represented as the mean ± SD (n=4).

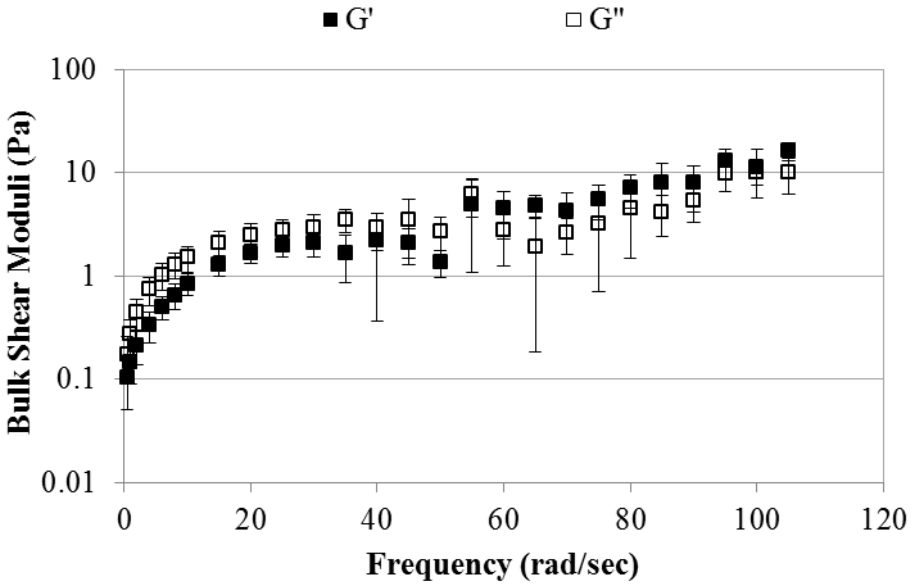

Figure 2-6: Frequency-dependence of bulk shear storage modulus G' and bulk shear loss modulus G" for mucin solution of 6% (w/v) PGM-type III. Data are represented as the mean ± SD (n=5).

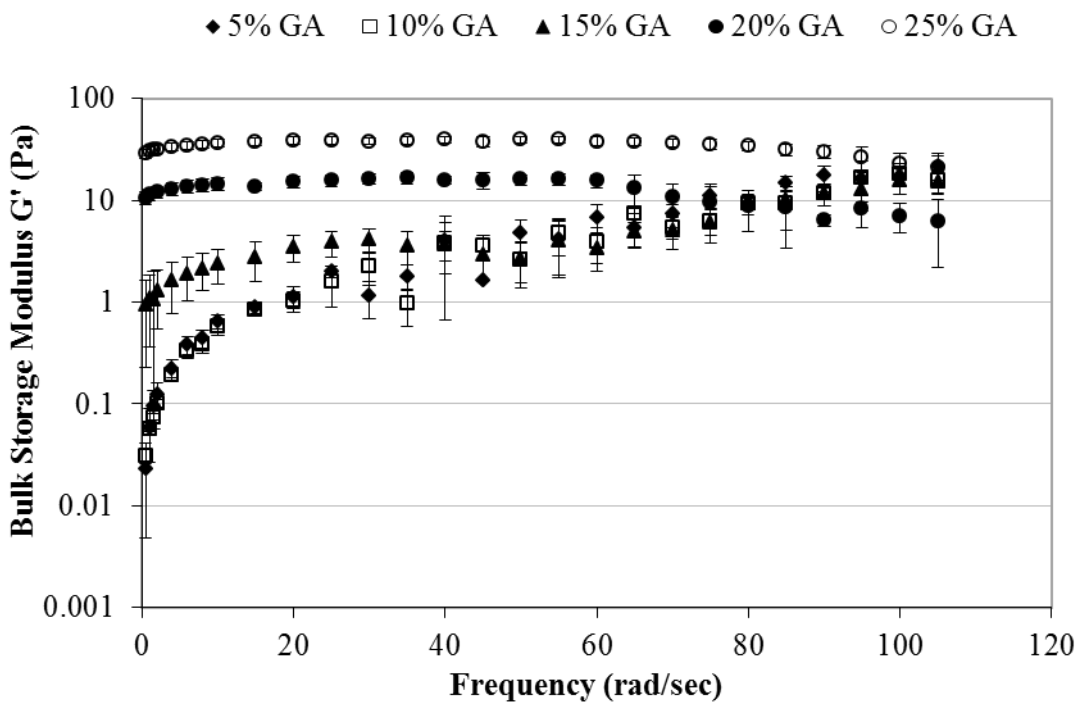

Figure 2-7: Frequency-dependence of bulk shear storage modulus G' for mucus mimetic cross-linked with various concentrations of GA solution (5% w/w, n=3; 10% w/w, n=4; 15% w/w, n=5; 20% w/w, n=3; and 25% w/w, n=5) for 3 days. Data are represented as the mean ± SD.

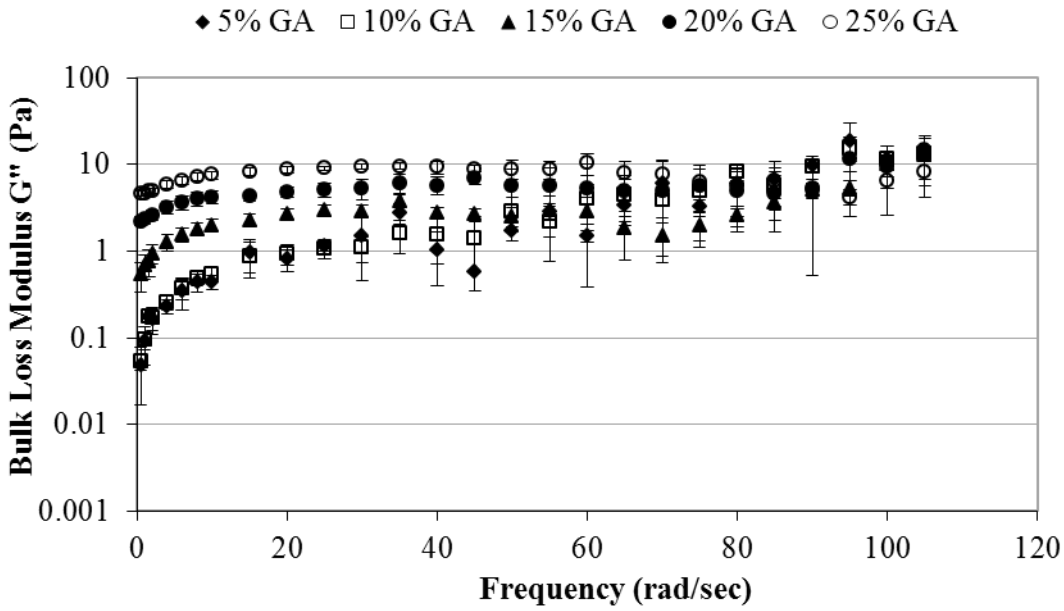

Figure 2-8: Frequency-dependence of bulk shear loss modulus G" for mucus mimetic cross-linked with various concentrations of GA solution (5% w/w, n=3; 10% w/w, n=4; 15% w/w, n=5; 20% w/w, n=3; and 25% w/w, n=5) for 3 days. Data are represented as the mean ± SD.

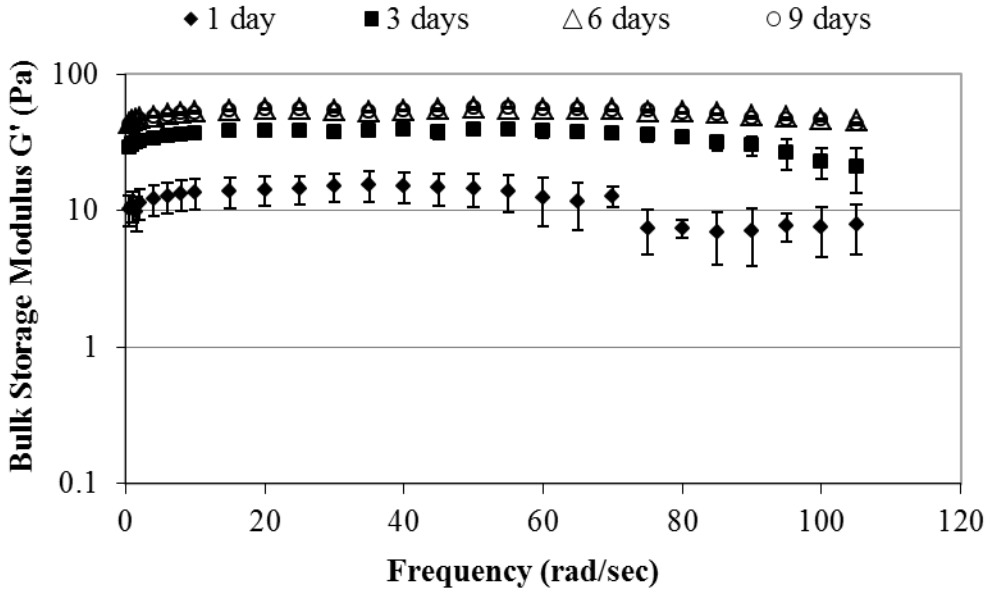

Figure 2-9: Frequency-dependence of bulk shear storage modulus G’ for mucus mimetic cross-linked using 0.5 ml-25% w/w GA solution at various cross-linking times (1 day, n=5; 3 days, n=5; 6 days, n=4; and 9 days, n=3). Data are represented as the mean ± SD.

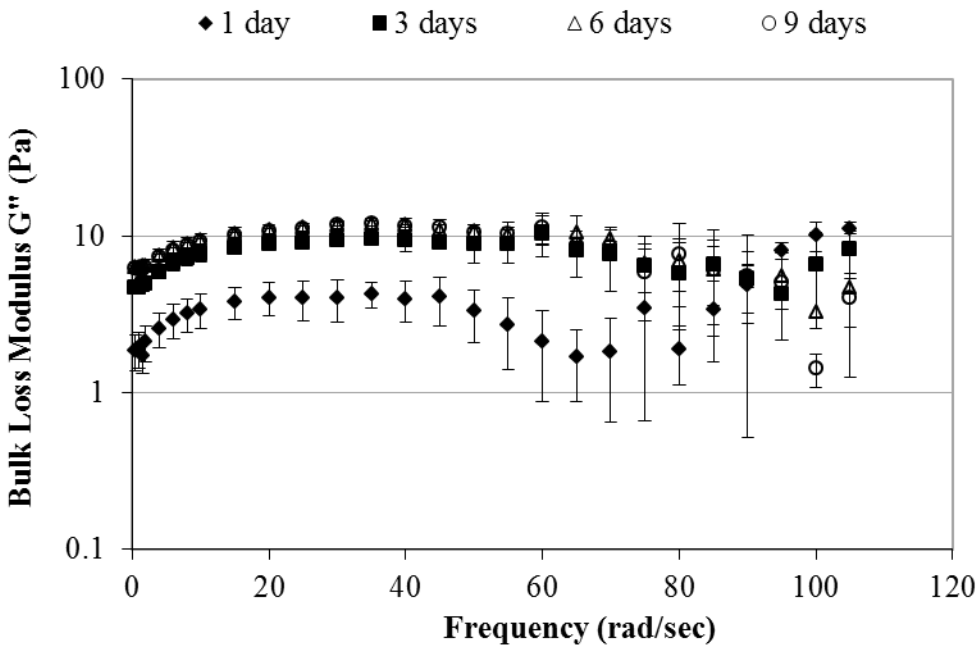

Figure 2-10**:** Frequency-dependence of bulk shear loss modulus G" for mucus mimetic cross-linked using 0.5 ml-25% w/w GA solution at various cross-linking times (1 day, n=5; 3 days, n=5; 6 days, n=4; and 9 days, n=3). Data are represented as the mean ± SD.

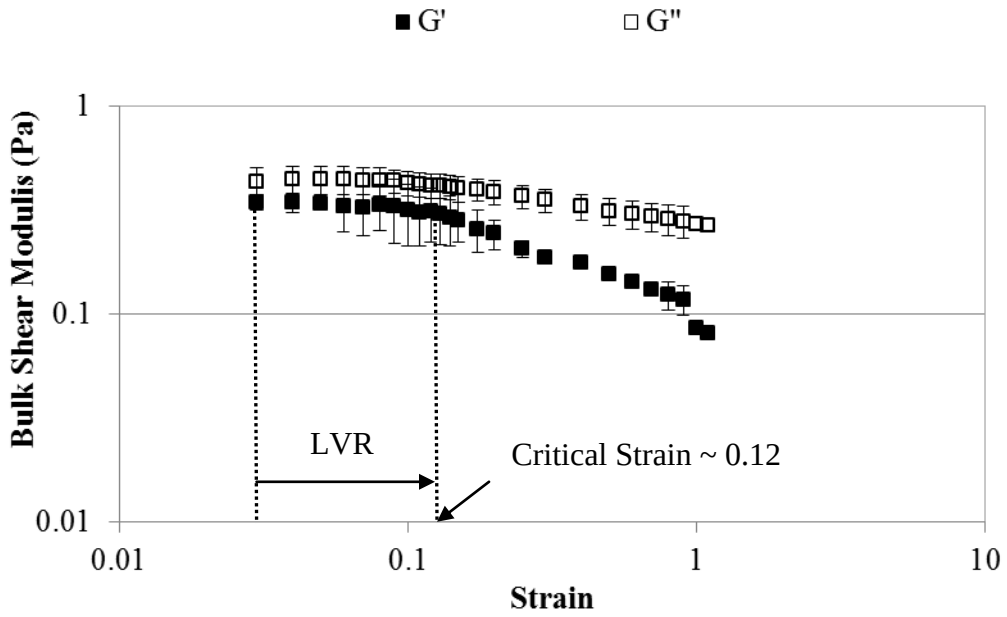

Figure 2-11: Strain-dependence of bulk shear storage modulus G' and bulk shear loss modulus G" for the mucus mimetic 1 over a strain range of 0.03 to 1.1 at a fixed frequency of 2 rad/sec. The linear viscoelastic region (LVR) and the critical strain (~ 0.12) at which the bulk viscoelastic moduli deviate from LVR are indicated by arrows. Data are represented as the mean ± SD (n=4).

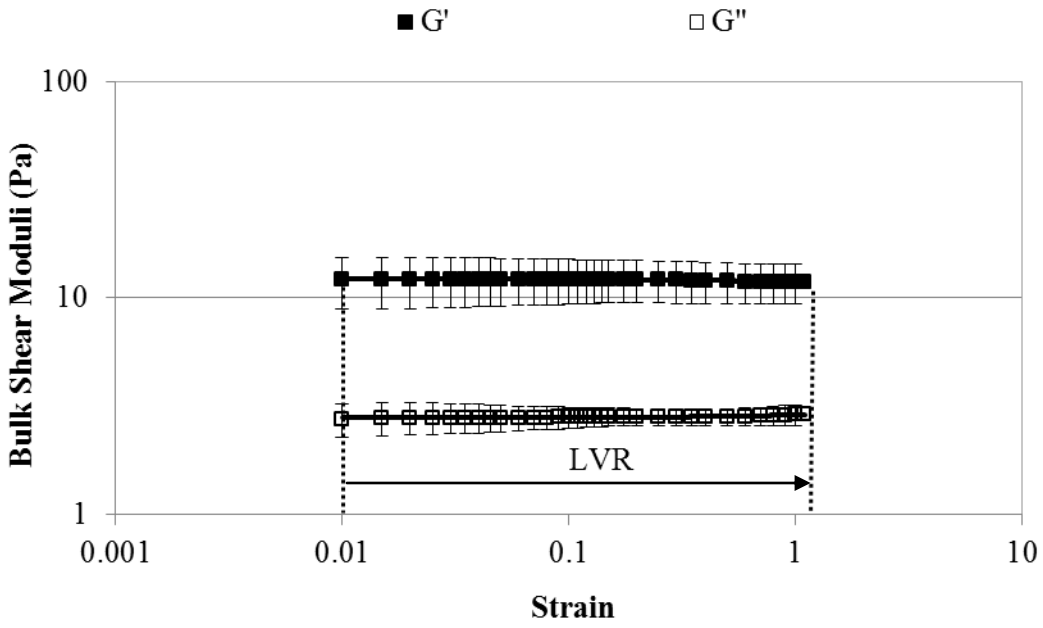

Figure 2-12: Strain-dependence of bulk shear storage modulus G' and bulk shear loss modulus G" for the mucus mimetic 2 over a strain range of 0.01 to 1.1 at a fixed frequency of 2 rad/sec. The LVR is extended from 0.01-1.1 and is indicated by an arrow. Data are represented as the mean ± SD (n=4).

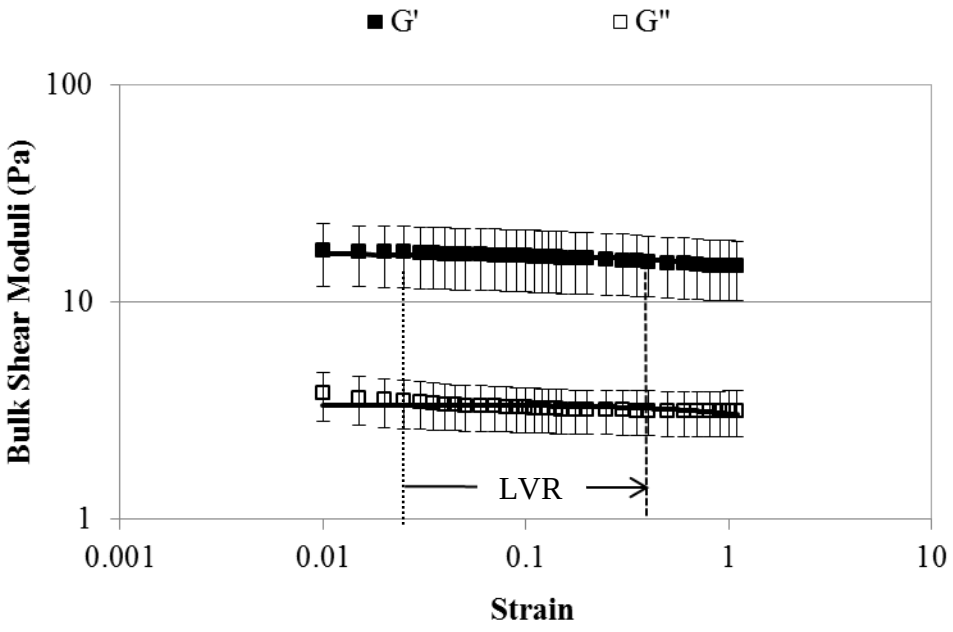

Figure 2-13: Strain-dependence of bulk shear storage modulus G' and bulk shear loss modulus G" for the mucus mimetic 3 over a strain range of 0.01 to 1.1 at a fixed frequency of 2 rad/sec. The LVR is extended from 0.025-0.40 and is indicated by an arrow. Data are represented as the mean ± SD (n=4).

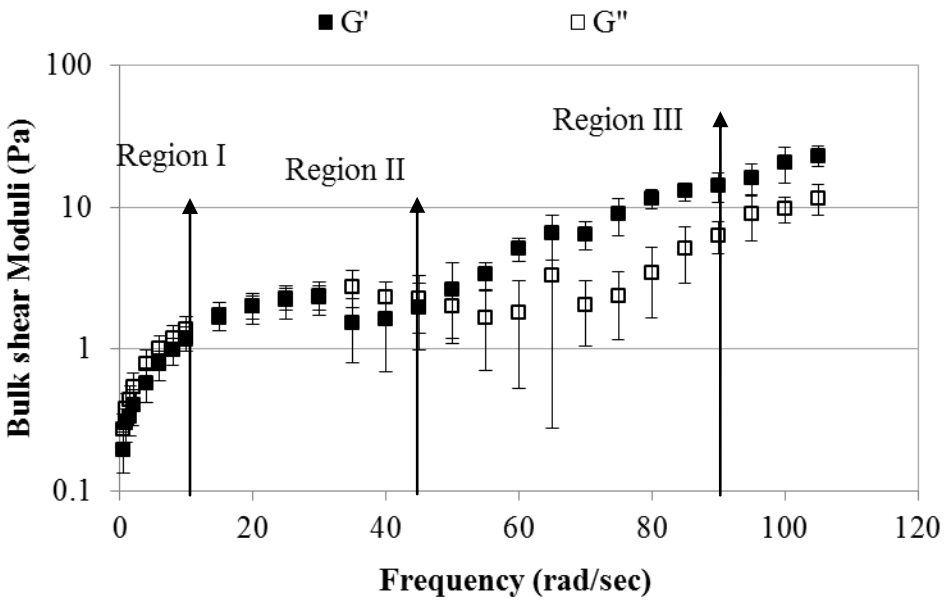

Figure 2-14: Frequency-dependence of bulk shear storage modulus G' and bulk shear loss modulus G" for the mucus mimetic 1 cross-linked using 0.5 ml-15% (w/w) GA solution for 24 hours. Data are represented as the mean ± SD (n=11).

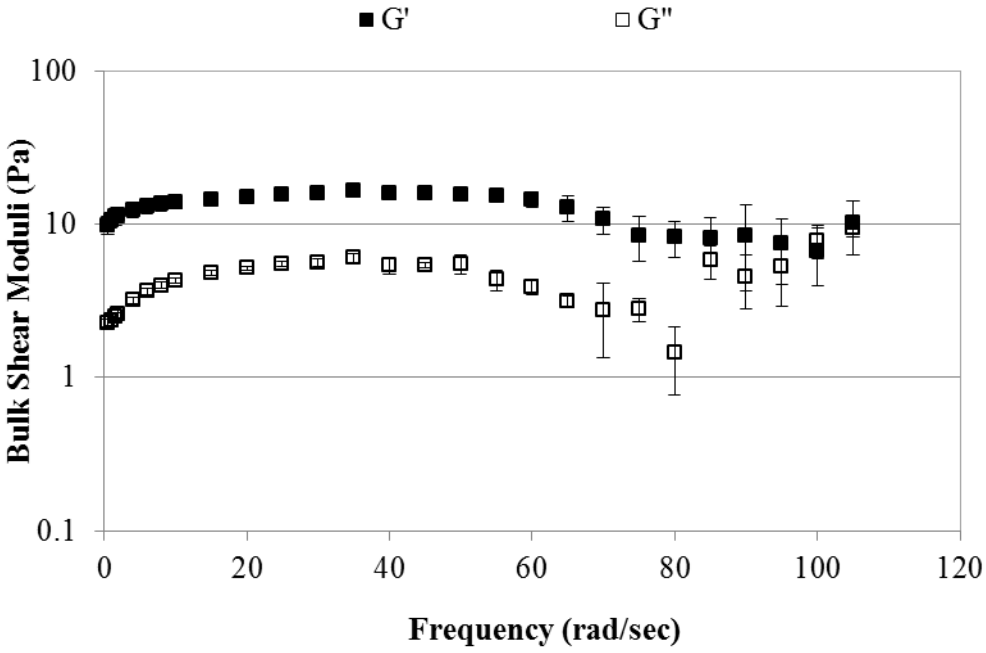

Figure 2-15**:** Frequency-dependence of bulk shear storage modulus G’ and bulk shear loss modulus G” for the mucus mimetic 2 cross-linked using 0.5 ml-25% (w/w) GA solution for 3 days. Data are represented as the mean ± SD (n=6).

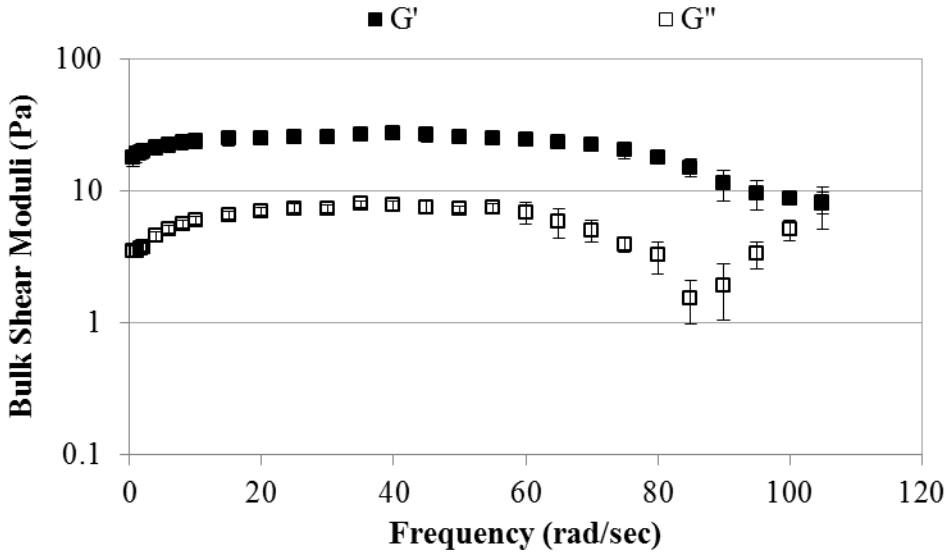

Figure 2-16**:** Frequency-dependence of bulk shear storage modulus G' and bulk shear loss modulus G" for the mucus mimetic 3 cross-linked using 1.0 ml-50% (w/w) GA solution for 3 days. Data are represented as the mean ± SD (n=5).

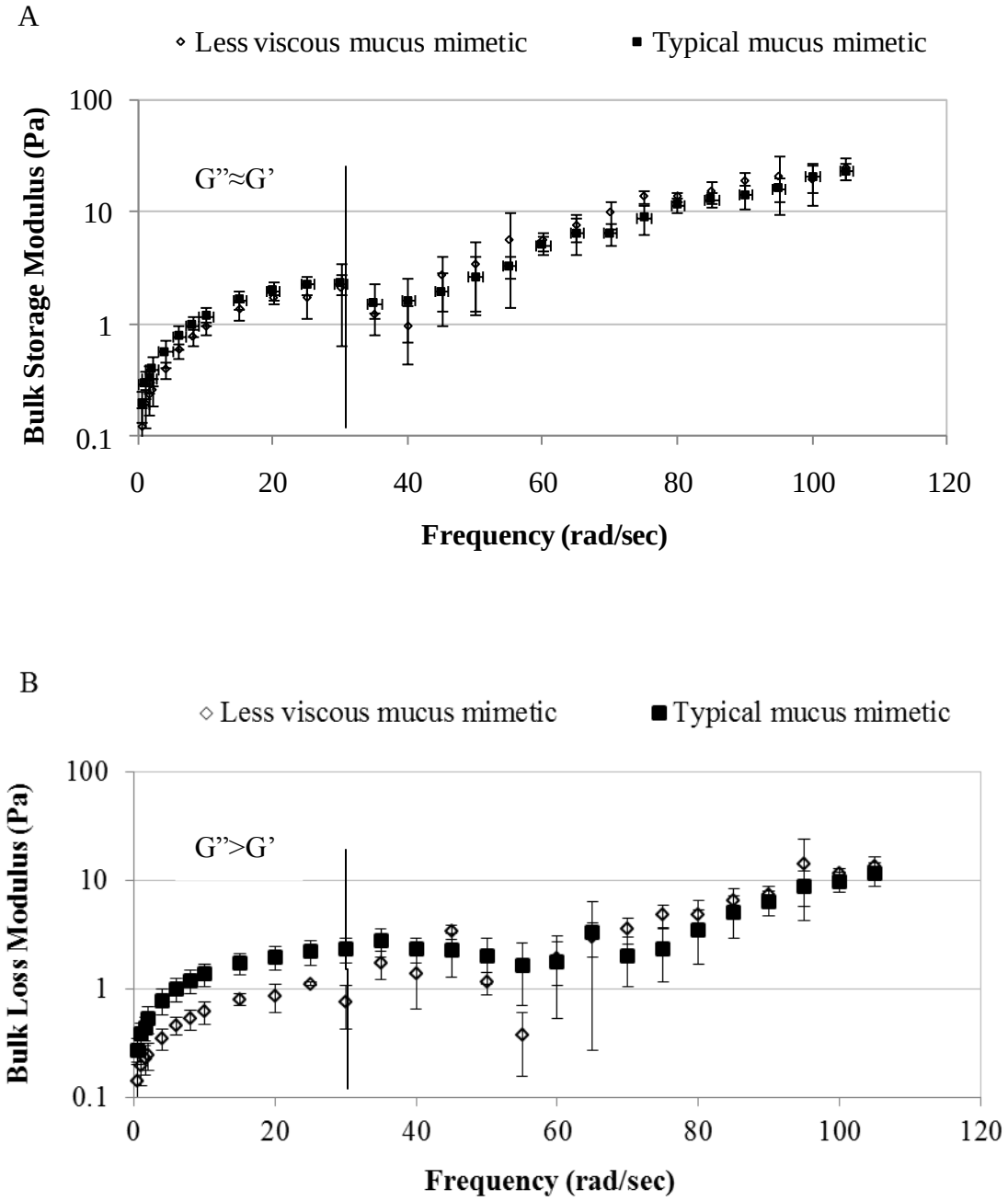

Figure 2-17: Frequency-dependence of: (A) bulk shear storage modulus G' and (B) bulk shear loss modulus G" of the less viscous mucus mimetic (n=3) and the typical mucus mimetic (n=11) discussed in section 2.3.8. Data are represented as the mean ± SD.

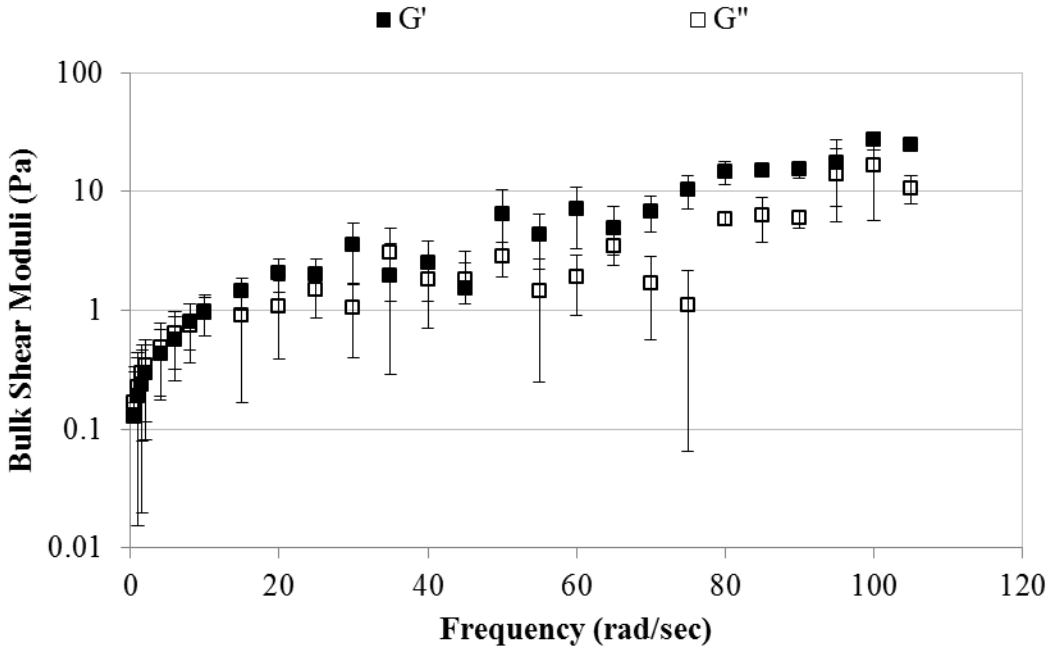

Figure 2-18: Frequency-dependence bulk shear storage modulus G' and bulk shear loss modulus G" of the less viscous mucus mimetic cross-linked using 0.5 ml-50% (w/w) GA for 24 hours. Data are represented as the mean ± SD (n=3).

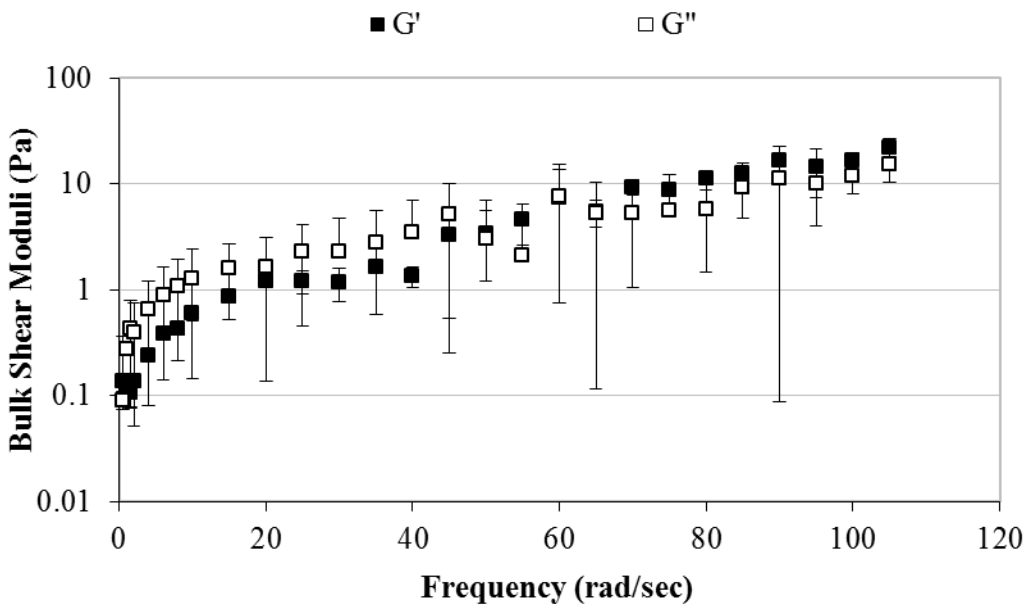

Figure 2-19: Frequency-dependence bulk shear storage modulus G' and bulk shear loss modulus G" for the cross-linked PGM (cross-linked by 0.5 ml-25% (w/w) GA solution for 3 days. Data are represented as the mean ± SD (n=5).

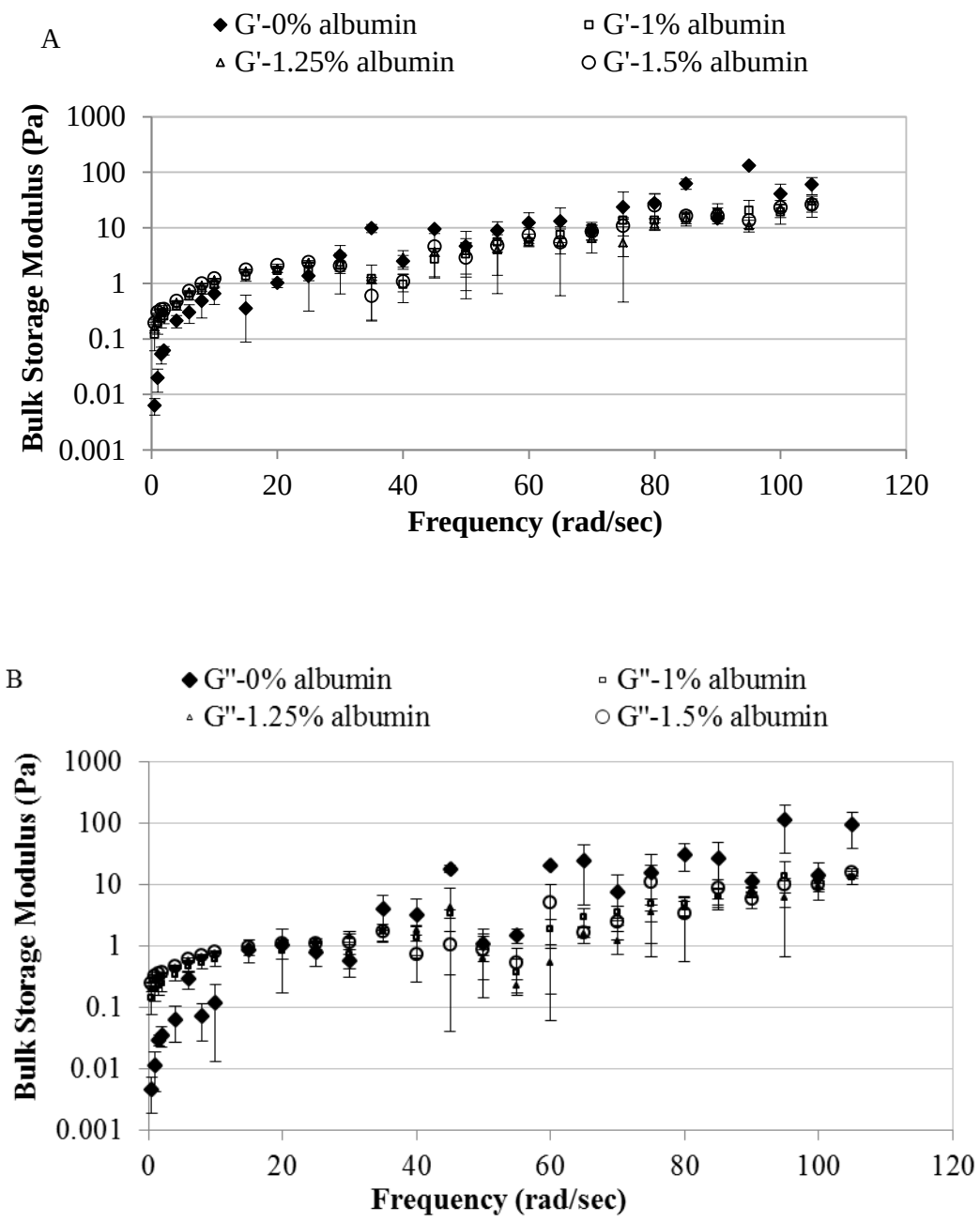

Figure 2-20: Frequency-dependence of: (A) bulk shear storage modulus and (B) bulk shear loss modulus G" of mucus mimetic formulations composed of 4% (w/v) PGM and various concentrations of albumin (0%, 1%, 1.25%,1.5%) cross-linked using 0.5 ml-15% (w/w) GA solution for 24 hours. Data are represented as the mean ± SD (n=3).

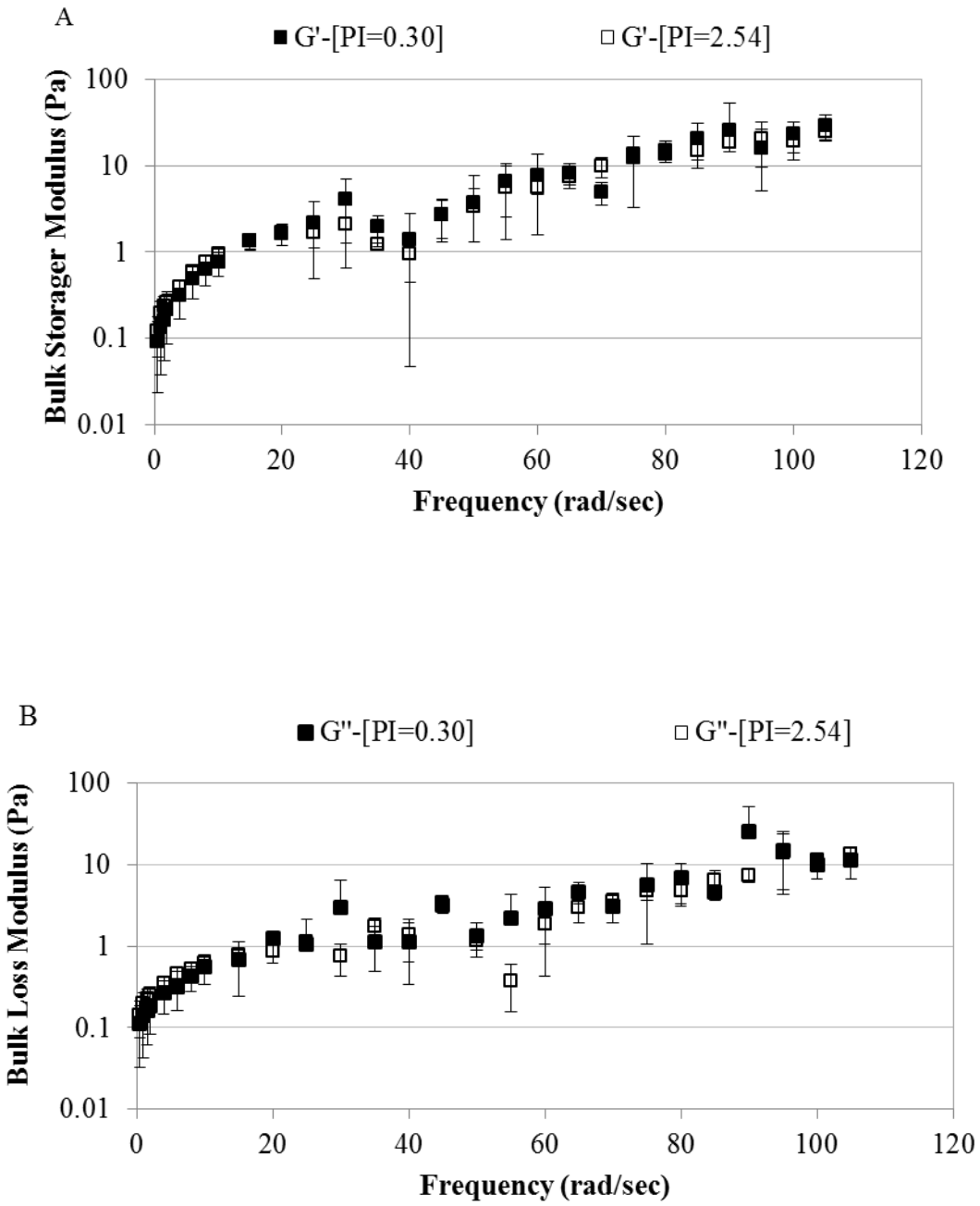

Figure 2-21: Frequency-dependence of: (A) bulk shear storage modulus G' and (B) bulk shear loss modulus G' of mucus mimetic cross-linked using 0.5 ml-15% (w/w) GA solution for 24 hours. Two types of GA with purification index of 0.3 (n=4) and 2.54 (n=3) were used. Data are represented as the mean ± SD.

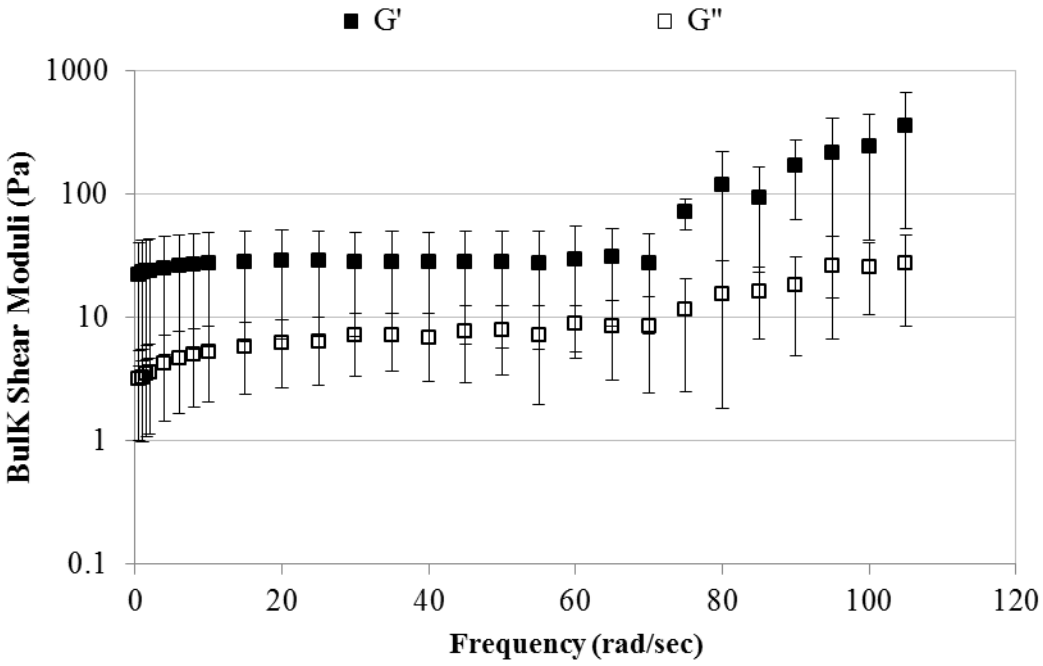

Figure 2-22: Frequency-dependence of bulk shear storage modulus G' and bulk shear loss modulus G" for mucus mimetic cross-linked using 0.5 ml-50% (w/w) GA solution using a modified method of preparation and cross-linked by kept stationary at room temperature for 24 hours. Data are represented as the mean ± SD (n=3).

A

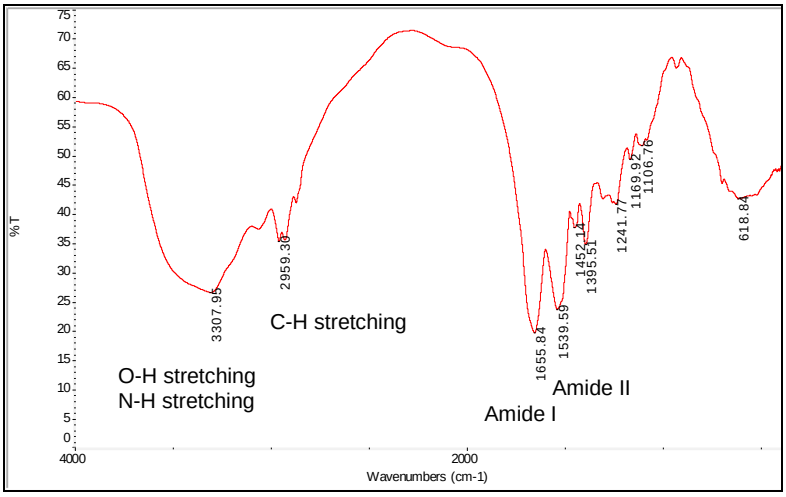

B

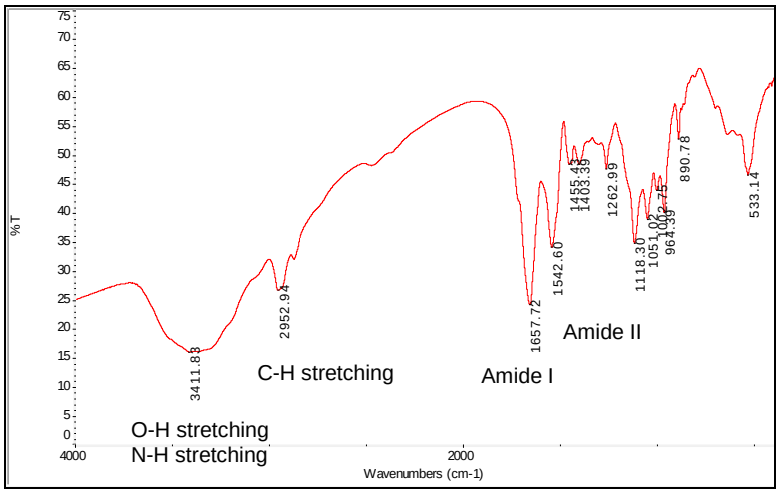

Figure 2-23: FT-IR spectra of: (A) native albumin and (B) 1% (w/v) albumin bovine cross-linked using 0.5 ml-50% (w/w) GA solution.

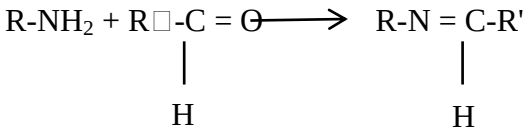

Figure 2-24: Schiff base formation upon the reaction of amine group with the aldehydic group.

A

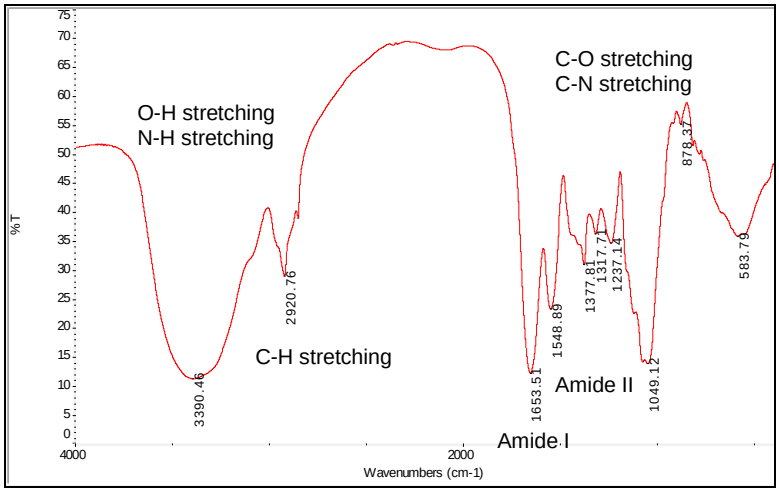

B

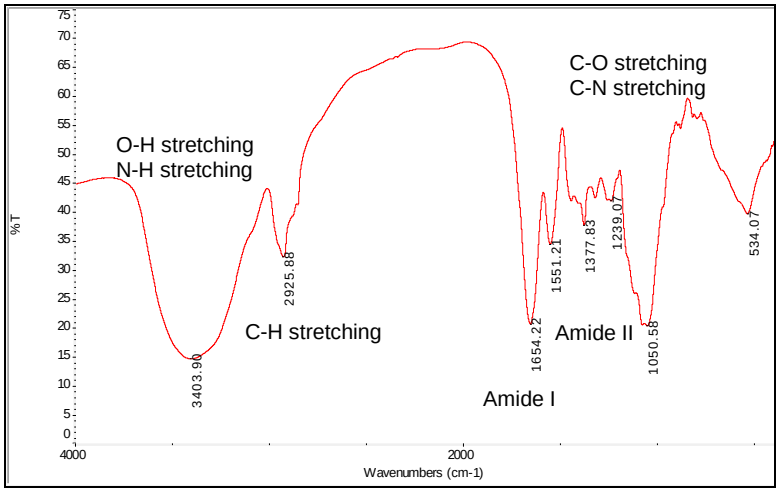

Figure 2-25: FT-IR spectra of: (A) native PGM-type III and (B) 4% (w/v) PGM-type III cross-linked using 0.5 ml-50% (w/w) GA solution.

A

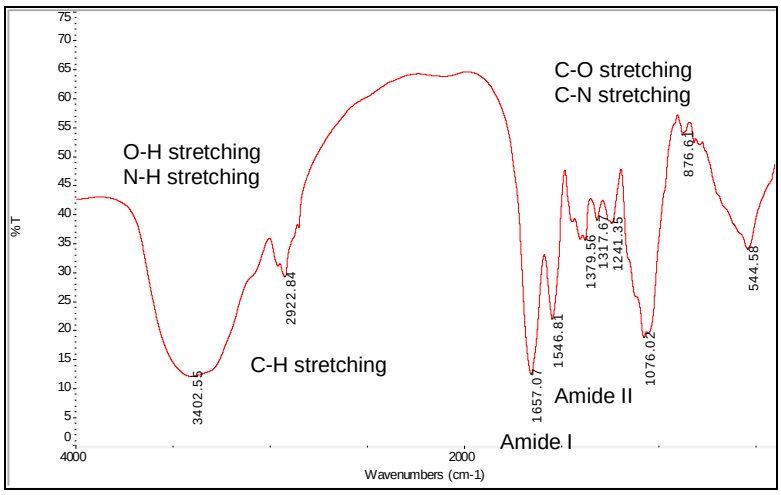

B

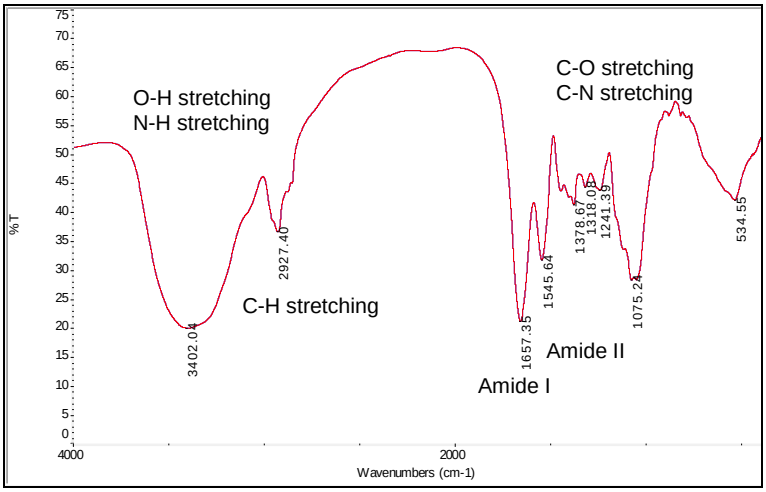

Figure 2-26: FT-IR spectra of: (A) uncross-linked mucus mimetic, (B) mucus mimetic cross-linked using 0.5 ml-50% (w/w) GA solution, (C) mucus mimetic cross-linked using 50% (w/w) GA solution then reduced with sodium borohydride.

C

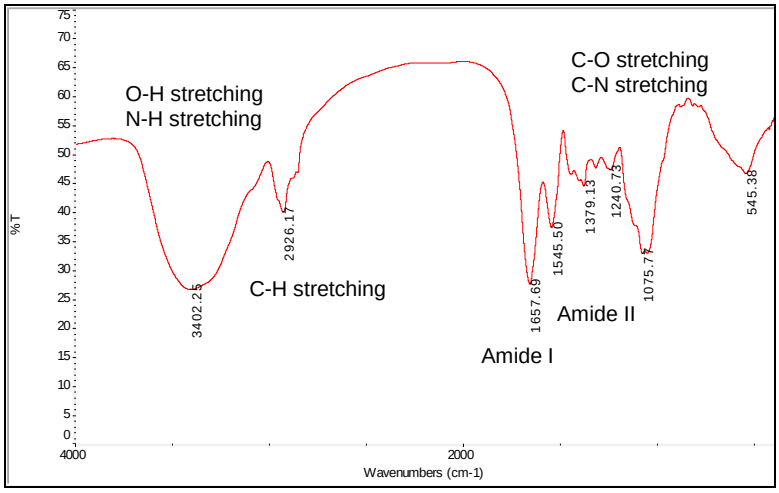

Figure 2-27 continued

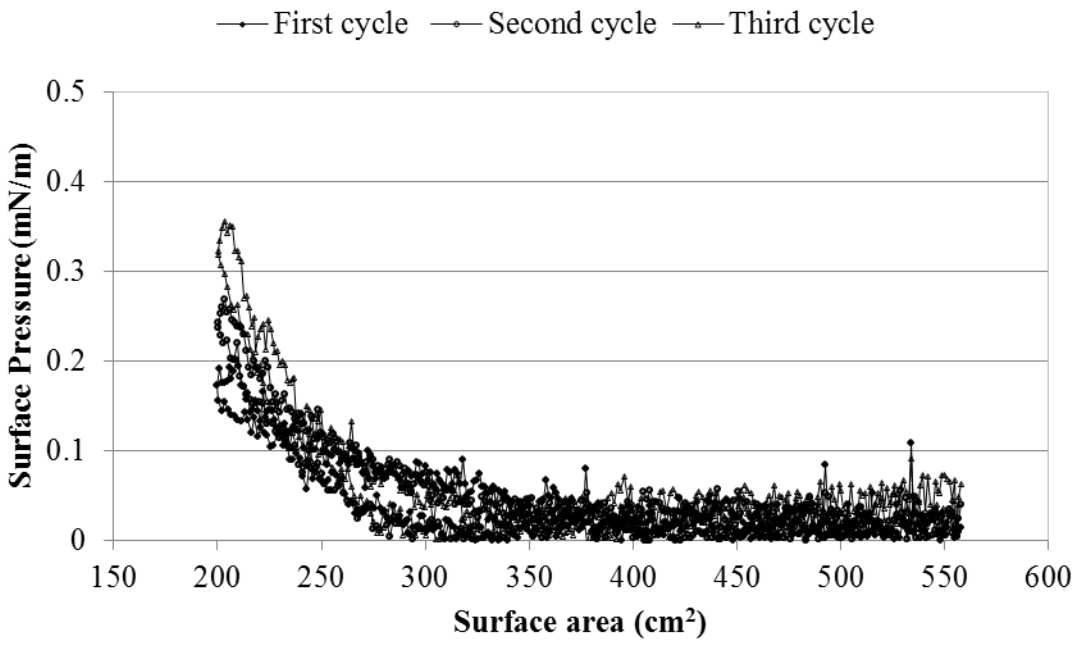

Figure 2-28: Surface pressure-surface area isotherm of the air-liquid interface after the addition of the spreading solvent n-hexane:methanol (95:5 v/v) during three compression-expansion cycles for one of the three experiments reported in Table 2-9. Surface pressure did not exceed 0.4 mN/m upon compression of the spreading solvent interface.

CHAPTER 3

SURFACE RHEOLOGICAL BEHAVIOR OF DIPALMITOYLPHOSPHATIDYLCHOLINE (DPPC) ON A MUCUS MIMETIC SUBPHASE

3.1. Introduction

The large conducting airways are coated with a continuous fluid film whose main functions include protecting the underlying lung tissues by trapping and clearing inhaled foreign material and hydrating the epithelial cells on the mucosal surface. This fluid film is composed of two primary layers: an aqueous periciliary fluid adjacent to the lung tissues which enables free ciliary movement for mucociliary clearance and a viscoelastic mucus gel layer which lies atop the periciliary layer and efficiently traps foreign material.[8, 76] The relatively low surface tension of the airway lining fluid (ALF) surface (~ 32 mN/m) suggests that the air-mucus interface of the large conducting airways is covered with a surface active material.[30, 31] Light and transmission electron micrographs have corroborated the presence of a surfactant film by demonstrating a continuous osmiophilic film at the air-mucus interface.[31, 34] This surfactant film is considered critical for normal function of the tracheobronchial tree by decreasing the surface tension of the interface to facilitate mucociliary and cough clearance,[35] aiding the penetration of foreign material (such as pathogens, environmental contaminants and therapeutics) into the gel phase for clearance,[30, 36] participating in innate lung defense,[111] and reducing evaporation of the subphase.[37]

Previous studies have confirmed that surfactants in the human tracheal secretions are transported up the surface tension gradient from the alveoli, with a secondary source via direct production by airway secretory cells in the epithelium and submucosal glands.[29, 31, 38, 45] Bernhard *et al.*[42] reported that the major phospholipid classes, including the phosphatidylcholine molecular species, in tracheal aspirates were similar to those in

bronchoalveolar lavage, showing a remarkable similarity in surfactant composition across the entire respiratory tract. Surfactant composition in tracheal aspirates was markedly different from those of the underlying airway mucosa, showing that secretion by the airway epithelium alone could not account for the levels of surfactants in the large conducting airways. Studies in rats have confirmed that the tracheal mucosa does not synthesize dipalmitoylphosphatidylcholine (DPPC), which therefore must be derived from the alveoli.[48] In terms of overall lipid composition in the tracheal secretions, about 40-45% is composed of neutral lipids, 22% phospholipids and 38% glycolipids.[13, 40, 41] Given the confirmed role of phospholipids as highly surface active species critical to the function of the pulmonary surfactant in the alveoli, phospholipids are likely major contributors in reducing the surface tension in the large conducting airways as well. Phosphatidylcholine is the most prevalent class of phospholipids in the tracheal secretions, representing 31-47 wt% (71-84 mol%) of the total phospholipid concentration.[13, 39, 42-44]

In the large conducting airways of mammalian lungs, the air-fluid interface experiences a variety of different stresses, such as shearing by air during inhalation-exhalation cycles and bulk fluid movement due to mucociliary clearance. The interfacial properties of surfaces can provide insight into how the interface functions under such stress. However, the interfacial properties of the fluids in the large conducting airways remain largely unstudied, despite their importance in a variety of physiological processes. Therefore, a better understanding of the properties of surfactants at the air-mucus interface would provide critical information about the function of the tracheobronchial tree.[112-115] The interfacial behavior of an air-fluid surface is influenced by the surface composition as well as the physical properties of the underlying fluid.[116, 117] Given the viscoelastic nature of the mucus underlying the surfactant film at the interface,[12, 22, 23, 56, 77] it is expected that the surface behavior of this fluid will be distinct from the commonly studied Newtonian case.

In this work, the effect of a viscoelastic subphase on the surface rheological properties of a DPPC model lipid layer was studied. Of the phosphatidylcholine species in the tracheal secretions, DPPC represents the predominant species at 49-57 mol% of the phosphatidylcholine composition and, therefore, was chosen as a representative surfactant for the investigation.[42, 44] The *in-vitro* mimetic of tracheal mucus developed in Chapter 2 was used as the model subphase. Surface shear rheology was used to investigate the mechanical properties of DPPC on a mucus subphase and was compared to the mechanical properties of DPPC on a water subphase.

The three mimetics developed in Chapter 2 exhibited varying bulk viscoelastic properties at different frequencies. Mucus mimetic 1 exhibited extremely low G' and G" values at 1 rad/sec. However, at high frequency (100 rad/sec) G' and G" considerably increased to values similar to native, non-diseased mucus. Therefore, probing the surface rheology of the mimetic 1 will provide information on the surface behavior of the tracheal mucus during high shear maneuvers such as cough. Mimetic 2 exhibited G' and G" similar to that of native, non-diseased mucus at 1 rad/sec. Therefore, probing the surface rheology of mimetic 2 will provide insight on the surface behavior of the tracheal mucus during normal breathing, which occurs at low frequencies.

3.2. Materials and Methods

3.2.1. Materials

Pig gastric mucin (PGM)-type III was purchased from Sigma-Aldrich, Inc. (St. Louis, MO), bovine serum albumin (fraction V, lyophilized powder) from Spectrum (New Brunswick, NJ) and 1, 2-dipalmitoyl-sn-glycero-3-phosphocholine (DPPC) from Genzyme Pharmaceuticals (Cambridge, MA). Glutaraldehyde (GA, 50% w/w solution), n-hexane (99.0% purity) and methanol (99.9% purity) were purchased from Fisher Scientific (Fair Lawn, NJ). Texas Red-DHPE (1, 2-dihexadecanoyl-sn-glycero-3-phosphoethanolamine, triethylammonium salt) was purchased from Invitrogen. Purified

water (18 MΩ cm) was used in all experiments obtained from a NANOpure Infinity Ultrapure Water System, Barnstead International (Northbrook, IL). All other chemical reagents were of analytical grade and used without further purification.

3.2.2. Preparation of Mucus Mimetics

The *in-vitro* model mucus mimetics of low and medium bulk viscoelasticity were used in this study. Mucus mimetic (composed of 4% (w/v) PGM-type III, 1% (w/v) ions, 1% (w/v) albumin, and 94 ml water) was prepared for surface rheology studies as discussed in section 2.2.3 in Chapter 2. Briefly, to prepare 30 ml of the mimetic, 0.3 g albumin, 1.2 g PGM-type III and 28.5 ml buffer (154 mM NaCl, 3 mM $CaCl_2$, 15 mM NaH_2PO_4/Na_2HPO_4; pH 7.4) were added to an amber glass bottle. Ingredients were mixed at 4°C on a tube rotator (Glas-Col, IN) for at least 6 days to mix the sample. The mucus mimetic 1 was prepared by cross-linking the mimetic formulation using GA solution. A 0.5 ml-15% (w/w) GA solution was added to the 30 ml of mimetic formulation and mixed at 4°C on a tube rotator (Glas-Col, IN) for 24 hours.

For surface rheology studies, the mucus mimetic 2 was cross-linked *in-situ* using a Plexiglas mini-trough. Two samples of mimetic formulation (30 ml each) were used to prepare the mucus mimetic. To each 30 ml of the mimetic formulation, 0.5 ml-25% (w/w) GA solution was added and mixed at 4°C on a tube rotator (Glas-Col, IN) for 5 hours. After 5 hours, the two samples were poured into a Plexiglas mini-trough (7.5 cm x 12 cm) with a glass channel (100 mm length, 9.6 mm width, 6.5 mm height) positioned in the middle of the mini-trough (Figure 3-1). A Plexiglas lid was used to cover the mimetic within the mini-trough to minimize evaporation. Mimetic within the mini-trough was kept at 4°C for about 5 days to crosslink *in-situ* and to attain bulk viscoelastic properties of the mucus mimetic 2 [i.e. bulk shear storage modulus G' (9.0-12.0 Pa) and bulk shear loss modulus G" (1.5-3.0 Pa), at 1 rad/sec].

3.2.3. Modification and Measurement of Surface Tension

1, 2-dipalmitoyl-sn-glycero-3-phosphocholine (DPPC) was spread onto mucus mimetic 1 and water surfaces within a Plexiglas mini-trough (7.5 cm x 12 cm) (Figure 3-1) placed in a home-built environmental chamber capable of maintaining temperature at ~ 25°C and relative humidity at ~ 40% (Figure 3-2). DPPC was dissolved in a solution of (n-hexane:methanol) (95:5 v/v) and was added at the air-fluid interface using a Hamilton micro-syringe until a surface tension of ~ 32 mN/m was achieved. Ten minutes were allowed to elapse for the solvents to evaporate. The surface tension of each interface was then determined using a Wilhelmy plate balance (KSV Instruments, Finland) equipped with a platinum plate (20 mm x 10 mm) at ~ 25°C. At least three surface tension measurements were conducted for each interface.

3.2.4. Fluorescence Microscopy

For microscopic studies, 1 mg/ml DPPC in n-hexane:methanol (95:5 v/v) was doped with 0.5 mol% of the fluorescent lipid Texas Red-DHPE® (1, 2-dihexadecanoyl-sn-glycero-3-phospho-ethanolamine, triethylammonium salt), which has excitation and emission wavelengths of 582 and 607 nm, respectively. The doped DPPC solution was spread onto uncross-linked and cross-linked mucus mimetic surfaces in a round Petri-dish using a micro-syringe until a surface tension of ~ 32 mN/m was achieved. Fluorescence images of each surface were obtained using a florescence microscope (Olympus BX-51) equipped with an excitation band pass filter of 515-560 nm and emission of 575-647 nm and a 20x objective. Image analysis was performed using Image J.[118]

3.2.5. Surface Pressure (Π)-Surface Area (A) Isotherm

The surface pressure (Π)-surface area (A) isotherms of the mucus mimetic 1 before and after spreading DPPC were studied. The surface pressure (Π) = γ_0-γ[119], where γ_0 is the surface tension of a surfactant-free interface and γ is the surface tension of the surfactant covered interface, and surface area (A) is the surface area of the Langmuir

trough. To investigate the effect of albumin on the surface activity of DPPC on mimetic subphase, the Π/A isotherms of 1% albumin solution in phosphate buffer (pH 7.4) was studied as a control. The Π/A isotherms were performed at room temperature (23°C). A Langmuir-Blodgett (LB) Teflon coated trough (KSV Instruments, Finland) of a working area of 558 cm^2 was placed on a vibration isolation table inside a home-built environmental chamber. The LB trough is equipped with a double barrier system and a Wilhelmy platinum plate (20 ×10 mm) plate attached to a microbalance (KSV Instruments, Finland) to record the surface pressure. Before each experiment, the LB trough and barriers were thoroughly cleaned with ethanol and de-ionized water, and the surface was aspirated by a tube connected to a vacuum-aspirator. A volume of 300 ml of subphase was poured into the LB trough. The Wilhelmy plate was dipped into the subphase and the surface pressure was monitored. The subphase was allowed to equilibrate for 15 minutes at room temperature, and the initial surface tension was recorded. For the Π/A isotherms of the DPPC film on the mucus mimetic subphase and the aqueous subphase containing 1% albumin, 223 µL of 1.0 mg/ml DPPC in n-hexane:methanol (95:5 v/v) was spread at the air-fluid using Hamilton micro-syringe. The amount of DPPC added to the surface is equivalent to the amount required to achieve a surface tension of ~ 32 mN/m on a water subphase. After spreading DPPC, 15 minutes were allowed for the solvent to evaporate and the initial surface tension was reported. The barriers were then compressed a rate of 15 mm/min to an area reduction of 91.4% and the surface tension monitored using LayerBuilder software. The isotherm for each compression cycle was recorded for at least three samples.

3.2.6. Surface Shear Rheology

Figure 3-3 illustrates the four systems used in this study: bare mucus mimetic 2, bare mucus mimetic 1, DPPC spread onto the mucus mimetic 1 subphase, and DPPC spread onto water subphase. The surface shear rheology of the four systems was probed

using an interfacial stress rheometer (ISR 400; KSV Instruments, Finland). The ISR, equipped with a Wilhelmy plate balance to measure surface tension, was placed on a vibration isolation table inside a home-built environmental chamber (Figure 3-2). The mucus mimetic 2 cross-linked *in-situ* was used without further modification for surface tension.

The mucus mimetic and water subphases were spread into a Plexiglas mini-trough (7.5 cm x 12 cm) with a glass channel (100 mm length, 9.6 mm width, 6.5 mm height) positioned in the middle of the trough (Figure 3-1). For each experiment, 60 ml of subphase was poured into the mini-trough until a meniscus was formed within the glass channel and climbed the top of the channel walls. Then the surface tension for the fluid subphases was modified, as described in section 3.2.3. A Teflon-coated magnetized needle (32 mm length, 546 μm diameter) was placed at the air-fluid interface within the channel and was subjected to an oscillatory magnetic force generated by a pair of Helmholtz coils to create a surface shear stress. The resulting needle motion was detected by tracking the needle tip using a Firewire camera (Basler A601f, Go Edmund Industrial Optics) with 512 x 480 pixel resolution. From the magnetic force applied to the needle (surface stress, σ_s) and the resulting surface strain (γ_s), the dynamic surface modulus (G_s^*) was determined by relating the surface stress (σ_s) to the surface strain (γ_s):

$$G_s^*(\omega) = \sigma_s(\omega) / \gamma_s(\omega)$$

The dynamic surface modulus (G_s^*) is a complex number which can be described by:

$$G_s^* = G_s' + iG_s''$$

where the real part, G_s', is the surface shear storage (or elastic) modulus and the imaginary part, G_s'', is the surface shear loss (or viscous) modulus. G_s' and G_s'' were determined from the phase lag (δ) (Figure 3-) between the surface strain (γ_s) and the surface stress (σ_s), where:

$$G_s' = G_s^* \cos\delta \text{ and } G_s'' = G_s^* \sin\delta$$

For surface rheological studies, the surface linear viscoelastic region (SLVR) was determined for each interface by conducting strain-dependent surface rheology. In this test, strain amplitude was varied sinusoidally with time at a fixed frequency of 1.56 rad/sec [equivalent to 0.25 Hz which corresponds to normal breathing frequency[50]]. On the basis of this test, a value of desired amplitude was selected over a region where G_s' and G_s" were independent of strain or exhibited weak dependence on strain. Subsequently, time-dependent and frequency-dependent surface rheological tests were performed. In the time-dependent tests, G_s' and G_s" were determined every 15 minutes for 120 or 165 minutes at a fixed frequency of 1.56 rad/sec. In the frequency-dependent tests, G_s' and G_s" were determined over a range of frequencies from 0.63-25.04 rad/sec. G_s' and G_s" were determined for at least three separate samples.

3.2.7. Statistical Analysis

Differences between groups of the time-dependent G' and G" were analyzed by one-way analysis of variance (ANOVA). Statistical significance was determined by 2-way ANOVA analysis for comparing the time-dependent surface rheological shear moduli among surface systems for an unbalanced number of samples using a general linear model. Levels of significance were accepted at the $p<0.05$ level. Statistical analyses were performed using Minitab 15 software.

3.3. Results and Discussion

3.3.1. Altering the Surface Tension of Mucus Mimetic

Table 3-1 illustrates surface tension measurements of the mucus mimetic 1 after different volumes (30, 60, 90 and 100 µL) of a 1.02 mg/ml solution of DPPC in n-hexane:methanol (95:5 v/v) were added to the air-mimetic interface. The surface tension of the mucus mimetic was lowered from 53.25 ± 1.22 mN/m to 30.16 ± 2.38 mN/m by spreading 100 µL DPPC onto the air-mimetic interface. However, a volume of only 36

μL of the DPPC solution was required to lower the surface tension of a water subphase to 33.18 ± 1.74 mN/m (n=12). The surface molecular area of DPPC on the water subphase was determined to be 33 $Å^2$/ molecule, in good agreement with that reported by Notter *et al*. (36-40 $Å^2$/ molecule).[120]

If the DPPC created a monolayer on the mimetic subphase, the equivalent surface molecular area would be 12$Å^2$/molecule. This is physically impossible given the molecular size of the DPPC polar headgroups. The greater amount of DPPC needed to lower the surface tension of the mucus mimetic to ~ 32 mN/m compared to that of water (ratio 3:1) suggests that that multilayers were formed on the surface.

Spreading DPPC onto the mimetics with high viscoelastic properties at low frequency (mimetics 2 and 3) encountered difficulties due to the more solid-like behavior of the surfaces. Kaneko *et al.*[116] have studied the spreading of liquids (ethanol, silicon oil and diethyl ether) onto polymeric aqueous solutions of 2-acrylamido-2-methyl-propanesulfonic acid (PAMPS) and onto chemically cross-linked gels of PAMPS with different amounts of cross-linking agent. It has been shown that the spreading exponent (α) decreases linearly with an in the elasticity (G') of the underlying viscoelastic subphase. However, for the chemically cross-linked PAMPS gel, it was found that α is independent on PAMPS concentration and that the spreading on an elastic gel surface is similar to that on a solid surface. Due to these difficulties, only mimetic with low viscoelastic properties at low frequency (mimetic 1) was used for the further studies.

3.3.2. Fluorescence Microscopy of Surfaces

Fluorescence microscopy was used to monitor the spreading of DPPC on the interface and to visualize the equilibrium surfactant structure at the interface. Texas Red-DHPE was added to the surfactant solution prior to spreading to enable visualization of the fluid front during spreading and the disordered fluid phases during equilibrium (the liquid condensed phases squeeze out the probe and therefore are visualized as black

domains).[121] However, clear differences in surfactant structure were observed when comparing the uncross-linked mimetic subphase (Figures 3-5) to the cross-linked mimetic subphase (Figure 3-6). When DPPC was spread on the uncross-linked mimetic surface, small spherical domains of ordered phase (black) interspersed within red regions of disordered phase were observed (Figure 3-5B). Similar spherical domains of DPPC are commonly observed on an aqueous subphase during surface compression, though notably at lower surface tensions.[122, 123] On the cross-linked mimetic surface, DPPC showed longer-range ordering, creating fairly large blocks of condensed fluid phases with thin finger-like projections of the disordered fluid phase (Figure 3-6B). Similar surface structures have been observed during the spreading of droplets on gel and solid surfaces, where surfactant spreading is resisted by the rigidity and viscous drag of underlying subphase.[116, 117, 124, 125] Note that slight background auto-fluorescence was observed for the mucus mimetic surface due to the unreacted aldehyde groups of GA (Figure 3-6A), hence the images appear brighter.[126] Albumin which is present in the mimetic subphase, may penetrate to the surface, due to its surface activity, forming a mixed DPPC/albumin film. Although the solubility of the dye is probably affected in the mixed DPPC/albumin film, the large amount of DPPC added to the surface showed the ordered phase. [127]

3.3.3. Surface Pressure-Area Isotherm

To study the phase states and surface activity of albumin and PGM, the surface pressure-surface area (Π/A) isotherm for the bare cross-linked mucus mimetic was obtained (Figure 3-7, Table 3-2). The initial surface tension of the mucus mimetic was 50.68 ± 0.29. The relatively low surface tension of the mucus mimetic, compared to that of water (surface tension of 72 mN/m), suggests that albumin and or mucin glycoproteins are surface active and adsorb to the interface.[128] During compression, the surface pressure exhibits a smooth non-linear increase over the entire compression range. Upon a 91.4% reduction in surface area, the air-mimetic interface was compressed up to a surface

pressure of 23.08 ± 1.31 mN/m. The Π/A isotherm of the mucus mimetic lacks the solid, liquid-condensed, liquid-expanded, and gas phases, which are normally observed in Π/A isotherm of the DPPC monolayer onto water subphase.

To study the phase states and surface activity of DPPC in the presence of albumin in the subphase, 1% albumin solution was added to the subphase and surface tension measured during compression (Figure 3-8, Table 3-3). The initial surface tension of the 1% albumin solution was 54.34 ± 0.29 mN/m. Upon the addition of 100 µL of 1 mg/ml DPPC to the surface, the surface tension decreased to 42.39 ± 1.54 mN/m. This surface tension was higher than that obtained when the equivalent amount of DPPC was added on the water subphase 33.18 ± 1.74 mN/m (n=12). This indicates that the adsorption of DPPC onto the surface is decreased by the presence of albumin. It has been shown by Zasadzinski *et al.*[128] that albumin reduces surfactant adsorption at the interface, thus does not allow sufficient lowering in surface tension. Upon compression, the surface pressure initially increases rapidly up to 18.5% compression. Upon further compression (from 18.5 to 28% reduction in maximum surface area), the isotherm exhibited a small shoulder. Compression beyond 28% led to a plateau region at a surface pressure of 42.39 ±1.54 mN/m. the wide plateau region is indicative of a film collapse, where multilayers are formed.

In addition, to study the phase states and surface activity of DPPC spread at the air-mimetic interface of the cross-linked mucus mimetic, the Π/A isotherm was obtained (Figure 3-9, Table 3-4). The initial surface tension of the mucus mimetic before the addition of DPPC was 51.5 ± 2.4. Upon the addition of 100 µL of 1.0 mg/ml DPPC, the surface tension decreased to 45.28 ± 1.17 mN/m. This surface tension is higher than that obtained for DPPC on the water subphase with and without albumin. The Π/A isotherm of mimetic covered with DPPC sharply differs than that of the typical Π/A isotherm for DPPC spread on water. Initially, when the interface compressed to 54% of the maximum surface area, the Π/A isotherm showed a shallow slope where surface pressure increases

slowly with the reduction in the mean molecular area of DPPC. Upon further compression (41% reduction in maximum surface area), the isotherm exhibited a steep slope, where surface pressure increases rapidly with little change in surface area. When the interface is further compressed (91.4% reduction in maximum surface area), DPPC film collapse occurs with a plateau region of a surface pressure of 43.46 ± 2.62 mN/m. The high surface pressure values for the DPPC film onto the mimetic surface during compression indicated that the DPPC film exhibited the liquid condensed phase. The ordered phase of the DPPC domains observed in fluorescence image of the cross-linked mimetic covered with DPPC was in good agreement with its Π/A isotherm (Figure 3-6B). Comparing the three Π/A isotherms (bare mucus mimetic, DPPC film on mimetic subphase, DPPC film on 1% albumin subphase), the following observation were noted:

1) in the bare mimetic, no plateau region was observed.
2) DPPC film on 1% albumin attained the plateau region upon lower surface area reduction compared to that of DPPC on mimetic subphase (maximum surface area reduction: 30% for DPPC film on 1% albumin vs. 60% for DPPC film on mucus mimetic).
3) Both DPPC films on 1% albumin and mimetic subphases attain relatively equal value for the surface pressure of the plateau region.

3.3.4. Surface Shear Rheology

It is known that surfactants adsorbed at fluid interfaces exhibit a complex viscoelastic rheological property, where resistance of the film to flow can be attributed to surface viscosity and rigidity of the film can be attributed to surface elasticity. If surface viscosity dominates surface elasticity (G_s”>G_s’), then the surface is more viscous (or liquid-like) in nature. However, if surface elasticity dominates surface viscosity (G_s’>G_s”), then the surface is more elastic (or solid-like) in nature.[119]

3.3.4.1. Surface Linear Viscoelastic Region

Surface rheological studies were conducted to determine the surface linear viscoelastic region (SLVR) for each system. Exceeding the critical deformation is destructive to the surface. However, no definitive values for the acceptable percent of deviation from the linear region have previously defined for the surface rheological studies. In this study, a percent deviation in the surface moduli of less than 15% was considered within the linear region. The SLVR was determined at a frequency of 1.56 rad/sec for each surface by systematically increasing the oscillation strain amplitude.

The strain-dependence of surface shear rheology for the mucus mimetic 2 was probed over a strain amplitude range of 0.004-0.017 (Figure 3-10). G_s' and G_s" exhibited weak dependence on strain amplitude increasing by ~ 9% and ~ 7% for G_s' and G_s", respectively, over the entire range probed.

The strain-dependence of surface shear rheology for the mucus mimetic 1 was probed over a larger strain amplitude range of 0.004-0.025 (Figure 3-11). G_s' and G_s" of mucus mimetic exhibited weak dependence on strain amplitude increasing by ~ 14% over the entire range probed. Therefore, the SLVR was limited to small strains (0.004-0.017).

Upon addition of DPPC to the mucus mimetic 1 surface, the surface viscoelasticity decreased, allowing a wider range of strain amplitudes to be probed (Figure 3-12). G_s" exhibited a weak dependence on strain amplitude over the entire range probed (0.007-0.166). Beyond a critical strain of 0.044, G_s" decreased with deformation by ~ 13%, whereas, G_s' decreased with deformation by ~ 42%. Therefore, the SLVR for the mucus mimetic with DPPC was limited to strains of 0.007-0.044.

Upon addition of DPPC to the water surface, the surface viscoelastic properties decreased allowing a range of strain amplitudes of 0.010-0.090 to be probed (Figure 3-13). G_s" exhibited a weak dependence on strain amplitude over the entire range probed (0.01-0.09), decreasing by ~ 14%. G_s' decreased with deformation by ~ 62%. Therefore, the SLVR for water with DPPC was limited to strains of 0.010 to 0.090.

3.3.4.2. Time-Dependent Surface Shear Rheology

The time-dependence of surface shear rheology at a constant frequency of 1.56 rad/sec was probed to gain insight into the behavior of the large conducting airways during normal breathing. Time-dependent studies for each surface were conducted at a constant strain amplitude within the LVR.

The mucus mimetic 2 exhibited high surface viscoelasticity with large G_s' and G_s" values over the entire time profile (120 min). The surface of the mucus mimetic was primarily more elastic, where G_s' dominated G_s" (Figure 3-14, Table 3-5). For the mucus mimetic 1 at all time points, G_s' dominated G_s", indicating a more elastic surface (Figure 3-15, Table 3-5). The mucus mimetic exhibited an increase in surface viscoelastic properties over the time profile. This increase in surface viscoelastic properties suggests either aging of the system or further cross-linking due to unreacted GA.

To test if further cross-linking of the mucus mimetic was observed in the bulk phase, the time-dependent bulk rheological behavior of the mimetic was probed (using the cone and plate rheometer) at frequency of 1.56 rad/sec. The bulk shear storage modulus G' and bulk shear loss modulus G" showed continuous increase over the first 30 minutes of measurement (Figure 3-16). Although no significant changes in the bulk viscoelastic properties were observed for the mucus mimetic after 30 min of cross-linking, it is possible that further cross-linking was observed via the surface rheological studies given the higher sensitivity of the ISR technique. In addition, it has been reported that GA cross-linking is enhanced at high temperatures.[91] Thus continuous cross-linking of mimetic subphase by GA may be observed due to the change in mimetic temperature where mimetic cross-linking was taken place at 4°C while surface rheological studies were conducted at room temperature (22°C).

When DPPC was spread at the air-mimetic interface, the surface exhibited a more viscous behavior, where G_s" dominated G_s' (Figure 3-17, Table 3-5). This change in behavior of the mimetic surface from more elastic to more viscous was due to a

considerable decrease in the surface elastic modulus after DPPC spreading ($p<0.05$). More viscous behavior was also observed for DPPC monolayers on an aqueous Newtonian subphase ($p<0.05$) (Figure 3-18, Table 3-5) in agreement with previous studies on DPPC monolayers.[114, 115]

Probing the surface rheological behavior of the tracheal mucus is important for understanding the surface properties of the large conducting airways. To date the surface properties of the air-mucus interface, which has a surface tension of ~ 32 mN/m, is still not well understood. Although the tracheal mucus is viscoelastic (non-Newtonian) fluid,[15, 129] the presence of surfactants at the air-mucus interface, influences mucus surface properties giving it more viscous behavior.

3.3.4.3. Frequency-Dependent Surface Shear Rheology

The frequency-dependence of surface shear rheology was probed to provide new behavior of the large conducting airways with increasing the rate of surface deformation. The surface rheological behavior of each interface was determined over a frequency range of 0.63-25.04 rad/sec.

For the mucus mimetic 2, G_s' and G_s" increased with increasing frequency. G_s' dominated G_s" for all frequencies probed (0.63 to 25.04 rad/sec), indicating a more elastic surface (Figure 3-19, Table 3-5). The mucus mimetic 1 exhibited more elastic behavior over a smaller frequency range of 0.63 to 10 rad/sec (Figure 3-20, Table 3-5). Beyond a frequency of 10 rad/sec, G_s' decreased with frequency, leading to a crossover point at 15 rad/sec. Since G_s" increased over the entire frequency range, the surface exhibited more viscous behavior after the crossover point.

Upon spreading DPPC at the air-mimetic interface, the surface exhibited a more viscous behavior over the entire frequency range (Figure 3-21, Table 3-5). G_s' increased with frequency over a frequency range of 0.63-8 rad/sec, and then decreased with frequency over the range of 10-25.04 rad/sec. G_s" of the increased throughout the entire

frequency range (0.63-25.04 rad/sec). The surface elastic modulus G_s' significantly decreased with the addition of DPPC to the surface [1.45 mN/m at 1 rad/sec and 2.82 mN/m at 10 rad/sec for the mucus mimetic with DPPC versus 6.06 mN/m at 1 rad/sec and 9.97 mN/m at 10 rad/sec for the bare mucus mimetic], while no significant change in the surface viscous modulus was observed. This suggests that the measured surface moduli were primarily influenced by surface forces, although subphase drag on the needle cannot be completely ignored (see section 3.3.4.4).

As a control experiment, the surface rheological properties of a water subphase with DPPC spread at the interface were probed. The DPPC-water surface exhibited a more viscous behavior over the entire frequency probed (0.63-25.04 rad/sec), where G_s" dominated G_s' (Figure 3-22, Table 3-5). G_s' increased with frequency over a frequency range (0.63-8 rad/sec), and then a reduction in G_s' values was observed over the high frequency range (10-25.04 rad/sec). G_s" of the DPPC monolayer increased with frequency throughout the entire frequency range (0.63-25.04 rad/sec).

Therefore, bare mimetics 1 and 2 exhibited a more elastic surface behavior. However, spreading DPPC on the mimetic 1 subphase altered the physical behavior of the surface to more viscous. DPPC on water subphase exhibited a more viscous surface, similar to that of DPPC on mimetic subphase. However, lower values for G_s' and G_s were observed for water with DPPC compared to that of mimetic with DPPC, suggesting the subphase effect.

As mentioned above, a significant drop in G_s' values was observed at high frequencies for the mucus mimetic 1, mucus mimetic 1 with DPPC and water with DPPC surfaces (Figures 3-20, 3-21, and 3-22). However, no deviation in G_s' was observed for the mucus mimetic 2 at high frequency (Figure 3-15). It has been shown by Brooks that at high frequencies, the needle dynamic motion, which is proportional to the rod inertia, is dominated by the viscous forces from the subphase. However at low frequency, the subphase viscous force dominates the needle's behavior, thus the rod inertia has no effect

in this case.[119] The drop in G_s' of the DPPC covered surfaces (both mimetic and water subphase) occurred at a frequency lower than that of the bare mucus mimetic (8 rad/sec vs. 10 rad/sec). This decrease in the drop frequency is attributed to the less elastic behavior of the DPPC covered surfaces.

3.3.4.4. Boussinesq Number

The sensitivity of the ISR is dependent on the coupling of both the measurement probe (the magnetic needle) and the monolayer with the surrounding bulk subphase. The presence of a drag force exerted by the bulk phase complicates the interfacial analysis.[119] The Boussinesq number (Bo) is a dimensionless number which indicative of the relative importance of the surface and subphase contributions. It measures the ratio of interfacial to bulk viscous effects:[119,130]

$$Bo = \frac{\eta_s}{\eta \cdot a}$$

where η_s is the interfacial shear viscosity (Pa· s· m), η is the bulk shear viscosity (Pa·s), and a is the characteristic length scale (m). The interfacial shear viscosity (η_s) can be approximated as $\eta_s = G_s''/\omega$ and the bulk shear viscosity $\eta = G''/\omega$, where ω is the frequency. The characteristic length scale in this system is the diameter of the needle.

Bo was determined in this study to verify the contribution of the subphase stresses to the reported surface rheological data. If coupling is present between the subphase and the surface, then the stress that is applied to the surface may be dissipated into the subphase instead through the film. When Bo>1, the surface stress is larger than subphase stress; however, when Bo<1, the subphase stress is larger than surface stress.[50, 131] Brooks showed that Bo should exceed 100 for a surface to be completely decoupled from the subphase and for a surface to behave as a two-dimensional fluid.[119] However, all the experimental work of Brooks was based on an aqueous Newtonian (water) subphase,

where polymers (such as phthalocyaninatopolysiloxane and poly(ethylene imine-co ethyl oxazoline)) were spread onto the air-water interface. The spreading of these polymers on clean water increased the elastic contribution at the interface and made the interface non-Newtonian by increasing the surface elastic modulus G_s' and surface viscous modulus G_s". However, if the bulk viscosity is higher than that of water, a subphase drag contribution is expected. Recently, it has been shown that the additive method[130 132]can be used to determine the true viscoelastic properties of the monolayer. In this method, the surface viscoelastic properties for a reference test with pure water (subphase or surfactant-free interface) is obtained and then subtracted from the surface viscoelastic properties obtained with the monolayer (subphase + interface). Although, the additive method may lead to substantial errors, it can account for the subphase drag. Erni *et al.*[130] calculated the values for the surface loss modulus G_s" of adsorption layers formed by modified starch by subtracting the blank value of the subphase stress from the total stress response (interface + bulk), assuming simple additivity of the interface and subphase rheological properties. They found that these calculated values were higher than those obtained for the interface + bulk that account for the coupling between the interface and bulk. The subtraction of the subphase is an approximation method, where the interfacial moduli might be overpredicted.

In this study, Bo was determined by relating the time-dependent surface shear rheology of the mucus mimetic 1 covered with DPPC (Figure 3-13) to the time-dependent bulk shear rheology of the mucus mimetic 1 (Figure 3-12). Bo was estimated using the following equation:

$$Bo = G_s'' / (G'' \cdot d)$$

where G_s" = surface shear loss modulus of mucus mimetic covered with DPPC, G" = bulk shear loss modulus of mucus mimetic, and d = diameter of the magnetic needle (0.546 mm).

Bo was found to be between 11-18 at all-time points (Figure 3-23); indicating that the surface viscoelastic forces dominated the bulk viscoelastic forces. However, it is obvious that Bo was smaller than those reported by Brooks[119] (Bo>100), indicating that subphase is coupled to the surface. The small values of Bo were attributed to high bulk viscoelastic properties of the subphase. Therefore, G_s' and G_s" should be considered "apparent" properties.

One method that could be used to increase the sensitivity of the interfacial rheometer would be to use a thinner rod. With a thinner rod, interfacial effects become more dominant since Bo is proportional to ~1/a. However, reducing the rod diameter also reduces the amount of magnetic material per unit rod length.[119] Therefore, optimization of the rod diameter, while maintaining the ability to move the rod using a magnetic field, would be required.

3.4. Conclusions

Although the mucus layer of the airway lining fluid (ALF) exhibited a bulk viscoelastic property, the continuous surfactant at the air-mucus interface that lowers the surface tension to ~ 32 mN/m, influence ALF surface properties. In addition, mucus contains serum proteins (albumin) and mucin glycoproteins which are surface active and adsorb at the interface, may have an impact on the surface properties of the tracheal mucus. The surface properties of the ALF are considered critical for normal function of the large conducting airways. The surface rheological behavior of dipalmitoyl-phosphatidylcholine (DPPC) covered the air-mucus interface, where the underlying subphase is viscoelastic, was studied using the interfacial stress rheometer. Spreading DPPC onto the mimetic subphase altered the physical behavior of the mimetic surface, leading to more fluid-like surface. In addition, the surface viscoelastic moduli were influenced by the subphase type, where lower values for G_s' and G_s" were observed onto the water subphase compared to those onto the mimetic subphase, indicating the

subphase effect on the surface behavior. The more liquid-like behavior of the mucus surface more likely influences the bioaerosol formation in the large conducting airways.

Table 3-1: Surface tension of the mucus mimetic 1 and surface area per DPPC molecule (if DPPC was added to water subphase) after the addition of different volumes of 1.02 mg/ml DPPC in n-hexane:methanol (95:5 v/v), measured using the Wilhelmy plate method; data are represented as the mean ± SD.

Subphase	**Volume of DPPC added (µL)**	**Surface tension (mN/m)**	**Equivalent surface area/DPPC molecule**
Mucus mimetic	0 µL	53.3 ± 1.2 (n=9)	NA
Mucus mimetic	30 µL	47.4 ± 2.1 (n=5)	40
Mucus mimetic	60 µL	43.3 ± 2.1 (n=6)	20
Mucus mimetic	90 µL	36.4 ± 4.1 (n=6)	13
Mucus mimetic	100 µL	30.16 ± 2.4 (n=4)	12
Water	36 µL	33.2 ± 1.7 (n=12)	30

* Equate surface area per DPPC molecule if DPPC was added to water subphase.

** DPPC was not added to the surface.

Table 3-2: Summary of the initial surface tension of the mucus mimetic 1 before compression and minimum surface tension reached upon complete compression of the air-mimetic interface.

Experiment #	**Initial surface tension (mN/m)**	**Minimum surface tension (mN/m)**
1	50.7	29.1
3	51.0	26.9
4	50.4	26.9
Mean ±SD	**50.7±0.3**	**27.6±1.3**

Table 3-3: Initial surface tension of the 1% albumin solution before and after spreading DPPC and minimum surface tension reached upon complete compression of the air-fluid interface.

Experiment #	**Initial surface tension of 1% albumin (mN/m)**	**Initial surface tension of 1% albumin with DPPC (mN/m)**	**Minimum surface tension (mN/m)**
1	55.3	41.0	13.6
2	53.4	43.9	10.7
3	55.0	41.2	14.0
4	53.7	43.6	10.1
Mean ±SD	**54.3±0.9**	**42.4±1.5**	**12.1±1.1**

Table 3-4: Summary of the initial surface tension of the mucus mimetic 1 with DPPC before compression and minimum surface tension reached upon complete compression of the air-mimetic interface.

Experiment #	**Initial Surface tension of mimetic (mN/m)**	**Initial surface tension of mimetic with DPPC (mN/m)**	**Minimum surface tension (mN/m)**
1	51.2	44.4	8.1
2	49.3	44.8	8.3
3	54.0	46.6	7.8
Mean ±SD	**51.5±2.4**	**45.3±1.2**	**8.1±2.6**

Table 3-5: Surface properties of the mucus mimetic 2, mucus mimetic 1, mucus mimetic 1with DPPC and water with DPPC.

Interface	**Surface tension (mN/m)**	**G_s' at 1 rad/sec (mN/m)**	**G_s" at 1 rad/sec (mN/m)**	**Surface behavior**
Mucus mimetic 2	76.8 ± 5.8 (n=3)	26.0 ± 2.1 (n=3)	6.9 ± 1.2 (n=3)	$G_s' > G_s''$ more elastic
Mucus mimetic 1	53.3 ± 1.2 (n=9)	6.1 ± 1.8 (n=3)	2.7 ± 1.6 (n=3)	$G_s' > G_s''$ more elastic
Mucus mimetic 1 with DPPC	30.2 ± 2.4 (n=4)	1.5 ± 0.9 (n=4)	1.9 ± 0.6 (n=4)	$G_s' < G_s''$ more viscous
Water with DPPC	33.2 ± 1.7 (n=12)	0.4 ± 0.1 (n=4)	1.1 ± 0.3 (n=4)	$G_s' < G_s''$ more viscous

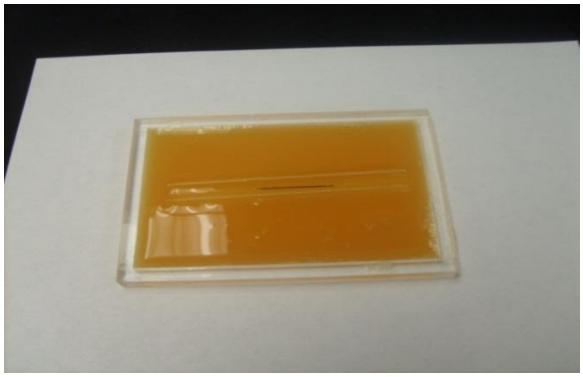

Figure 3-1: A Plexiglas mini-trough (7.5 cm x12 cm) with a glass channel (100 mm length, 9.6 mm width, 6.5 mm height) positioned in the middle of the trough to place a magnetized needle at the air-fluid interface.

Figure 3-2: The interfacial stress rheometer (ISR) placed on a vibration isolation table inside a home built environmental chamber used to measure the surface shear rheology of interfaces.

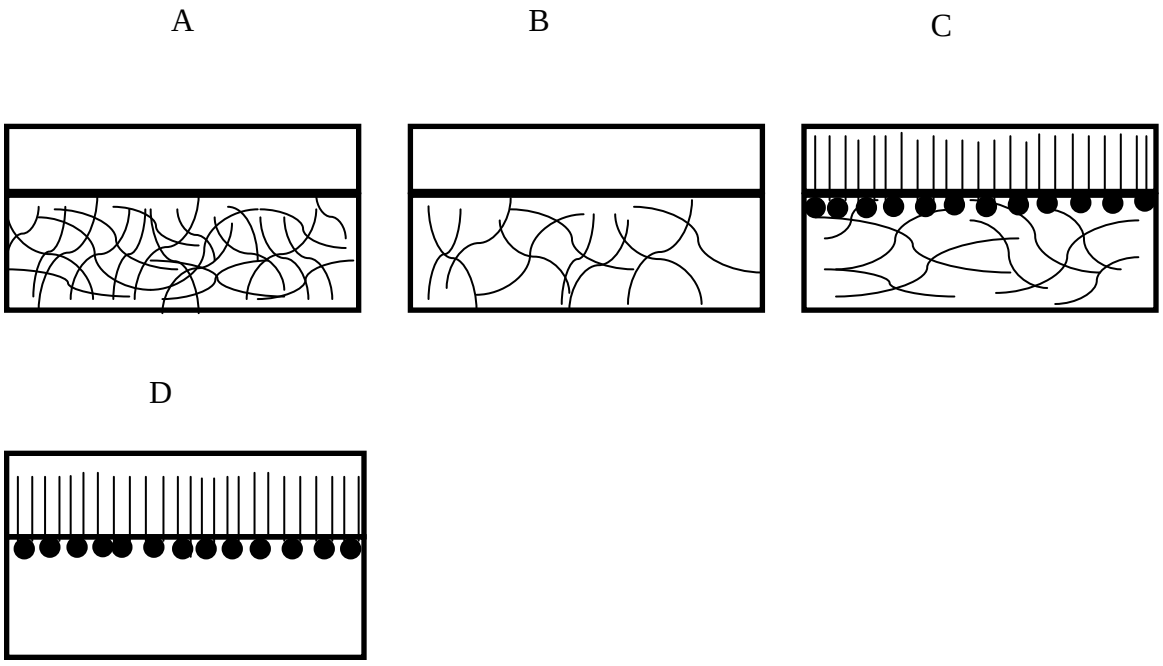

Figure 3-3: Sketches of (A) mucus mimetic 2, (B) mucus mimetic 1, (C) DPPC spread on mucus mimetic 1 subphase, and (D) DPPC spread on water subphase.

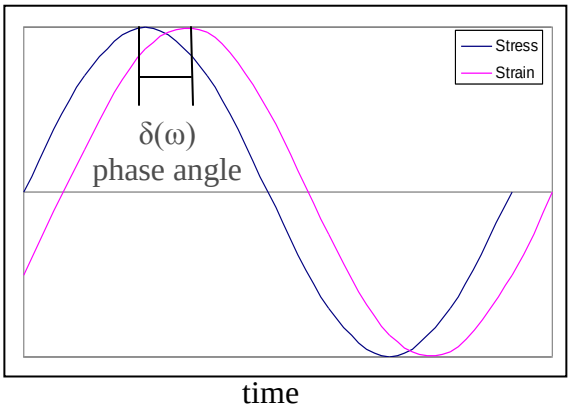

Figure 3-4: The phase angle (δ) shift between the surface strain (γ_s) and the surface stress (σ_s),

A

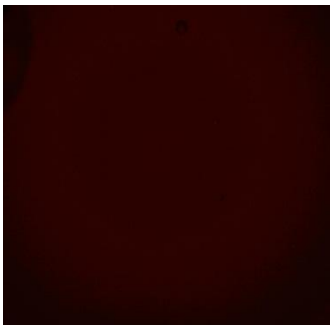

B

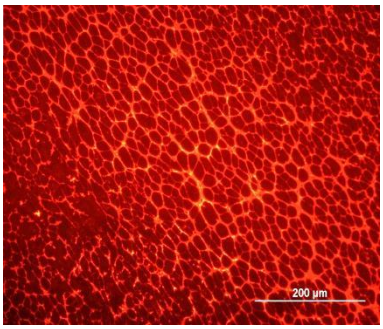

Figure 3-5: Fluorescence micrographs of (A) uncross-linked mucus mimetic surface (before the addition of DPPC), and (B) uncross-linked mucus mimetic surface with DPPC at the surface (surface tension=32 mN/m).

A

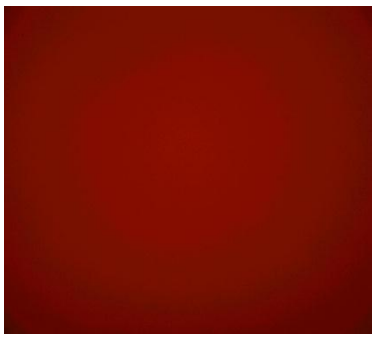

B

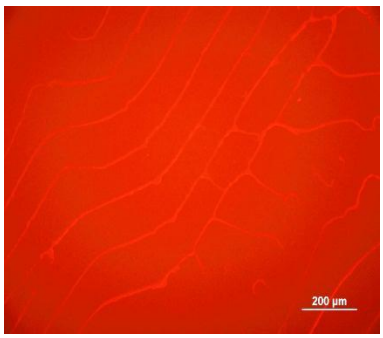

Figure 3-6: Fluorescence micrographs of (A) mucus mimetic 1 surface (before the addition of DPPC), and (B) mucus mimetic 1 surface with DPPC at the surface (surface tension=32 mN/m).

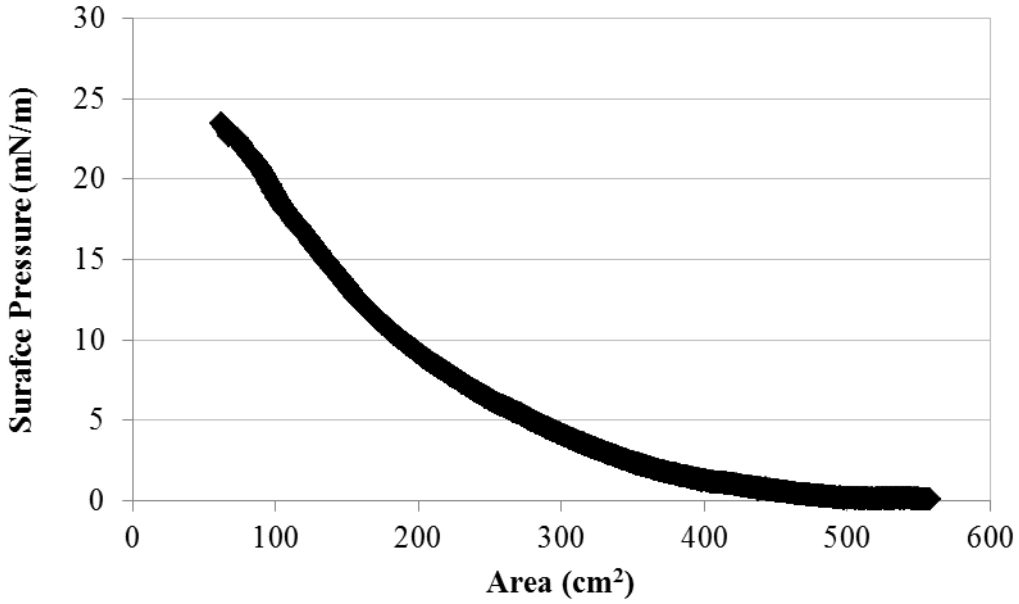

Figure 3-7: Surface pressure-surface area isotherm of the air-mimetic interface during compression.

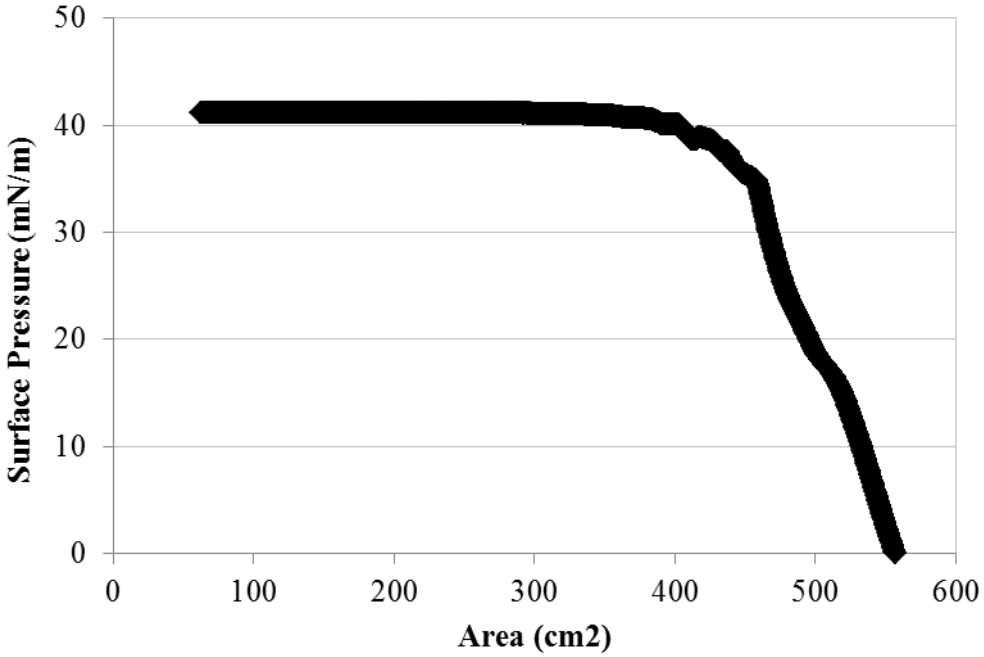

Figure 3-8: Surface pressure-surface area isotherm of a DPPC film on an aqueous subphase containing 1% albumin solution, during compression.

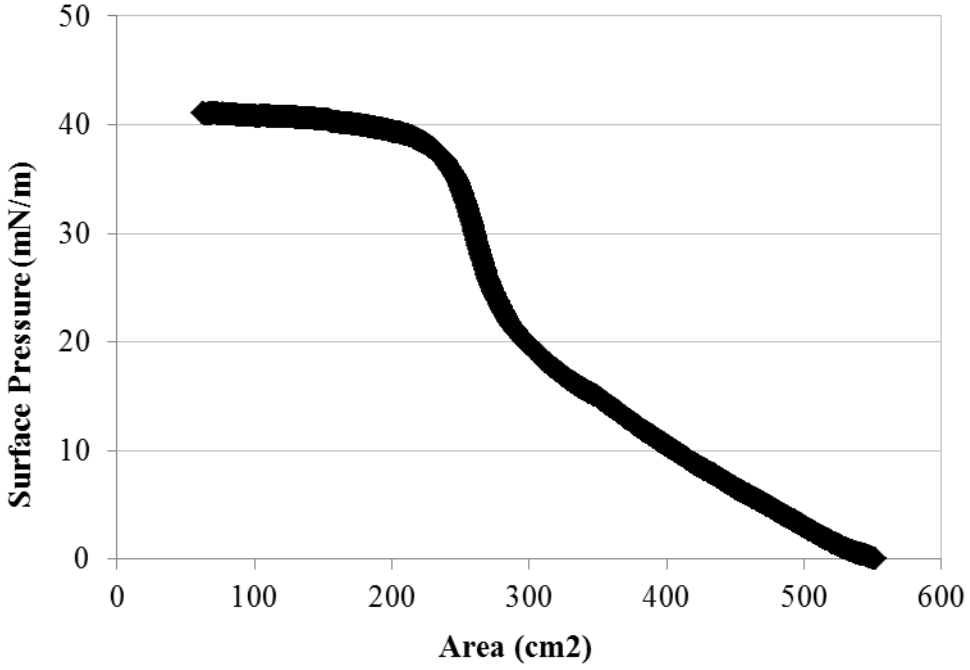

Figure 3-9: Surface pressure-surface area isotherm of the DPPC covered mucus mimetic interface, during compression.

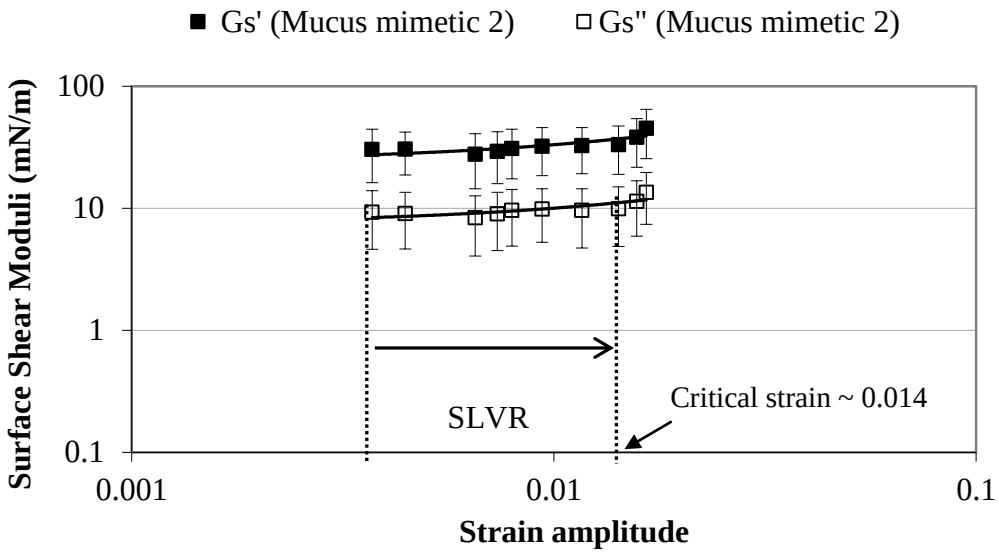

Figure 3-10: Strain-dependence of surface shear storage modulus G_s' and surface shear loss modulus G_s" at a fixed frequency of 1.56 rad/sec for the mucus mimetic 2 over strain range of (0.004-0.017). The surface linear viscoelastic region (SLVR) and the critical strain at which the interfacial moduli deviate from SLVR are indicated by arrows. Data are represented as the mean ± SD (n=3).

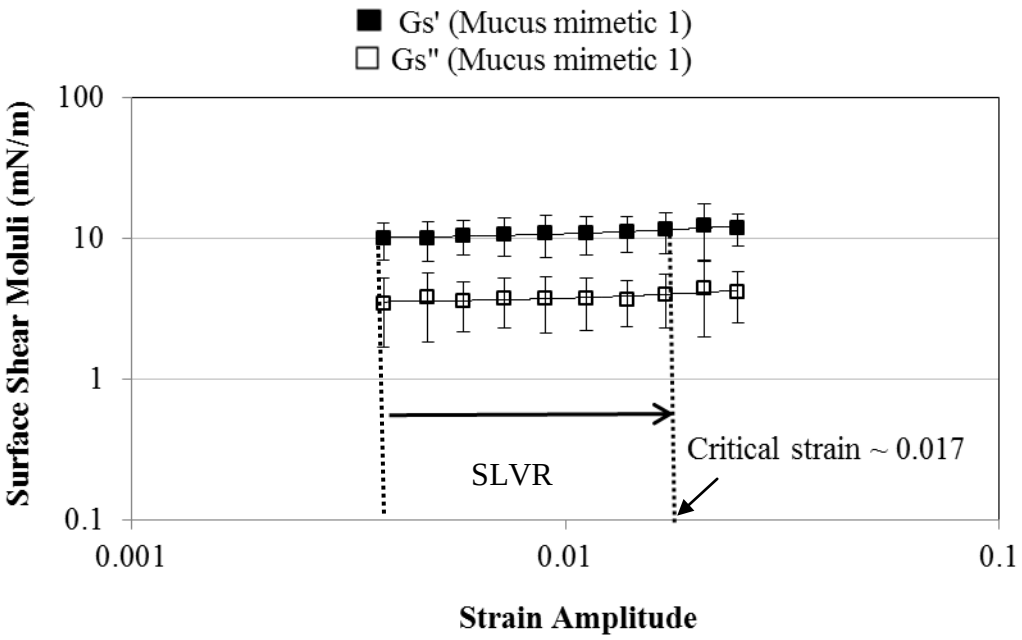

Figure 3-11: Strain-dependence of surface shear storage modulus G_s' and surface shear loss modulus G_s" at a fixed frequency of 1.56 rad/sec for the mucus mimetic 1 over strain range of (0.004-0.025). The surface linear viscoelastic region (SLVR) and the critical strain at which the interfacial moduli deviate from SLVR are indicated by arrows. Data are represented as the mean ± SD (n=3).

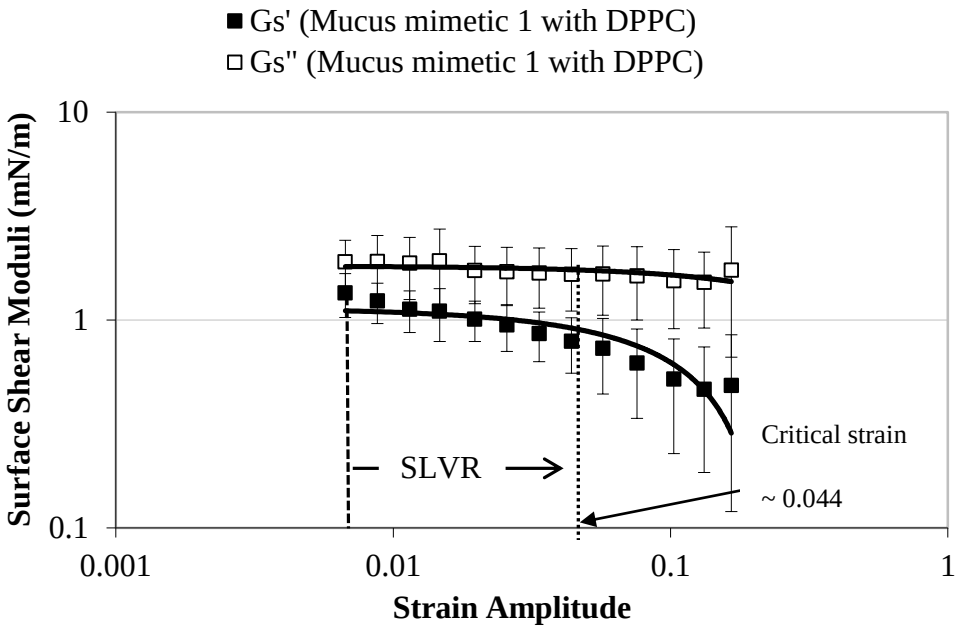

Figure 3-12: Strain-dependence of surface shear storage modulus G_s' and surface shear loss modulus G_s" at a fixed frequency of 1.56 rad/sec for DPPC spread at an air-mimetic interface over strain range of (0.007-0.166). The surface linear viscoelastic region (SLVR) and the critical strain at which the interfacial moduli deviate from SLVR are indicated by arrows. Data are represented as the mean ± SD (n=4).

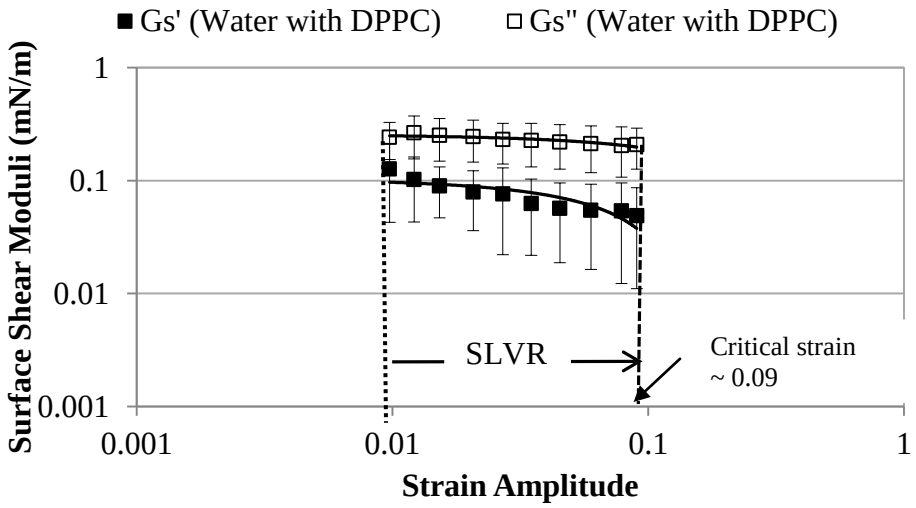

Figure 3-13: Strain-dependence of surface shear storage modulus G_s' and surface shear loss modulus G_s" at a fixed frequency of 1.56 rad/sec for DPPC spread at an air-water interface over strain range of (0.010-0.090). The surface linear viscoelastic region (SLVR) and the critical strain at which the interfacial moduli deviate from SLVR are indicated by arrows. Data are represented as the mean ± SD (n=3).

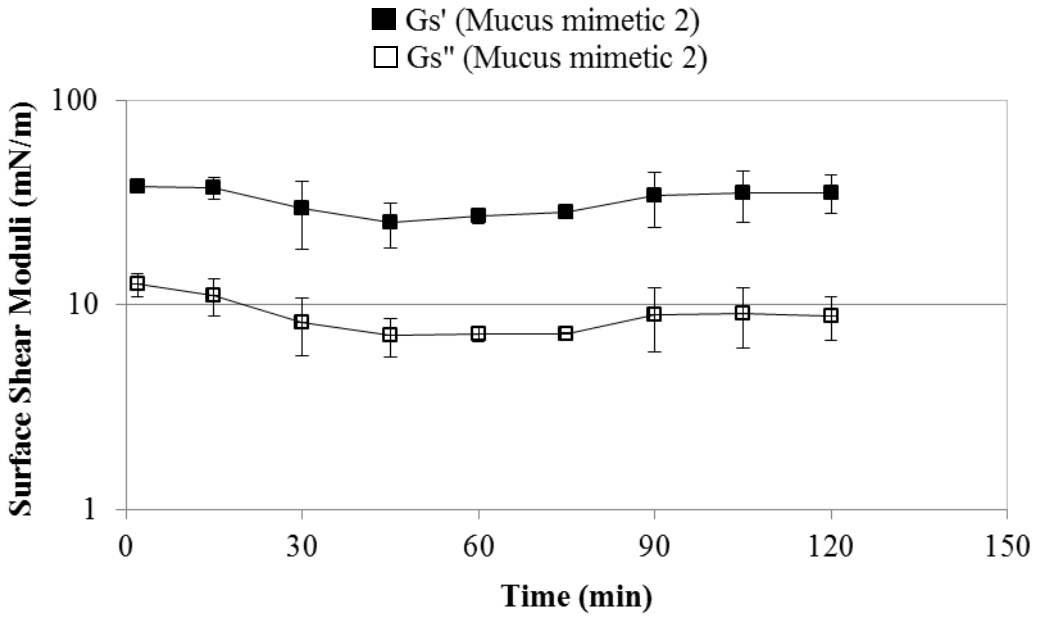

Figure 3-14: Time-dependence of surface shear storage modulus G_s' and surface shear loss modulus G_s" for the mucus mimetic 2. Data are represented as the mean ± SD (n=3).

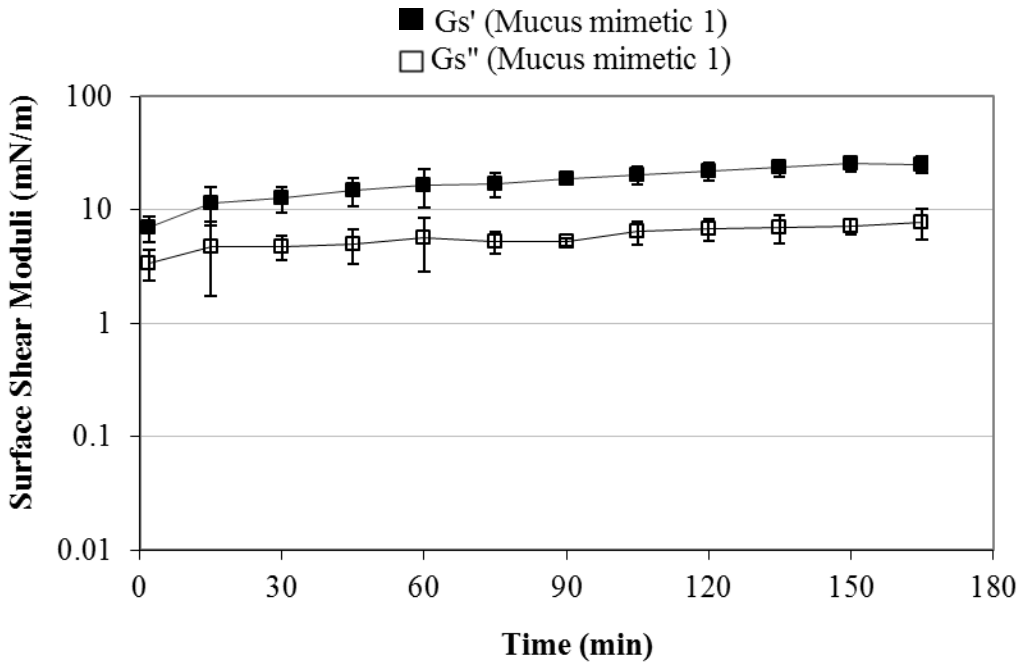

Figure 3-15: Time-dependence of surface shear storage modulus G_s' and surface shear loss modulus G_s" for the mucus mimetic 1. Data are represented as the mean ± SD (n=5).

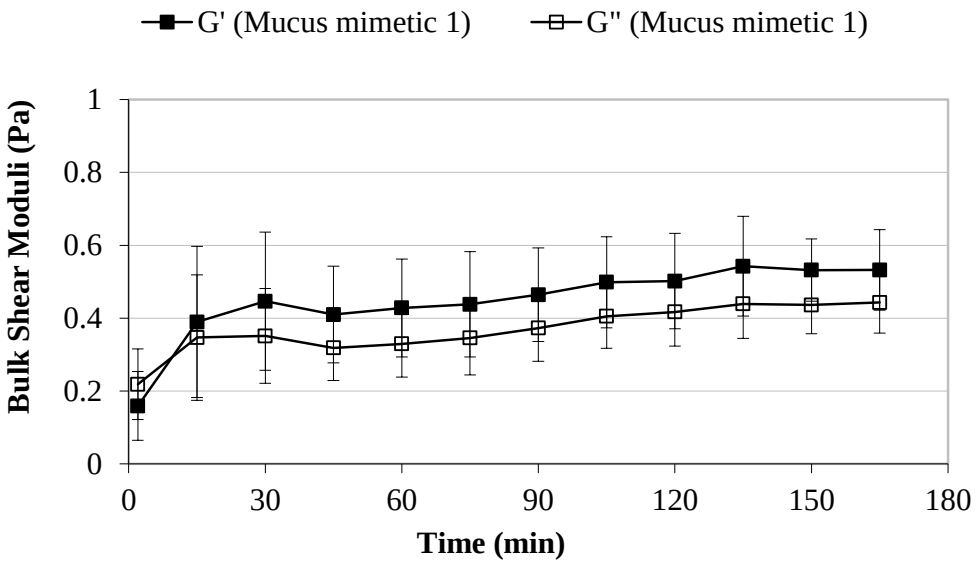

Figure 3-16: Time-dependence of bulk shear storage modulus G’ and bulk shear loss modulus G” of the mucus mimetic 1 at a frequency of 1.56 rad/sec. Data are represented as the mean ± SD (n=5).

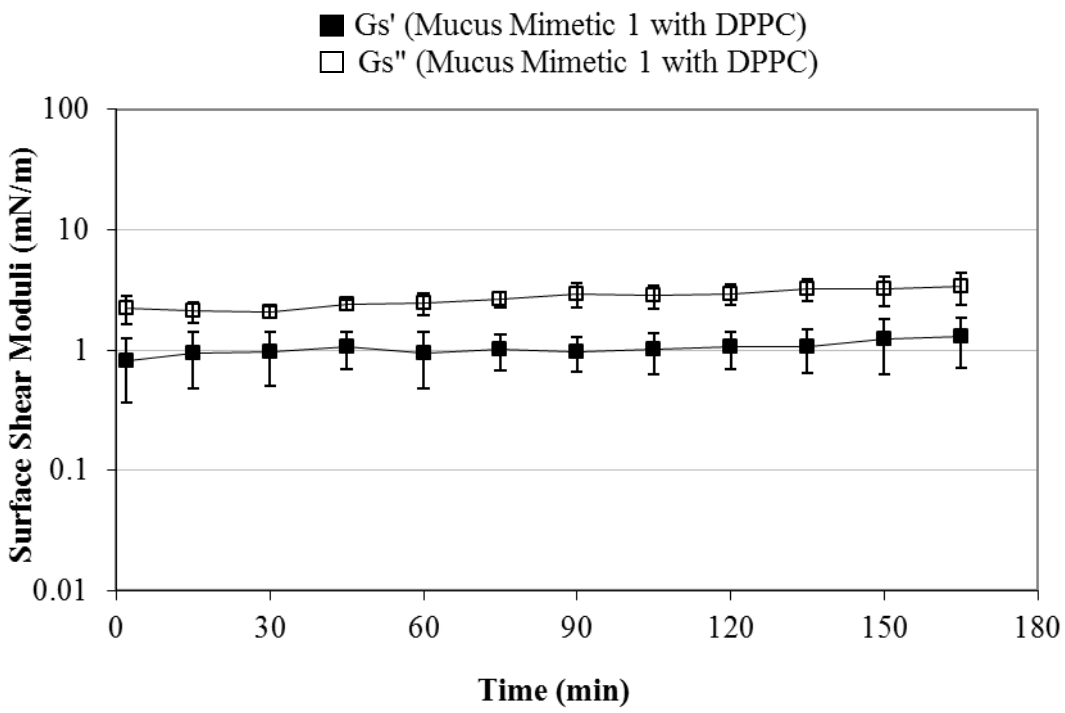

Figure 3-17: Time-dependence of surface shear storage modulus G_s' and surface shear loss modulus G_s" for DPPC spread at an air-mimetic interface. Data are represented as the mean ± SD (n=4).

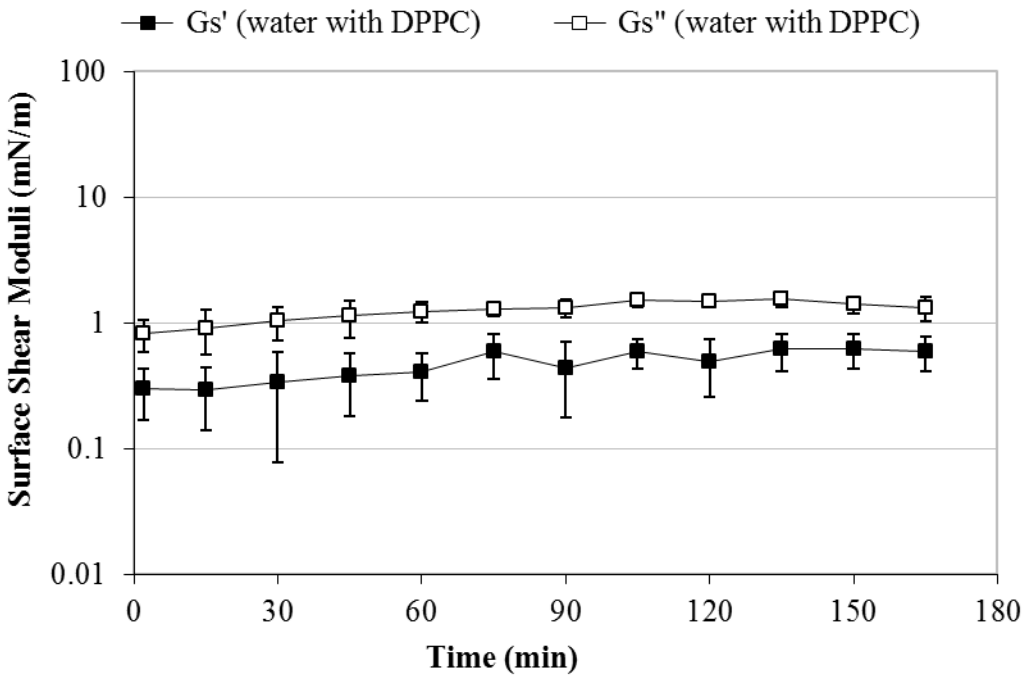

Figure 3-18: Time-dependence of surface shear storage modulus G_s' and surface shear loss modulus G_s" for DPPC spread at an air-water interface. Data are represented as the mean ± SD (n=4).

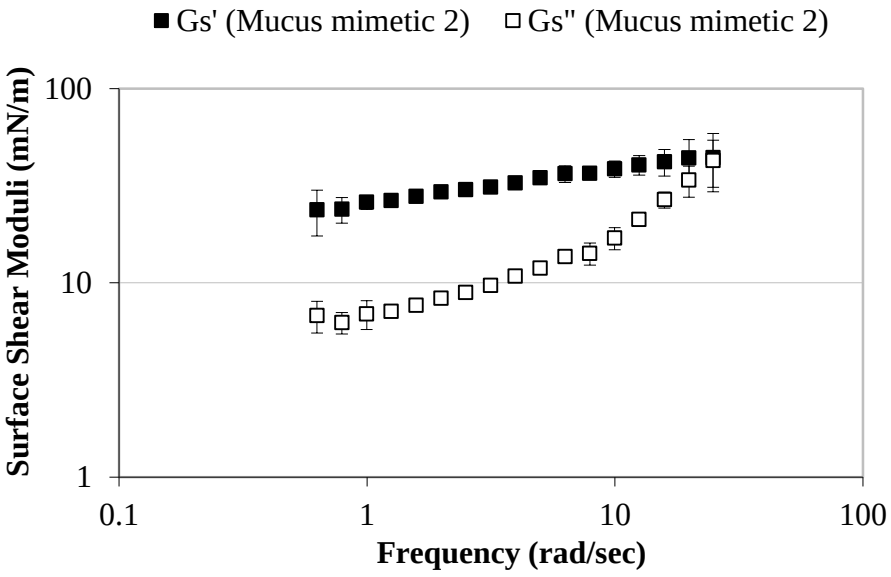

Figure 3-19: Frequency-dependence of surface shear storage modulus G_s' and surface shear loss modulus G_s" for the mucus mimetic 2. Data are represented as the mean ± SD (n=3).

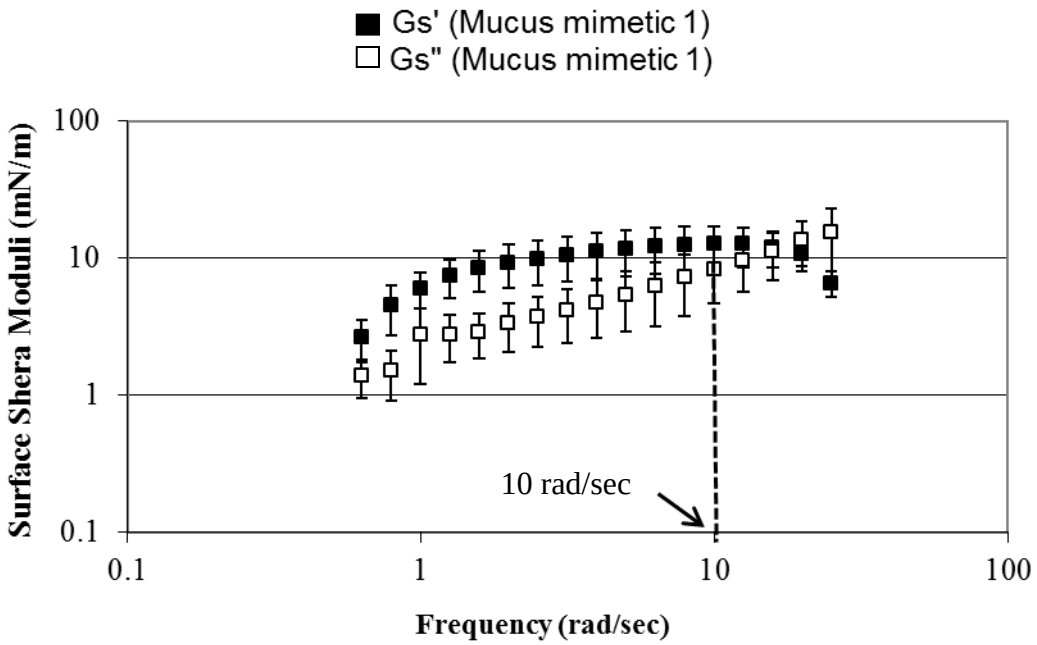

Figure 3-20: Frequency-dependence of surface shear storage modulus G_s' and surface shear loss modulus G_s" for the mucus mimetic 1. Dashed line indicates the frequency at which G_s' G_s' decreased with frequency. Data are represented as the mean ± SD (n=3).

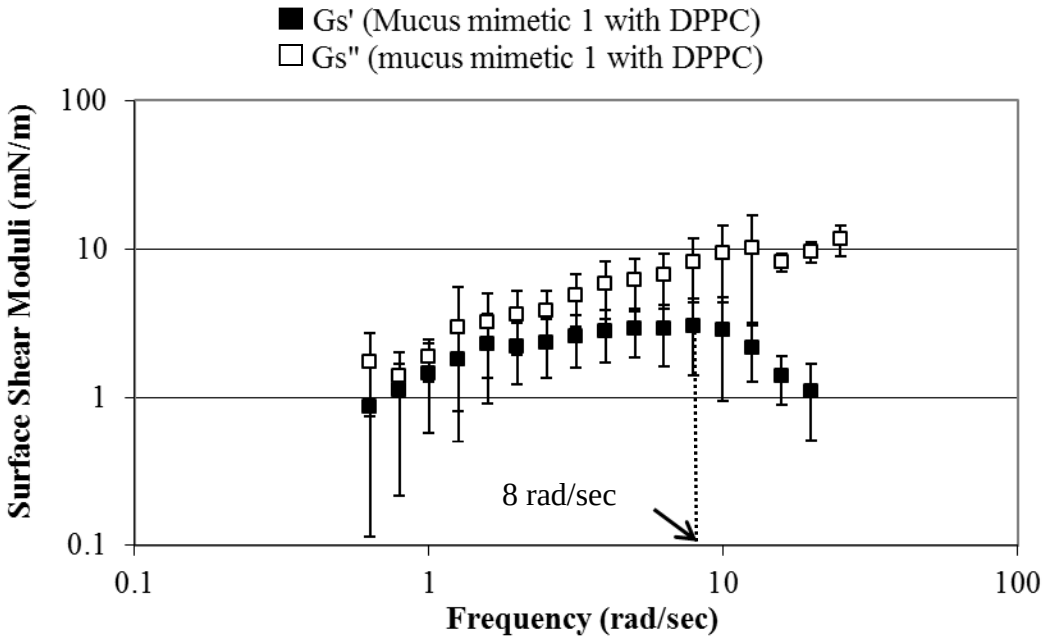

Figure 3-21: Frequency-dependence of surface shear storage modulus G_s' and surface shear loss modulus G_s" for DPPC spread at an air-mimetic interface. Dashed line indicates the frequency at which G_s' decreased with frequency. Data are represented as the mean ± SD (n=5).

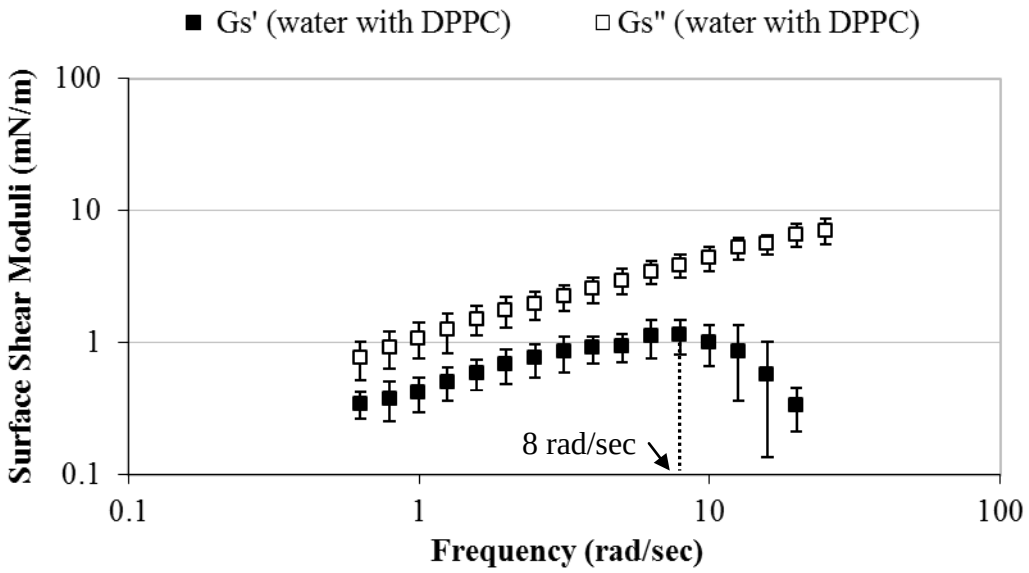

Figure 3-22: Frequency-dependence of surface shear storage modulus G_s' and surafce shear loss modulus G_s" for DPPC spread at an air-water interface. Dashed line indicates the frequency at which G_s' decreased with frequency. Data are represented as the mean ± SD (n=4).

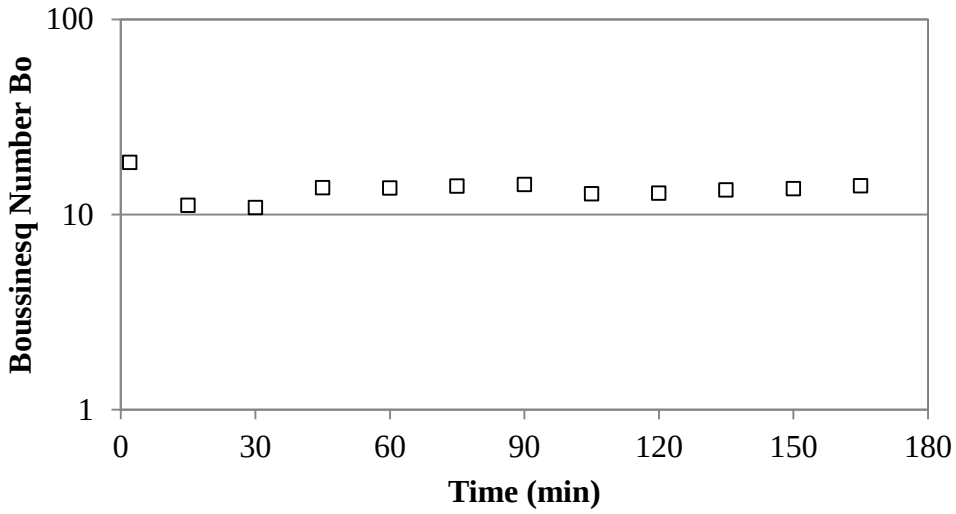

Figure 3-23: Boussinesq number (Bo) calculated based on the time-dependent G" of the mucus mimetic 1 (Figure 3-12) and the time-dependent G_s" of mucus mimetic 1 covered with DPPC (Figure 3-13) at different time points.

CHAPTER 4

CONDUCTIVE AIRWAY SURFACTANTS INFLUENCE THE SURFACE PROPERTIES OF THE TRACHEAL MUCUS

4.1. Introduction

The airway lining fluid (ALF) of the large conducting airways is coated with a heterogeneous complex mixture of surface-active components. Although the chemical composition of the alveolar surfactant in mammalian lungs has been well studied, the exact chemical composition of the conductive airway surfactants lining the ALF is still not well defined. This is due to major limitations encountered in the chemical analysis of the surface active materials in tracheal secretions, such as the association of lipids with mucus glycoproteins (mucins)[43] and the selection of a proper sampling method of lipids from the conducting airways.[37]

Although Girod *et al.*[45] have shown that the tracheal mucosa synthesizes airway surfactants, others have shown that surfactants reached large conducting airways by the overflow from the alveolar region via the surface tension gradient.[42, 48] For instance, Bernhard *et al.*[42] have shown that the phospholipid classes, particularly phosphatidyl-choline, in tracheal aspirates were similar to those in bronchoalveolar lavage and were markedly different from those of the underlying airway epithelium. In another study, Rau *et al.*[48] have shown that phospholipid classes on conductive airway surfaces are different from those secreted by the tracheal mucosa and that the tracheal mucosa in rats does not synthesize dipalmitoylphosphatidylcholine (DPPC) suggesting that DPPC originates from the alveolar region.

Analyses of human tracheobronchial aspirates have confirmed the presence of various surface active compounds such as phospholipids, neutral lipids, and glycolipids.[13, 39-44] The presence of hydrophobic surfactant proteins (SP-A, B, C and D) in conductive airway surfactants is still subject to controversy. It has been shown that the

hydrophobic surfactant proteins (SP-B and SP-C) are expressed in bronchi and bronchioles during lung development,[133] and that the hydrophilic surfactant proteins (SP-A and SP-D) are detected in human tracheal, bronchial and bronchiolar epithelium.[111, 134, 135] However, Bernhard *et al*.[42] have reported that SP-B and SP-C were absent in the tracheobronchial secretions.

Infasurf®, a complex lung surfactant derived from calf lungs, closely matches lavaged lung surfactant in composition compared to other available clinical exogenous surfactants such as Survanta®, Curosurf® and Exosurf®.[136] The other exogenous surfactants lack one or more of the surface-active components available in lung surfactants. For instance, Survanta® and Exosurf® lack surfactant-associated proteins.[136,47] In addition, Curosurf® contains less surfactant associated proteins than native bovine and porcine surfactant.[137] Infasurf® contains 90-94% phospholipids, of which 79% is phosphatidylcholine and the remainder is 6% phosphatidylglycerol, 6% neutral lipids and about 1% protein.[138] The hydrophilic proteins (SP-A and SP-D) are lost during Infasurf® preparation because of the organic solvent extraction of the calf lung surfactants, whereas hydrophobic proteins (SP-B and SP-C) are restored.[139] The surface activity and surface rheological behavior of Infasurf® spread onto an aqueous subphase has been studied.[136, 140] However, no study has been carried out to study the surface rheological behavior of Infasurf® spread onto a mucus-like subphase. It is likely that the surface rheological behavior of Infasurf® will be influenced by the viscoelastic properties of the underlying mucus gel layer of the ALF as well as the surface composition. Since it has been shown that surfactants in the human tracheal secretions are primarily derived from the alveolar region,[42, 48] Infasurf® may be a good model for large conducting airways surfactants.

The objective of the present study was to investigate the effect of a mucus subphase on the surface rheological behavior of a complex lung surfactant. Our hypothesis is that, while DPPC represents the principle pulmonary surfactant, other pulmonary surfactants such as unsaturated phospholipids, neutral lipids, and free fatty

acids may play a significant role in tuning the surface properties of the large conducting airways. Towards this aim, a natural calf lung extract (Infasurf®, Ony, Inc.) was used as a model for conductive airway surfactants. Surface shear rheology was used to investigate the mechanical properties of Infasurf® on mucus and water subphases. In addition, a comparison in the surface rheology of the *in-vitro* model mimetic of tracheal mucus before spreading surfactants (DPPC and Infasurf®) and after spreading Infasurf® and DPPC was illustrated.

4.2. Materials and Methods

4.2.1. Materials

Pig gastric mucin (PGM)-type III and chloroform (≥ 99.8 % purity) were purchased from Sigma-Aldrich, Inc. (St. Louis, MO), bovine serum albumin (fraction V, lyophilized powder) from Spectrum (New Brunswick, NJ), and Infasurf® was a generous gift from ONY Inc. (Amherest, NY). Glutaraldehyde (GA, 50% w/w solution) and methanol (99.9% purity) were purchased from Fisher Scientific (Fair Lawn, NJ). All other chemical reagents were of analytical grade and used without further purification. Purified water (18 MΩ cm) was used in all experiments obtained from NANOpure Infinity Ultrapure Water System, Barnstead International.

4.2.2. Preparation of Mucus Mimetic

The *in-vitro* model mucus mimetic of low bulk viscoelasticity was used in this study. The mucus mimetic 1 was prepared as mentioned in Materials and Methods section 2.2.3 in Chapter 2. Briefly, mucus mimetic was composed of 4% (w/v) PGM-type III, 1% (w/v) ions (Na^+, Ca^{+2}, P^{+5} and Cl^-), 1% (w/v) protein (albumin), and 94 ml water. To prepare 30 ml of the mimetic, 0.3 g albumin, 1.2 g PGM-type III and 28.5 ml buffer (154 mM NaCl, 3 mM $CaCl_2$, 15 mM NaH_2PO_4/Na_2HPO_4; pH 7.4) were added to an amber glass bottle. Ingredients were mixed at 4°C on a tube rotator (Glas-Col, IN) for at

least 6 days to mix the sample. The mucus mimetic was prepared by cross-linking the mimetic using 0.5 ml-15% (w/w) GA solution added to the 30 ml of the mimetic formulation and mixed at 4°C on a tube rotator (Glas-Col, IN) for 24 hours.

4.2.3. Control Experiments for the Spreading Solvent Chloroform:Methanol

To ensure that the spreading solvent chloroform:methanol is not surface active, a control experiment was conducted in our laboratory by Amir Farnoud (Chemical and Biochemical Engineering, The University of Iowa). In this experiment, a Langmuir-Blodgett (LB) Teflon coated trough (KSV Instruments, Finland) with a working area of 78 cm x 7.5 cm was placed on a vibration isolation table inside a home-built environmental chamber. The LB trough was equipped with a double barrier system and a Wilhelmy plate (KSV Instruments, Finland) attached to a microbalance to record the surface pressure or surface tension. Before each experiment, the LB trough and barriers were thoroughly cleaned with ethanol and de-ionized water and the surface was aspirated via a vacuum-aspirator. A liquid subphase composed of 150 mM NaCl and 1.5 mM $CaCl_2$, chosen in accordance with the chemical composition of the alveolar fluid, was used.[18] To ensure cleanliness of the surface, a zero reading of the surface pressure (Π) on complete compression of the interface was obtained. Surface pressure (Π) is defined as $\Pi = \gamma_o - \gamma$, where γ is the surface tension of the surfactant covered the interface and γ_o is the surface tension for a clean air-liquid interface. A volume of 250 ml of the liquid subphase was poured into the LB trough. The subphase was allowed to equilibrate for 30 minutes at room temperature (~ 22°C). The 20 mm x 10 mm Wilhelmy platinum plate was dipped into the subphase and the surface tension was reported. An amount of 50 µL of the spreading solvent chloroform was spread at the air-liquid interface using a micro-syringe. After spreading, 10 minutes were allowed for solvent to evaporate. Surface pressure-surface area isotherms for three successive compression-expansion cycles for the air-

liquid interface after the addition of the spreading solvent chloroform was recorded. A 77.4% area reduction of the maximum surface area, at a speed of 45.7 mm/min, was performed. All control experiments were performed at least three times. In addition, the surface activity of methanol as a spreading solvent was studied in Section 2.3.9.1 Chapter 2.

4.2.4. Modification and Measurement of Surface Tension

Infasurf® spreading solution was prepared by dissolving 28 µL of Infasurf® suspension containing 1 mg of total phospholipids in 1.0 ml chloroform:methanol (90:10 v/v) to obtain a final concentration of 1 mg phospholipid per 1 ml solution. Infasurf® was spread onto the mucus mimetic and water surfaces within a Plexiglas mini-trough (7.5 cm x 12 cm) placed in a home-built environmental chamber capable of maintaining temperature at ~ 25°C and relative humidity at ~ 40%, as mentioned in section 3.2.3 in Chapter 3. The surface tension of each interface was determined using a Wilhelmy plate balance (KSV Instruments, Finland) equipped with a platinum plate (20 mm x 10 mm). Infasurf® was added at the air-fluid interface using a micro-syringe until a surface tension of ~ 32 mN/m was achieved. Ten minutes were allowed to elapse for the solvents to evaporate. At least three surface tension measurements were conducted for each interface.

4.2.5. Surface Stress Rheology

Figure 4-1 illustrates sketches for the five surface systems discussed in this study: bare mucus mimetic, Infasurf® spread onto mucus mimetic subphase, DPPC spread onto mucus mimetic subphase, Infasurf® spread onto water subphase and DPPC spread onto water subphase. The surface rheology of Infasurf® spread at the air-mimetic interface and a pure Infasurf® film spread at an air-water interface were determined using an interfacial stress rheometer (ISR 400; KSV Instruments, Finland) as discussed in Materials and Methods section 3.2.5 in Chapter 3. Briefly, the mucus mimetic and water subphases

were spread into a Plexiglas mini-trough (7.5 cm x 12 cm) with a glass channel (100 mm length, 9.6 mm width, 6.5 mm height) positioned in the middle of the trough. For each experiment, 60 ml of subphase was poured into the mini-trough until a meniscus was formed within the glass channel and climbed the top of the channel walls. Then the surface tension for the fluid subphases was modified as described in section 4.2.3. A Teflon-coated magnetized needle (32 mm length) was placed at the air-fluid interface within the channel and was subjected to an oscillatory magnetic force generated by a pair of Helmholtz coils to create a surface shear stress. The resulting needle motion was detected by tracking the needle tip using a Firewire camera with 512 x 480 pixel resolution. From the magnetic force applied to the needle (surface stress, σ_s) and the resulting needle position (surface strain, γ_s), the dynamic surface modulus (G_s^*) was determined by relating the surface stress, (σ_s) to the surface strain (γ_s):

$$G_s^*(\omega) = \sigma_s(\omega) / \gamma_s(\omega)$$

The dynamic surface modulus (G_s^*) is a complex number, which can be described by:

$$G_s^* = G_s' + iG_s''$$

where the real part, G_s', is the surface shear storage (or elastic) modulus and the imaginary part, G_s'', is the surface shear loss (or viscous) modulus. G_s' and G_s'' were determined from the phase lag (δ) between the surface strain (γ_s) and the surface stress (σ_s), where:

$$G_s' = G_s^* \cos\delta \text{ and } G_s'' = G_s^* \sin\delta$$

For surface rheological studies, the surface linear viscoelastic region (SLVR) was determined for each interface by conducting strain-dependent surface rheology. In this test, strain amplitude was varied sinusoidally with time at a fixed frequency of 1.56 rad/sec (corresponding to normal breathing frequency of 0.25 Hz).[58] On the basis of this test, a value of desired amplitude was selected over a region where G_s' and G_s'' were independent of strain or exhibited weak dependence on strain. Subsequently, time-dependent and frequency-dependent surface rheological tests were performed. In the

time-dependent tests, G_s' and G_s" were determined every 15 minutes for 150 minutes at a fixed frequency of 1.56 rad/sec. In the frequency-dependent tests, G_s' and G_s" were determined over a range of frequencies from 0.63-25.04 rad/sec. G_s' and G_s" were determined for at least three separate samples.

4.2.6. Statistical Analysis

Statistical significance was determined by 2-way ANOVA analysis for comparing the time-dependent surface rheological shear moduli among surface systems for an unbalanced number of samples using a general linear model. A paired t-test was performed to compare the surface tension of the air-liquid interface before and after the addition of a spreading solvent. Levels of significance were accepted at the $p<0.05$ level. Statistical analyses were performed using Minitab 15 software.

4.3. Results and Discussion

4.3.1. Surface Activity of the Spreading Solvent

The surface activity of the spreading solvent chloroform at the air-liquid interface was determined during three successive compression-expansion cycles. Table 4-1 illustrates γ^* (initial surface tension of the air-liquid interface after the addition of the spreading solvent and before initiating the compression-expansion cycles), and γ_{min} and γ_{max} (the minimum and maximum surface tensions of the air-liquid interface with the spreading solvent for each compression-expansion cycle). No significant difference was observed between $\gamma_{subphase}$ and γ^* ($p>0.05$). The air-liquid interface with the spreading solvent exhibited no change in γ_{min} and γ_{max} compared to $\gamma_{subphase}$, during the three compression-expansion cycles ($p>0.05$), indicating that chloroform is not surface active. Figure 4-2 represents the surface pressure-surface area isotherm of the compression-expansion cycles conducted on the liquid-air interface with the spreading solvent for one of the three experiments reported in Table 4-1. Maximum surface pressure did not exceed

0.2 mN/m upon compression during the three cycles, indicating that the spreading solvent is not surface active. As mentioned in section 2.3.9.1 in Chapter 2, spreading solvents such as chloroform, toluene, and benzene have been previously shown to not significantly surface active when the maximum changes in surface pressure upon the compression.[105]

4.3.2. Altering the Surface Tension of an Air-Fluid Interface Using Infasurf®

The mucus mimetic was used as a representative subphase to study the surface rheological behavior of Infasurf® spread onto a viscoelastic mucus layer. The surface tension of the mucus mimetic, 53.25 ± 1.22 mN/m (n=9), was lowered to 31.40 ± 3.75 mN/m (n=5) by spreading Infasurf® at the air-mimetic interface (Table 4-2). About 28 µL of Infasurf® solution (1 mg/ml of total phospholipid) was needed to lower the surface tension of the mucus mimetic to 31.40 ± 3.75 mN/m (n=5). The amount of Infasurf® solution needed to lower the surface tension was 70.0% less than the amount of DPPC required (~ 93 µL of 1mg/ml DPPC) (Table 4-3). DPPC represents about 40% of Infasurf® composition.[141] Therefore, other compounds present in Infasurf® enhance its surface tension lowering effect. It has been shown in other studies that Infasurf® exhibits higher surface activity compared to DPPC.[142, 143] This is due to the slow adsorption of the disaturated phospholipid (DPPC) to the surface, and the adsorption enhancement afforded by the unsaturated phospholipids, neutral lipids, and SP-B and C in Infasurf®. Therefore, Infasurf® exhibits improved surface tension lowering capacity at both aqueous and viscoelastic interfaces.[136, 141, 142, 144]

4.3.3. Surface Rheology of Infasurf®

4.3.3.1. Surface Linear Viscoelastic Region

The surface linear viscoelastic region (SLVR) was determined at a frequency of 1.56 rad/sec for the mucus mimetic with Infasurf® by systematically increasing the

oscillation strain amplitude. The SLVR was within the strain range 0.005 to 0.169 where G_s' and G_s" were strain-independent over the entire range probed (Figure 4-3). The mucus mimetic covered with Infasurf® extended over longer SLVR (0.005 to 0.169) compared to the SLVR of the mucus mimetic which was limited to very small strains (0.003-0.025) (Figure 3-7), as discussed in section 3.3.2.1 in Chapter 3. This indicates that the surface behavior of mucus mimetic with Infasurf® exhibited more viscous behavior compared to that of bare mimetic.

4.3.3.2. Time-Dependence Surface Shear Rheology

The time-dependence of surface rheological behavior of Infasurf® spread at an air-mimetic and air-water interface was determined at constant strain amplitude of 0.033 and constant frequency of 1.56 rad/sec. Spreading Infasurf® at an air-mimetic interface led to a more viscous surface, where G_s" dominated G_s' (Figure 4-4). This change in surface rheological behavior of mimetic from more elastic (Figure 3-11) to more viscous was due to the considerable decrease in G_s' values after the addition of Infasurf®. Furthermore, G_s" exhibited very low values implying that Infasurf® remarkably fluidized the mimetic surface.

More viscous behavior was also observed for Infasurf® spread on water subphase (Figure 4-5). G_s" values were extremely low (~ 0.01 mN/m). G_s' values were below the ISR limit of detection (0.005 mN/m). Therefore, the Infasurf® interface exhibited no surface elasticity after 120 min. The surface rheological behavior of Infasurf® spread onto a water subphase described here is in good agreement with a previous study by Fuller *et al.*[140] In both studies, the Infasurf® film exhibited a remarkable fluidity and values of G_s' and G_s" were extremely low, at 0.001 mN/m.

4.3.3.3. Frequency-Dependence Surface Shear Rheology

The frequency-dependent surface rheological behavior of Infasurf® spread at an air-mimetic interface was determined over a frequency range of 0.63-25.04 rad/sec.

Spreading Infasurf® resulted in a more viscous surface, where G_s" dominated G_s' (Figure 4-6, Table 4-2). This change in surface behavior from more elastic surface, observed for the mucus mimetic where G_s' dominated G_s" (Figure 3-16), to more viscous surface was due to a considerable decrease in the surface elastic modulus after Infasurf® spreading. At high frequencies (above 12.5 rad/sec), this elastic surface behavior was no longer observed, which suggests the breakdown of the Infasurf® film at high shearing rate.

The Infasurf® film spread on a water subphase exhibited a viscous behavior only, where low values for G_s' (<0.03 mN/m) were only recorded at a low frequency range (0.63-1.25 rad/sec). This indicates that Infasurf® monolayer exhibits a remarkable fluidity (Figure 4-7, Table 4-2).

4.3.3.4. Comparison in the Surface Rheological Studies

Figures 4-8 and 4-10 compare the surface rheological behavior of the bare mucus mimetic, Infasurf® spread at an air-mimetic interface and DPPC spread at an air-mimetic interface. The bare mucus mimetic exhibited a more elastic surface, where G_s' dominated G_s" at all time points. Spreading Infasurf® or DPPC on the mucus mimetic altered the surface rheological behavior of mimetic from more elastic (G_s' dominated G_s") to more viscous (G_s" dominated G_s'). This viscous surface behavior for mucus mimetic after the addition of either DPPC or Infasurf® was expected if there was sufficient decoupling of the interface from the subphase. Previous studies have shown that DPPC or Infasurf® fluidize aqueous surfaces, leading to more viscous behavior.[114, 115,140] Lower values for the surface viscous modulus G_s" were observed for Infasurf® on the mucus mimetic compared to those of DPPC ($p<0.05$). The time dependent G_s" for the mucus mimetic with Infasurf® were 0.37 mN/m and 0.45 mN/m at 60 min and 120 min, respectively. However, G_s" for the mucus mimetic with DPPC were 2.45 mN/m and 2.93 mN/m at 60 min and 120 min, respectively. For the frequency-dependent surface rheological behavior, lower values for the elastic and viscous moduli were observed for Infasurf® on

the mimetic surface compared to those of DPPC (at 1 rad/sec, G_s' and G_s" were 0.03 mN/m and 0.29 mN/m, respectively, for Infasurf® with mimetic versus 1.45 mN/m and 1.86 mN/m, respectively, for DPPC with mimetic (Figure 4-10 and Table 4-2). In addition, Infasurf® film on mimetic subphase exhibited no surface elastic behavior at high frequencies (beyond 12.5 rad/sec); however, the DPPC film on mimetic subphase exhibited surface elastic behavior at high frequencies. The remarkable fluidity of Infasurf® films on mimetic was mainly attributed to the fluid surfactants, such as the unsaturated phospholipids and neutral lipids, present in Infasurf®. It has been shown that DPPC, due to its disaturated acyl chains, forms a rigid monolayer which sustains high surface pressure (~ 70 mN/m) preventing the condensed monolayer from collapse.[145] The intermolecular interaction between the disaturated acyl chains of DPPC at the interface, and between the headgroups increases the film strength and resulted in a viscoelastic surface with more elastic surface behavior.[146, 132] However, the unsaturated phospholipids and neutral lipids form a fluid monolayer due to the presence of the double bond which inhibit the formation of a condensed (rigid) monolayer and result in a more viscous surface behavior.[145]

These results show that surfactant composition plays a significant role in the surface behavior of the mimetic. Although DPPC is the most prevalent class of phospholipids in the tracheal secretions,[13, 39, 42-44] it does not capture the surface rheological behavior of the complex mixture of the surface active components present in the tracheal secretions. The mucus layer of the ALF exhibited a significant surface rheological behavior due to the presence of surfactants at air-mucus interface. This surfactant film is of critical importance for mucus function such as cough and mucociliary clearance[35] and retention of inhaled particles into the gel phase for clearance.[30, 36] The viscous surface behavior of the mucus layer of the ALF will more likely facilitate mucus function, despite its bulk viscoelastic properties.

On an aqueous subphase, Infasurf® and DPPC films exhibited similar behavior to that on a mucus subphase. More viscous behavior was observed at all time points for both DPPC and Infasurf® films (Figure 4-9). Infasurf® films exhibited lower viscoelastic properties than DPPC films. For example, lower values for the surface viscous modulus G_s" were observed for Infasurf® film compared to those of DPPC film ($p<0.05$) (0.009 mN/m and 0.009 mN/m at 60 min and 120 min, respectively, for Infasurf® films versus 1.23 mN/m and 1.48 mN/m at 60 min and 120 min time points, respectively, for DPPC films), providing further evidence of the influence of surfactant composition on surface behavior. For the frequency-dependent surface rheology, viscous behavior only was observed for Infasurf® film, where no surface elastic behavior values were observed at frequency beyond 1.25 rad/sec (Figure 4-11). In addition, G_s" of Infasurf® film was lower than that of DPPC film (G_s" at 1 rad/sec was 0.07 mN/m for Infasurf® on a water subphase versus 1.08 mN/m for DPPC on a water subphase, Table 4-2).

The surface rheological behavior of DPPC and Infasurf® films on aqueous subphase was studied as a control. The surface rheological behavior of DPPC and Infasurf® films on aqueous subphase was compared to that of DPPC and Infasurf® films on mimetic subphase. Lower values of time-dependent G_s' and G_s" were observed for DPPC and Infasurf® films on an aqueous subphase compared those on a mimetic subphase ($p<0.05$), indicating that the subphase significantly influences the surface rheological properties of these films.

4.3.3.5. Boussinesq Number

The Boussinesq number, Bo, as discussed in section 3.3.4.4 in Chapter 3, is the ratio of the surface drag to the subphase drag. Bo was determined by relating the time-dependent surface shear rheology of the mucus mimetic 1 covered with Infasurf® (Figure 4-4) to the time-dependent bulk shear rheology of the mucus mimetic 1, discussed in Chapter 3 (Figure 3-12). Bo was determined using the following equation:

$$Bo = G_s''/(G'' \cdot d)$$

where: G_s''= surface shear loss modulus of mucus mimetic covered with Infasurf®, G"= bulk shear loss modulus of mucus mimetic only, and d= diameter of the magnetic needle 0.546 mm.

Figure 4-12 illustrates the values of Bo at all-time points. It was found that Bo was between 2 to 3, indicating that the surface viscosity and bulk viscosity were about equal. This Bo value was much lower than what has been reported by Brooks (Bo ~ 100) to completely decouple the interface from subphase. The influence of the bulk viscoelastic mimetic subphase, in addition to the extremely low values of the time-dependent G_s'' after the addition of Infasurf® on the mimetic subphase, resulted in lower Bo values compared to those obtained for mimetic covered by DPPC. This indicates that G_s' and G_s'' moduli should be considered "apparent" properties of the mucus mimetic surface, where the surface viscoelastic moduli are influenced by the subphase.

The time-dependent G_s'' of mucus mimetic with Infasurf® at the time points 2, 30, 60, 90, 120 and 150 min were 0.37, 0.37, 0.37, 0.40, 0.45 and 0.52 mN/m, respectively. However, the time-dependent G_s' of bare mucus mimetic at the time points 2, 30, 60, 75, 90 and 120 min were 3.4, 4.8, 4.4, 5.2, 6.8 and 7.2 mN/m, respectively. The ratio of the time-dependent G_s'' of mucus mimetic with Infasurf® to that of bare mucus mimetic was between 7-11%. This shows that Infasurf® significantly influences the surface properties.

4.4. Conclusions

Infasurf® exhibited a higher surface activity at an air-mimetic interface compared to DPPC. This was reflected by the lower volume of Infasurf® solution used to lower the surface tension of the mucus mimetic to ~ 32 mN/m, compared to DPPC solution. The surface rheological behavior of Infasurf® spread onto a viscoelastic non-Newtonian and aqueous Newtonian subphases was probed using an interfacial stress rheometer (ISR). Infasurf® films on the mucus mimetic and water subphases exhibited a more viscous

surface, where G_s" dominated G_s'. For Infasurf® at an air-mimetic interface, the time-dependence surface elastic modulus, G_s' exhibited extremely low values. In addition, no surface elastic behavior was observed at high frequencies. Infasurf® film at an air-water interface exhibited a viscous surface behavior only. The substantial difference in the chemical composition of the two surfactants resulted in significant changes in the surface rheological behavior of Infasurf® and DPPC films on the mucus mimetic and water subphases. This indicates that while DPPC is the primary pulmonary surfactant, other components such as unsaturated phospholipids, neutral lipids, and surfactant associated proteins, likely influence the surface rheology of the airway lining fluid (ALF) of the large conducting airways. The more viscous surface behavior of the tracheal mucus, due to the presence of surfactants at the air-mucus interface, will more likely influence mucus functions such as, mucociliary and cough clearance, penetration of inhaled particles into the mucus layer for clearance and bioaerosol formation.

Table 4-1: Maximum and minimum surface tensions monitored during three successive compression-expansion cycles of the spreading solvent (chloroform) at the air-liquid interface.

Exp #	**$\gamma_{Subphase}$ (mN/m)**	**γ^* (mN/m)**	**Cycle 1 γ (mN/m)**	**Cycle 2 γ (mN/m)**	**Cycle 3 γ (mN/m)**
1	73.3	73.3	‡γ_{min} 73.2 †γ_{max} 73.3	γ_{min} 73.2 γ_{max} 73.3	γ_{min} 73.2 γ_{max} 73.4
2	73.0	73.0	γ_{min} 72.9 γ_{max} 73.0	γ_{min} 73.0 γ_{max} 73.1	γ_{min} 73.0 γ_{max} 73.2
3	72.6	72.7	γ_{min} 72.6 γ_{max} 72.7	γ_{min} 72.7 γ_{max} 72.9	γ_{min} 72.8 γ_{max} 72.9
Mean±SD	73.0±0.3	73.0±0.3	γ_{min} 72.9±0.3 γ_{max} 73.0±0.3	γ_{min} 73.0±0.3 γ_{max} 73.1±0.2	γ_{min} 73.0±0.2 γ_{max} 73.1±0.3

γ^* is the initial surface tension at the air-liquid interface after the addition of the spreading solvent and allowing 10 minutes for spreading solvent to evaporate.

‡γ_{min} is the minimum surface tension monitored upon compression.

†γ_{max} is the maximum surface tension monitored upon expansion.

Table 4-2: Comparison of surface tension and surface moduli of mucus mimetic with and without surfactant at the interface; data are represented as the mean ± SD.

Interface	**Surface tension (mN/m)**	**G_s' at 1 rad/sec (mN/m)**	**G_s" at 1 rad/sec (mN/m)**	**Surface behavior**
Bare mucus mimetic	53.3±1.2 (n=9)	6.1±1.8 (n=3)	2.7±1.6 (n=3)	G_s'> G_s" More elastic
Infasurf® spread at an air-mimetic interface	31.4±3.8 (n=5)	0.0±0.0 (n=6)	0.3±0.1 (n=6)	G_s'< G_s" More viscous
Infasurf® at an air-water interface	29.2±1.0 (n=6)	0.0±0.0 (n=4)	0.1±0.1 (n=4)	G_s'< G_s" More viscous
DPPC spread at an air-mimetic interface	30.2±2.4 (n=4)	1.5±0.9 (n=4)	1.9±0.6 (n=4)	G_s'< G_s" More viscous
DPPC spread at an air-water interface	30.2±2.4 (n=4)	0.4±0.1 (n=4)	1.1±0.3 (n=4)	G_s'< G_s" More viscous

Table 4-3: Volume of Infasurf® solution (1 mg/ml of total phospholipid in chloroform:methanol (90:10 v/v) and DPPC solution (1mg/ml DPPC in n-hexane:methanol 95:5 v/v) used to lower the surface tension of mucus mimetic 1 and water to ~ 32 mN/m.

Subphase	**Infasurf® solution**	**DPPC solution**
Mucus mimetic 1	27.9 ± 0.5 µL (n=9)	92.7 ± 7.5 µL (n=9)
Water	28.0 ± 0.6 µL (n=6)	36.6 ± 1.2 µL (n=12)

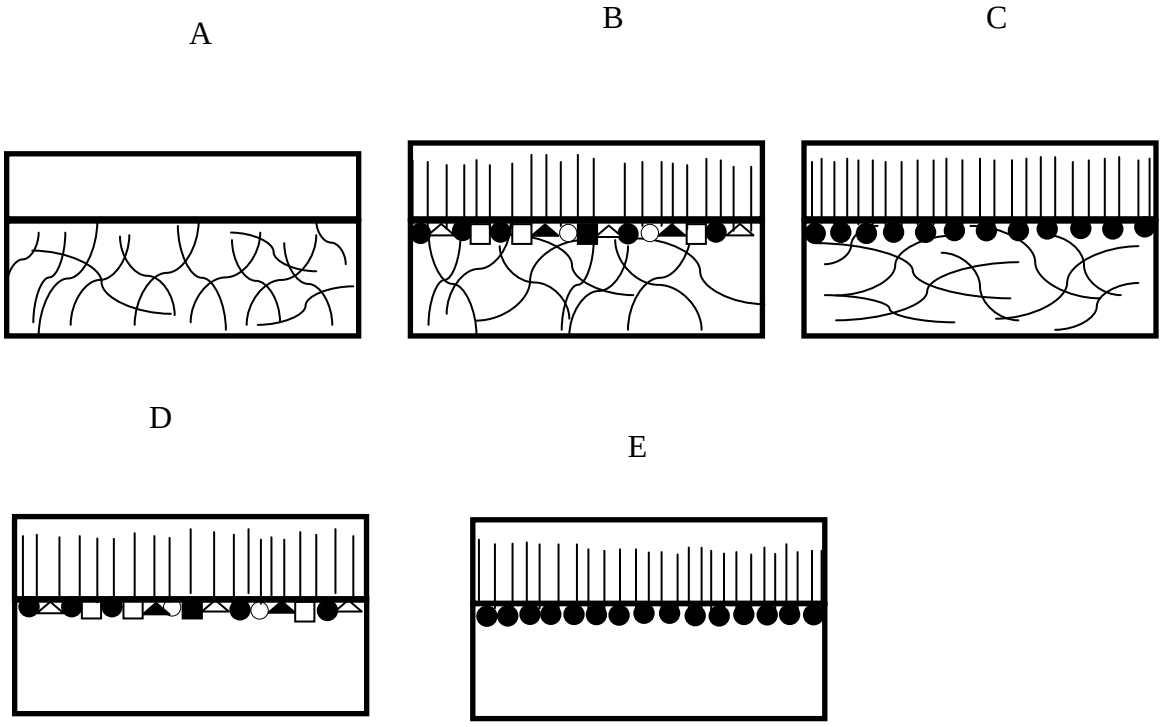

Figure 4-1: Sketches of: (A) mucus mimetic, (B) Infasurf® spread at an air-mimetic interface, (C) DPPC spread at an air-mimetic interface, (D) Infasurf® spread at the air-water interface , and (E) DPPC spread at an air-water interface.

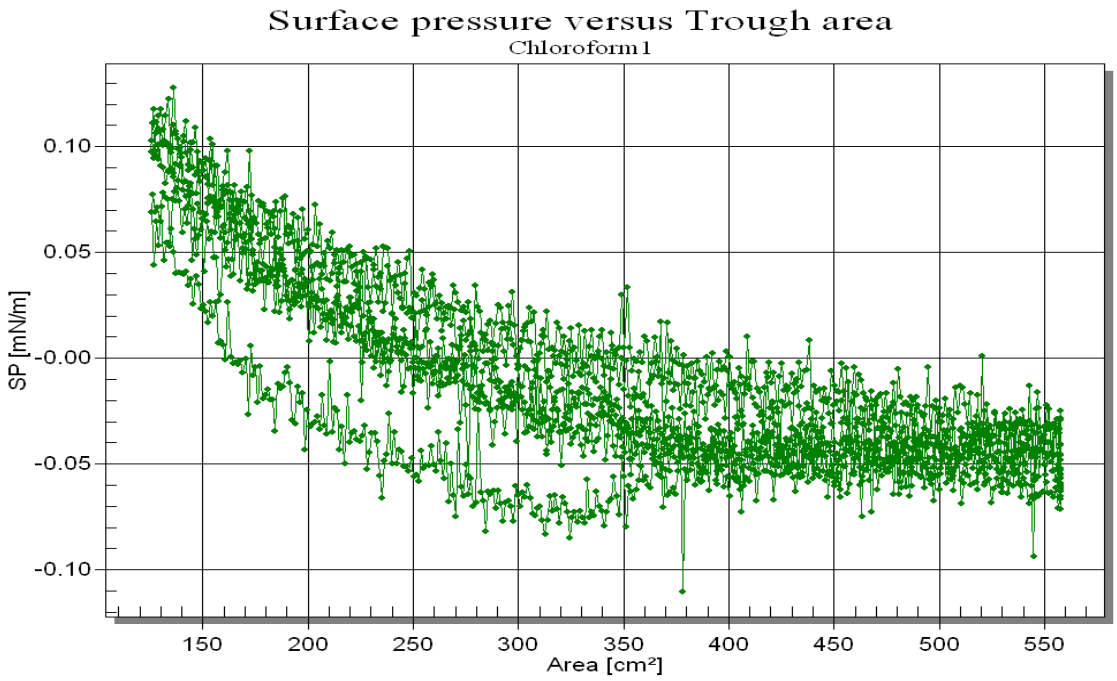

Figure 4-2: Surface pressure-surface area isotherm of the air-liquid interface after the addition of the spreading solvent (chloroform) during three compression-expansion cycles for one of the three experiments reported in Table 4-1. Surface pressure did not exceed 0.2 mN/m upon compression of the spreading solvent interface.

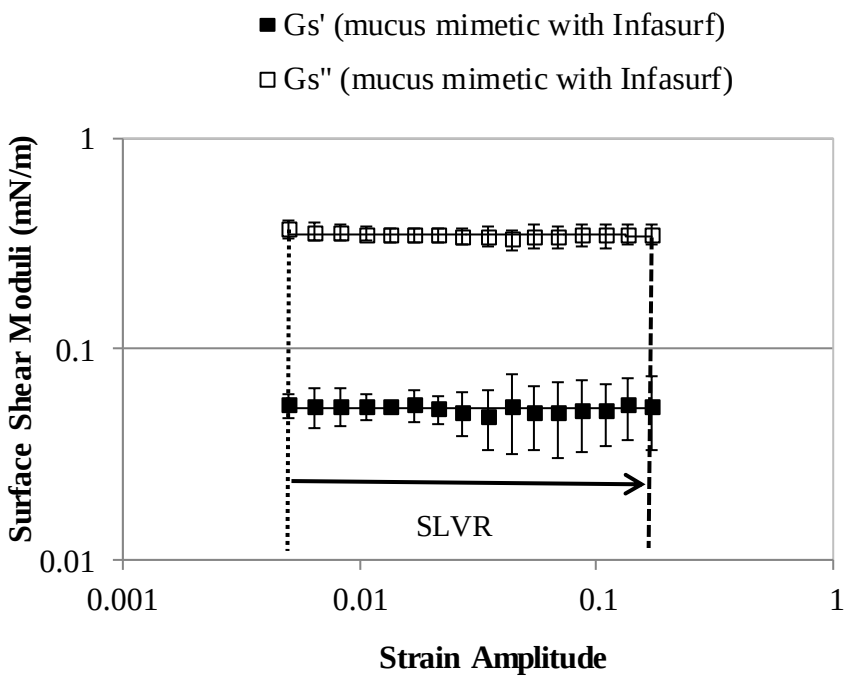

Figure 4-3: Strain-dependence of surface shear storage modulus G_s' and surface shear loss modulus G_s" at a fixed frequency of 1.56 rad/sec for Infasurf® spread at an air-mimetic interface over strain range of (0.005-0.169). The surface linear viscoelastic region (SLVR) is indicated by an arrow. Data are represented as the mean ± SD (n=3).

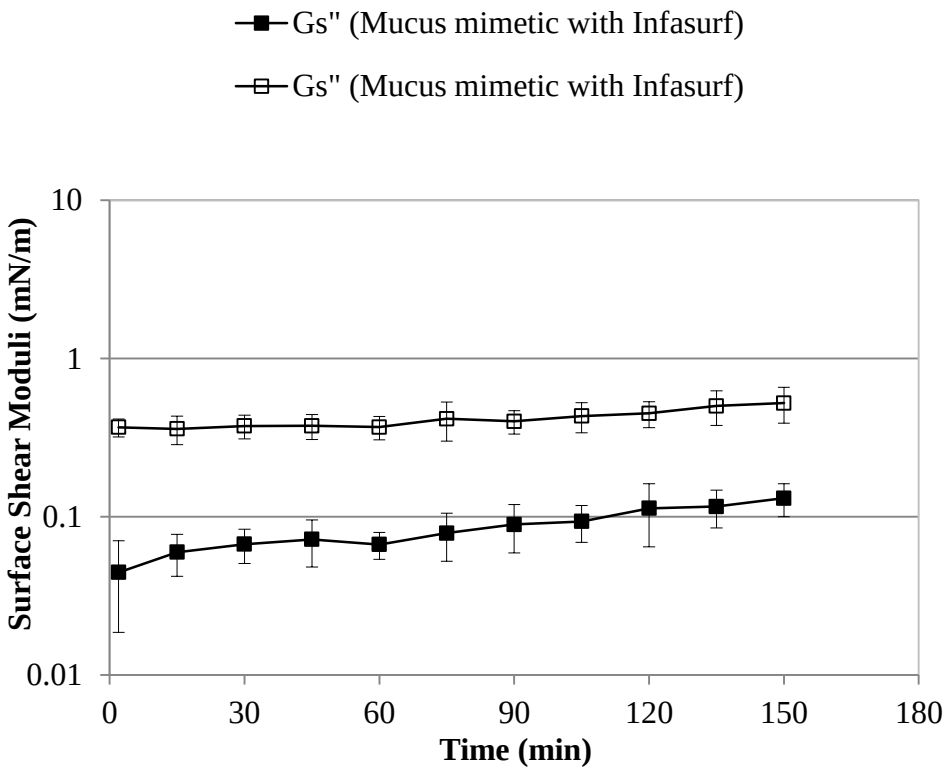

Figure 4-4: Time-dependence of surface shear storage modulus G_s' and surface shear viscous modulus G_s" for Infasurf® spread at an air-mimetic interface. Data are represented as the mean ± SD (n=3).

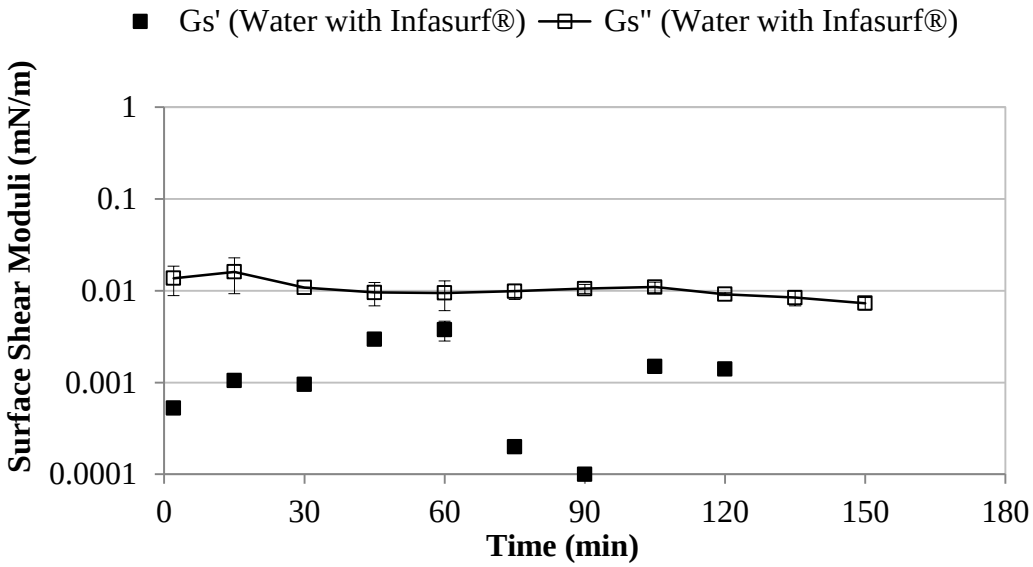

Figure 4-5: Time-dependence of surface shear storage modulus G_s' and surface shear viscous modulus G_s" for Infasurf® spread at an air-water interface. The G_s' values were below the detection limit (0.005 mN/m) and G_s" values were ~ 0.01 mN/m. Data are represented as the mean ± SD (n=3).

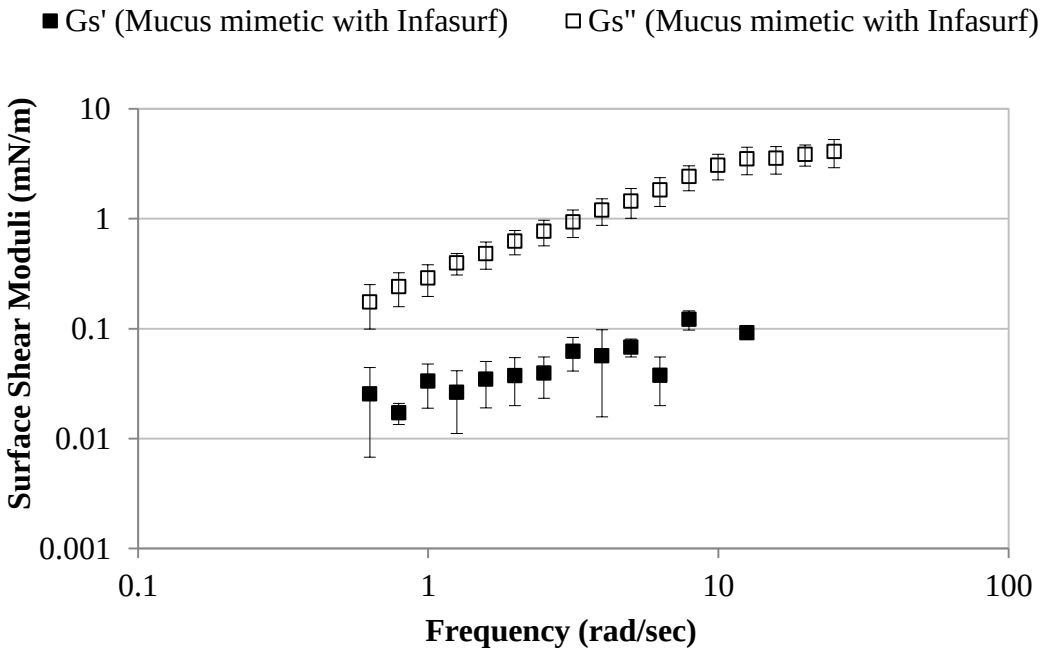

Figure 4-6: Frequency-dependence of surface shear storage modulus G_s' and surface shear viscous modulus G_s" for Infasurf® spread at an air-mimetic interface. No surface elasticity was observed above frequency of 12.5 rad/sec. Data are represented as the mean ± SD (n=6).

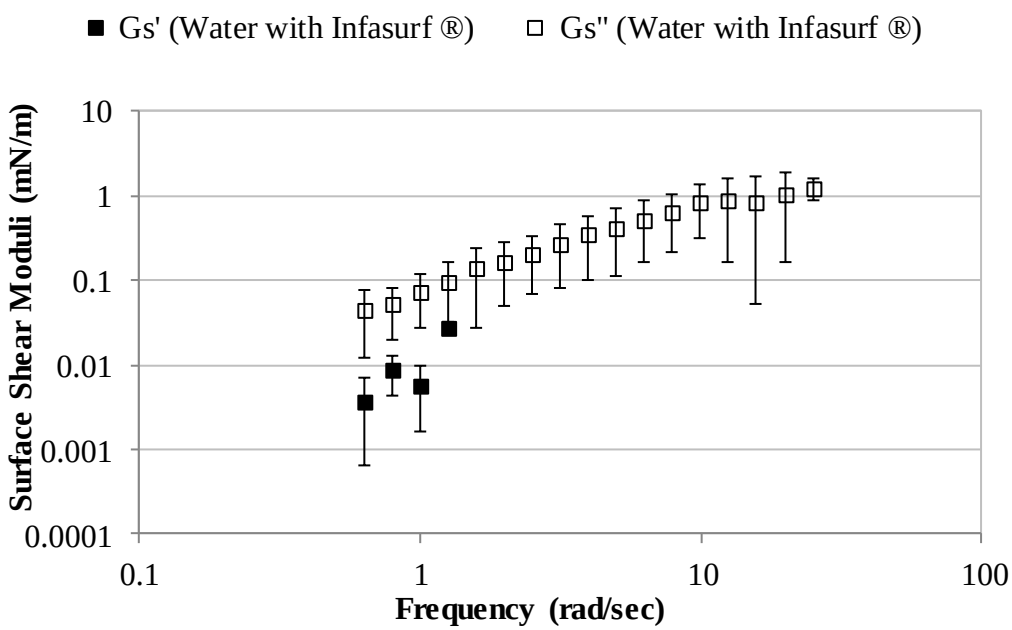

Figure 4-7: Frequency-dependence of surface shear storage modulus G_s' and surface shear viscous modulus G_s" for Infasurf® spread at an air-water interface. The interface exhibited a viscous behavior only. Data are represented as the mean ± SD (n=4).

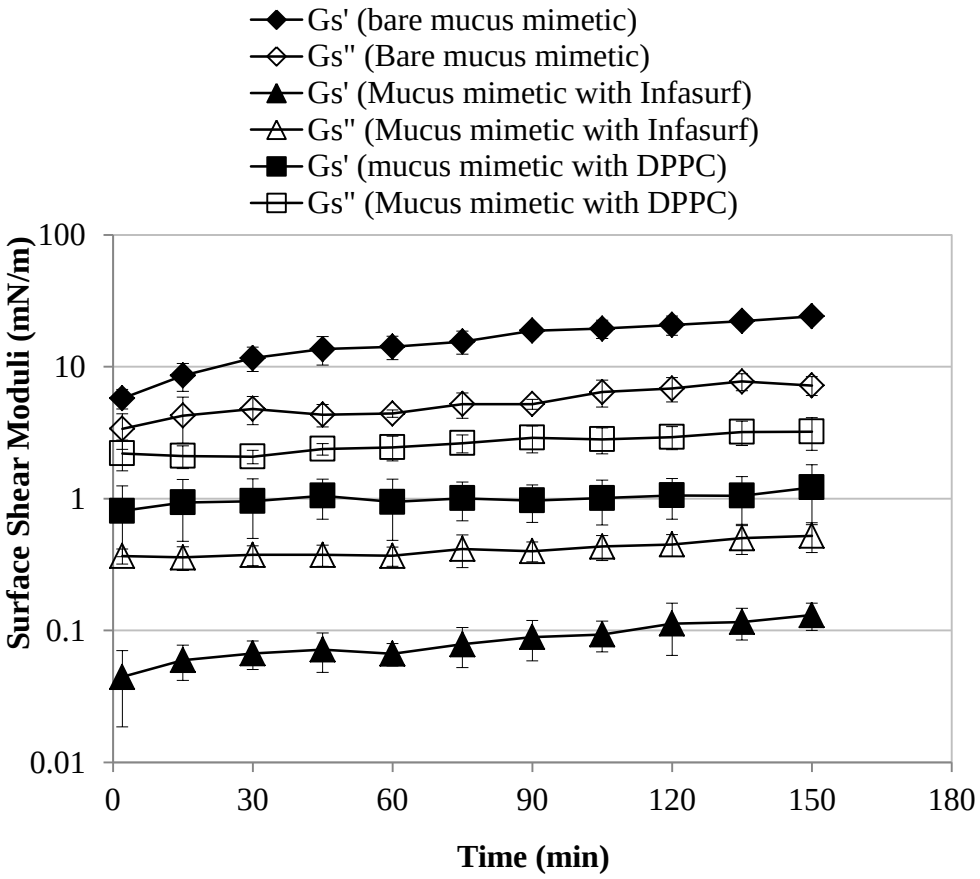

Figure 4-8: Time-dependence of surface shear storage modulus G_s' and surface shear viscous modulus G_s" of bare mucus mimetic (n=5), Infasurf® spread at an air-mimetic interface (n=3) and DPPC spread at an air-mimetic interface (n=4). Data are represented as the mean ± SD.

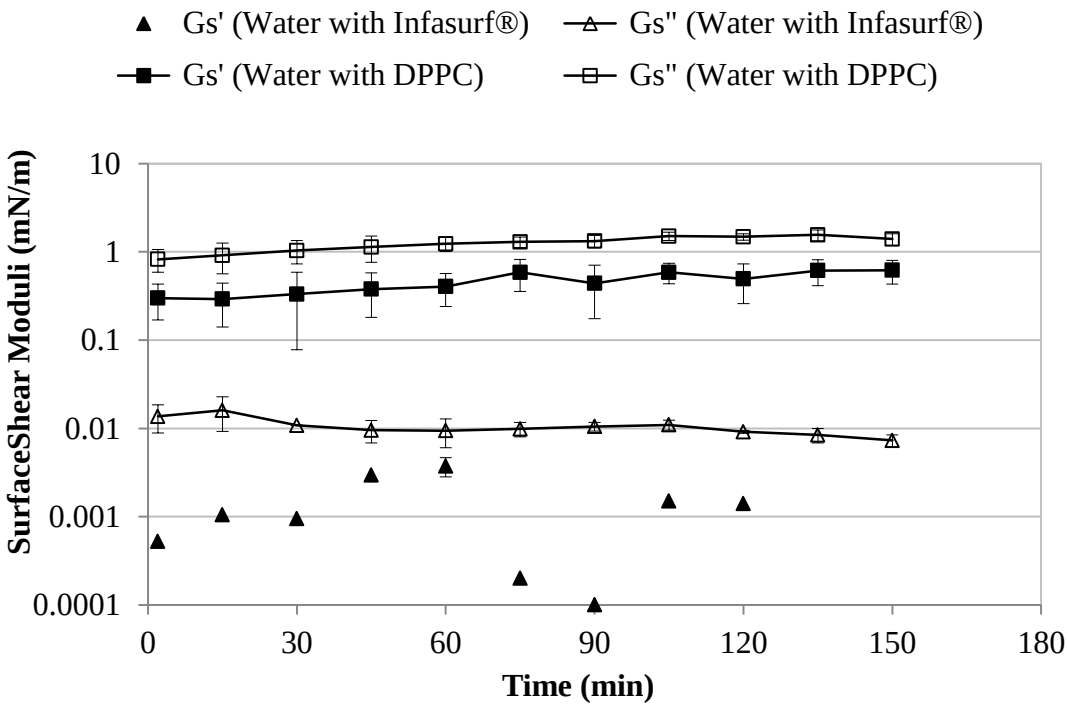

Figure 4-9: Time-dependence of surface shear storage modulus G_s' and surface shear viscous modulus G_s" for Infasurf® spread at an air-water interface (n=3) and DPPC spread at an air-water interface (n=4). The G_s' values for Infasurf® on a water subphase were below the detection limit (0.005 mN/m). Data are represented as the mean ± SD.

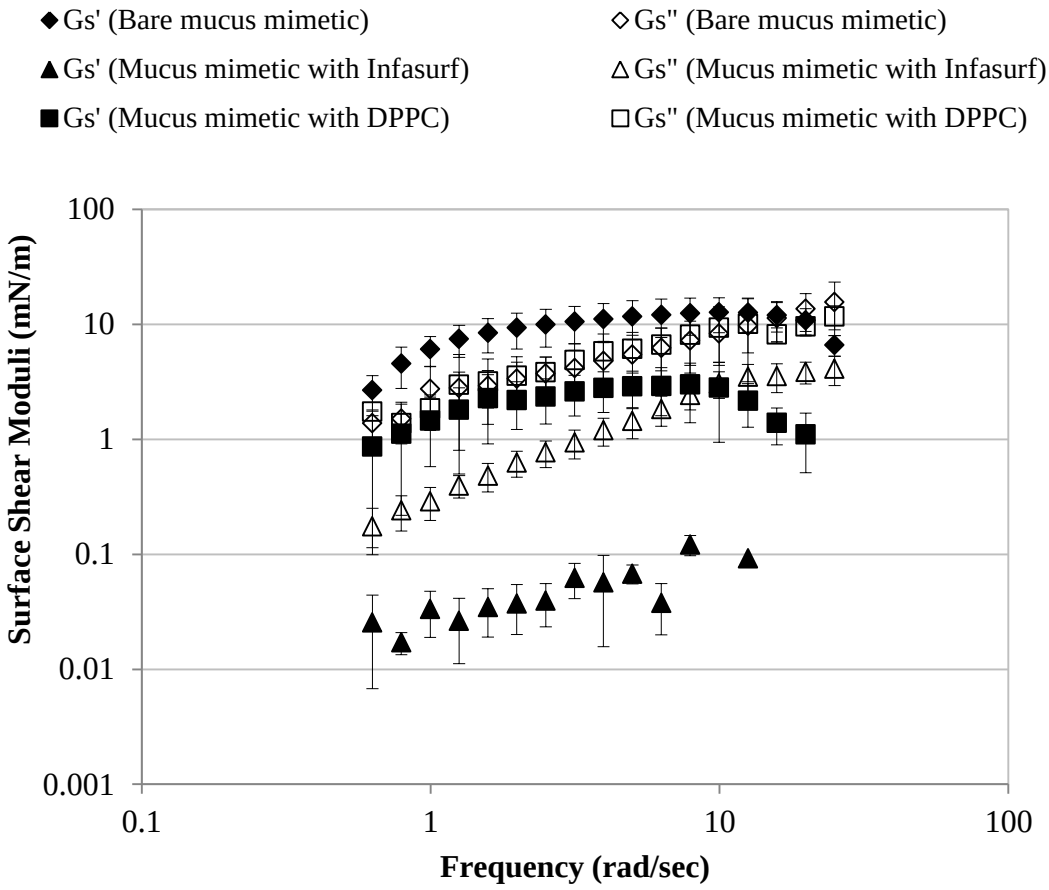

Figure 4-10: Frequency-dependence surface shear storage modulus G_s' and surface shear viscous modulus G_s" for the bare mucus mimetic (n=3), Infasurf® spread at an air-mimetic interface (n=6) and DPPC spread at an air-mimetic interface (n=5). Data are represented as the mean ± SD.

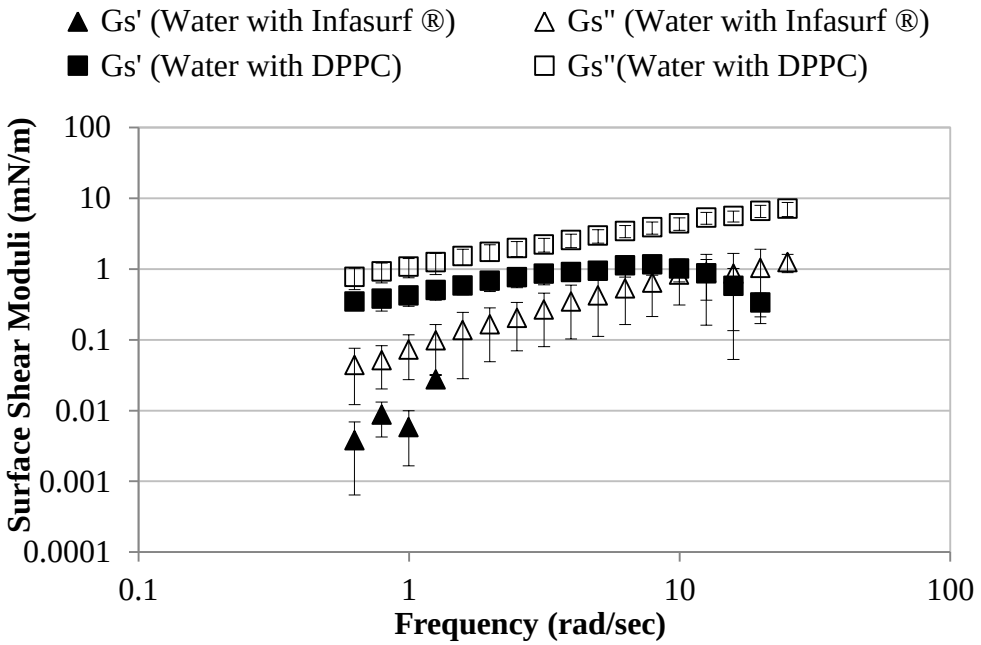

Figure 4-11: Frequency-dependence of surface shear storage modulus G_s' and surface shear viscous modulus G_s" for Infasurf® spread at an air-water interface (n=4) and DPPC spread at an air-water interface (n=4). The G_s' values for Infasurf® on a water subphase were below the detection limit (0.005 mN/m). Data are represented as the mean ± SD.

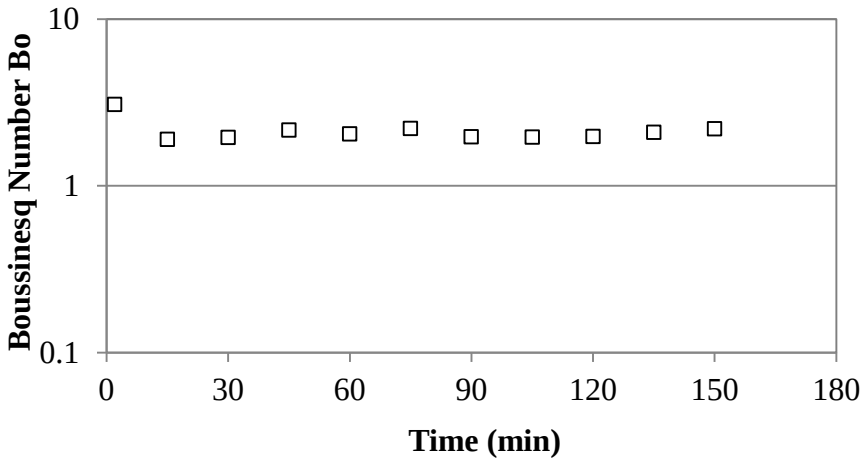

Figure 4-12: Boussinesq number Bo calculated based on the time-dependent G" of mucus mimetic (Figure 3-12) and the time-dependent G_s" of the mucus mimetic covered with Infasurf® (Figure 4-3) at different time points.

CHAPTER 5

ENHANCEMENT OF THE SIMULATED COUGH MACHINE

5.1. Introduction

A better understanding of the function of pulmonary mucus and the mechanisms underlying these functions can be gained through the use of model *in vitro* systems. One *in vitro* system, the simulated cough machine (SCM), was originally developed by King *et al.* to study mucus clearance by cough.[49, 73, 147] More recently, the SCM has been used to study the formation of bioaerosols from the fluid surface of the large conducting airways.[15, 50, 58] In these studies, a compressed airstream was passed over a mucus simulant to simulate air flow during a cough maneuver and to generate droplets from the mucus simulant surface. In all these cases, the SCM was operated at room temperature and at an uncontrolled relative humidity (%RH). In addition, a dry air stream was used to shear the mucus simulant surface. However, McRae *et al.*[148] have measured the temperature and %RH of the tracheal airways in sixteen healthy volunteers and found tracheal temperatures of 35.8-36.4°C and %RH of 98.8-99.7% during expiration. Thus, the tracheal air on expiration is almost fully saturated with water vapor with a temperature of ~ 1°C below the core body temperature. Therefore, conditions during *in vitro* studies have not accurately mimicked those in the trachea. Droplets generated under these conditions would have been highly susceptible to drying prior to measurement. While these *in vitro* studies have provided key information on the ability of exhaled bioaerosols to remain suspended and therefore potentially transmit disease, they do not address bioaerosol formation mechanisms.

Droplets will shrink due to drying based on their initial size, their nonvolatile component concentration and the environment in which they are contained. If a droplet is sufficiently small, it will remain suspended in air for several minutes or more. Larger droplets can undergo rapid drying to become sufficiently small to remain suspended in air

for a similar duration.[149] The evaporation of water droplets when expired into an environment of lower temperature and %RH than in the respiratory tract have been addressed in literature.[68, 149] It has been shown by Wells[150] that respiratory droplets with diameters <100 µm rapidly evaporate to become droplet nuclei (<5 µm). However, a recent model by Nicas *et al.*[149] have demonstrated that an emitted droplet of diameter >20 µm can may not become droplet nuclei, depending on the presence of nonvolatile components or the relative humidity of the surrounding air. In this model, Nicas *et al.*[149] showed that respiratory droplets contain nonvolatile components, such as ions and glycoproteins, which reduce the tendency of these droplets to shrink. The emitted particles quickly decrease in diameter, due to evaporation, to an equilibrium diameter equal to about one half of their initial size (the diameter of particle at which there is no net change in water content of droplet, i.e. there is a balance between water vapor evaporation from and condensation on the particle). This analysis was based on calculation of respiratory droplets that are composed of an aqueous solution containing inorganic ions (Na^+, 91± 8 mM; K^+, 60 ± 11 mM; and Cl^-,102 ± 17 mM) and other mucus components (lactate, 44 ± 17 mM; and glycoprotein, 76 ± 18 g/L).

In complete drying, it was assumed that the mass of nonvolatile species in the dry particle equals the mass of the emitted particle:

$$d_{eq} = d_0 \left(C_{nonvolatile} / \rho_{nonvolatile}\right)^{1/3}$$

where d_{eq} is the equilibrium particle diameter and d_0 is the initial particle diameter. If the total mass concentration ($C_{nonvolatile}$) for the five non-volatile species is taken as 88 g/L and the density of nonvolatile components ($\rho_{nonvolatile}$) is estimated as the density of water (1000 g/L), since the dry density of the complex mixture of solutes in the respiratory fluid is unknown, this model predicts an equilibrium diameter $d_{eq} = 0.44 \times d_0$. In comparison, if the droplets of the respiratory fluid were treated as purely salt particles containing NaCl at 150 mM, then $d_{eq} = 0.16 \times d_0$.

The primary theory of bioaerosol formation suggests that exhaled droplets are generated due to the shearing of the surface of the airway lining fluid by the passage of air during normal breathing, sneezing and coughing.[7, 58, 62] Therefore, these droplets likely contain various mucus components, including ions, proteins and surfactants. We expect, then, that the former model is more appropriate as an estimate the equilibrium size of respiratory droplets. If the exhaled droplets are treated as containing only NaCl, then the estimated equilibrium size will be much smaller than that estimated for droplet containing all mucus components.

The relative humidity of the surrounding air in which the droplet is suspended significantly affects the final equilibrium size of the droplet. At a higher RH of 50%, the equilibrium diameter for a salt particle containing 150 mM NaCl would be ~19% of its initial size.[149] In this case, $d_{eq} = 0.19 \times d_{0.}$ Nicas *et al.*[149] used this same approximation to determine the equilibrium diameter for incomplete dry particle of respiratory fluid at 50% RH, where a rough estimate was given as $d_{eq} = 1.19 \times 0.44\ d_0 = 0.52\ d_0$. Under an indoor %RH range of 30% to 70%, the estimated equilibrium diameters were $d_{eq} = 0.47 \times d_0$ (30% RH) to $0.61 \times d_0$ (70% RH).

The time required to attain the equilibrium diameter (t_{eq}) has been calculated based on the following equation:

$$t_{eq} = \frac{\varepsilon}{P_{sat} - P_{water}} (d_o^2 - d_{eq}^2)$$

where $\varepsilon = 9.35 \times 10^8$ g/(cm^3·sec) = kT/8v_mD (T = 293 K (20°C) in these calculations, k = Boltzmann's constant = 1.38×10^{-16} erg/K, v_m = condensed-phase volume occupied by a single water molecule = 3×10^{-23} cm^3, and D = molecular diffusivity of water vapor in air = 0.18 cm^2/sec), P_{sat} is partial pressure of water vapor in equilibrium with the surface of droplet, and P_{water} is the partial pressure of water vapor in ambient air. It has been shown that the estimated time for a respiratory particle with d_0 of 20 µm to attain d_{eq} of 10 µm, under temperature of 20°C and %RH range of 50% was 0.24 sec. However, at 30% and

70% RH, the estimated equilibrium time was 0.17 sec and 0.40 sec, respectively. In addition, particles of d_0 <20 µm will attain their equilibrium diameter even faster. For instance, based on Nicas *et al.*[149] model, a particle with d_0 of 10 µm would need 0.05, 0.06 and 0.08 sec to reach d_{eq} of 4.7 µm, 5.2 µm and 6.1 µm at %RH of 30%, 50% and 70%, respectively. Based on these extremely short time scales, this model assumes that respiratory particles of initial diameters of ≤20 µm are susceptible to evaporation immediately after being emitted at room temperature of ~ 20°C and typical %RH (30-70%). Therefore, the submicron median particle size measured in previous studies[50, 58] was more likely the equilibrium particle diameter, where equilibrium diameter can be attained instantaneously (t_{eq} would expected to be less than that calculated for a particle with d_0 of 1 µm) at room temperature of a typical range of indoor %RH (30%-70%).

The objective of this study was to better simulate the conditions of the trachea during cough to limit droplet drying and mimic trachea temperature. This was achieved by placing our home-built SCM inside an enclosure system conditioned at 37°C, and warming and humidifying the air used to generate the simulated cough. Therefore, this chapter focuses on developing an enhanced SCM with features that better mimic the conditions of the trachea to generate bioaerosols from mucus mimetic surfaces. By enhancing the features of the SCM, droplets generated from mucus mimetic surfaces are expected to be more representative of the exhaled droplets generated from humans. Enhancing the SCM should enable a better understanding of the mechanism of bioaerosol formation from the large conducting airways, as will be discussed in Chapter 6.

5.2. Materials and Methods

5.2.1. Simulated Cough Machine

The simulated cough machine (SCM) was developed as has been described in detail by King *et al.*[49] A 6.25-liter lung tank was equipped with a digital pressure gauge (Ashcroft, model #595-02 with a measuring range 0-15 psi) and a pressure relief valve

(F.C. Kingston Co., model #111x-2-010) to supply a volume of air representative of average lung capacity.[58] A dry medical compressed air cylinder was connected to the air reservoir to provide the volume of air and to pressurize the air tank for cough simulation. An air filter (Domnick Hunter) of 0.2 μm was connected to the compressed air cylinder to remove particulates from the air before entering the 6.25-liter lung tank. The outlet of the air reservoir was connected to a solenoid valve (Asco, Florham Park, NJ) to control the release of air. The solenoid valve was connected to a Fleisch pneumotachograph (Model no. 4, Phipps and Bird) with a differential pressure transducer (Model no. DP 45-14, Validyne, North Ridge, CA) to measure the pressure drop over the course of the simulated cough. The pneumotachograph was calibrated twice during this study in the Biomedical Engineering Laboratory at The University of Iowa. The differential pressure transducer measures the pressure drop through the pneumotachograph, amplifies the signal and converts it to a flow rate profile using LABVIEW software (National Instruments, Austin, TX). The pneumotachograph was connected to a rectangular Plexiglas trough (31 cm x 1.6 cm x 1.2 cm) used as a model trachea. The distal end of the model trachea was connected to a particle sizer (Sympatec, HELOS laser diffraction system) that was used to measure the size range from 0.1 to 35 μm of bioaerosols exiting the SCM.

Prior to a cough, the trough was lined with 20 cm of mucus mimetic (corresponding to the length of the trachea) at a depth ≈ 2 mm. The 6.25-liter lung tank was pressurized to ~ 6.5 psi. The solenoid valve was opened to release the compressed air, generating a simulated biphasic cough profile with a peak flow rate between 10 and 14 L/sec over ≈ 0.5 sec (Figure 5-2). The opening of the solenoid valve was controlled by the LABVIEW software. The passage of air over the mucus mimetic sheared the mucus surface and led to the breakup of the surface and bioaerosol formation. The size distribution of droplets entrained within the air stream and exiting the SCM was determined via the particle sizer. Prior to particle sizing, a vacuum connected to the end

of particle sizer was opened to draw the generated particles through the particle sizer. The valve for the house vacuum was opened simultaneously with the start of the particle sizing measurements.

5.2.2. Generation of Bioaerosols from Mucus Mimetic Surfaces

Bioaerosols were generated from the surface of the mucus mimetic with DPPC using the SCM that was developed by King *et al*.[49] and described in section 5.2.1. The mucus mimetic was used in this study because of its more liquid-like bulk rheological properties at low shear rates, which allowed spreading of surfactants onto its surface, and its high viscoelastic properties at high shear, which mimics the tracheal mucus properties. Mimetic was lined on the bottom of a Plexiglas trough at a depth ~ 2.0 mm to create a model trachea. A dry air stream during a simulated cough maneuver was passed across the mucus mimetic surface. The passage of air over the mucus mimetic results in shearing of the mimetic surface and in creating surface disturbances which lead to breakup of the surface and to aerosol formation. The size distribution of droplets entrained within the air stream and exiting the SCM was determined via the particle sizer (Sympatec, HELOS laser diffraction system) which was connected to the outlet of the trough. The size distributions for bioaerosols were generated from mimetic surfaces during a single cough. Before each experiment, a reference measurement was made for dry air during a simulated cough maneuver as a background. This background data was stored and subtracted out from the detector readings recorded during the sample measurement. The difference between background and measurement intensity is the diffraction pattern, or raw data, used to calculate the size distribution. At least three bioaerosol measurements were taken for mucus mimetic with DPPC sample.

5.2.3. Mimicking Tracheal Conditions in the SCM

The SCM was placed inside a home-built Plexiglas enclosure system (Figure 5-3). Three sides of the enclosure system were insulated with extruded polystyrene to minimize heat loss except one side, which could be opened to enable access to the SCM. Two electrical heaters (Hoffman, Cat no. DAH-8001B, China; and Honeywell, model HZ-315, China), each adjusted between 37-39°C, were used to maintain the temperature inside the enclosure system to ~ 37°C, to simulate human body temperature. Air during a simulated cough was conditioned as follows: dry air from the compressed air cylinder was passed through an inlet air tube into a pressure cooker (Presto®, capacity 23 Quart) equipped with digital pressure gauge (Ashcraft, Model #1309, China; measuring range 0-20 psi) and a temperature sensor (TREND, China; measuring range 0-200°F) (Figure 5-4). The pressure cooker was filled with deionized water up to two third of its capacity. Water within the pressure cooker was heated using a hotplate/stirrer (VWR, Cat. #12365-382; Batavia, IL) adjusted at ~ 300°C. This led to an air temperature within the pressure cooker of 54.4-60.0°C at a pressure of 4-5 psi. The air inlet tube (19.6 cm x 0.5 cm) of the pressure cooker was extended into the water at the bottom of pressure cooker (Figure 5-5). The outlet air tube of the pressure cooker was extended into the air space above the body of water (Figure 5-5). This outlet air tube was then passed to the 6.25-liter lung tank. A one-way valve (Eastman Imperial Company, Baltimore, MD) was placed on the pressure cooker to control flow of dry air from the compressed air cylinder to the pressure cooker in one direction. To condition the model trachea, the 6.25-liter lung tank was pressurized continuously and a simulated biphasic cough profile of warmed and humidified air was passed through the SCM. Two temperature/RH probes (Model RH-USB, Omega engineering Inc., Stamford, CT) with temperature ranges of -17 to 49°C and %RH range of 2-98% were used to measure the temperature and %RH of the conditioned air. One probe was inserted into the 6.25-liter lung tank to measure the temperature and %RH of air inside the tank and the other was inserted into a small

chamber immediately before the trough to measure the temperature and %RH of air entering the model trachea.

In the model trachea, two pieces of Plexiglas of 1.5 mm thickness were placed and glued at the bottom of the two ends of the trough to control the thickness of the mimetic layer and minimize the edge effect of the mimetic within the trough (Figure 5-6). The distance between droplet generation source and probe inlet of the HELOS particle sizer was reduced to the minimum (3 cm) to minimize impaction and sedimentation of the large particles.

Parameters that were kept constant (i.e. similar to the SCM of King *et al*. [49, 73, 147]) included: 1) size of the Plexiglas trough (31 cm x1.6 cm x 2 cm), 2) size of the air holding tank (6.25-liter lung tank), and 3) the dry compressed air source. Parameters that were changed were: 1) use of a more physiologically relevant *in-vitro* model mucus mimetic, 2) thickness of the mucus layer (1.5 mm), 3) temperature and %RH of air entering model trachea, 4) temperature and %RH of air inside the 6.25-liter lung tank, and 5) temperature inside the enclosure system.

5.3. Results and Discussion

5.3.1. Size Distribution of Bioaerosols during a Simulated Cough Maneuver

Bioaerosols were generated from the mucus mimetic surface without conditioning the SCM, where the heaters inside the enclosure system were turned off and the air entering the model trachea was dry, room temperature air. The temperature and %RH in the SCM and enclosure system remained relatively constant throughout the bioaerosol experiments (Table 5-1). The temperature and %RH inside the enclosure system were 23.80 ± 0.45°C and 26.20 ± 0.45%, respectively. The temperature of the air entering the model trachea was 24.56 ± 0.11°C and %RH of 29.30 ± 2.66%. The temperature of the air inside the 6.25-liter lung tank was 27.10 ± 0.86°C.

The optical concentration (Copt%), which is a measure of the amount of laser light that is being blocked by the sample, was used as an indicator of the relative concentration of the aerosol produced by the mimetic surface. Table 5-2 illustrates the Copt% for bioaerosols generated from six mimetic samples during a simulated cough maneuver with the peak air flow rate for each cough. The Copt% of bioaerosols generated from five samples was 0.0%, indicating no measurable quantity of bioaerosols was formed during cough. In addition, the Copt% for the sixth sample was low (0.19%). The low Copt% suggested that any bioaerosols being formed were rapidly evaporated due to the low humidity of the air stream. Therefore, conditioning the SCM to a higher %RH may help the aerosols maintain their original size for longer periods of time and improve our ability to detect the aerosols. Therefore, bioaerosols were generated from mucus mimetic surfaces using the enhanced SCM where the temperature inside the enclosure system was maintained at ~ 37°C and the air entering the model trachea was conditioned (bioaerosol detection under high temperature and RH conditions will be discussed in Chapter 6).

5.3.2. Enhancement of the Simulated Cough Machine

To mimic the conditions of the trachea, the two heaters inside the enclosure system were maintained at a temperature between 37-39°C, close to body core temperature, and the water within the pressure cooker was heated at 300°C to generate an air stream at body temperature. Table 5-3 illustrates the temperature and %RH of air entering model trachea, air inside 6.25-liter lung tank, and inside the enclosure system recorded during warming and humidifying the air and warming the enclosure system. The air entering the model trachea was conditioned to 34.8 ± 0.7°C and 39.0 ± 2.8% RH (n=11). Therefore, the maximum %RH that was achieved for air entering the model trachea was ~ 39%. The temperature and %RH for the air inside the 6.25-liter lung tank was 33.4 ± 0.2°C and 103.2 ± 0.3% RH (n=11). This high %RH inside the 6.25-liter lung

tank may be due to a condensation on the probe resulting from a temperature difference between air coming from the pressure cooker (~ 48°C) and air inside the 6.25-liter lung tank (~ 33°C). In addition, condensation may be due to the reduction in the temperature of air after its expansion into the 6.25-liter lung tank. The temperature and %RH inside the enclosure system was 31.6 ± 0.5°C and 25.3 ± 1.8% (n=11), respectively. The %RH inside the enclosure system was low since no humidification took place inside the enclosure system.

To further increase the %RH of the air entering the model trachea, warmed and humidified air was purged through the SCM via multiple simulated coughs. Table 5-4 summarizes the conditions of the enhanced SCM via multiple cough maneuvers. After three cough maneuvers, the %RH of air entering the model trachea increased from 39.0 ± 2.8% to 61.5 ± 6.2% (n=3). While this was a significant increase in %RH over the original SCM design, it is not as high as that in the mammalian trachea (98.8-99.7%)[148]. A reduction in %RH (46.7 ± 8.5, n=3) was observed immediately after performing a simulated cough profile. This reduction was due to the opening of the vacuum system attached to the particle sizer. Low %RH (30%) was observed inside the enclosure system, where no humidification took place.

The conditioning of air entering the model trachea is expected to have an impact on the size of droplets exiting the SCM, where increasing the %RH reduces the rate of droplet evaporation. Based on Nicas's model, the time required for a droplet to reach its equilibrium size, t_{eq}, can be compared to the average time required for the same droplet to reach the detector. This will provide an estimate of whether the droplets have reached their equilibrium size or maintained a size closer to their original size when they reach the detector. Using the above equation for t_{eq}, a particle with an initial size of 10 µm would require about $3x10^{-2}$ sec to reach its equilibrium size (assuming T = 35ºC and RH = 61.5%; therefore, $d_{eq} \approx 0.57d_o$ and $P_{sat} \approx 6000$ Pa). Likewise, a 1 µm particle would require $3x10^{-3}$ sec; a 0.1 µm particle would require $3x10^{-4}$ sec. The time to reach the

detector, t_{det}, was calculated assuming the droplets flow with the air stream. The shortest time needed for the droplet to reach the detector of the particle sizer was estimated as 4.1×10^{-3} sec. This value was calculated using t=l/V, where l is the length of the path the droplet would take to get to the detector [25.5 cm = length of the model trachea (20 cm) plus the distance between the distal end of the model trachea and the outlet connected to the particle sizer (5.5 cm)] and V is the velocity of the air used to shear the mimetic surface [6250 cm/sec, calculated using V= Q/A, where Q is the peak air flow rate entering the model trachea of an average of 12 L/sec and A is cross-sectional area of the model trachea of 1.6 cm×1.2 cm]. Given a lower average air flow rate (i.e. not taking the peak flow rate), the time to reach the detector would be longer; for example, at 625 cm/sec on average, $t_{det} = 4.1x10^{-2}$ sec. These calculations suggest that all particles will have reached their equilibrium size, or very close to their equilibrium size, by the time they reach the detector. Given the higher RH conditions in the present studies, however, the equilibrium size will be larger than in previous studies, thereby increasing the ability to detect the droplets and likely providing a more accurate measure of equilibrium particle size. Finally, by controlling the environmental conditions during bioaerosol formation and detection, these equations could be used to estimate the original droplet size generated during bioaerosol formation.

5.4. Conclusions

Bioaerosols were generated from mucus mimetic surfaces using the simulated cough machine (SCM) as described by King *et al*.[49], where the temperature and humidity of the system were not specifically maintained. The optical concentration measured during simulated coughs was extremely low, suggesting the need to prevent aerosol drying. Therefore, of the relative humidity within the SCM was increased to ~ 62% by conditioning the inlet air stream prior to the simulated cough. In addition, the temperature of the entire SCM system was maintained at ~ 37°C by placing the SCM inside a home-

built enclosure chamber. Since temperature and %RH are important factors in determining droplet size, increasing these factors within the SCM will significantly alter the measured size of bioaerosols generated during simulated cough. By better mimicking the conditions with the mammalian trachea, we expect to gain a better understanding of bioaerosol formation within the conducting airways using this improved SCM system.

Table 5-1: Conditions of the SCM as developed based on King *et al. 's*[49, 73, 147] during a simulated cough maneuver while generating bioaerosols from mucus mimetic with DPPC surfaces.

Parameter	**Air entering model Trachea**	**Air inside 6.25-liter lung tank**	**Enclosure system**
Temperature (°C)	24.56 ± 0.11	27.1 ± 0.86	23.8 ± 0.45
RH (%)	29.3 ± 2.66	NR*	26.2 ± 0.45

†Temperature was off inside the enclosure system and air was not conditioned.

*NR = not recorded due to problems with the RH probe.

Table 5-2: Copt% and peak air flow rate (L/sec) for each sample of the mucus mimetic with DPPC during a simulated cough maneuver.

Sample #	**Copt%**	**Flow rate (L/sec)**
1	0.0	9.50
2	0.0	11.20
3	0.0	10.50
4	0.0	10.80
5	0.0	14.50
6	0.19	11.84
Mean ±SD	**0.03±0.08**	**11.39±1.71**

†Temperature was off inside the enclosure system and air was not conditioned.

Table 5-3: Conditions of the enhanced SCM during a single cough maneuver: temperature and %RH of air entering the model trachea, air inside the 6.25-liter lung tank, inside the enclosure system, temperature and pressure of air within pressure cooker, and peak air flow rate during a simulated cough maneuver.

Run #	Air entering model trachea		Air inside 6.25-liter lung tank		Enclosure system		Pressure cooker		Peak flow rate (L/sec)
	Temp. (°C)	%RH	Temp (°C)	%RH	Temp (°C)	%RH	Air Temp. (°C)	Pressure (psi)	
1	35.9	32.1	33.9	102.2	32.4	22.0	47.8	5.0	11.7
2	35.6	37.3	33.6	103.0	32.1	23.0	47.8	5.0	7.5
3	35.5	39.1	33.5	103.1	32.0	24.0	47.8	5.0	28.0
4	35.2	36.9	33.4	103.3	31.8	24.0	47.8	5.0	8.2
5	35.1	38.5	33.4	103.3	31.7	25.0	47.8	5.0	31.0
6	34.9	41.4	33.3	103.2	31.6	26.0	47.8	5.0	18.8
7	34.8	39.2	33.3	103.3	31.5	26.0	47.8	5.0	10.7
8	34.3	40.1	33.2	103.3	31.2	27.0	47.8	5.0	8.5
9	34.2	41.3	33.2	103.3	31.1	27.0	47.8	5.0	15.0
10	34.0	41.1	33.1	103.3	31.0	27.0	47.8	5.0	10.1
11	33.8	41.7	33.1	103.3	30.8	27.0	47.8	5.0	28.5
Mean± SD	**34.8 ± 0.7**	**39.0 ± 2.8**	**33.4 ± 0.2**	**103.2 ± 0.3**	**31.6 ± 0.5**	**25.3 ± 1.8**	**47.8 ± 0.0**	**5.0 ± 0.0**	**16.2 ± 9.0**

Table 5-4: Conditions of the enhanced SCM during multiple maneuvers: temperature and %RH of air entering the model trachea and air inside the 6.25-liter lung tank.

Run #	**Air entering model trachea**		**Air inside 6.25-liter lung tank**	
	Temp (°C)	**%RH**	**Temp. (°C)**	**%RH**
1	34.9	57.0	33.1	103.4
2	34.3	58.9	32.8	103.4
3	36.1	68.6	34.7	103.2
Mean ± SD	**35.1 ± 0.9**	**61.5 ± 6.2**	**33.5 ± 1.0**	**103.3 ± 0.1**

†The temperature inside the enclosure system was maintained at ~ 37°C.

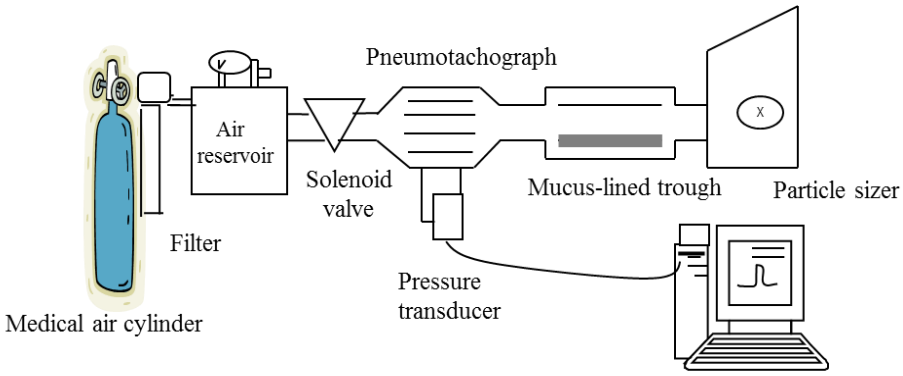

Figure 5-1: Sketch of the home-built simulated cough machine (SCM).

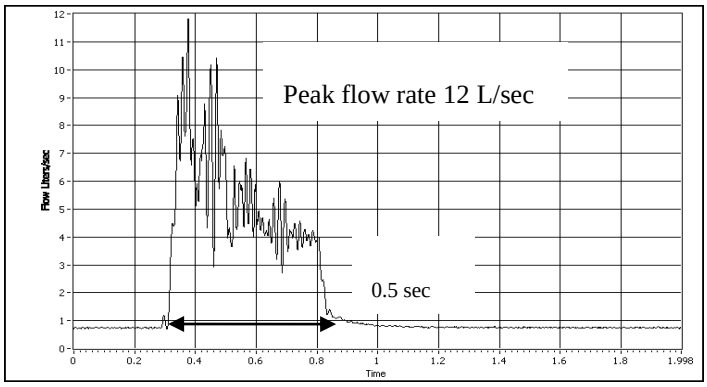

Figure 5-2: Simulated cough profile generated from the SCM.

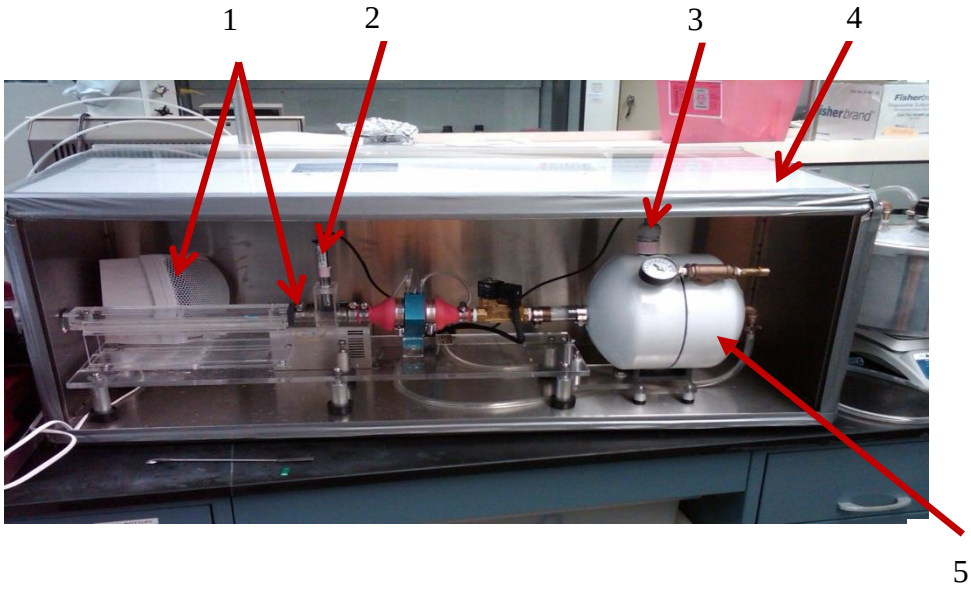

Figure 5-3: Enhanced SCM: (1) two heaters inside the chamber to increase the temperature up to ~ 37°C, (2) probe inside a small chamber to record the temperature and %RH of air entering the model trachea, (3) probe to record the temperature and %RH of air in the 6.25-liter lung tank, (4) enclosure system for the SCM, and (5) inlet for the conditioned air to the 6.25-liter lung tank.

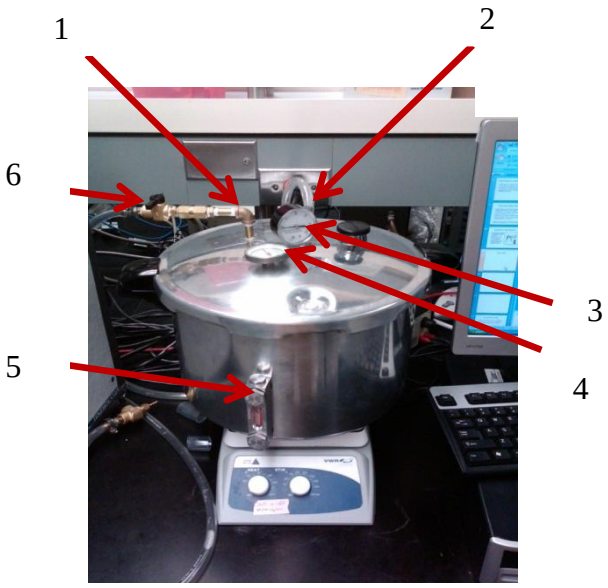

Figure 5-4: Pressure cooker used to warm and humidify air entering the model trachea: (1) inlet for dry air which comes from the compressed air cylinder (2) outlet of warmed and humidified air that goes to the 6.25-liter lung tank, (3) pressure gauge to record pressure inside the pressure cooker (4) temperature sensor to measure the temperature of air inside the pressure cooker, (5) volume gauge to indicate water volume inside the pressure cooker, and (6) one-way valve which allows the flow of air from the compressed air cylinder to the pressure cooker in one-direction.

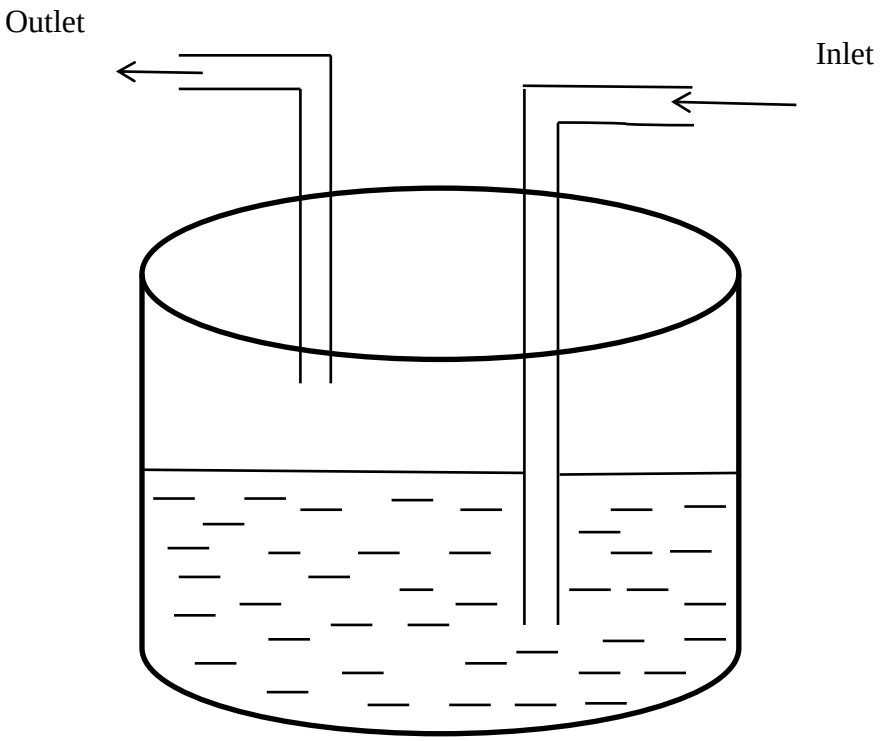

Figure 5-5: Schematic diagram for conditioning the air entering the model trachea using the pressure cooker. The inlet air tube (19.6 cm x 0.5 cm), which comes directly from the dry compressed air cylinder, extends inside the water, and the outlet tube of conditioned air, which passes to the 6.25-liter lung tank, extends above the water within the pressure cooker.

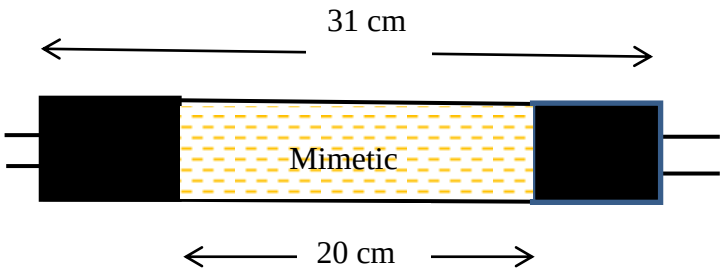

Figure 5-6: Trough of 31 cm length with mucus mimetic lined 20 cm of the trough representing the model trachea. Two pieces of Plexiglas (~ 1.5 mm thickness) placed at each end of the trough to remove the edge effects of mimetic within the trough.

CHAPTER 6

BIOAEROSOL FORMATION FROM THE TRACHEA

6.1. Introduction

The rapid spread of airborne infectious diseases remains a critical threat to the health of the human population. The emergence of new infectious diseases and re-emergence of diseases considered under control has spurred increased attention to the development of new therapies or strategies to halt their spread. However, the lack of knowledge about the mechanism of formation of bioaerosols and pathogen-containing bioaerosols in the human lungs has hindered the development of new alternative strategies to halt the transmission of airborne infectious diseases. It is now understood that airborne infectious diseases are transmitted from person to person by droplets or droplet nuclei carried in exhaled breath known as bioaerosols.[58, 59] These droplets can be loaded with pathogens and exhaled out of the lungs of infected individual and into the environment; those who inhale ambient aerosols can become infected.

The proposed mechanisms of bioaerosol formation were discussed in detail in section 1.5 in Chapter 1. Briefly, the primary theory for bioaerosol formation suggested that droplets are formed by the passage of air over the airway lining fluid (ALF) during inhalation and exhalation, which shears the ALF surface and breaks it up into small droplets.[58] An alternative theory suggested that these exhaled droplets are formed through the reopening of closed peripheral airways, particularly in the lower bronchioles, during the inhalation phase while breathing.[60]

To date, the exact mechanism of bioaerosol formation in the large conducting airways is still not known and little information is available on the size distribution of bioaerosol droplets generated from tracheal surface. The size of bioaerosol droplets is an important factor in determining: 1) the fate of the droplets since large droplets (>10 μm) quickly settle on near surfaces and small droplets (≤10 μm) can remain suspended in the

air for long times, 2) the types of pathogenic organisms that can be transported by airborne route, as the size of viruses is on the order of 100's of nanometers while that of bacteria tends to be in the micron size range, and 3) the control measures that can be used to prevent the spread of droplets and disease since size directly impacts filtration efficiency.[8, 59]

Various control strategies (such as ventilation, filtration, UV irradiation and vaccination) traditionally have been used to halt the spread of airborne infectious diseases, with varying degrees of success due to their limited effectiveness, high cost and limited practicality. For instance, well-fitted surgical masks, face shields and other respiratory protective equipment cannot be worn for long periods of time as they impair the performance of users. In addition, although vaccination is the main strategy used to control airborne infectious disease, its immediate availability remains a major limitation. Therefore, new, cost effective strategies are needed to fight airborne infectious diseases. One new strategy aims to prevent the aerosolization of exhaled droplets by limiting their formation in the lungs. Edwards *et al*.[8, 50, 58, 71] have shown that this strategy can be effectively implemented *in-vivo* by depositing simple salt solutions in the lungs. They have shown that delivery of isotonic saline (0.9% sodium chloride, NaCl) to bull calves and humans reduces the number of exhaled bioaerosols and promotes the formation of larger droplet sizes. Delivery of ~ 1 g normal saline into human lungs for 6 min diminished the exhaled bioaerosol production of super-producers (individuals who produce >500 droplets/liter of air during normal breathing) by 72% over a six hour period. *In-vitro* studies suggested that the diameter of these exhaled droplets shifted to values >10 μm. The large size of these aerosols would cause them to be filtered by the respiratory tract via inertial deposition or to settle quickly upon exhalation due to gravitational forces. The opposite trend was observed for low producers (individuals who produce <500 droplets/liter of air during normal breathing). These individuals expired more particles after inhaling isotonic saline. In a follow up study,[50] Watanabe *et al*. have

shown that the nebulization of isotonic saline to the lungs of bull calves for 6 min reduces their exhaled bioaerosols for 120 minutes by more than 50% compared to pretreatment. This diminution in bioaerosol counts was reversible, where animals returned to baseline exhaled bioaerosol counts after 180 minutes post-treatment. In addition, the delivery of isotonic saline to the lungs of bull calves was not associated with negative health effects.[71]

The studies by Edwards *et al*. also found that the divalent cation Ca^{+2} produced greater suppression of exhaled bioaerosols than monovalent cation Na^{+}.[8] The reduction in exhaled bioaerosols following the *in-vivo* delivery of $CaCl_2$ solution into the lung was attributed to increased surface elasticity of ALF by ionic interaction between the positively charged cations and the negatively charged mucin glycoproteins. This was hypothesized to lead to a reduction in the ability of ALF surface to breakup into small droplets. The *in-vitro* deposition of NaCl and $CaCl_2$ onto mucus simulant surfaces was shown to increase the surface viscoelastic properties of the mucus simulant, and consequently reduced the ability of mucus simulant to break up into droplets in the SCM. This was suggested to be the primary mechanism of the $CaCl_2$ solution in suppressing the formation of aerosols.[8, 50]

Certain limitations were observed in these studies. Of those, the chemical composition and surface properties (particularly surface tension) of tracheal mucus were not modeled in the *in vitro* model systems. Given that bioaerosol formation due to the shear is a surface phenomenon, matching the surface tension to that *in-vivo* is expected to have a significant effect on the resulting particle count and size. Edwards *et al*. have shown that the delivery of surfactant mixtures of dipalmitoyl-phosphatidylcholine (DPPC) and 1-palmitoyl-2-oleoyl-sn-glycero-3-phosphoglycerol (POPG), 7:3 (w/w) suspended at 100 mg/ml in 0.9% saline, onto mucus simulant surfaces reduced the size of droplets relative to saline delivery.[58] Therefore, the results of these previous studies have

urged us to better understand the surface properties of the tracheal mucus after delivery of simple salt solutions.

Therefore, the first focus of this study is to elucidate the mechanism of bioaerosol generation from the surface of airway lining fluid (ALF) of the large conducting airways. In particular, we aim to determine key parameters that control the size distribution of bioaerosols generated from the large conducting airways via *in-vitro* simulated cough studies. The hypothesis of this study was that physical properties (bulk viscoelasticity, surface tension and surface rheology) of tracheal mucus control the size distribution of bioaerosols generated from ALF surface. Toward this objective, the *in-vitro* model mimetic developed in Chapter 2 was used as a representative model for native tracheal mucus to generate bioaerosols. The physical properties of the mucus mimetic (bulk and surface viscoelasticity, and surface tension) were correlated to the size distribution of bioaerosols generated from mimetic surfaces. The *in-vitro* model mimetic of low bulk viscoelasticity (mucus mimetic 1) was used in this study. The enhanced simulated cough machine (SCM) discussed in Chapter 5, which better simulates lung conditions, was used to perform cough maneuver and generate bioaerosols from mimetic surfaces.

The second objective of this study was to better understand the surface rheology of the ALF of the large conducting airways aerosolized with 1.29% $CaCl_2$, to aid further development of new aerosolizable strategies to suppress the formation of pathogenic bioaerosols at the source. This work, as discussed above, stems from previous studies which have shown that the delivery of $CaCl_2$ solutions *in-vivo* and *in-vitro* has the ability to temporarily reduce the number of exhaled bioaerosols by reversibly altering the surface properties of the large conducting airways by increasing the surface elasticity causing surface gelation of the tracheal mucus. Towards this objective, the *in-vitro* model mimetic of native tracheal mucus, discussed in Chapter 2, was used. The primary surface-active component, DPPC, was spread at the air-mimetic interface to lower the surface

tension to ~ 32 mN/m. The surface rheology of the mucus mimetic with DPPC and post-aerosolization with 1.29% $CaCl_2$ was probed using an interfacial stress rheometer (ISR).

6.2. Materials and Methods

6.2.1. Materials

Pig gastric mucin (PGM)-type III, n-hexane (99.0% purity) were purchased from Sigma-Aldrich, Inc. (St. Louis, MO), bovine serum albumin (fraction V, lyophilized powder) from Spectrum (New Brunswick, NJ) and 1, 2-dipalmitoyl-sn-glycero-3-phosphocholine (DPPC) from Genzyme Pharmaceuticals (Cambridge, MA). Infasurf® was a generous gift from ONY Inc. (Amherest, NY). Glutaraldehyde (GA, 50% w/w solution) and methanol (99.9% purity) were purchased from Fisher Scientific (Fair Lawn, NJ). Purified water (18 MΩ cm) was used in all experiments obtained from a NANOpure Infinity Ultrapure Water System, Barnstead International (Northbrook, IL). All other chemical reagents: sodium chloride (NaCl), calcium chloride ($CaCl_2.2H_2O$), sodium phosphate monobasic ($NaH_2PO_4.H_2O$), and sodium phosphate dibasic (Na_2HPO_4) were of analytical grade and used without further purification.

6.2.2. Altering the Bulk Rheology of Mucus Mimetic

The *in-vitro* model mucus mimetic used in the bioaerosols study were prepared using the modified method of preparation as mentioned in section 2.2.5 in Chapter 2. Briefly, to prepare 30 ml of the mimetic, 0.3 g albumin, 1.2 g PGM-type III and 28.5 ml buffer (154 mM NaCl, 3 mM $CaCl_2$, 15 mM NaH_2PO_4/ Na_2HPO_4; pH 7.4) were added to an amber glass bottle. Ingredients were mixed at 4°C on a tube rotator (Glas-Col, IN) for 24 hours to mix the sample. The uncross-linked mucus mimetic was used without further treatment with GA solution. The mucus mimetic was prepared by cross-linking the mimetic formulation using GA solution. A 0.5 ml-15% (w/w) GA solution was added to the 30 ml of the mimetic formulation, mixed manually at room temperature (~ 22°C) for

5 minutes, and kept stationary at room temperature for 24 hours. The *in-vitro* model mucus mimetic used in the salt solution study was prepared as mentioned in Materials and Methods section 2.2.3 in Chapter 2. Briefly, to prepare 30 ml of the mimetic, 0.3 g albumin, 1.2 g PGM-type III and 28.5 ml buffer (154 mM NaCl, 3 mM $CaCl_2$, 15 mM NaH_2PO_4/Na_2HPO_4; pH 7.4) were added to an amber glass bottle. Ingredients were mixed at 4°C on a tube rotator (Glas-Col, IN) for at least 6 days to mix the sample. The mucus mimetic was prepared by cross-linking the mimetic formulation using GA solution. A 0.5 ml-15% (w/w) GA solution was added to the 30 ml of the mimetic formulation and mixed at 4°C on a tube rotator (Glas-Col, IN) for 24 hours.

6.2.3. Altering the Surface Tension of Mucus Mimetic

The surface tension of the mucus mimetic (53.25 ± 1.22 mN/m, n=9) was lowered using two surfactants: dipalmitoylphosphatidylcholine (DPPC) and Infasurf® as discussed in Sections 3.3.1 and 4.3.1 in Chapters 3 and 4, respectively. The mucus mimetic was lined onto the model trachea of the SCM. The surface area of the model trachea lined with mucus mimetic was 32 cm^2 (20 cm length x 1.6 cm width). A volume of 52 µL of 1 mg/ml DPPC in n-hexane:methanol (95:5 v/v) solution or a volume of 17 µL of Infasurf® solution, prepared as mentioned in Materials and Methods section 4.2.3 Chapter 4, was needed to lower the surface tension of the mucus mimetic within the model trachea to ~ 32 mN/m. DPPC and Infasurf® spreading solutions were spread at an air-mimetic interface using a micro-syringe.

6.2.4. Determination of Background Aerosols

The quantity of background aerosols was determined by measuring the optical concentration (Copt%) and size distribution for three control situations: 1) aerosols entrained within dry air released directly from the compressed air cylinder, 2) aerosols entrained within dry air generated during a simulated cough maneuver, and 3) aerosols entrained within conditioned air generated during a simulated cough maneuver. The

Copt% or obscuration is the percent of laser beam intensity blocked by particles on the focus zone. Copt% measures the amount of light, from the laser beam, that is being blocked by the sample. The light blockage from particles being dispersed in the measuring zone can vary greatly. It is affected by the amount of sample in the measuring zone and the optical properties of the sample. Copt% gives a general guide to how much material is moving thru the measuring zone.

The average Copt% measured for the three control situations was used to remove background aerosols and to obtain a meaningful measurement for the size distribution of bioaerosols generated from mucus mimetic surfaces. Therefore, the average Copt% obtained was used to trigger conditions of the detector to determine the start and stop of a particle sizer measurement.

For background aerosols of dry air, the outlet of the compressed air cylinder was introduced directly into the inlet of the HELOS particle sizer and the Copt% for the aerosols entrained within airstream was determined. For background aerosols entrained within dry air generated during a simulated cough maneuver, the Copt% was determined during a simulated cough maneuver at a peak air flow rate of 10 to 14 L/sec over ~ 0.5 sec. Dry air during a simulated cough maneuver was passed through the enhanced SCM. No mucus mimetic lined the model trachea and conditions of the enhanced SCM were illustrated in Table 5-1 (Chapter 5). For background aerosols entrained within conditioned air, the Copt% was determined during a simulated cough maneuver at a peak air flow rate of 10 to 14 L/sec over ~ 0.5 sec. No mucus mimetic lined the model trachea during that test and conditions of the enhanced SCM were illustrated in Table 5-3 in Chapter 5.

6.2.5. Generation of Bioaerosols from Mucus Mimetic Surfaces

Table 6-1summarizes the physical properties (bulk and surface rheology, and surface tension) of mucus mimetics used to generate bioaerosols. Bioaerosols were generated from the surfaces of the uncross-linked mucus mimetic, mucus mimetic 1, mucus mimetic 1 with DPPC or Infasurf® spread on mimetic surface using the enhanced SCM described in Section 5.3.2 in Chapter 5. The mucus mimetic was used in this study because of its more liquid-like bulk rheological properties at low shear rates, which allowed spreading of surfactants onto its surface, and its high viscoelastic properties at high shear, which mimics the tracheal mucus properties. Mimetic was lined on the bottom of a Plexiglas trough at a depth ~1.5 mm to create a model trachea. A conditioned air stream during a simulated cough maneuver and repetitive cough maneuvers was passed across the mucus mimetic surface. The passage of air over the mucus mimetic results in shearing of the mimetic surface and in creating surface disturbances which lead to breakup of the surface and to aerosol formation. The size distribution of droplets entrained within the air stream and exiting the SCM was determined via the particle sizer (Sympatec, HELOS laser diffraction system) which was connected to the outlet of the trough. The size distributions for bioaerosols generated from mimetic surfaces during a single cough and three repetitive coughs were recorded for 5 seconds.

Before each experiment, a reference measurement was made for conditioned air during a simulated cough maneuver as a background. This background data was stored and subtracted out from the detector readings recorded during the sample measurement. The difference between background and measurement intensity is the diffraction pattern, or raw data, used to calculate the size distribution. At least three bioaerosol measurements were taken for each mucus mimetic sample.

6.2.6. Aerosolizing of $CaCl_2$ Solution

To study the effect of 1.29% $CaCl_2$ on the surface rheology of the *in-vitro* model mimetic of tracheal mucus, four subphases were tested. They included the mucus mimetic, 4% PGM solution in phosphate buffer (pH7.4) cross-linked with 0.5 ml-15% GA for 24 hrs, 1% albumin solution in phosphate buffer (pH7.4) cross-linked with 0.5 ml-15% GA for 24 hrs and water. The subphase was lined in a Plexiglas mini-trough (7.5 cm x 12 cm) as mentioned in section 3.2.3 in Chapter 3. A volume of 100 µL of 1 mg/ml DPPC in n-hexane:methanol (95:5 v/v) was spread onto the subphase. This volume is equivalent to the volume of DPPC required to lower the surface tension of the mucus mimetic to ~ 32 mN/m. The test solution 1.29% $CaCl_2$ was delivered onto the surface covered with DPPC for 2 minutes through an Aeroneb Lab nebulizer (Aerogen, Mountain View, CA) within a closed nebulization chamber (Figure 6-1). The home-built Plexiglas nebulization chamber (14.2 cm x 9.8 cm x 3.7 cm) was used to tightly cover the mini-trough during nebulization. A round hole of 2.2 cm diameter was made on the top of the nebulization chamber to fit the Aeroneb Lab nebulizer tightly inside during nebulization. At the end of the nebulization, the nebulizer was removed and the hole was covered by a round Plexiglas piece of 5.0 cm diameter, while allowing the $CaCl_2$ solution to settle onto the surface. The Aeroneb Go nebulizer utilizes vibration mesh technology to aerosolize $CaCl_2$ solution. Three minutes were allowed to elapse for aerosols generated by nebulization to settle onto the surface. This time period was chosen since the difference in the weight of the chamber before and after 2 minutes of $CaCl_2$ nebulization was 0.65%, indicating that >99% of nebulized $CaCl_2$ was deposited onto the surface. The amount of $CaCl_2$ deposited on the mimetic surface was estimated as follows: the weight of the condensed formulation on the chamber was determined by taking the difference in the weight of the nebulization chamber with the hole cover before aerosolization and three minutes post-aerosolization, to allow the deposition of $CaCl_2$ onto mimetic surface.

6.2.7. Surface Shear Rheology

The surface rheology of the mucus mimetic with DPPC and aerosolized with 1.29% $CaCl_2$ solution for 2 minutes was probed using an interfacial stress rheometer (ISR 400; KSV Instruments, Finland), Section 3.2.5 in Chapter 3. The time-dependence of G_s' and G_s" was determined every 15 minutes for ~ 120 minutes at a fixed frequency of 1.56 rad/sec (corresponds to normal breathing frequency of 0.25 Hz [58]). The time-dependence surface shear rheology was determined for at least three samples.

6.2.8. Data Analysis

The cumulative volume and number distributions as a function of particle size for background aerosols and bioaerosols generated from mimetic surfaces were determined using a HELOS particle sizer. Mix function[151] (Mixdist package, R-software Version 2.12.1) was used to analyze the multimodal size distributions. The Mix function analyzes mixtures of normal and/or lognormal distributions. From the cumulative volume or number distribution of each sample, a histogram of grouped data, which represents the mixture or multimodal size distributions, was obtained. A smooth curve was drawn to match the shape of the histogram plot using the maximum-likelihood estimation (MLE) for grouped data. MLE estimated two parameters of a mixture distribution, the mean and standard deviation. The probability density function for a variable characteristic X in the mixed distribution is:

$$g(x) = \pi 1\, f1(x) + \ldots + \pi k\, fk(x)$$

where k is the number of mixture components, πi represents the proportion of the total population that the *ith* component population constitutes (where proportions $\pi 1 + \ldots + \pi k = 1$), and $fi(x)$ represent the probability density function for some variable characteristic X within the *ith* component population. The Mix function estimates the parameters $\pi 1, \ldots, \pi k$; $\mu 1, \ldots, \mu k$; $\sigma 1, \ldots, \sigma k$, where μi is the mean and σi is the standard deviation. The positions of the means, which represent the modes for each peak, were indicated with

triangles. The mode for each peak in the multimodal or mixture distributions of background aerosols and bioaerosols was determined.

6.2.9. Statistical Analysis

Statistical significance was determined by one-way ANOVA analysis for comparing the modes of the size distribution of bioaerosols. Statistical significance was determined by 2-way ANOVA analysis for comparing the time-dependent surface rheological shear moduli among surface systems for an unbalanced number of samples using a general linear model. Levels of significance were accepted at the $p<0.05$ level. Statistical analyses were performed using Minitab 15 software.

6.3. Results and Discussion

6.3.1. Optical Concentration of Background Aerosols

The optical concentration (Copt%) for background aerosols in the dry air released directly from the air cylinder and introduced into the HELOS particle sizer was obtained for five samples. The Copt% measured for four samples was $0.14 \pm 0.17\%$ (n=4) and one sample gave poor signal where Copt% was not recorded. The Copt% for dry and conditioned air obtained during a simulated cough maneuver, without mucus mimetic, were $0.09 \pm 0.15\%$ (n=8) and $0.16 \pm 0.32\%$ (n=5), respectively. Table 6-2 illustrates the measured values of Copt% of background aerosols for the three control situations. The reported Copt% values were relatively low ($\leq 0.13\%$) except for one value reported in each control test. Large standard deviations were reported in the three control tests. This may be due to inadequate purging of air through the SCM. The average Copt% measured for the three sources of background aerosols was $0.12 \pm 0.20\%$, n=17. This implies that a very small amount of aerosol was entrained by the air. Based on the average Copt% value for background aerosols, the initial trigger condition was setup at Copt% of 0.1%. As

long as the Copt% was above 0.1%, the detector continued to record the data; however, when the Copt% dropped below 0.1%, the detector stopped recording.

6.3.2. Multimodal Size Distribution

The size distributions, based on cumulative volume and number distributions, of background aerosols and bioaerosols generated from a mucus mimetic surface were determined. The cumulative volume distribution was able to determine the size of coarse particles, even if they were present in small amounts, as they make up a large percentage of the total volume. However, in the cumulative number distribution, they are insignificant. The size distributions indicated the presence of multiple peaks. Figure 6-2 represents an example of the multimodal size distribution of bioaerosols generated from a mucus mimetic surface determined using the HELOS particle sizer. Figure 6-3 illustrates a best fit to the three histograms, obtained from the cumulative volume distribution illustrated in Figure 6-2, using MIX function. The continuous line closely matches the shape of the three histograms and the triangles mark the mean (mode) of each peak. The mode of each peak in the mixture of distributions or multimodal distribution was determined. The average and standard deviation of peak modes for background and mucus mimetic samples were determined. Figure 6-4 illustrates averaging of the modes over all peaks located approximately in the same range generated from surfaces of a specific mucus mimetic system.

6.3.3. Size Distribution of Background Aerosols

Based on the cumulative volume distribution, Figures 6-5, 6-6 and 6-7 illustrate the multimodal size distributions of background aerosols entrained within dry air released directly from air cylinder, and dry and conditioned air during a simulated cough maneuver, respectively. Tables 6-3, 6-4 and 6-5 summarize the modes, Copt% and peak air flow rate for each background sample of the three control situations. For aerosols entrained within dry air released directly from air cylinder, three distinct modes were

observed at 0.15, 2.18 and 9.79 µm (Figure 6-5, Table 6-3). The Copt% of aerosols reported for all samples (n=5) were relatively low (≤0.12%), except for one sample of Copt%=0.38% with a mode peaking at 0.15 µm. However, the modes at 2.18 and 9.79 µm were reported in only one sample of Copt%=0.05% (Table 6-3). For aerosols entrained within dry air during a simulated cough maneuver, four distinct modes were observed at 0.13, 2.70, 6.02 and 15.50 µm (Figure 6-6, Table 6-4). The Copt% reported for all samples (n=8) were relatively low (≤0.13%), except for one sample of Copt%=0.44% with a mode peaking at 0.13 µm. However, the modes at 2.70, 6.02 and 15.50 µm were reported at low Copt% (Table 6-4). For aerosols entrained within conditioned air during a simulated cough maneuver, four distinct modes were observed at 0.13, 1.82, 4.89 and 15.64 µm (Figure 6-7, Table 6-5). The Copt% reported for all samples (n=5) were relatively low (≤0.03%), except for one sample of Copt%=0.73% with a mode peaking at 0.13 µm. However, the modes at 0.82, 4.89 and 15.64 µm were reported at low Copt% (Table 6-5). This indicates that modes at 0.13, 0.14 and 0.15 µm represent aerosols entrained within the air stream.

The size distribution, based on cumulative number distribution, of background aerosols during a single simulated cough maneuver was obtained by back calculation from the volume distribution using the HELOS particle sizer software. Figures 6-8, 6-9 and 6-10 illustrate the multimodal size distributions of background aerosols entrained within dry air released directly from air cylinder, and dry and conditioned air during a simulated cough maneuver, respectively. Tables 6-6, 6-7 and 6-8 illustrate the modes, Copt% and peak air flow rate for each background sample of the three control situations. For aerosols entrained within dry air released directly from air cylinder, three distinct modes were observed at 0.16, 2.10 and 8.15 µm (Figure 6-8, Table 6-6). For aerosols entrained within dry air during a simulated cough maneuver, four distinct modes were observed at 0.13, 2.43, 6.94 and 14.59 µm (Figure 6-9, Table 6-7). For aerosols entrained within conditioned air during a simulated cough maneuver, five distinct modes were

observed at 0.13, 0.76, 1.99, 4.56 and 14.08 μm (Figure 6-10, Table 6-8). Comparing the modes of the volume distribution to those of the number distribution, a shift was observed in the largest modes.

6.3.4. Size Distribution of Bioaerosols during a Simulated Cough Maneuver

It has been shown that the Copt% of bioaerosols generated from the surface of mucus mimetic with DPPC, using the SCM described by King *et al.*[49] without conditioning the air, was relatively low (0.03%), Section 5.3.1, Chapter 5. Bioaerosols were generated from mucus mimetic surfaces using the enhanced SCM where the temperature inside the enclosure system was maintained at ~ 37°C, and the air entering the model trachea was conditioned to 35.1± 0.9°C and 61.5 ± 6.2% RH (Table 5-3). Figures 6-11 to 6-14 illustrate the multimodal size distribution of bioaerosols, based on cumulative volume distribution, generated from surfaces of the bare mucus mimetic, mucus mimetic with DPPC, uncross-linked mucus mimetic and mucus mimetic with Infasurf®, respectively. Based on 38 separate measurements of the size distribution of bioaerosols generated during a simulated cough maneuver, the conditions (temperature and %RH) of air entering the model trachea, air within the 6.25-liter lung tank, and inside the enclosure system) of the enhanced SCM were reported (Table 6-9). The temperature inside the enclosure system was maintained at temperature of 33.98 ± 1.62°C and %RH of 24.68 ± 1.49%. Air entering the model trachea was warmed at 36.35 ± 2.22°C and humidified at 57.88 ± 7.08%. In the enhancement of the SCM, the temperature of air entering the model trachea was close to that reported for tracheal temperature (35.8-36.4°C), however, the %RH was much lower than that of trachea (98.8-99.7%). Air inside the 6.25-liter lung tank maintained at temperature of 35.57 ± 0.96°C and 103.34 ± 0.28%. The flow rate of the air stream used to generate bioaerosols from mimetic surfaces shows

large variability 12.26 ± 5.44 L/sec. However, small variation in the pressure of 6.25-liter lung tank was reported, 6.68 ± 0.22 psi.

Tables 6-10 to 6-13 illustrate the modes, Copt% and peak air flow rate for each sample of the bare mucus mimetic, mucus mimetic with DPPC, uncross-linked mucus mimetic and mucus mimetic with Infasurf®. All four surfaces produced five modes, at similar sizes. The bare mucus mimetic exhibited five modes at 0.16, 0.81, 2.20, 6.18 and 13.55 µm (Figure 6-11, Table 6-10). There was some evidence that smallest modes of 0.14 and 0.17 µm were generated only with highest air flow rate (>19 L/sec). However, smallest modes were not generated at flow rates <19 L/sec. Similar modes were obtained with the mucus mimetic with DPPC with modes at 0.14, 0.64, 2.78, 5.81 and 14.96 µm (Figure 6-12, Table 6-11). Similarly, the smallest mode (0.14 µm) was only visible at the greatest air flow rate (19.91 L/sec). In the uncross-linked mucus mimetic, the five modes were 0.13, 0.77, 2.16, 5.03 and 15.54 µm (Figure 6-13, Table 6-12). The modes at 0.11 and 0.13 µm were detected at both low and high air flow rates (6.63-15.7 L/sec). In the mucus mimetic with Infasurf®, the five modes were 0.15, 0.76, 3.05, 7.58 and 17.26 µm (Figure 6-14, Table 6-13). Then mode at 0.15 was detected at both low and high air flow rates (6.57-11.08 L/sec). The smallest modes for the uncross-linked mimetic and mimetic with Infasurf® were observed at low and high flow rates, suggesting the ability of the mimetic surfaces to break up into small droplets at low flow rate. This may be due to the low bulk viscoelastic properties of the uncross-linked mimetic compared to the cross-linked mimetic, and to the more viscous surface behavior of mimetic with Infasurf® compared to the bare mimetic and mimetic with DPPC.

Figure 6-15 provides a comparison of the multimodal size distributions for bioaerosols generated from the surface of the four mucus mimetic systems. The multimodal distribution of bioaerosols has been reported by Yang *et al.*,[68] who found that the size distributions of coughed droplets, collected in a sampling bag that had a higher %RH (95%) than the surrounding air, exhibited three peaks at approximately 1, 2 and 8

μm. Those three modes were observed in the size distributions of the four mucus mimetic systems studied here. In addition, a comprehensive study by Morawska *et al.*[70] reported the size distribution of droplets generated during different respiratory activities including coughing. Multimodal distribution was observed, where for all respiratory activities the majority of particles were of diameters below 0.8 μm and a second mode was at 1.8 μm, which are also in good agreement with that was observed in bioaerosols generated from mimetic surfaces.

Although the four types of mucus mimetic varied in their bulk viscoelastic and surface properties, they all show similar multimodal size distribution. This suggests that the variation in the physical properties (bulk and surface viscoelastic properties and surface tension) of mimetics were not sufficient to induce significant changes in the size distribution of bioaerosols. Investigating the range of the physical properties of the four mimetics used in this study, the physical properties for the mucus mimetics were as follows:

1) Bulk viscoelastic properties: G' from ~ 0.3 Pa at 1 rad/sec and ~ 21 Pa at 100 rad/sec for bare mucus mimetic, and G' from ~ 0.01 Pa at 1 rad/sec to ~ 16 Pa at 100 rad/sec for uncross-linked mimetic. G" from ~ 0.08 Pa at 1 rad/sec and ~ 6 Pa at 100 rad/sec for bare mucus mimetic, and G" from ~ 0.03 Pa at 1 rad/sec to ~ 28 Pa at 100 rad/sec for uncross-linked mucus mimetic.
2) Surface tension: from ~ 53 mN/m for bare mucus mimetic to ~ 32 mN/m for mucus mimetic with surfactant.
3) Surface viscoelastic properties: G_s' from ~ 3 mN/m at 0.6 rad/sec to ~ 6 mN/m at 25 rad/sec for the bare mucus mimetic, G_s' from ~ 0.9 mN/m at 0.6 rad/sec to ~ 1.1 mN/m at 20 rad/sec for mucus mimetic with DPPC, and G_s' from ~ 0.03 mN/m at 0.6 rad/sec to ~ 0.1 mN/m at 13 rad/sec for mucus mimetic with Infasurf®. G_s" from ~ 1 mN/m at 0.6 rad/sec and ~ 16 mN/m at 25 rad/sec for the bare mucus mimetic, and G_s" from ~ 2 mN/m at 0.6 rad/sec and 12 mN/m at 25

rad/sec for the mucus mimetic with DPPC, and G_s" from ~ 0.2 mN/m at 0.6 rad/sec and ~ 4 mN/m at 25 rad/sec.

These physical properties of the mimetics represent a fairly narrow range. Therefore, a wider range for mimetic physical properties may be suggested, where the variation in the size distribution of bioaerosols can be observed. In the two mathematical models studies by Vasudevan and Lange, [63,64] wider range was considered for the typical fluid properties of the mucus layer were the elastic storage modulus G' ranges from 0.1-150 Pa and surface tension ranges from 10-100 N/m.

Table 6-14 summarizes the Copt% for bioaerosols generated from each mimetic surface during a simulated cough maneuver. Large variations were observed in measured Copt% values (0.14-5.71%), reflected by the large standard deviation calculated. No significant differences were observed in amount of aerosols generated for each surface on average, as reflected by Copt%. However, it was observed that the bare mucus mimetic surface did not generate a measurable quantity of aerosol for half of the runs (Table 6-10). In comparison, the other surfaces generated measurable aerosols in almost all runs (at most 1 run failed to generate aerosols; Tables 6-11 to 6-13). This suggests that the properties of the bare mucus mimetic surface did not easily allow for bioaerosol formation. Therefore, fluidization of the fluid surface through either addition of surfactant to the surface or lack of cross-linking in the mimetic enabled bioaerosol formation. Interestingly, though, no relation was observed between Copt% values and flow rate (Tables 6-10 to 6-13).

Figure 6-20 summarizes the multimodal size distribution of bioaerosols, based on cumulative number distribution, generated from surfaces of the mucus mimetic, mucus mimetic with DPPC, uncross-linked mucus mimetic and mucus mimetic with Infasurf®, respectively. Tables 6-15 to 6-18 illustrate the modes, Copt% and peak air flow rate for each sample of the mucus mimetic, mucus mimetic with DPPC, uncross-linked mucus mimetic and mucus mimetic with Infasurf®. In the mucus mimetic, the five modes were

at 0.12, 0.42, 1.62, 4.52 and 11.07 µm (Figure 6-16, Table 6-15). In the mucus mimetic with DPPC, modes were observed at 0.14, 0.46, 2.37, 4.86 and 15.07 µm (Figure 6-17, Table 6-16). In the uncross-linked mucus mimetic, the five modes were 0.11, 0.75, 2.15, 5.27 and 14.78 µm (Figure 6-18, Table 6-17). In the mucus mimetic with Infasurf®, the four modes were 0.15, 0.67, 2.64, and 17.52 µm (Figure 6-19, Table 6-18). The modes for the four mimetic surfaces were relatively equal, in agreement to what have been reported in the cumulative volume distribution (the cumulative number distribution is a back calculation of the cumulative volume distribution). However, for mimetic with Infasurf® four modes were observed.

6.3.5. Size Distribution of Bioaerosols Generated During Three Repetitive Simulated Cough Maneuvers

The size distribution of bioaerosols generated from the surfaces of the mucus mimetic with DPPC was determined during three repetitive simulated cough maneuvers. Based on 33 separate measurements, the conditions of the model trachea, the enclosure system and the 6.25-liter lung tank were reported for the first, second and third cough (Table 6-19). The temperature of air entering the model trachea was 36.5 ± 1.7°C, 37.4 ± 0.7°C and 37.2 ±1.9°C during the first, second and third coughs, respectively. The temperature of the air entering the model trachea was relatively constant during coughs, suggesting that the time between the coughs was not long enough to recondition the air after each cough. The %RH of air entering the model trachea was 58.0 ± 8.7%, 49.9 ± 4.3% and 50.3 ± 8.4% during the first, second and third coughs, respectively. Reduction in %RH was observed during the three successive coughs due to opening of the vacuum system used to pull droplets toward the particle detector. However, the change in %RH between the second and third coughs was insignificant ($P>0.05$). The temperature of air inside the 6.26-liter tank was maintained at ~ 35°C during successive coughs. The %RH of air inside the 6.26-liter tank was recorded as >100% during the successive coughs. The

high %RH (~ 103%) inside the tank may be either due to a condensation on the probe resulting from a temperature difference between air coming from the pressure cooker (48°C) and air inside the tank (33°C), or a reduction in temperature of the air inside the tank after its expansion upon opening the solenoid valve. The temperature and %RH inside the enclosure system during the three repetitive coughs were maintained at 34.2°C and 24%, respectively. This indicates that the model trachea was maintained at a temperature close to that of body temperature. In addition, since no humidification was taken place inside the enclosure system, the %RH was relatively low (24%). However, this low %RH is expected to have no effect on the size of bioaerosols, since the model trachea was sealed and droplets directly exited to the particle sizer. The peak air flow rate, reported during the first, second and third coughs, was 12.2 ± 5.8 L/sec, 15.2 ± 3.1 L/sec and 14.7 ± 3.3 L/sec, respectively. Large variation was observed in the peak air flow rate during coughs. Pressure in the 6.26-liter tank, reported during the first, second and third coughs, was 6.2 ± 1.3, 6.8 ± 0.2 and 6.8 ± 0.2 psi, respectively, indicating that the pressure inside the tank was accurately controlled. In spite of this, very small changes to the tank pressure led to significant variation in the peak air flow rate.

Based on the cumulative volume distribution, Tables 6-20 and 6-21 illustrate the modes, Copt% and peak air flow rate for each sample of the mucus mimetic with DPPC for the second and third coughs. No significant change in the modes was observed between coughs (Figures 6-12, 6-22 and 6-23). This suggests that the surface behavior of mimetic was not affected between successive coughs. Although similar multimodal distributions were observed between coughs in this study, no *in-vivo* data has been reported for the size distribution of bioaerosols during repetitive coughs.

Based on the cumulative number distribution, four modes rather than five modes (as was observed in the cumulative volume distribution) were observed during the second and third coughs. This indicates that particles of this missing size mode were present in small amounts, making up insignificant percentage of the total number. In the second

cough, no mode was observed above 4.33 µm (Figure 6-24, Table 6-22). Since particle > 10 µm are expected to settle near surfaces due to gravity, they will not highly contribute in spreading the airborne diseases. In the third cough, no mode was observed between 2.79 and 15.19 µm (Figure 6-25, Table 6-23). Particles <10 µm loaded with pathogens will remain suspend in air for long periods of time, thereby giving more time for disease transmission.

Although the same method was used to generate bioaerosols from mimetic surfaces, bioaerosols were not generated from all mimetic surfaces during a simulated cough maneuver and during the three repetitive simulated cough maneuvers. This implies that shearing of the surface by the high air flow rate (10-14 L/min) did not always lead to bioaerosol formation. Table 6-24 illustrates the total number of runs for each mimetic surface and the number of runs that generate bioaerosols. Bioaerosols were generated in most samples of the uncross-linked mucus mimetic (5 of 6 samples), mucus mimetic with DPPC (11 of 12 samples) and mucus mimetic with Infasurf® (6 of 6 samples). In comparison, bioaerosols were generated from the mucus mimetic in only 5 of 10 samples. This may be due to the more elastic surface behavior of the bare mucus mimetic, which reduces the propensity of the mimetic to break up into droplets during the simulated cough maneuver. This indicates that the presence of surfactants plays a role in bioaerosol formation from the large conducting airways. This observation is in accordance with that of Edwards *et al.*[50, 58] who found that surface tension and mucus surface viscoelasticity may have a primary role in the formation of droplets. In addition, more bioaerosols were generated from mucus mimetic surface covered with DPPC during the first cough (11 of 12 samples) than during the second and third cough (6 of 12 samples in each), Table 6-24. This suggests that material is sheared off the mucus surface during a simulated cough maneuver, leading to alteration of the mimetic surface properties after the first cough.

6.3.6. Surface Rheology of Mucus Mimetic Aerosolized with $CaCl_2$

In this study, an estimated 0.764 ± 0.003 gm of 1.29% $CaCl_2$ was aerosolized on the mucus mimetic with DPPC after 2 minutes period of nebulization., The weight of the condensed $CaCl_2$ formulation on the nebulization chamber was 0.005 ± 0.002 gm (n=3), which represents ~ 0.65% of the total amount of nebulized $CaCl_2$ (Table 6-25). Figures 6-27A and 6-27B illustrate the time-dependent G_s' and G_s", respectively, for the mucus mimetic, mucus mimetic with DPPC, and mucus mimetic with DPPC post-aerosolization with 1.29% $CaCl_2$. G_s' rose following deposition of the divalent cation onto the mimetic surface at a time point of 15 minutes (indicated by arrow). At this point and beyond, G_s' dominated G_s", indicating a more elastic surface. Therefore, a dramatic alteration in the surface rheological behavior was observed following $CaCl_2$ deposition. This change in behavior of the mimetic surface from more viscous, after spreading DPPC, to more elastic, was due to a considerable increase in G_s" after $CaCl_2$ deposition ($p<0.05$). However, the deposition of $CaCl_2$ onto the mimetic surface did not affect its surface loss modulus G_s".

The increase in surface elasticity after the deposition of $CaCl_2$ onto mimetic surface was in agreement with the *in-vitro* studies of Edwards *et al.,* who found that the deposition of NaCl and $CaCl_2$ solutions enhance surface viscoelastic properties relative to the mucus simulants (locust bean gum cross-linked with sodium borate) alone.[8, 50] To verify that this rise in the surface elasticity of mimetic is due to the deposition of $CaCl_2$, the surface rheological behavior for the mucus mimetic was initially probed before the addition of DPPC. For the first 15 minutes, G_s' dominated G_s" indicating a more elastic surface, a characteristic surface behavior for the mucus mimetic (Figure 6-28, region I). After spreading DPPC onto the mimetic surface, the surface behavior transitioned from more elastic to more viscous, a characteristic surface behavior for the mucus mimetic with DPPC (Figure 6-28, region II). Deposition of $CaCl_2$ resulted in a crossover point,

where G_s' (ω) = G_s" (ω). After this crossover point a phase-transition in surface behavior was observed, where the surface exhibited a more elastic behavior due to continuous increase in the surface elastic modulus with time and G_s' dominated G_s" (Figure 6-28, region III).

Furthermore, to investigate the mechanism of $CaCl_2$ solution in enhancing the surface elastic property of the mucus mimetic post-aerosolization, the surface viscoelastic properties of single component subphases (cross-liked PGM and cross-linked albumin) with DPPC spread at the surface were probed post-aerosolization with $CaCl_2$ solution. Figure 6-29 illustrates the time-dependent G_s' and G_s" for the cross-linked 4% PGM solution. At the time point 2 min, G_s" dominated G_s'. A cross-over point, where G_s'= G_s", was observed at the time point of 15 min. After time point 15 min, a transition in the surface behavior was observed, where G_s' dominated Gs", indicating a more elastic surface. Figure 6-30 illustrates the time-dependent G_s' and G_s" for the cross-linked 1% albumin solution. Both G_s' and G_s" were relatively close to each other at all time points. For the water subphase (Figure 6-31), the interface exhibited a viscous behavior only of low G_s" values. In addition, extremely low values for G_s' (<0.03 mN/m) were recorded at few time points (2, 15, 75, 90, 105 and 120). The DPPC monolayer with $CaCl_2$ exhibited similar surface viscous behavior of the DPPC monolayer. This may due to that divalent cations such as calcium ions are known to interact moderately with zwitterionic lipids such as DPPC,[152] hence no change in the surface behavior was observed. These data suggest that the increase in the surface elastic behavior of mucus mimetic post-aerosolization with $CaCl_2$ solution may be reasoned to the ionic interaction between the positively charged cations (Ca^{+2}) and the negatively charged mucins glycoproteins or due to the bulk viscoelastic properties of the cross-linked 4% PGM and 1% albumin subphases.

6.4. Conclusions

Enhancements to the simulated cough machine (SCM) were necessary to better mimic the formation of bioaerosols from lung fluid surfaces. The size distribution of bioaerosols generated from the surfaces of the mucus mimetics, of different bulk and surface properties, during a simulated cough maneuver was multimodal. No significant changes in the modes of bioaerosols generated from different mimetic surfaces were observed. This suggests that large variation in mimetic physical properties may be necessary to show a significant change in the size distribution of bioaerosols. The modes of the three repetitive coughs performed to generate bioaerosols from mucus mimetic with DPPC peaked at relatively equal modes. This may suggest that no alteration in mimetic surface properties has occurred during the three repetitive coughs cough. There was some evidence that the smallest modes of 0.14 and 0.17 μm of bioaerosols generated only with the highest air flow rate. The air of high flow rare shears the mimetic surface and break it up into small droplets. The Copt% of background aerosols was relatively low ($0.12 \pm 0.2\%$), indicating that background aerosols were not interfering with the bioaerosols generated from mimetic surfaces. Deposition of $CaCl_2$ onto mimetic surface altered mimetic surface behavior from more viscous to more elastic. The increase in the surface elastic modulus G_s' of the mucus mimetic after $CaCl_2$ deposition may reasoned to the ionic interaction between the positively charged cation (Ca^{+2}) and the negatively charged mucin glycoproteins. We believe that further studies of this behavior will ultimately guide the development of simple, safe alternative strategies to suppress the formation of bioaerosols in the lungs and thereby halt airborne disease transmission.

Table 6-1: Summary of the physical properties of mucus mimetics used to generate bioaerosols from mimetic surfaces; data are represented as the mean ± SD.

Mucus Mimetic	**Bulk shear moduli at 1 rad/sec (Pa)**	**Bulk shear moduli at 100 rad/sec (Pa)**	**Surface tension (mN/m)**	**Surface behavior**
Uncross-linked mucus mimetic	G'= 0.08 ± 0.04 G"= 0.10 ± 0.04 (n=4)	G'=15.31 ± 4.08 G"=11.89 ± 1.44 (n=4)	49.45 ± 3.54 (n=4)	$G_s'>G_s"$ more elastic
Mucus mimetic	G'= 0.30 ± 0.08 G"= 0.38 ± 0.10 (n=11)	G'=20.65 ± 5.86 G"=9.80 ± 2.02 (n=11)	53.25 ± 1.22 (n=9)	$G_s'>G_s"$ more elastic
Mucus mimetic with DPPC	NT*	NT	30.16 ± 2.38 (n=4)	$G_s'<G_s"$ more viscous
Mucus mimetic with Infasurf®	NT	NT	31.40 ± 3.75 (n=5)	$G_s'<G_s"$ more viscous

* Not tested.

Table 6-2: Optical concentration (Copt%) reported for background aerosols of the three control situations.

Sample #	**Dry air-directly from air cylinder (Copt%)**	**Dry air-simulated cough maneuver (Copt%)**	**Conditioned air-simulated cough maneuvers (Copt%)**
1	Poor signal, no data recorded	0.02	0.00
2	0.00	0.01	0.00
3	0.05	0.07	0.73
4	0.12	0.01	0.03
5	0.38	0.01	0.03
6	ND*	0.44	ND
7	ND	0.13	ND
8	ND	0.00	ND
Ave ± SD	0.14 ± 0.17	0.09 ± 0.15	0.16 ± 0.32

* Measurement was not determined.

Table 6-3: Modes of background aerosols based on cumulative volume distribution and Copt% for each sample of dry air released directly from air cylinder; data are represented as the mean ± SD.

Sample #	**Mode 1 (µm)**	**Mode 2 (µm)**	**Mode 3 (µm)**	**Copt%**
1	Poor signal, no data recorded			
2	0.14	NR*	NR	0.00
3	0.14	2.18	9.79	0.05
4	0.18	NR	NR	0.12
5	0.14	NR	NR	0.38
Mean ± SD	**0.15 ± 0.02**	**2.18**	**9.79**	**0.14 ± 0.17**

* No data recorded.

Table 6-4: Modes of background aerosols based on cumulative volume distribution, Copt% and peak air flow rate for each sample of dry air entrained during a simulated cough maneuver; data are represented as the mean ± SD.

Sample #	**Mode 1 (µm)**	**Mode 2 (µm)**	**Mode 3 (µm)**	**Mode 4 (µm)**	**Copt (%)**	**Peak air Flow rate (L/sec)**
1	0.13	NR*	4.27	17.34	0.02	8.50
2	0.11	1.87	NR	17.18	0.01	9.30
3	0.17	NR	7.31	NR	0.07	14.00
4	0.14	3.27	NR	11.88	0.01	8.40
5	0.15	1.91	NR	15.72	0.01	24.20
6	0.14	3.88	NR	NR	0.44	7.40
7	0.12	2.57	NR	NR	0.13	8.50
8	0.11	NR	6.23	15.36	0.00	10.20
Mean ± SD	**0.13 ± 0.02**	**2.70 ± 0.87**	**5.94 ± 1.54**	**15.50 ± 2.20**	**0.09 ± 0.15**	**11.31 ± 5.58**

* No data recorded.

Table 6-5: Modes of background aerosols based on cumulative volume distribution, Copt%, and peak air flow rate for each sample of conditioned air entrained during a simulated cough maneuver; data are represented as the mean ± SD.

Sample #	**Mode 1 (µm)**	**Mode 2 (µm)**	**Mode 3 (µm)**	**Mode 4 (µm)**	**Copt (%)**	**Peak air Flow rate (L/sec)**
1	0.14	NR*	4.89	16.73	0.0	22.50
2	NR	2.65	NR	15.02	0.0	8.00
3	0.13	NR	NR	11.94	0.73	ND**
4	0.13	NR	NR	17.05	0.03	ND
5	0.11	2.09	NR	17.46	0.03	ND
Mean ± SD	**0.13 ± 0.01**	**2.37 ± 0.40**	**4.89**	**15.64 ± 2.27**	**0.16 ± 0.32**	**15.25 ± 10.25**

* No data recorded.

** Measurement was not determined.

Table 6-6: Modes of background aerosols based on cumulative number distribution and Copt% for each sample of dry air released directly from air cylinder; data are represented as the mean ± SD.

Sample #	**Mode 1 (µm)**	**Mode 2 (µm)**	**Mode 3 (µm)**	**Copt (%)**
1	Poor signal, no data reported			
2	0.15	NR*	NR	0.00
3	0.21	2.10	8.15	0.05
4	0.12	NR	NR	0.12
5	0.14	NR	NR	0.38
Mean ± SD	**0.16 ± 0.04**	**2.10**	**8.15**	**0.14 ± 0.17**

* No data recorded.

Table 6-7: Modes of background aerosols based on cumulative number distribution, Copt %, and peak air flow rate for each sample of dry air entrained during a simulated cough maneuver; data are represented as the mean ± SD.

Sample #	**Mode 1 (µm)**	**Mode 2 (µm)**	**Mode 3 (µm)**	**Mode 4 (µm)**	**Copt (%)**	**Peak air Flow rate (L/sec)**
1	0.12	NR*	NR	16.73	0.02	8.50
2	0.10	NR	6.94	NR	0.01	9.30
3	0.16	NR	NR	NR	0.07	14.00
4	0.14	3.11	NR	10.57	0.01	8.40
5	0.15	1.85	NR	14.32	0.01	24.20
6	0.12	NR	NR	NR	0.44	7.40
7	0.13	NR	NR	NR	0.13	8.50
8	NR	NR	NR	16.74	0.00	10.20
Mean ± SD	**0.13 ± 0.02**	**2.48 ± 0.89**	**6.94**	**14.59 ± 2.91**	**0.09 ± 0.15**	**11.31 ± 5.58**

* No data recorded.

Table 6-8: Modes of background aerosols based on cumulative number distribution, Copt %, and peak air flow for each sample of conditioned air entrained during a simulated cough maneuver; data are represented as the mean ± SD.

Sample #	**Mode 1 (µm)**	**Mode 2 (µm)**	**Mode 3 (µm)**	**Mode 4 (µm)**	**Mode 5 (µm)**	**Copt (%)**	**Peak air Flow rate (L/sec)**
1	0.12	NR*	NR	NR	NR	0.0	22.50
2	NR	NR	2.30	NR	13.97	0.0	8.00
3	0.12	0.76	NR	NR	11.51	0.73	ND**
4	0.11	NR	1.67	4.56	16.75	0.03	ND
5	0.11	NR	NR	NR	NR	0.03	ND
Mean ± SD	**0.12 ± 0.00**	**0.76**	**1.99 ± 0.45**	**4.56**	**14.08 ± 2.62**	**0.16 ± 0.32**	**15.25 ± 10.25**

* No data recorded.

** Measurement was not determined.

Table 6-9: Conditions of the enhanced SCM during a simulated cough maneuver at a peak air flow rate of 12.26 ± 5.44 L/sec. Pressure of the 6.25-liter air tank was 6.68 ± 0.22 psi; data are represented as the mean ± SD (n=38).

Parameter	**Air entering model trachea**	**Air inside 6.25-liter lung tank**	**Enclosure system**
Temperature (°C)	36.35 ± 2.22	35.57 ± 0.96	33.98 ± 1.62
RH (%)	57.88 ± 7.08	103.34 ± 0.28	24.68 ± 1.49

Table 6-10: Modes of bioaerosol size based on cumulative volume distribution, Copt%, and peak air flow rate (L/sec) for each sample of the mucus mimetic during a simulated cough maneuver; data are represented as the mean ± SD.

Sample #	**Mode 1 (µm)**	**Mode 2 (µm)**	**Mode 3 (µm)**	**Mode 4 (µm)**	**Mode 5 (µm)**	**Copt%**	**Peak air Flow rate (L/sec)**
1	0.17	NR*	1.37	5.36	NR	0.47	19.52
2	0.14	NR	3.71	NR	NR	0.26	19.28
3	NR	0.68	1.99	NR	11.47	0.5	13.10
4	NR	0.93	1.74	7.05	15.91	0.15	18.64
5	NR	NR	NR	6.12	13.26	0.5	14.38
6	Poor signal, no data recorded						20.37
7	Poor signal, no data recorded						ND**
8	Poor signal, no data recorded						6.90
9	Poor signal, no data recorded						10.89
10	Poor signal, no data recorded						7.21
Mean ± SD	**0.16 ± 0.02**	**0.81 ± 0.18**	**2.20 ± 1.04**	**6.18 ± 0.85**	**13.55 ± 2.23**	**0.38 ± 0.16**	**14.48 ± 5.31**

* No data recorded.

** Measurement was not determined.

Table 6-11: Modes of bioaerosol size based on cumulative volume distribution, Copt %, and peak air flow rate (L/sec) for each sample of the mucus mimetic with DPPC during a simulated cough maneuver; data are represented as the mean ± SD.

Sample #	**Mode 1 (µm)**	**Mode 2 (µm)**	**Mode 3 (µm)**	**Mode 4 (µm)**	**Mode 5 (µm)**	**Copt (%)**	**Peak air Flow rate (L/sec)**
1	0.14	NR*	1.45	NR	NR	2.12	19.91
2	NR	0.94	NR	6.18	14.25	5.71	5.57
3	NR	0.61	3.48	7.04	NR	1.00	21.83
4	NR	0.68	NR	4.47	NR	3.58	4.18
5	NR	0.75	NR	6.04	NR	0.86	10.38
6	NR	0.45	3.06	NR	10.95	0.23	9.72
7	NR	0.53	3.33	NR	17.63	0.40	6.78
8	NR	0.82	2.71	NR	NR	0.22	13.04
9	NR	0.3	2.89	NR	17.84	0.37	13.11
10	NR	NR	1.87	5.3	12.07	1.90	19.60
11	NR	NR	3.46	NR	17.02	0.28	8.59
12	Poor signal, no data recorded						13.23
Mean ± SD	**0.14**	**0.64 ± 0.21**	**2.78 ± 0.75**	**5.81 ± 0.97**	**14.96 ± 2.99**	**1.52 ± 1.75**	**12.16 ± 5.80**

* No data recorded.

Table 6-12: Modes of bioaerosol size based on cumulative volume distribution, Copt%, and peak air flow rate (L/sec) for each sample of uncross-linked mucus mimetic during a simulated cough maneuver; data are represented as the mean ± SD.

Sample #	**Mode 1 (µm)**	**Mode 2 (µm)**	**Mode 3 (µm)**	**Mode 4 (µm)**	**Mode 5 (µm)**	**Copt (%)**	**Peak air Flow rate (L/sec)**
1	0.11	NR*	NR	5.21	15.58	0.92	15.7
2	0.13	NR	3.79	NR	15.50	0.20	7.69
3	0.13	0.68	NR	4.03	NR	0.23	6.63
4	NR	0.86	2.98	NR	NR	2.07	6.12
5	NR	NR	1.68	5.44	NR	0.15	16.16
6	Poor signal, no data recorded						9.31
Mean ± SD	**0.12 ± 0.01**	**0.77 ± 0.13**	**2.82 ± 1.06**	**4.89 ± 0.76**	**15.54 ± 0.06**	**0.71 ± 0.82**	**10.27 ± 4.52**

* No data recorded.

Table 6-13: Modes of bioaerosol size based on cumulative volume distribution, Copt%, and peak air flow rate (L/sec) for each sample of the mucus mimetic with Infasurf® during a simulated cough maneuver; data are represented as the mean ± SD.

Sample #	**Mode 1 (µm)**	**Mode 2 (µm)**	**Mode 3 (µm)**	**Mode 4 (µm)**	**Mode 5 (µm)**	**Copt (%)**	**Peak air Flow rate (L/sec)**
1	0.15	0.41	2.88	7.97	17.63	0.22	6.57
2	0.15	0.66	3.24	NR	17.26	0.49	11.08
3	0.16	NR	3.32	NR	17.45	0.14	9.16
4	NR	0.77	2.76	8.44	17.68	0.36	12.87
5	NR	1.00	3.11	6.34	16.12	0.27	6.40
6	NR	0.98	2.99	17.41	NR	0.14	14.32
Mean ± SD	**0.15 ± 0.01**	**0.76 ± 0.24**	**3.05 ± 0.21**	**7.58 ± 1.10**	**17.26 ± 0.58**	**0.27 ± 0.12**	**10.07 ± 3.27**

* No data recorded.

Table 6-14: Measured values of Copt% for bioaerosols generated from each mimetic surface during a simulated cough maneuver; data are represented as the mean ± SD.

Mucus mimetics	**Copt% ± SD**
Uncross-linked mucus mimetic	0.71 ± 0.82 (n=5)
Mucus mimetic	0.38 ± 0.16 (n=5)
Mucus mimetic with DPPC	1.52 ± 1.75 (n=11)
Mucus mimetic with Infasurf®	0.27 ± 0.12 (n=6)

Table 6-15: Modes of bioaerosol size based on cumulative number distribution, Copt%, and peak air flow rate (L/sec) for each sample of the mucus mimetic during a simulated cough maneuver; data are represented as the mean ± SD.

Sample #	**Mode 1 (µm)**	**Mode 2 (µm)**	**Mode 3 (µm)**	**Mode 4 (µm)**	**Mode 5 (µm)**	**Copt (%)**	**Peak air Flow rate (L/sec)**
1	NR*	NR	1.35	NR	NR	0.47	19.52
2	0.10	NR	NR	NR	NR	0.26	19.28
3	NR	0.46	1.86	NR	10.19	0.5	13.10
4	0.14	NR	1.64	NR	NR	0.15	18.64
5	NR	NR	NR	4.52	11.94	0.5	14.38
6	Poor signal, no data recorded						20.37
7	Poor signal, no data recorded						ND**
8	Poor signal, no data recorded						6.90
9	Poor signal, no data recorded						10.89
10	Poor signal, no data recorded						7.21
Mean ± SD	**0.12 ± 0.03**	**0.46**	**1.62 ± 0.26**	**4.52**	**11.07 ± 1.24**	**0.38 ± 0.16**	**14.48 ± 5.31**

* No data recorded.

** Measurement was not determined.

Table 6-16: Modes of bioaerosol size based on cumulative number distribution, Copt%, and peak air flow rate (L/sec) for each sample of the mucus mimetic with DPPC during a simulated cough maneuver; data are represented as the mean ± SD.

Sample #	**Mode 1 (µm)**	**Mode 2 (µm)**	**Mode 3 (µm)**	**Mode 4 (µm)**	**Mode 5 (µm)**	**Copt (%)**	**Peak air Flow rate (L/sec)**
1	0.12	0.37	NR*	NR	NR	2.12	19.91
2	0.14	0.43	NR	NR	NR	5.71	5.57
3	0.12	NR	1.87	NR	NR	1.00	21.83
4	0.16	NR	NR	NR	NR	3.58	4.18
5	0.16	0.3	NR	NR	NR	0.86	10.38
6	NR	NR	NR	NR	10.23	0.23	9.72
7	NR	0.4	NR	NR	NR	0.40	6.78
8	NR	0.71	2.21	NR	NR	0.22	13.04
9	0.15	NR	2.69	NR	17.48	0.37	13.11
10	NR	0.27	1.76	4.86	17.49	1.90	19.60
11	NR	0.87	3.32	NR	NR	0.28	8.59
12	Poor signal, no data recorded						13.23
Mean ± SD	**0.14 ± 0.02**	**0.48 ± 0.22**	**2.37 ± 0.64**	**4.86**	**15.07 ± 4.19**	**1.52 ± 1.75**	**12.16 ± 5.80**

* No data recorded.

Table 6-17: Modes of bioaerosol size based on cumulative number distribution, Copt %, and peak air flow rate (L/sec) for each sample of uncross-linked mucus mimetic during a simulated cough maneuver; data are represented as the mean ± SD.

Sample #	**Mode 1 (µm)**	**Mode 2 (µm)**	**Mode 3 (µm)**	**Mode 4 (µm)**	**Mode 5 (µm)**	**Copt (%)**	**Peak air Flow rate (L/sec)**
1	NR*	NR	NR	4.82	14.76	0.92	15.7
2	0.11	NR	NR	NR	NR	0.20	7.69
3	0.11	0.75	NR	NR	NR	0.23	6.63
4	NR	0.75	2.28	NR	NR	2.07	6.12
5	NR	NR	2.01	5.71	NR	0.15	16.16
6	Poor signal, no data recorded						9.31
Mean ± SD	**0.11 ± 0.00**	**0.75 ± 0.00**	**2.15 ± 0.19**	**5.27 ± 0.63**	**14.76**	**0.71 ± 0.82**	**10.27 ± 4.52**

* No data recorded.

Table 6-18: Modes of bioaerosol size based on cumulative number distribution, Copt%, and peak air flow rate (L/sec) for each sample of the mucus mimetic with Infasurf® during a simulated cough maneuver; data are represented as the mean ± SD.

Sample #	**Mode 1 (µm)**	**Mode 2 (µm)**	**Mode 3 (µm)**	**Mode 4 (µm)**	**Copt (%)**	**Peak air Flow rate (L/sec)**
1	0.14	0.36	NR*	NR	0.22	6.57
2	0.13	NR	NR	NR	0.49	11.08
3	0.11	NR	NR	NR	0.14	9.16
4	0.19	0.54	2.50	17.52	0.36	12.87
5	NR	0.85	2.85	NR	0.27	6.40
6	NR	0.95	2.56	NR	0.14	14.32
Mean ± SD	**0.15 ± 0.03**	**0.67 ± 0.27**	**2.64 ± 0.19**	**17.52**	**0.27 ± 0.14**	**10.07 ± 3.27**

* No data recorded.

Table 6-19: Conditions of the enhanced SCM with peak air flow rate and pressure at the 6.25-liter lung tank reported during three repetitive cough maneuvers for the mucus mimetic with DPPC; data are represented as the mean ± SD.

	Air entering model trachea		**Air inside 6.25-liter lung tank**			
Cough maneuver	**Temp (°C)**	**RH (%)**	**Temp (°C)**	**RH (%)**	**Peak air flow rate (L/sec)**	**Pressure (psi)**
First cough (n=12)	36.51 ± 1.74	58.03 ± 8.65	35.10 ± 0.60	103.45 ± 0.19	12.17 ± 5.80	6.15 ± 1.30
Second cough (n=10)	37.44 ± 0.70	49.91 ± 4.28	35.18 ± 0.55	103.50 ± 0.14	15.23 ± 3.11	6.77 ± 0.15
Third cough (n=11)	37.15 ± 1.88	50.27 ± 8.40	35.30 ± 0.56	103.53 ± 0.17	14.67 ± 3.30	6.77 ± 0.15

†Temperature and %RH inside the enclosure system was 34.2°C and 24%, respectively.

Table 6-20: Modes of bioaerosol size based on cumulative volume distribution, Copt%, and peak air flow rate (L/sec) for each sample of mucus mimetic with DPPC during the second simulated cough maneuver; data are represented as the mean ± SD.

Sample #	**Mode 1 (µm)**	**Mode 2 (µm)**	**Mode 3 (µm)**	**Mode 4 (µm)**	**Mode 5 (µm)**	**Copt (%)**	**Peak air Flow rate (L/sec)**
1	NR	0.82	NR	4.75	NR	4.38	19.12
2	ND						
3	NR	NR	2.45	7.47	NR	0.28	20.89
4	0.23	0.66	2.53	NR	NR	1.21	ND
5	0.23	0.91	NR	7.33	NR	0.86	13.04
6	Poor signal, no data recorded						16.28
7	NR	0.80	2.72	NR	NR	0.35	15.18
8	Poor signal, no data recorded						13.95
9	Poor signal, no data recorded						11.44
10	NR	0.89	NR	5.15	14.20	1.33	20.58
11	Poor signal, no data recorded						11.86
12	Poor signal, no data recorded						11.44
Mean ± SD	**0.23 ± 0.00**	**0.82 ± 0.10**	**2.57 ± 0.10**	**6.18 ± 1.43**	**14.20**	**1.40 ± 1.52**	**15.38 ± 3.70**

* No data recorded.

** Measurement was not determined.

Table 6-21: Modes of bioaerosol size based on cumulative volume distribution, Copt %, and peak air flow rate (L/sec) for each sample of the mucus mimetic with DPPC during the third simulated cough maneuver; data are represented as the mean ± SD.

Sample #	**Mode 1 (µm)**	**Mode 2 (µm)**	**Mode 3 (µm)**	**Mode 4 (µm)**	**Mode 5 (µm)**	**Copt (%)**	**Peak air Flow rate (L/sec)**
1	NR*	0.96	NR	6.16	NR	2.11	15.80
2	ND**						
3	0.27	NR	NR	5.73	NR	0.26	20.54
4	0.12	NR	2.23	NR	11.19	0.92	ND
5	NR	0.74	NR	7.67	17.52	0.90	13.48
6	Poor signal, no data recorded						10.28
7	NR	0.66	2.84	NR	NR	0.23	14.09
8	Poor signal, no data recorded						14.16
9	Poor signal, no data recorded						12.01
10	NR	0.86	NR	4.80	12.5	1.45	18.19
11	Poor signal, no data recorded						11.05
12	Poor signal, no data recorded						16.76
Mean ± SD	**0.20 ± 0.11**	**0.81 ± 0.13**	**2.54 ± 0.43**	**6.09 ± 1.20**	**13.74 ± 3.34**	**0.98 ± 0.72**	**14.64 ± 3.23**

* No data recorded.

** Measurement was not determined.

Table 6-22: Modes of bioaerosol size based on cumulative number distribution, Copt%, and peak air flow rate (L/sec) for each sample of the mucus mimetic with DPPC during the second simulated cough maneuver; data are represented as the mean ± SD.

Sample #	**Mode 1 (µm)**	**Mode 2 (µm)**	**Mode 3 (µm)**	**Mode 4 (µm)**	**Copt (%)**	**Peak air Flow rate (L/sec)**
1	NR*	0.47	1.18	NR	4.38	19.12
2	ND**					
3	NR	0.9	1.48	NR	0.28	20.89
4	0.15	0.53	NR	NR	1.21	ND
5	NR	NR	NR	NR	0.86	13.04
6	Poor signal, no data recorded					16.28
7	NR	0.61	2.08	NR	0.35	15.18
8	Poor signal, no data recorded					13.95
9	Poor signal, no data recorded					11.44
10	NR	0.42	NR	4.33	1.33	20.58
11	Poor signal, no data recorded					11.86
12	Poor signal, no data recorded					11.44
Mean ± SD	**0.15**	**0.59 ± 0.19**	**1.58 ± 0.46**	**4.33**	**1.40 ± 1.52**	**15.38 ± 3.70**

* No data recorded.

** Measurement was not determined.

Table 6-23: Modes of bioaerosol size based on cumulative number distribution, Copt%, and peak air flow rate (L/sec) for each sample of the mucus mimetic with DPPC during the third simulated cough maneuver; data are represented as the mean ± SD.

Sample #	**Mode 1 (µm)**	**Mode 2 (µm)**	**Mode 3 (µm)**	**Mode 4 (µm)**	**Copt (%)**	**Peak air Flow rate (L/sec)**
1	NR*	0.40	1.29	NR	2.11	15.80
2	ND**					
3	NR	NR	NR	NR	0.26	20.54
4	0.11	NR	2.67	17.49	0.92	ND
5	NR	0.23	3.71	16.71	0.90	13.48
6	Poor signal, no data recorded					10.28
7	NR	0.31	NR	NR	0.23	14.09
8	Poor signal, no data recorded					14.16
9	Poor signal, no data recorded					12.01
10	NR	0.39	3.84	11.37	1.45	18.19
11	Poor signal, no data recorded					11.05
12	Poor signal, no data recorded					16.76
Mean ± SD	**0.11**	**0.33 ± 0.08**	**2.87 ± 1.18**	**15.19 ± 3.33**	**0.98 ± 0.72**	**14.64 ± 3.23**

* No data recorded.

** Measurement was not determined.

Table 6-24: Number of experiments that generated bioaerosols from mucus mimetic surface during repetitive coughs.

		Number of experiments generating Bioaerosols		
Mimetic sample	**Total # of runs**	**First cough**	**Second cough**	**Third cough**
Uncross-linked mucus mimetic	6	5	ND*	ND
Mucus mimetic	10	5	ND	ND
Mucus mimetic with DPPC	12	11	6	6
Mucus mimetic with Infasurf®	6	6	ND	ND

* No data recorded.

Table 6-25: The difference in weight of the nebulization chamber and hole cover before nebulization and three minutes post nebulization; data are represented as the mean ± SD.

Sample #	**Before nebulization (g)**	**Three minutes post-aerosolization (g)**	**Difference in weight (g)**
1	112.265	112.268	0.003
2	112.264	112.271	0.007
3	112.278	112.282	0.004
Mean ± SD	**112.269 ± 0.008**	**112.274 ± 0.007**	**0.005 ± 0.002**

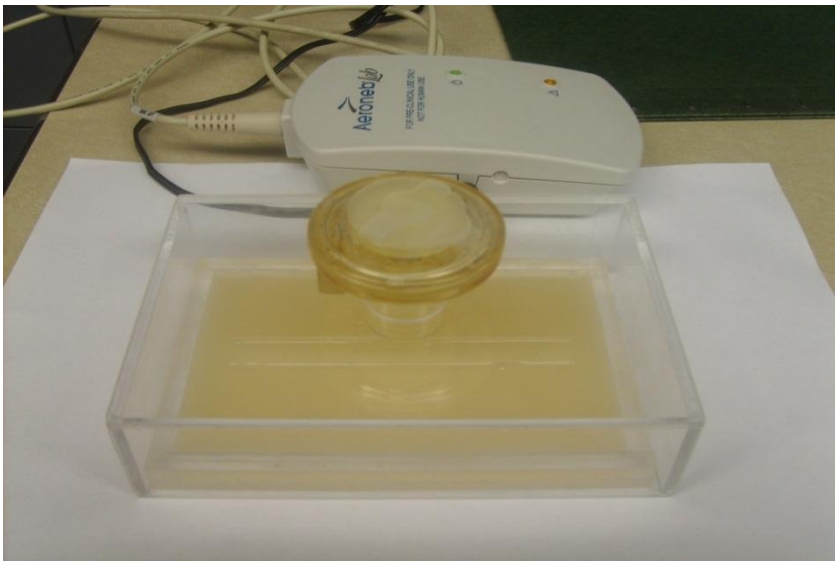

Figure 6-1: A closed home-built nebulization chamber made of Plexiglas used to aerosolize1.29% $CaCl_2$ solution onto the mucus mimetic with DPPC through Aeroneb Lab nebulizer.

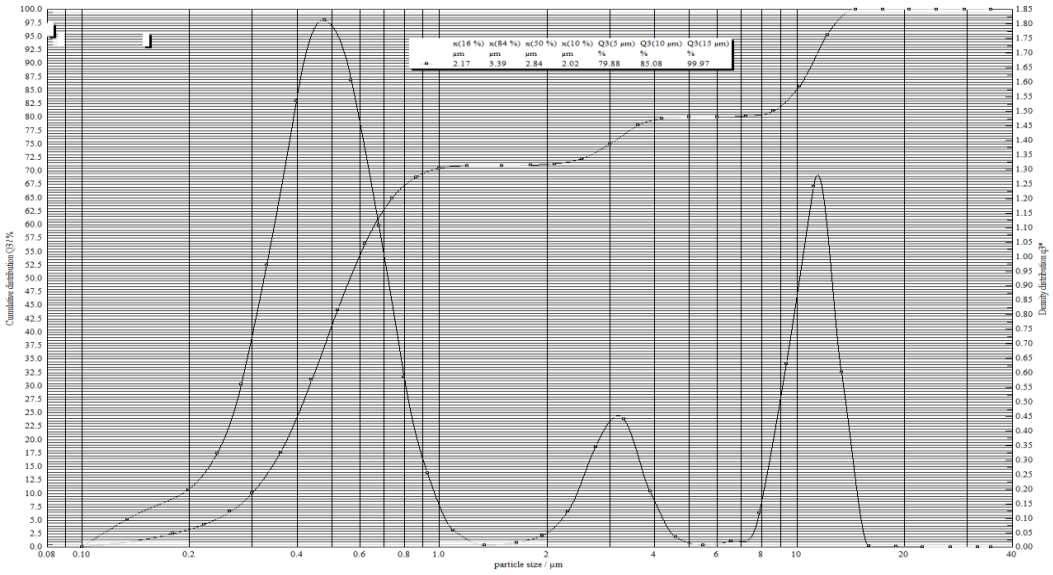

Figure 6-2: Multimodal size distribution of bioaerosols generated from a mucus mimetic surface determined using the HELOS particle sizer.

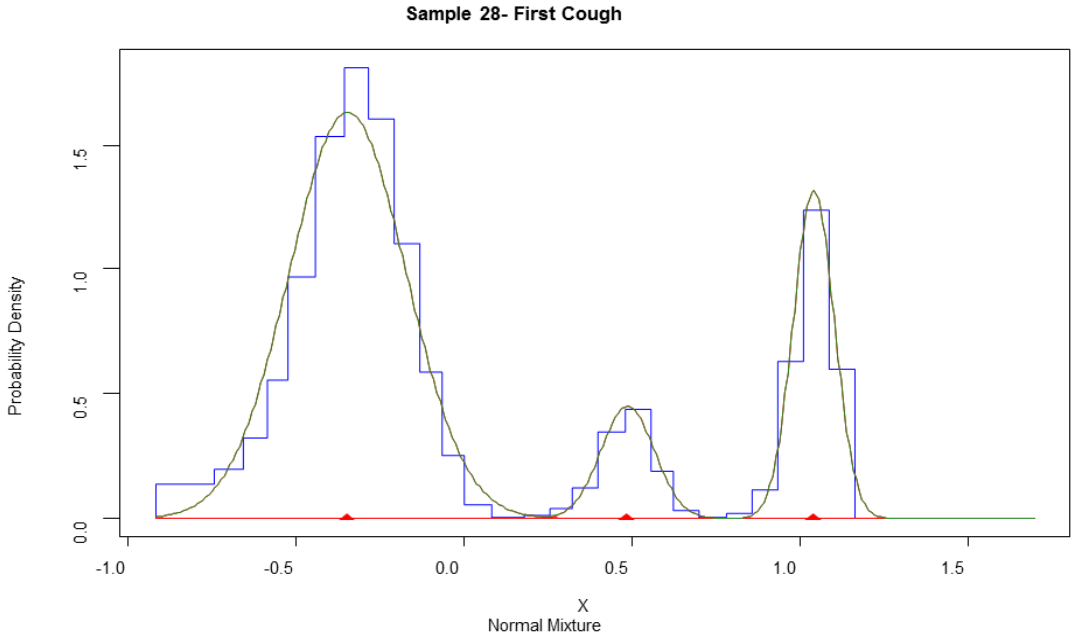

Figure 6-3: Fitted distributions (MIX function) to histogram particle size distributions.

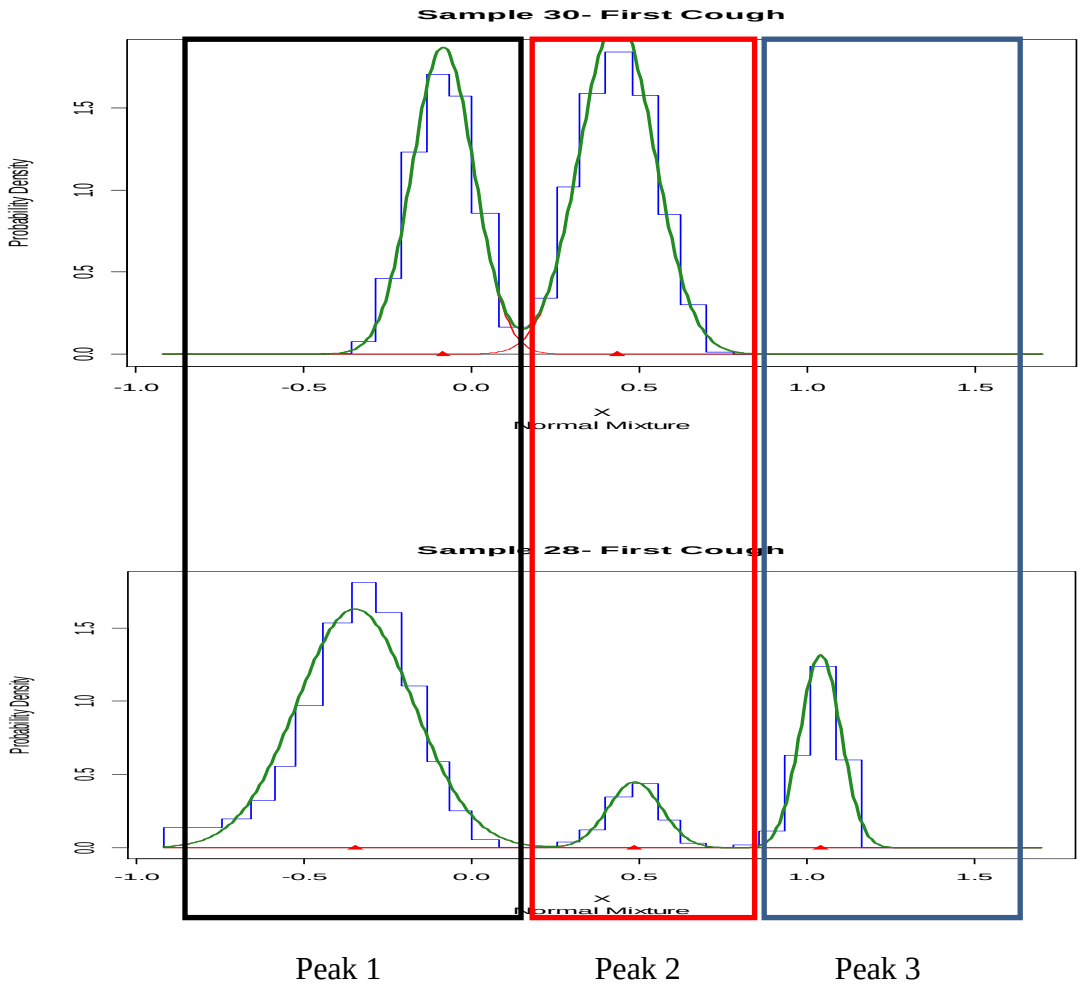

Figure 6-4: Calculated average and standard deviation of each mode for two cough samples from fitted (MIX function) histogram size distribution.

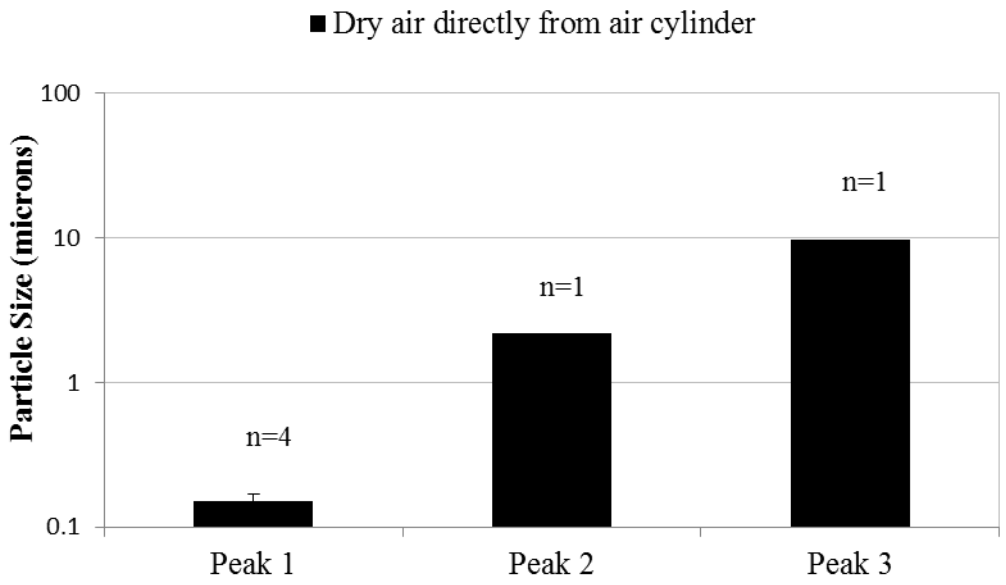

Figure 6-5: Multimodal size distributions, based on cumulative volume distribution, of aerosols entrained within dry air released directly from compressed air cylinder. Data are represented as the mean ± SD (n=4).

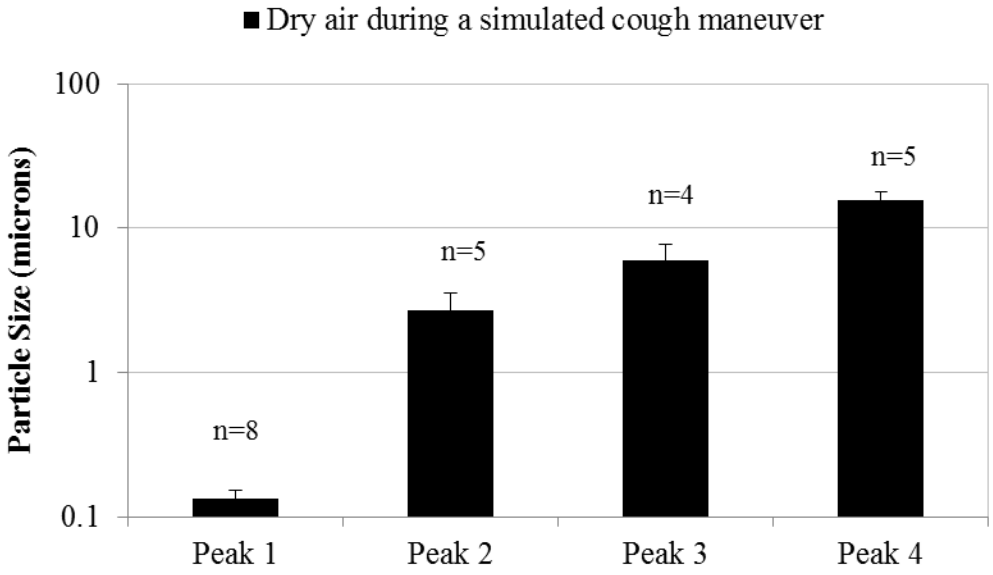

Figure 6-6: Multimodal size distributions, based on cumulative volume distribution, of aerosols entrained within dry air during a simulated cough maneuver. Data are represented as the mean ± SD (n=8).

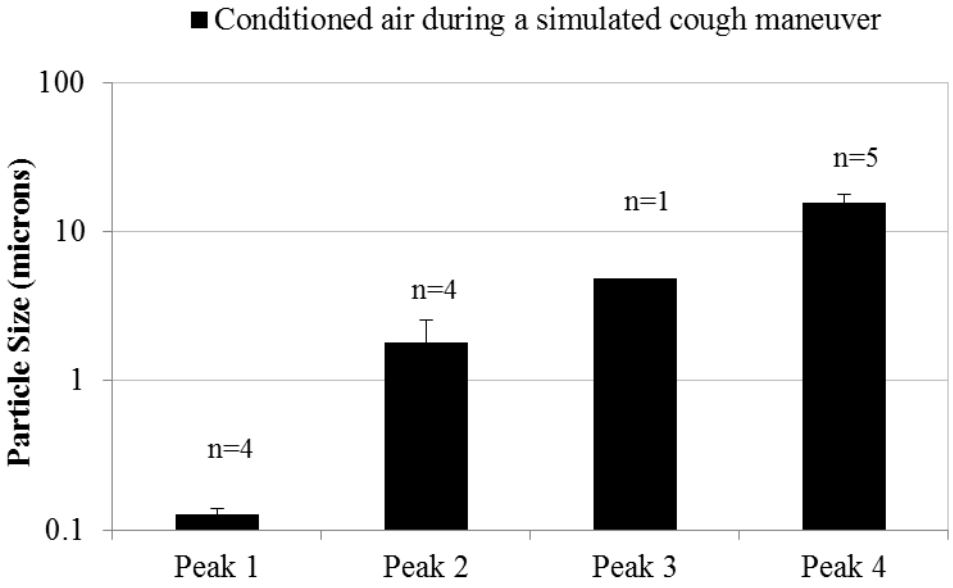

Figure 6-7: Multimodal size distributions, based on cumulative volume distribution, of aerosols entrained within conditioned air during a simulated cough maneuver. Data are represented as the mean ± SD (n=5).

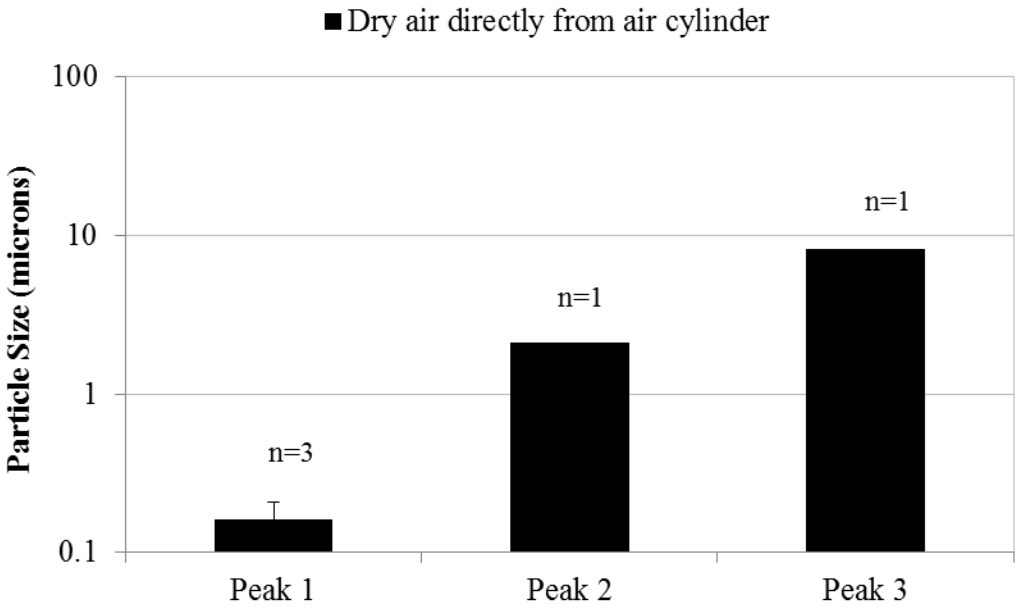

Figure 6-8: Multimodal size distributions, based on cumulative number distribution, of aerosols entrained within dry air released directly from compressed air cylinder. Data are represented as the mean ± SD (n=4).

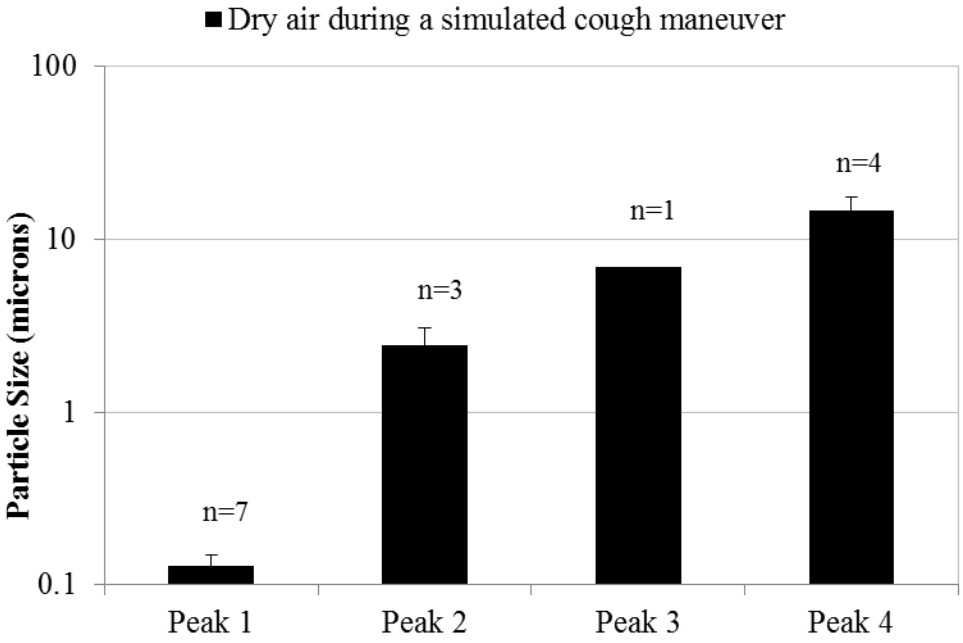

Figure 6-9: Multimodal size distributions, based on cumulative number distribution, of aerosols entrained within dry air during a simulated cough maneuver. Data are represented as the mean ± SD (n=8).

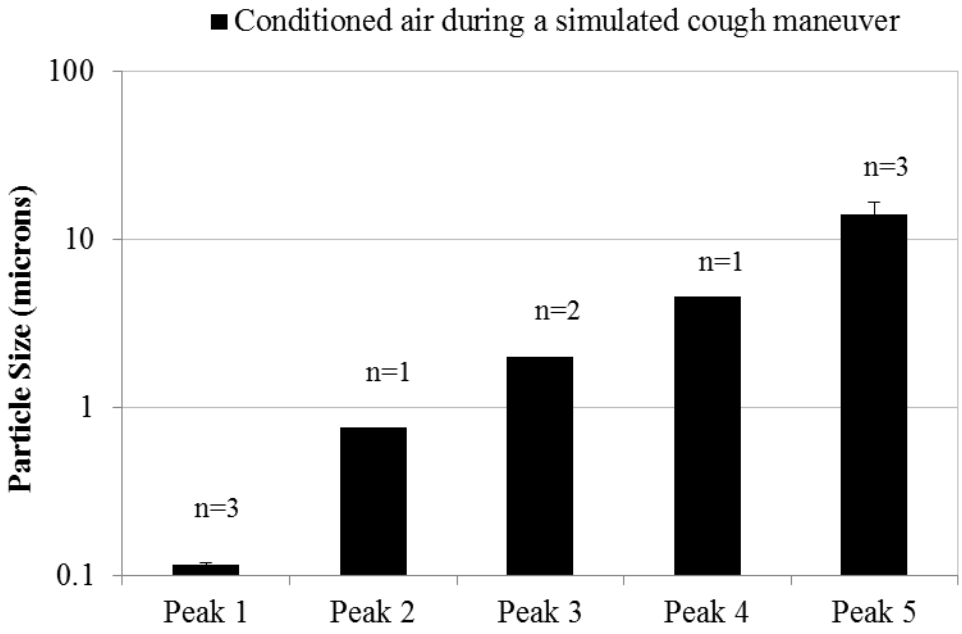

Figure 6-10: Multimodal size distributions, based on cumulative number distribution, of aerosols entrained within conditioned air during a simulated cough maneuver. Data are represented as the mean ± SD (n=5).

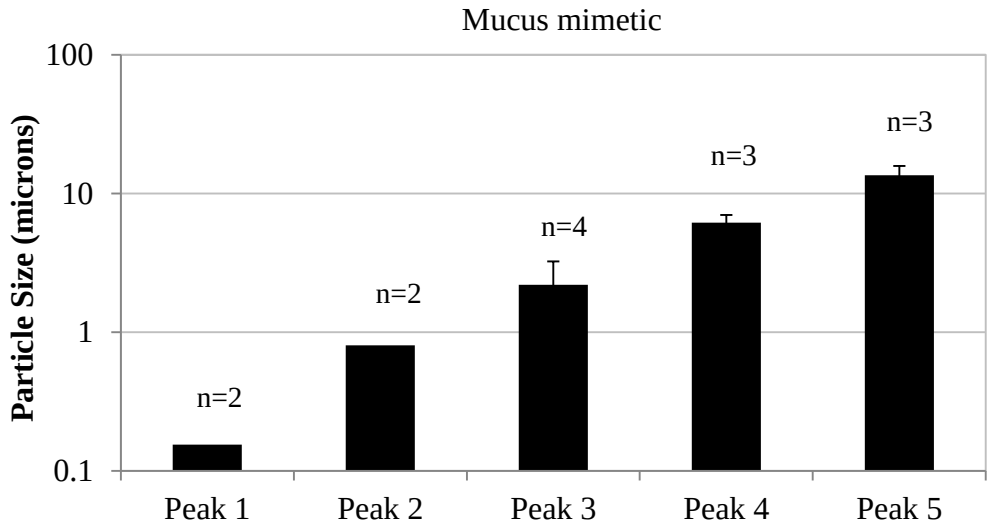

Figure 6-11: Multimodal size distributions, based on cumulative volume distribution, of bioaerosols generated from the surfaces of the mucus mimetic during a simulated cough maneuver. Data are represented as the mean ± SD (n=5).

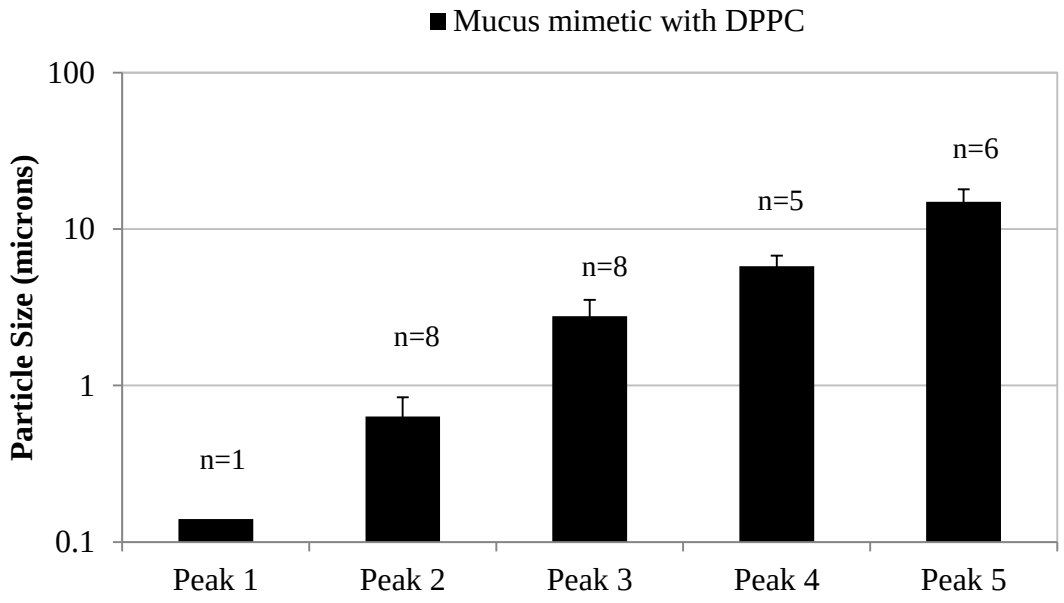

Figure 6-12: Multimodal size distributions, based on cumulative volume distribution, of bioaerosols generated from the surfaces of the mucus mimetic with DPPC during a simulated cough maneuver. Data are represented as the mean ± SD (n=11).

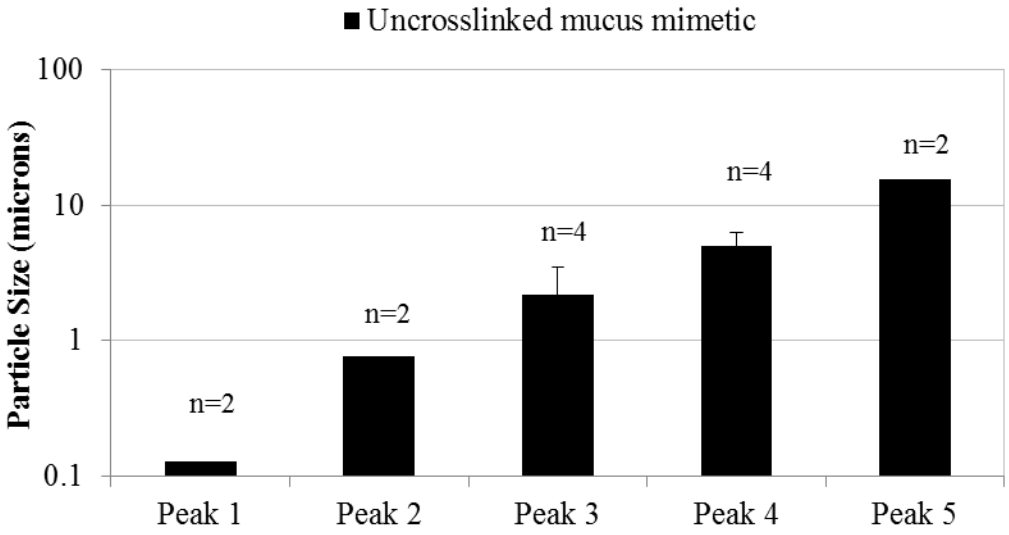

Figure 6-13: Multimodal size distributions, based on cumulative volume distribution, of bioaerosols generated from the surfaces of the uncross-linked mucus mimetic during a simulated cough maneuver. Data are represented as the mean ± SD (n=5).

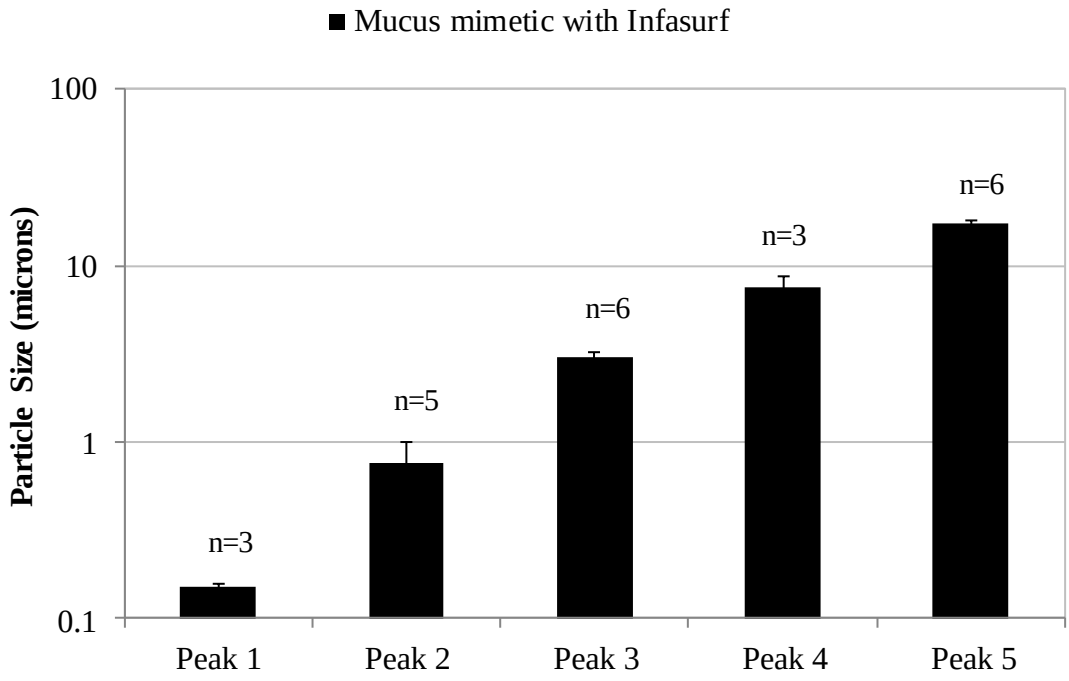

Figure 6-14: Multimodal size distributions, based on cumulative volume distribution, of bioaerosols generated from the surfaces of the mucus mimetic with Infasurf® during a simulated cough maneuver. Data are represented as the mean ± SD (n=6).

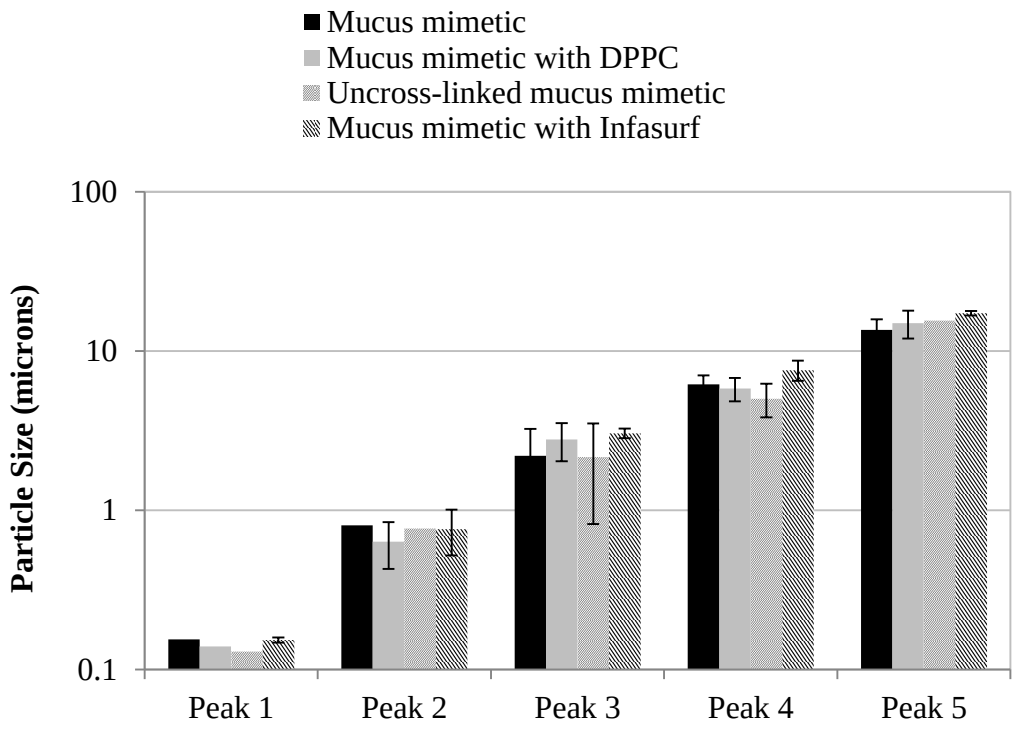

Figure 6-15: Multimodal size distributions, based on cumulative volume distribution, of bioaerosols generated from surfaces of the mucus mimetic (n=5), mucus mimetic with DPPC (n=11), uncross-linked mucus mimetic (n=5), and mucus mimetic with Infasurf® (n=6) during a simulated cough maneuver. Data are represented as the mean ± SD.

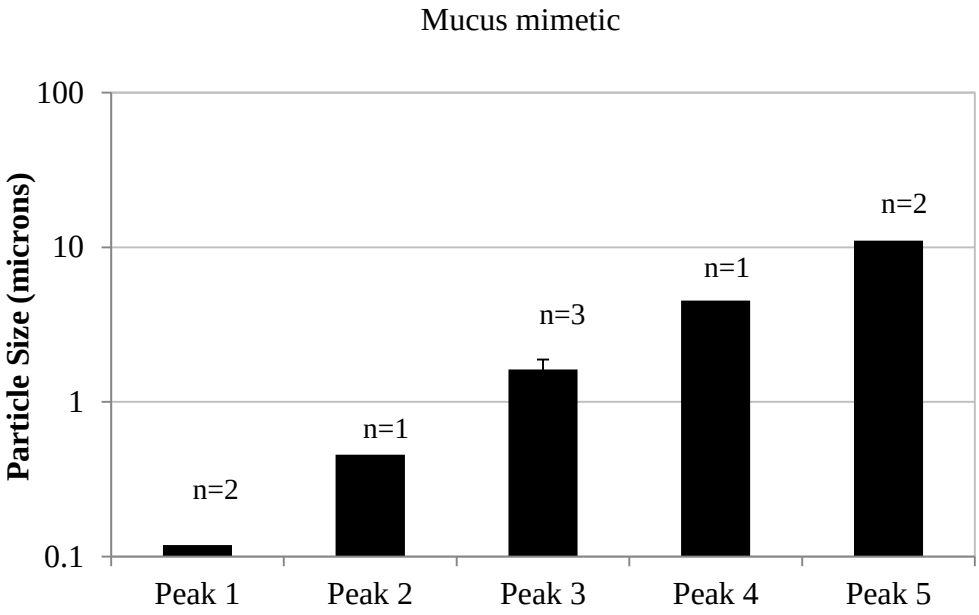

Figure 6-16: Multimodal size distributions, based on cumulative number distribution, of bioaerosols generated from the surfaces of the mucus mimetic during a simulated cough maneuver. Data are represented as the mean ± SD (n=5).

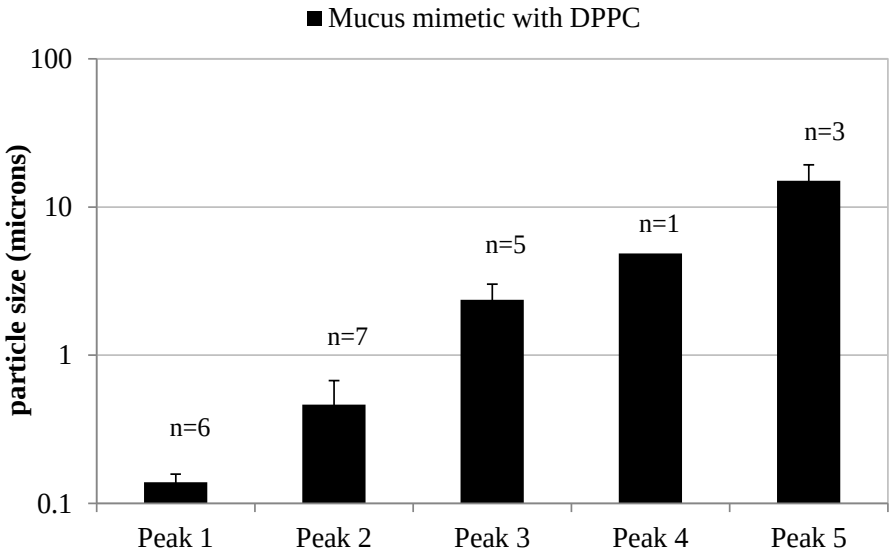

Figure 6-17: Multimodal size distributions, based on cumulative number distribution, of bioaerosols generated from the surfaces of the mucus mimetic with DPPC during a simulated cough maneuver. Data are represented as the mean ± SD (n=11).

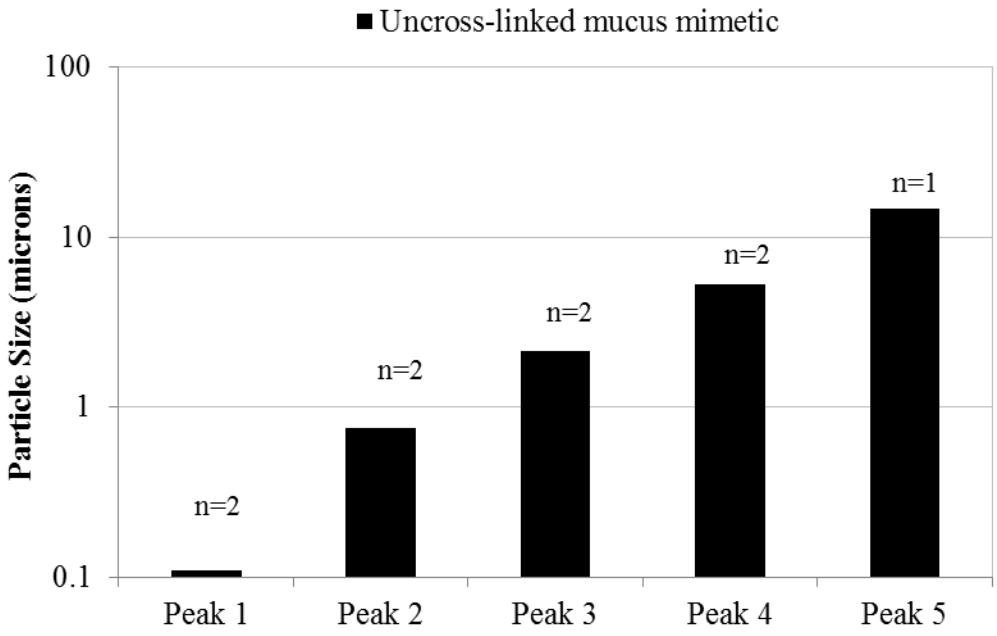

Figure 6-18: Multimodal size distributions, based on cumulative number distribution, of bioaerosols generated from the surfaces of the uncross-linked mucus mimetic during a simulated cough maneuver. Data are represented as the mean ± SD (n=5).

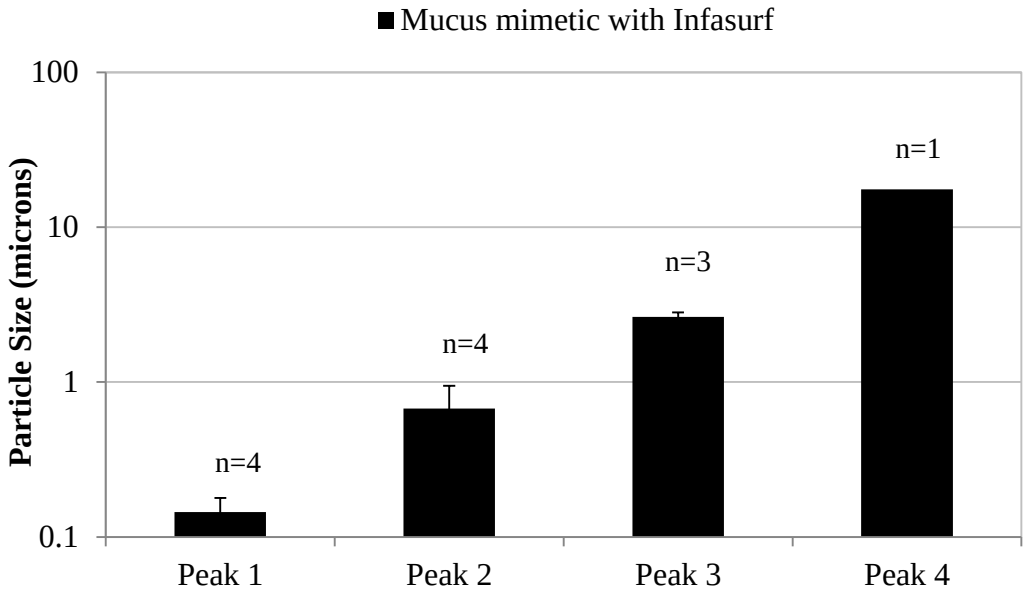

Figure 6-19: Multimodal size distributions, based on cumulative number distribution, of bioaerosols generated from the surfaces of the mucus mimetic with Infasurf® during a simulated cough maneuver. Data are represented as the mean ± SD (n=6).

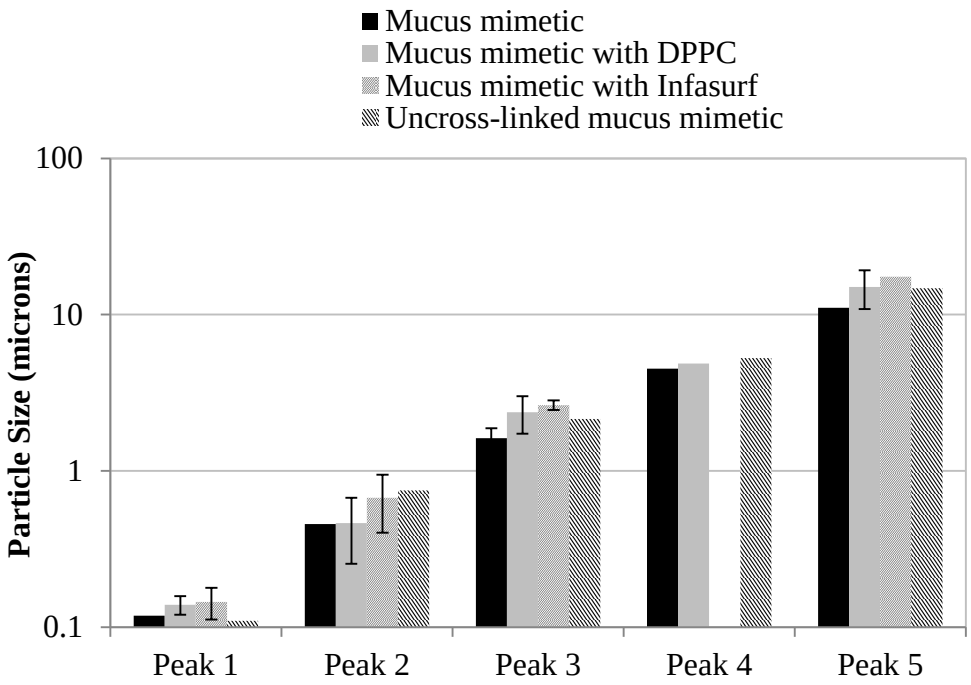

Figure 6-20: Multimodal size distributions, based on cumulative number distribution, of bioaerosols generated from surfaces of the mucus mimetic (n=5), mucus mimetic with DPPC (n=11), uncross-linked mucus mimetic (n=5), and mucus mimetic with Infasurf® (n=6) during a simulated cough maneuver. Data are represented as the mean ± SD.

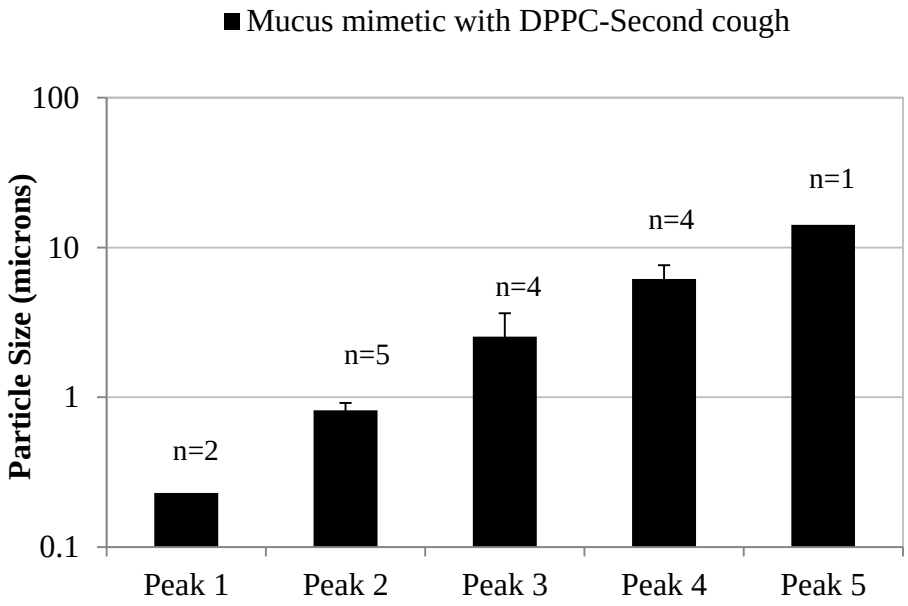

Figure 6-21: Multimodal size distributions, based on cumulative volume distribution, of bioaerosols generated from the surfaces of the mucus mimetic with DPPC during a second simulated cough maneuver. Data are represented as the mean ± SD (n=6).

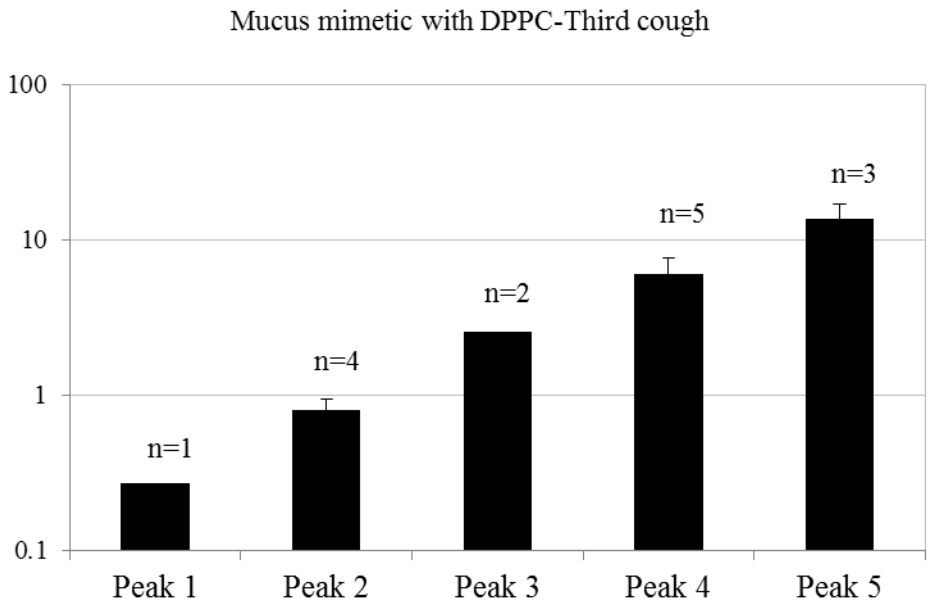

Figure 6-22: Multimodal size distributions, based on cumulative volume distribution, of bioaerosols generated from the surfaces of the mucus mimetic with DPPC during a third simulated cough maneuver. Data are represented as the mean ± SD (n=6).

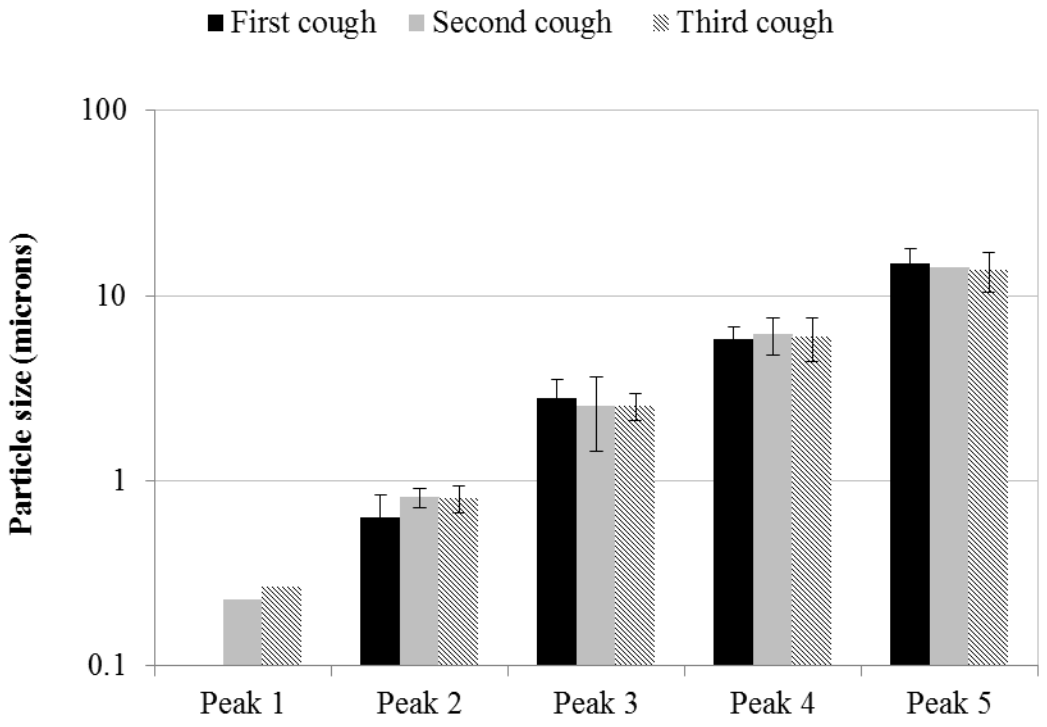

Figure 6-23: Multimodal size distributions, based on cumulative volume distribution, of bioaerosols generated from the surfaces of the mucus mimetic with DPPC during first cough (n=11), second cough (n=6), and third cough (n=6). Data are represented as the mean ± SD.

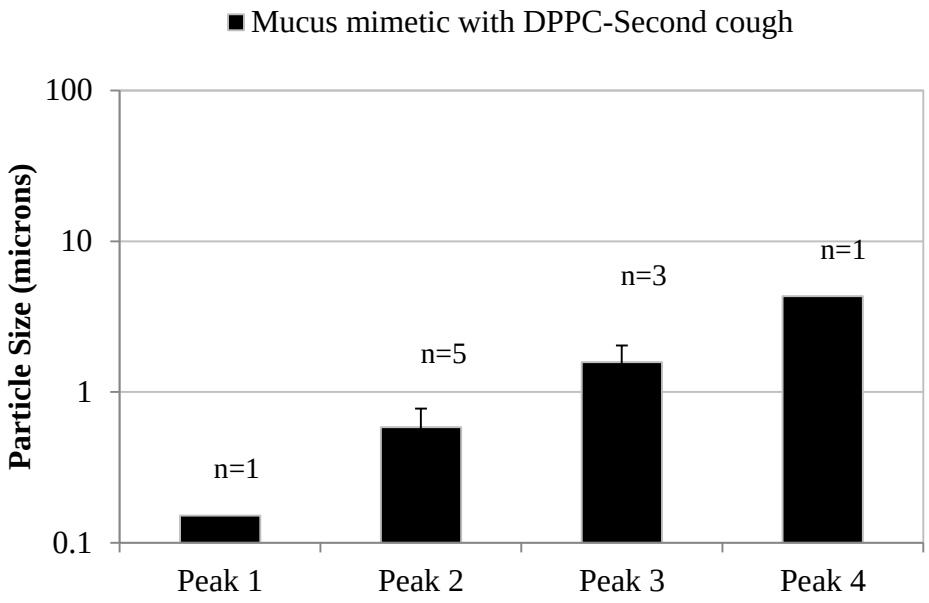

Figure 6-24: Multimodal size distributions, based on cumulative number distribution, of bioaerosols generated from the surfaces of the mucus mimetic with DPPC during a second simulated cough maneuver. Data are represented as the mean ± SD (n=6).

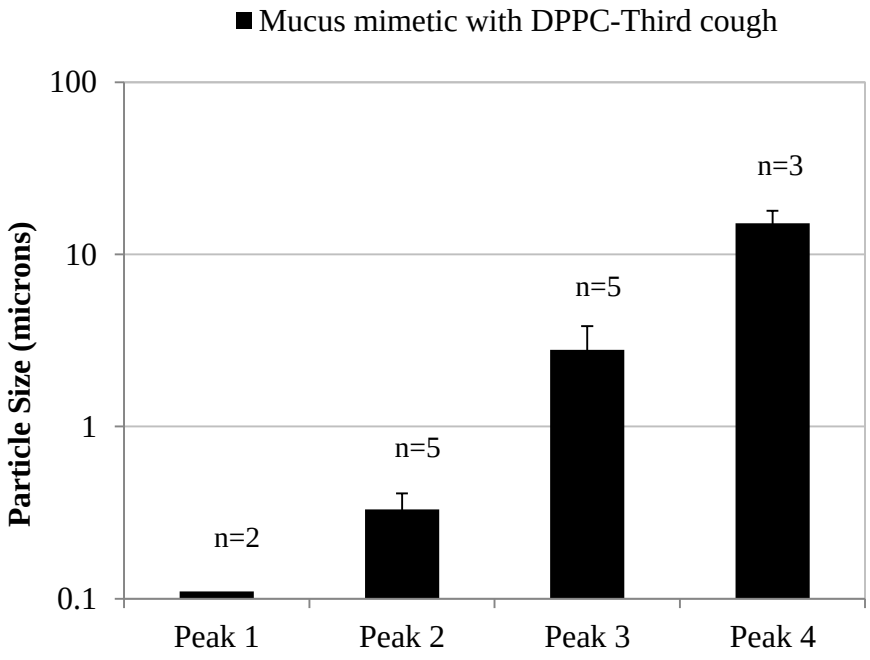

Figure 6-25: Multimodal size distributions, based on cumulative number distribution, of bioaerosols generated from the surfaces of the mucus mimetic with DPPC during a third simulated cough maneuver. Data are represented as the mean ± SD (n=6).

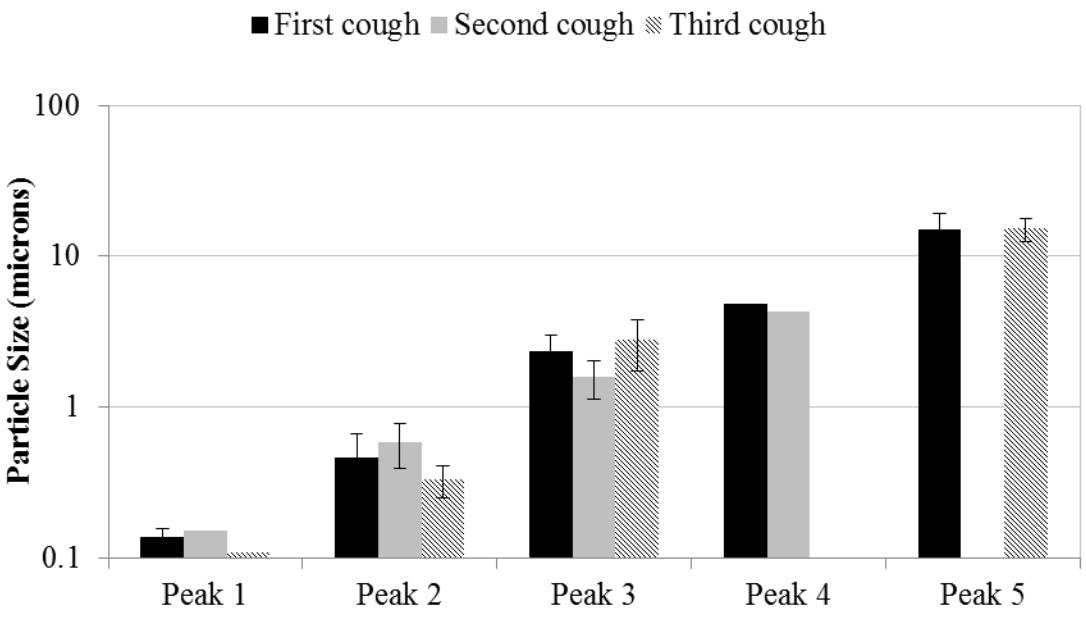

Figure 6-26: Multimodal size distributions, based on cumulative number distribution, of bioaerosols generated from the surfaces of the mucus mimetic with DPPC during first cough (n=11), second cough (n=6), and third cough (n=6). Data are represented as the mean ± SD.

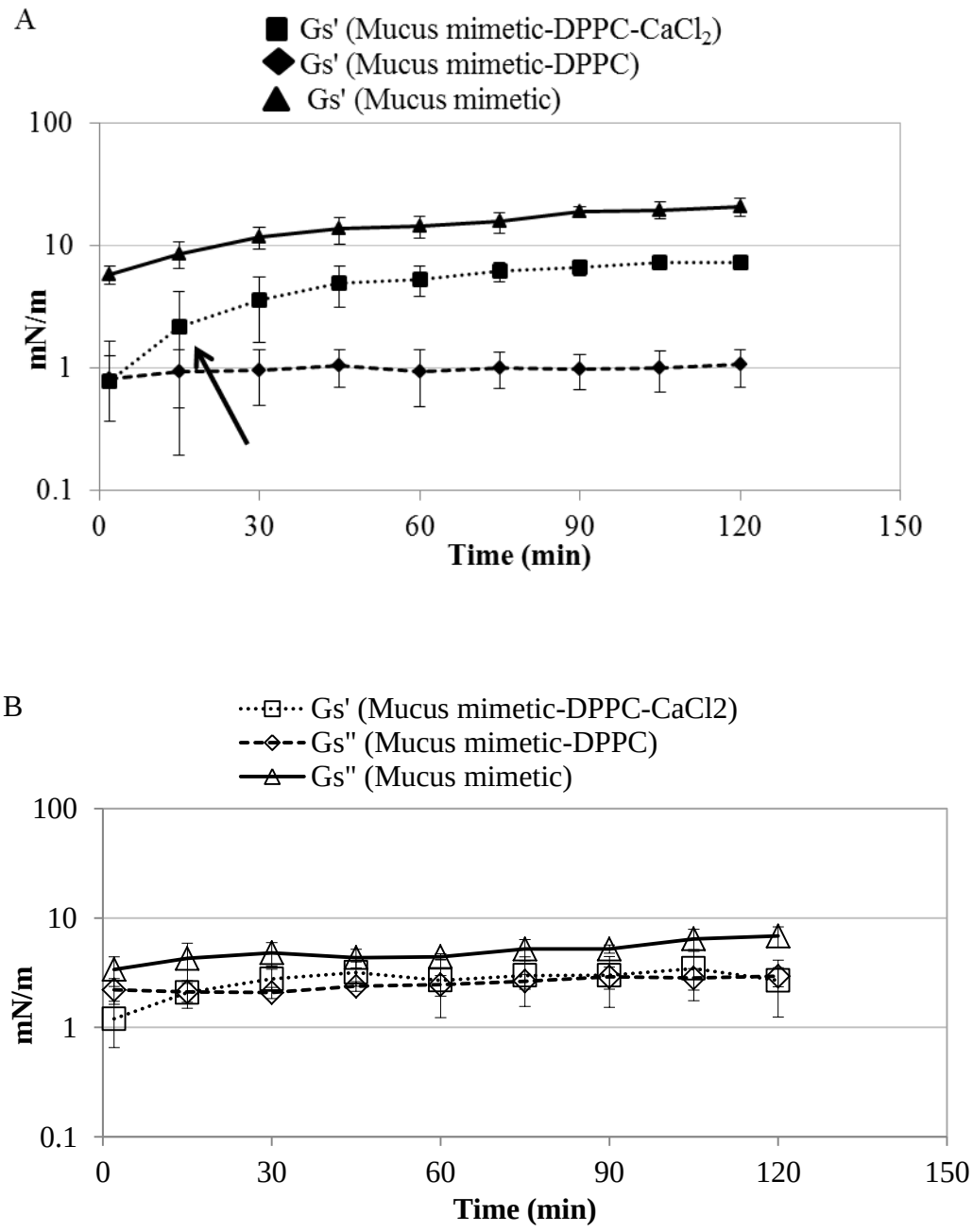

Figure 6-27: Time-dependence of: (A) surface shear storage modulus G_s' and (B) surface shear loss modulus G_s" for the mucus mimetic (n=5), mucus mimetic with DPPC (n=4), and mucus mimetic with DPPC and post-aerosolization with 1.29% $CaCl_2$ for 2 minutes (n=3). The enhancement in surface elastic modulus G_s' after 15 minutes of $CaCl_2$ deposition was indicated by arrow. Data are represented as the mean ± SD.

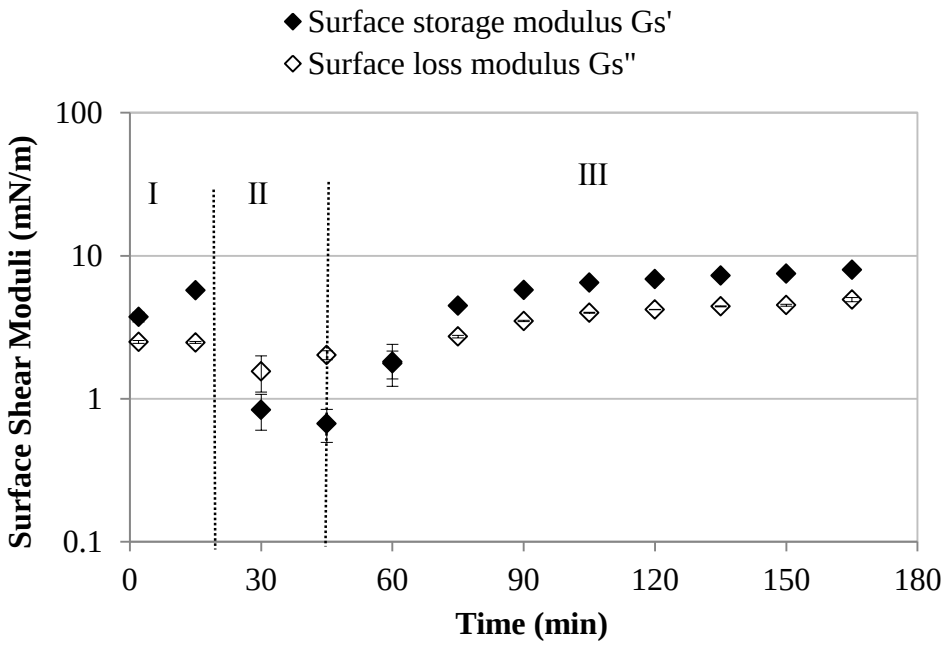

Figure 6-28: Time-dependence of surface shear storage modulus G_s' and surface shear loss modulus G_s" for the mucus mimetic (region I), after spreading DPPC onto mimetic surface (region II), and post- aerosolization with 1.29% $CaCl_2$ onto mimetic covered with DPPC for 2 minutes (region III).

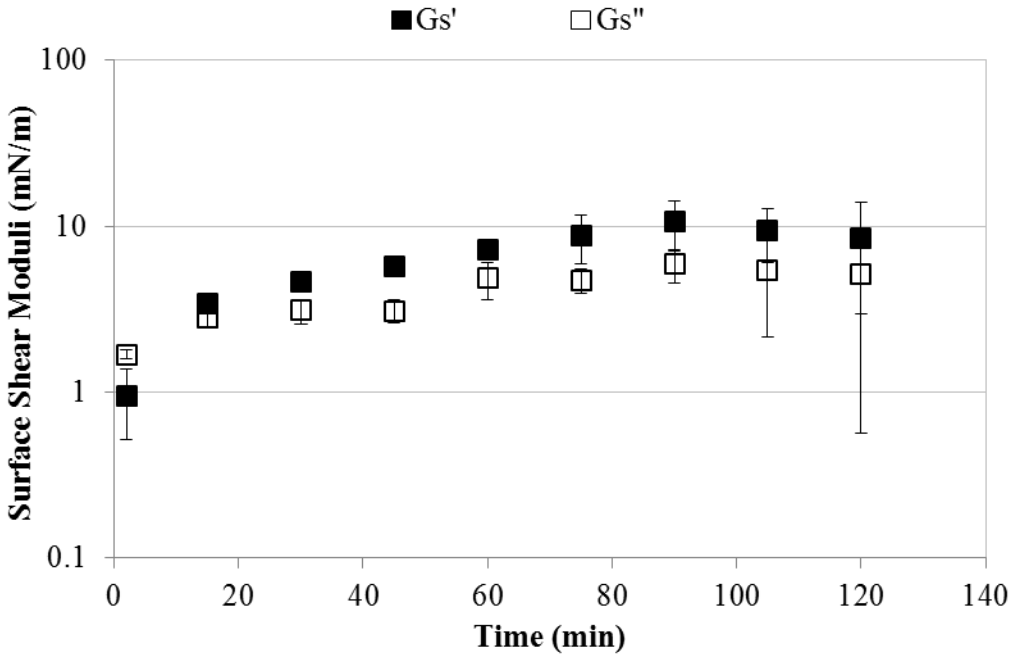

Figure 6-29: Time-dependence of surface shear storage modulus G_s' and surface shear loss modulus G_s" for the 4% PGM with DPPC and post-aerosolization with 1.29% $CaCl_2$ onto for 2 minutes. Data are represented as the mean ± SD (n=3).

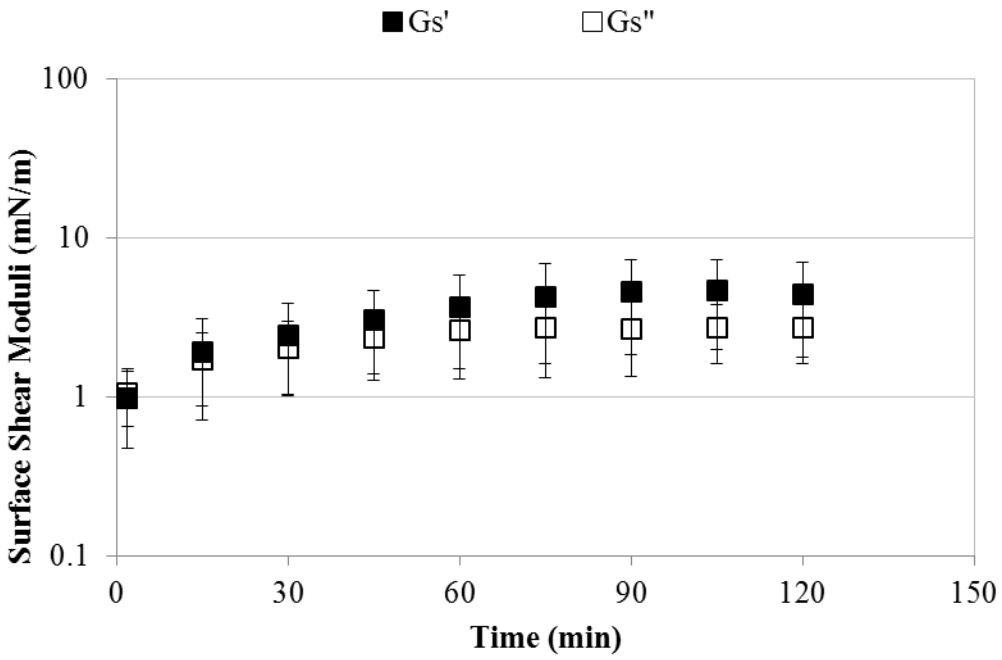

Figure 6-30: Time-dependence of surface shear storage modulus G_s' and surface shear loss modulus G_s" for the 1% albumin solution with DPPC and post-aerosolization with 1.29% $CaCl_2$ onto for 2 minutes. Data are represented as the mean ± SD (n=3).

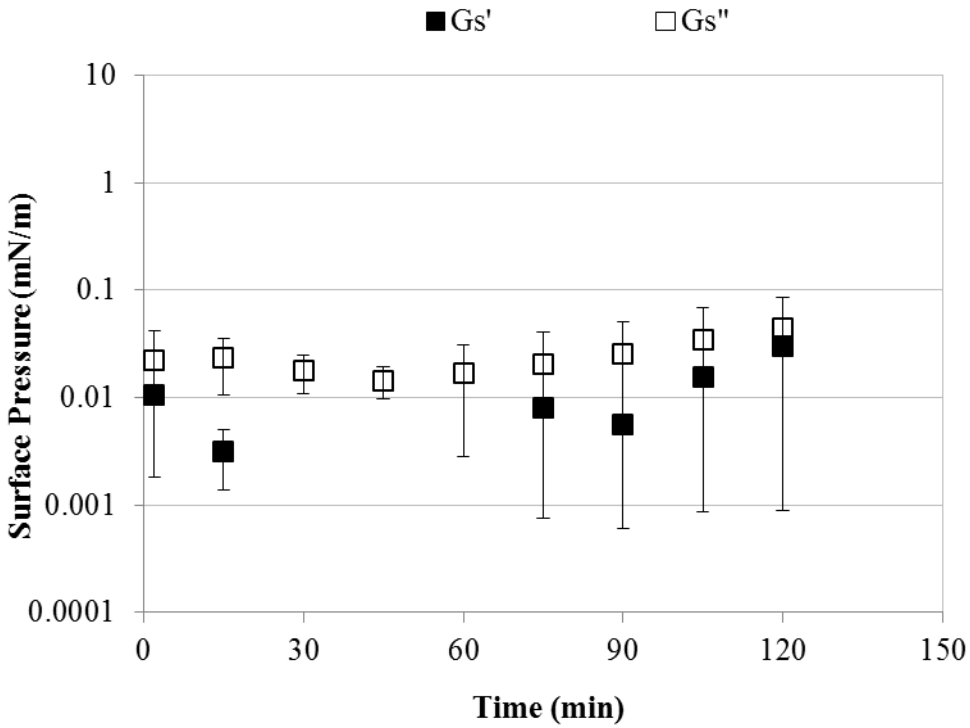

Figure 6-31: Time-dependence of surface shear storage modulus G_s' and surface shear loss modulus G_s" for water with DPPC and post-aerosolization with 1.29% $CaCl_2$ for 2 minutes. Data are represented as the mean ± SD

CHAPTER 7

CONCLUSIONS AND FUTURE PERSPECTIVES

7.1. Conclusions

This research developed a more physiologically relevant *in-vitro* model system for the generation and characterization of exhaled bioaerosols. Synthetic tracheal mucus was first developed for use as a representative viscoelastic subphase for studying the surface rheology of surfactants spreading at the airway lining fluid (ALF) of the large conducting airways. The new system can be used to study the mechanism of bioaerosol formation in the trachea. It may also be used to understand mucus clearance, drug and particle distribution and penetration in the trachea.

In chapter 2, the chemical composition and physical properties (bulk viscoelasticity and surface tension) of the *in-vitro* model mimetic, were matched to that of native tracheal mucus. The *in-vitro* model mimetic was composed based on the most abundant components in lung mucus and their similarity to components found natively. The physical properties of the tracheal mucus are determined by its chemical composition and component concentration; therefore matching the chemical composition and component concentrations of the mucus mimetic was of critical important. The bulk rheological properties of the mimetic were precisely controlled via tailoring of the cross-linking agent (glutaraldehyde, GA) concentration and/or cross-linking time. Three types of mucus mimetics were classified according to their bulk viscoelasticity: mucus mimetics 1, 2 and 3. The wide range of the bulk viscoelastic properties of the three mimetics provide an insight on the rheological behavior of the tracheal mucus at low frequency (i.e. during normal breathing) and at high frequency (i.e. during cough maneuver). The surface tension of the mucus mimetic 1 was matched to that of native tracheal mucus (~ 32 mN/m) via spreading dipalmitoylphosphatidylcholine (DPPC) at the air-mimetic interface. Matching the surface tension of the mucus mimetic helped in better

understanding the surface rheological behavior of the tracheal mucus. DPPC showed good spreadability on the mucus mimetic. However, lowering the surface tension for the mucus mimetics 1 and 2 encountered difficulty due to the more solid-like surface. Therefore, the mucus mimetic 1 was selected to be used in the surface rheological studies and bioaerosol formation.

In chapter 3, lowering the surface tension of the mucus mimetic 1, using DPPC, to ~ 32 mN/m required three-fold the amount that would need to form a DPPC monolayer on an aqueous subphase of equivalent surface tension. The mucus mimetic was used as a representative viscoelastic subphase in this study. The surface rheological behavior of the most abundant phospholipid in tracheal secretions, DPPC, spread on the mucus mimetic was probed using an interfacial stress rheometer (ISR). DPPC alters the surface rheological behavior of the mucus mimetic from more elastic to more viscous surface, where surface shear viscous modulus G_s" dominated surface shear elastic modulus G_s'. In addition, lower values of G_s' and G_s" moduli were observed for DPPC on an aqueous Newtonian subphase compared to pure DPPC on the viscoelastic, non-Newtonian subphase, at a surface tension of ~ 32 mN/m, showing the importance of the subphase type on surface behavior. Understanding the surface properties of the tracheal mucus provide an insight in better understanding the normal function of the tracheal mucus (mucociliary and cough clearance) and bioaerosol formation.

In chapter 4, Infasurf® was used as a model lung surfactant to study the surface rheological properties of the heterogeneous complex mixture of surface active components covered the ALF of the airway conducting airways. Although the surface properties of DPPC onto mimetic subphase was studied in Chapter 3, DPPC did not capture the surface properties of the complex surfactant mixture covers the air-mucus interface. Infasurf® exhibited a higher surface activity at an air-mimetic interface compared to DPPC. This was reflected by the lower amount of Infasurf® required to lower the surface tension of the mucus mimetic to ~ 32 mN/m compared to that of DPPC.

Infasurf® films on the mucus mimetic and water subphases exhibited a more viscous surface, where G_s" dominated G_s'. The substantial difference in the chemical composition of the two surfactants resulted in significant changes in the surface rheological behavior of Infasurf® and DPPC films on the mucus mimetic and water subphases. Therefore, it is expected that the Infasurf® will have more influence on the mucus functions and bioaerosol formation.

In chapter 5, the optical concentration of bioaerosols generated from mimetic surfaces, using the simulated cough machine (SCM) described by King *et al.*,[49] was extremely low, indicating no bioaerosols were formed. Therefore, the SCM was enhanced by mimicking the features of the trachea, where tracheal temperature and relative humidity (%RH) in healthy individuals were reported to be 35.8-36.4°C and %RH of 98.8-99.7%, respectively, during expiration. In the enhanced SCM, the air passing through the SCM and entering the model trachea was warmed to 35.1 ± 0.9°C and humidified to 61.5 ± 6.2% RH. In addition, SCM was placed inside an enclosure chamber maintained at temperature of ~ 37°C. Mimicking the conditions (temperature and %RH) of the trachea is critical to better determine the initial (original) droplet size, thereby understand the mechanism of bioaerosol formation.

In chapter 6, the size distribution of bioaerosols generated from mucus mimetic surfaces was determined. The size of bioaerosol droplets is an important factor in determining the fate of the droplets and the types of pathogenic organisms that can be transported by airborne route. Bioaerosols were generated from mucus mimetic surfaces of varying bulk and surface properties during a simulated cough maneuver using the enhanced SCM. The size distributions of bioaerosols were multimodal, where four to five modes were observed and were relatively equal. This indicates that the variation in the bulk viscoelastic and surface properties of mimetics was not significant to show changes in modes. The size of bioaerosols generated from the mucus mimetic with DPPC during the second and third cough peaked at relatively equal modes. Equal modes of the size

distribution suggests no alteration in surface properties after each cough. The surface viscoelastic properties of mucus mimetic with DPPC and post-aerosolization with 1.29% $CaCl_2$ solution was probed using the ISR. Deposition of $CaCl_2$ onto mimetic surface altered mimetic surface behavior from more viscous to more elastic, where G_s' dominated G_s". Further studies will ultimately guide the development of simple, safe inhalants to suppress the formation of bioaerosols.

7.2. Future Perspectives

The more physiologically relevant *in-vitro* model mimetic of the tracheal mucus showed great potential for better understanding the surface rheological properties of surfactants spread at an air-mucus interface of the ALF and bioaerosols formation from the large conducting airways. However, better matching the bulk rheological properties of the mimetic to those of native mucus at high frequencies (100 rad/sec) requires further evaluation. In addition, this *in-vitro* model mimetic needs further evaluation for the cross-linking process and the selection of the cross-linking agent used in this study. The cross-linking process of the mimetic using GA was a continuous process where GA was not washed out (to remove unreacted GA) from mucus mimetic formulations. Thus a continuous increase in both G' and G" was expected to be observed with time. Therefore, an alternative cross-linking method needs to be investigated. One alternative method is the oxidation of the free thiol groups in mucin glycoproteins to disulfides using an oxidizing agent such as iodine.[153] The introduction of the disulfide bridges will covalently cross-link two (or more) polypeptide chains of mucins, thus enhance the viscoelastic properties of the mucus mimetic. In addition, this mucus mimetic needs to be evaluated for its usefulness in mucociliary studies.

The surface rheology of surfactants spread at an air-mucus interface needs to be determined using a mucus mimetic of average bulk viscoelasticity that matched that of native tracheal mucus (such as mucus mimetic 2). The surface rheological studies

discussed in this work were probed using mucus mimetic of a low bulk viscoelasticity (mucus mimetic 1). Therefore, spreading of surfactants onto the mucus mimetic 2 subphase needs further evaluation. In addition, surface rheological studies can be conducted at 37°C to simulate body temperature by placing the mini-trough inside a small heater connected to an external circulating water bath maintained at 37°C.

Better enhancement of the SCM by increasing the relative humidity (%RH) of air entering the model trachea needs to be considered to more accurately determine the original (initial) size distribution of bioaerosols generated from mucus mimetic surfaces. In addition, flow rate and %RH of air entering the model trachea during a simulated cough maneuver using the SCM should be better controlled. The peak air flow rate during a simulated cough maneuver can be better controlled by placing a control valve between the pressure cooker and the 6.25-liter air tank.

Future work in bioaerosol studies will aim to determine the size distribution of bioaerosols generated from mimetic surfaces during three repetitive cough maneuvers to ensure sufficient bioaerosol production for particle size characterization. Furthermore, an alteration in mimetic surface properties after the first cough should be directly investigated and correlated to bioaerosol formation during the second and third coughs. In addition, the key parameters that determine pathogen loading into bioaerosols by correlating pathogen physical properties (size and shape of pathogen) to bioaerosol formation should be identified.

To aid further development of new aerosolizable strategies to suppress the formation of pathogenic bioaerosols in the lungs, further studies are needed to study the effect of 0.9% NaCl and 1.29% $CaCl_2$ solutions on the surface viscoelastic properties of mucus mimetic as a function of concentration. These studies will ultimately guide the development of simple, safe alternative strategies to suppress the formation of bioaerosols in the lungs and thereby halt airborne disease transmission.

REFERENCES

1. Hinds WC. Respiratory deposition. In: Aerosol Technology: properties, behavior, and measurement of airborne particles. 2nd edition. John Wiley & Sons, Inc.; 1999:pp 233-259. New York.

2. Hickey AJ, Thompson DC. Physiology of the airways. In: Pharmaceutical Inhalation Aerosol Technology. 2nd edition. Marcel Dekker; 2004:pp 1-29. New York.

3. Wine JJ. The genesis of cystic fibrosis lung disease. J Clin Invest. 1999;103(3):309-312.

4. Patton JS. Mechanisms of macromolecule absorption by the lungs. Adv Drug Deliv Rev. 1996;19(1):3-36.

5. Jayaraman S, Song Y, Vetrivel L, Shankar L, Verkman AS. Noninvasive in vivo fluorescence measurement of airway-surface liquid depth, salt concentration, and pH. J Clin Invest. 2001;107(3):317-324.

6. Song Y, Namkung W, Nielson DW, Lee JW, Finkbeiner WE, Verkman AS. Airway surface liquid depth measured in ex vivo fragments of pig and human trachea: Dependence on Na+ and Cl^- channel function. Am J Physiol Lung Cell Mol Physiol. 2009;297(6):L1131-40.

7. Moriarty JA, Grotberg JB. Flow-induced instabilities of a mucus-serous bilayer. J Fluid Mech. 1999;397:1-22.

8. Edwards DA, Fiegel J, DeHaan W, Brande M, Man J, Clarke R. Novel inhalants for control and protection against airborne infections. Respir Drug Deliv. 2006;1:41-48.

9. Puchelle E, Zahm JM, Duvivier C, Didelon J, Jacquot J, Quemada D. Elasto-thixotropic properties of bronchial mucus and polymer analogs. I. Experimental results. Biorheology. 1985;22(5):415-423.

10. Gehr P, Annexe A. Anatomy and morphology of the respiratory tract. Ann ICRP. 1994;24(1-3):121-166.

11. Sleigh MA. Ciliary function in transport of mucus. Eur J Respir Dis Suppl. 1983;128 (Pt 1):287-292.

12. Matthews LW, Spector S, Lemm J, Potter JL. Studies on pulmonary secretions. I. The over-all chemical composition of pulmonary secretions from patients with cystic fibrosis, bronchiectasis, and laryngectomy. Am Rev Respir Dis. 1963;88:199-204.

13. Slomiany A, Murty VL, Aono M, Snyder CE, Herp A, Slomiany BL. Lipid composition of tracheobronchial secretions from normal individuals and patients with cystic fibrosis. Biochim Biophys Acta. 1982;710(1):106-111.

14. Boat TF, Cheng PW, Leigh MW. Biochemistry of mucus. In: Lung Biology in Health and Disease. Volume 72. Dekker 1994:pp 217-282. New York.

15. Zayas G, Dimitry J, Zayas A, O'Brien D, King M. A new paradigm in respiratory hygiene: Increasing the cohesivity of airway secretions to improve cough interaction and reduce aerosol dispersion. BMC Pulm Med. 2005;5:11.

16. Kocevar-Nared J, Kristl J, Smid-Korbar J. Comparative rheological investigation of crude gastric mucin and natural gastric mucus. Biomaterials. 1997;18(9):677-681.

17. King M, Rubin BK. Pharmacological approaches to discovery and development of new mucolytic agents. Adv Drug Deliv Rev. 2002;54(11):1475-1490.

18. Nielson DW. Electrolyte composition of pulmonary alveolar subphase in anesthetized rabbits. J Appl Physiol. 1986;60(3):972-979.

19. Yoneda K. Mucous blanket of rat bronchus: An ultrastructural study. Am Rev Respir Dis. 1976;114(5):837-842.

20. Low FN. The pulmonary alveolar epithelium of laboratory mammals and man. Anat Rec. 1953;117(2):241-263.

21. Yu SH, Possmayer F. Dipalmitoylphosphatidylcholine and cholesterol in monolayers spread from adsorbed films of pulmonary surfactant. J Lipid Res. 2001;42(9):1421-1429.

22. Jeanneret-Grosjean A, King M, Michoud MC, Liote H, Amyot R. Sampling technique and rheology of human tracheobronchial mucus. Am Rev Respir Dis. 1988;137(3):707-710.

23. Rubin BK, Ramirez O, Zayas JG, Finegan B, King M. Collection and analysis of respiratory mucus from subjects without lung disease. Am Rev Respir Dis. 1990;141(4 Pt 1):1040-1043.

24. Zayas JG, Man GC, King M. Tracheal mucus rheology in patients undergoing diagnostic bronchoscopy. Interrelations with smoking and cancer. Am Rev Respir Dis. 1990;141(5 Pt 1):1107-1113.

25. Litt M, Khan MA, Chakrin LW, Wardell JR,Jr, Christian P. The viscoelasticity of fractionated canine tracheal mucus. Biorheology. 1974;11(2):111-117.

26. Lai SK, Wang YY, Wirtz D, Hanes J. Micro- and macrorheology of mucus. Adv Drug Deliv Rev. 2009;61(2):86-100.

27. Homnick DN, Marks JH, Rubin BK. The effect of a first-generation antihistamine on sputum viscoelasticity in cystic fibrosis. J Aerosol Med. 2007;20(1):45-49.

28. Davis SS, Dippy JE. The rheological properties of sputum. Biorheology. 1969;6(1):11-21.

29. Im Hof V, Gehr P, Gerber V, Lee MM, Schurch S. In vivo determination of surface tension in the horse trachea and in vitro model studies. Respir Physiol. 1997;109(1):81-93.

30. Schurch S, Gehr P, Im Hof V, Geiser M, Green F. Surfactant displaces particles toward the epithelium in airways and alveoli. Respir Physiol. 1990;80(1):17-32.

31. Lee MM, Schurch S, Roth SH, Jiang X, Cheng S, Bjarnason S, Green FH. Effects of acid aerosol exposure on the surface properties of airway mucus. Exp Lung Res. 1995;21(6):835-851.

32. Rubin BK. Mucus, phlegm, and sputum in cystic fibrosis. Respir Care. 2009;54(6):726-32.

33. Morgenroth K. Morphology of the bronchial lining layer and its alteration in IRDS, ARDS and COLD. Eur J Respir Dis Suppl. 1985;142:7-18.

34. Sims DE, Horne MM. Heterogeneity of the composition and thickness of tracheal mucus in rats. Am J Physiol. 1997;273(5 Pt 1):L1036-41.

35. King M, Rubin BK. Rheology of airway mucus: Relationship with clearance function. In: Airway Secretions; Physiological Bases for the Control of Mucus Hypersecretion. M. Dekker; 1994:pp283-314. New York.

36. Im Hof V, Patrick G. Particle retention and clearance. J Aerosol Med. 1994;7(1):39-47.

37. Hohlfeld JM. The role of surfactant in asthma. Respir Res. 2002;3:4.

38. Widdicombe JG. Role of lipids in airway function. Eur J Respir Dis Suppl. 1987;153:197-204.

39. Bhaskar KR, Drazen JM, O'Sullivan DD, Scanlon PM, Reid LM. Transition from normal to hypersecretory bronchial mucus in a canine model of bronchitis: Changes in yield and composition. Exp Lung Res. 1988;14(1):101-120.

40. Bhaskar KR, O'Sullivan DD, Opaskar-Hincman H, Reid LM, Coles SJ. Density gradient analysis of secretions produced in vitro by human and canine airway mucosa: Identification of lipids and proteoglycans in such secretions. Exp Lung Res. 1986;10(4):401-422.

41. Bhaskar KR, O'Sullivan DD, Seltzer J, Rossing TH, Drazen JM, Reid LM. Density gradient study of bronchial mucus aspirates from healthy volunteers (smokers and nonsmokers) and from patients with tracheostomy. Exp Lung Res. 1985;9(3-4):289-308.

42. Bernhard W, Haagsman HP, Tschernig T, Poets CF, Postle AD, van Eijk ME, and von der Hardt H. Conductive airway surfactant: Surface-tension function, biochemical composition, and possible alveolar origin. Am J Respir Cell Mol Biol. 1997;17(1):41-50.

43. Griese M, Duroux A, Schams A, Lenz AG, Kleinsasser N. Tracheobronchial surface active material in cystic fibrosis. Eur J Med Res. 1997;2(3):114-120.

44. Wright SM, Hockey PM, Enhorning G, Strong P, Reid KBM, Holgate ST, Ratko Djukanovic R, Postle AD. Altered airway surfactant phospholipid composition and reduced lung function in asthma. J Appl Physiol. 2000;89(4):1283-1292.

45. Girod S, Fuchey C, Galabert C, Lebonvallet S, Bonnet N, Ploton D, Puchelle E. Identification of phospholipids in secretory granules of human submucosal gland respiratory cells. J Histochem Cytochem. 1991;39(2):193-198.

46. Marcinkowski AL, Garoff S, Tilton RD, Pilewski JM, Corcoran TE. Postdeposition dispersion of aerosol medications using surfactant carriers. J Aerosol Med Pulm Drug Deliv. 2008;21(4):361-370.

47. Banerjee R, Puniyani RR. Exogenous surfactant therapy and mucus rheology in chronic obstructive airway diseases. J Biomater Appl. 2000;14(3):243-272.

48. Rau GA, Dombrowsky H, Gebert A, Thole HH, von der Hardt H, Bernhard,W. Phosphatidylcholine metabolism of rat trachea in relation to lung parenchyma and surfactant. J Appl Physiol. 2003;95(3):1145-1152.

49. King M. The role of mucus viscoelasticity in cough clearance. Biorheology. 1987;24(6):589-597.

50. Watanabe W, Thomas M, Clarke R, Klibanov AM, Langer R, Katstra J, Fuller GG, Griel LC, Fiegel J, David Edwards D. Why inhaling salt water changes what we exhale. J Colloid Interface Sci. 2007;307(1):71-78.

51. Banerjee R, Puniyani RR. Effects of clove oil-phospholipid mixtures on rheology of gum tragacanth - possible application for surfactant action on mucus gel simulants. Biomed Mater Eng. 2000;10(3-4):189-197.

52. Zahm JM, King M, Duvivier C, Pierrot D, Girod S, Puchelle E. Role of simulated repetitive coughing in mucus clearance. Eur Respir J. 1991;4(3):311-315.

53. Mujica-Lopez KI, Pearce MA, Narron KA, Perez J, Rubin BK. In vitro evaluation of endotracheal tubes with intrinsic suction. Chest. 2010;138(4):863-869.

54. Basser PJ, McMahon TA, Griffith P. The mechanism of mucus clearance in cough. J Biomech Eng. 1989;111(4):288-297.

55. Rancourt RC, Tai S, King M, Heltshe SL, Penvari C, Accurso FJ, White CW. Thioredoxin liquefies and decreases the viscoelasticity of cystic fibrosis sputum. Am J Physiol Lung Cell Mol Physiol. 2004;286(5):L931-8.

56. King M, Macklem PT. Rheological properties of microliter quantities of normal mucus. J Appl Physiol. 1977;42(6):797-802.

57. Lutz RJ., Litt M, Chakrin LW. Physical-chemical factors in mucus rheology. In: Rheology of Biological Systems. 1973:pp119-157. Springfield, IL.

58. Edwards DA, Man JC, Brand P, Katstra JP, Sommerer K, Stone HA, Edward Nardell E, Scheuch G. Inhaling to mitigate exhaled bioaerosols. Proc Natl Acad Sci U S A. 2004;101(50):17383-17388.

59. Papineni RS, Rosenthal FS. The size distribution of droplets in the exhaled breath of healthy human subjects. J Aerosol Med. 1997;10(2):105-116.

60. Johnson GR, Morawska L. The mechanism of breath aerosol formation. J Aerosol Med Pulm Drug Deliv. 2009;22(3):229-237.

61. Fiegel J, Clarke R, Edwards DA. Airborne infectious disease and the suppression of pulmonary bioaerosols. Drug Discov Today. 2006;11(1-2):51-57.

62. Evrensel CA, Khan RU, Elli S, Krumpe PE. Viscous airflow through a rigid tube with a compliant lining: A simple model for the air-mucus interaction in pulmonary airways. J Biomech Eng. 1993;115(3):262-270.

63. Vasudevan M, Lange CF. Property dependence of onset of instability in viscoelastic respiratory fluids. Int J Eng Sci. 2005;43(15-16):1292-1298.

64. Vasudevan M, Lange CF. Surface tension effects on instability in viscoelastic respiratory fluids. Math Biosci. 2007;205(2):180-194.

65. Duguid JP. The size and the duration of air-carriage of respiratory droplets and droplet-nuclei. J Hyg (Lond). 1946;44(6):471-479.

66. Loudon RG, Roberts RM. Droplet expulsion from the respiratory tract. Am Rev Respir Dis. 1967;95(3):435-442.

67. Fairchild CI, Stampfer JF. Particle concentration in exhaled breath. Am Ind Hyg Assoc J. 1987;48(11):948-949.

68. Yang S, Lee GW, Chen CM, Wu CC, Yu KP. The size and concentration of droplets generated by coughing in human subjects. J Aerosol Med. 2007;20(4):484-494.

69. Chao CYH, Wan MP, Morawska L, Johnson GR, Ristovski ZD, Hargreaves M, Mengersen K, Corbett S, Li Y, Xie X, Katoshevski D. Characterization of expiration air jets and droplet size distributions immediately at the mouth opening. J Aerosol Sci. 2009;40(2):122-133.

70. Morawska L, Johnson GR, Ristovski ZD, Hargreaves M, Mengersen K, Corbett S, Chao CYH, Katoshevski D. Size distribution and sites of origin of droplets expelled from the human respiratory tract during expiratory activities. J Aerosol Sci. 2009;40(3):256-269.

71. Clarke R, Katstra J, Man J, Dehaan W, Edwards D, Griel L. Pulmonary delivery of anti-contagion aerosol to diminish exhaled bioaerosols and airborne infectious disease. Am J Infect Control. 2005;33(5):e85-e85.

72. Girod S, Galabert C, Pierrot D, Boissonnade MM, Zahm JM, Baszkin A, Puchelle E. Role of phospholipid lining on respiratory mucus clearance by cough. J Appl Physiol. 1991;71(6):2262-2266.

73. King M, Brock G, Lundell C. Clearance of mucus by simulated cough. J Appl Physiol. 1985;58(6):1776-1782.

74. Galabert C, Jacquot J, Zahm JM, Puchelle E. Relationships between the lipid content and the rheological properties of airway secretions in cystic fibrosis. Clin Chim Acta. 1987;164(2):139-149.

75. Martin GP, Marriott C, Kellaway IW. Direct effect of bile salts and phospholipids on the physical properties of mucus. Gut. 1978;19(2):103-107.

76. Boat TF, Cheng PW. Biochemistry of airway mucus secretions. Fed Proc. 1980;39(13):3067-3074.

77. Potter JL, Matthews LW, Spector S, Lemm J. Studies on pulmonary secretions. II. osmolality and the ionic environment of pulmonary secretions from patients with cystic fibrosis, bronchiectasis, and laryngectomy. Am Rev Respir Dis. 1967;96(1):83-87.

78. Yu SH, Possmayer F. Interaction of pulmonary surfactant protein A with dipalmitoylphosphatidylcholine and cholesterol at the air/water interface. J Lipid Res. 1998;39(3):555-568.

79. Adamson AW, Gast AP. Capillarity. In: Physical Chemistry of Surfaces. 6th edition. John Wiley and Sons, Inc.; 1997:pp4-47. New York

80. Kaliner M, Shelhamer JH, Borson B, Nadel J, Patow C, Marom Z. Human respiratory mucus. Am Rev Respir Dis. 1986;134(3):612-621.

81. Sachdev GP, Myers FJ, Horton FO, Fox OF, Wen G, Rogers RM, Carubelli R. Isolation, chemical composition, and properties of the major mucin component of normal human tracheobronchial secretions. Biochem Med. 1980;24(1):82-94.

82. Reid LM, Bhaskar KR. Macromolecular and lipid constituents of bronchial epithelial mucus. Symp Soc Exp Biol. 1989;43:201-219.

83. Madsen F, Eberth K, Smart JD. A rheological evaluation of various mucus gels for use in in-vitro mucoadhesion testing. J Pharm Sci. 1996;2:563-566.

84. Litt M, Khan MA, Wolf DP. Mucus rheology: Relation to structure and function. Biorheology. 1976;13(1):37-48.

85. Gelman RA, Meyer FA. Mucociliary transference rate and mucus viscoelasticity dependence on dynamic storage and loss modulus. Am Rev Respir Dis. 1979;120(3):553-557.

86. Molin SO, Nygren H, Dolonius L. A new method for the study of glutaraldehyde-induced crosslinking properties in proteins with special reference to the reaction with amino groups. J Histochem Cytochem. 1978;26(5):412-414.

87. Denton R, Forsman W, Hwang SH, Litt M, Miller CE. Viscoelasticity of mucus. its role in ciliary transport of pulmonary secretions. Am Rev Respir Dis. 1968;98(3):380-391.

88. Rudraraju VS, Wyandt CM. Rheology of microcrystalline cellulose and sodiumcarboxymethyl cellulose hydrogels using a controlled stress rheometer: Part II. Int J Pharm. 2005;292(1-2):63-73.

89. Migneault I, Dartiguenave C, Bertrand MJ, Waldron KC. Glutaraldehyde: Behavior in aqueous solution, reaction with proteins, and application to enzyme crosslinking. BioTech. 2004;37(5):790-6, 798-802.

90. Hopwood D. Theoretical and practical aspects of glutaraldehyde fixation. Histochem J. 1972;4(4):267-303.

91. Ruijgrok JM, Dewijn JR, Boon ME. Optimizing glutaraldehyde crosslinking of collage: Effects of time, temperature and concentration as measured by shrinkage temperature. J Mater Sci: Mater Med. 1994;5:80-87.

92. Hopwood D, Callen CR, McCabe M. The reactions between glutaraldehyde and various proteins. an investigation of their kinetics. Histochem J. 1970;2(2):137-150.

93. Qin C, Xu J, Zhang Y. Spectroscopic investigation of the function of aqueous 2-hydroxyethylmethacrylate/glutaraldehyde solution as a dentin desensitizer. Eur J Oral Sci. 2006;114(4):354-359.

94. Farris S, Song J, Huang Q. Alternative reaction mechanism for the cross-linking of gelatin with glutaraldehyde. J Agric Food Chem. 2010;58(2):998-1003.

95. Tomihata K, Ikada Y. Crosslinking of hyaluronic acid with glutaraldehyde. J Polym Sci Part A. 1997;35(16):3553-3559.

96. Gupta KC, Ravi Kumar MNV. Semi-interpenetrating polymer network beads of crosslinked chitosan-glycine for controlled release of chlorphenramine maleate. J Appl Polym Sci. 2000;76(5):672-683.

97. Capra RH, Baruzzi AM, Quinzani LM, Strumia MC. Rheological, dielectric and diffusion analysis of mucin/carbopol matrices used in amperometric biosensors. Sensors Actuators B: Chem. 2007;124(2):466-476.

98. Bansil R, Turner BS. Mucin structure, aggregation, physiological functions and biomedical applications. Curr Opin Colloid Interf Sci. 2006;11(2-3):164-170.

99. Grdadolnik J, Marechal Y. Bovine serum albumin observed by infrared spectrometry. I. methodology, structural investigation, and water uptake. Biopolymers. 2001;62(1):40-53.

100. Feng Y, Zhou Y, Zou Q, Wang J, Chen F, Gao Z. Preparation and characterization of bisphenol A-cationized bovine serum albumin. J Immunol Methods. 2009;340(2):138-143.

101. Sheu MT, Huang JC, Yeh GC, Ho HO. Characterization of collagen gel solutions and collagen matrices for cell culture. Biomaterials. 2001;22(13):1713-1719.

102. Pavia DL, Lampman GM, Kriz GS. Infrared spectroscopy. In: Introduction to Spectroscopy. 2nd edition. Saunders College Publishing; 1996: pp14-95. Orlando, FL.

103. Kildeeva NR, Permino PA, Vladimiro LV, Novikov VV, Mikhailov SN. About mechanism of chitosan cross-linking with glutaraldehyde. Russ J Bioorg Chem. 2009;35:360-369.

104. Fen-NiFu, DeOliveira D,B., Trumble W,R., Sarkar H,K., Singh B,Ram. Secondary structure estimation of proteins using the amide III region of fourier transform infrared spectroscopy: Application to analyze calcium-binding-induced structural changes in calsequestrin. Appl Spectrosc. 1994;48:1432-1441.

105. Orbulescu J, Leblanc RM. Importance of the spreading solvent evaporation time in langmuir monolayers. J Phys Chem C. 2009;113:5313-5315.

106. Baszkin A, Proust JE, Monsenego P, Boissonnade MM. Wettability of polymers by mucin aqueous solutions. Biorheology. 1990;27(3-4):503-514.

107. Deneuville E, Perrot-Minot C, Pennaforte F, Roussey M, Zahm, JM, Clavel C, Puchelle E, de Bentzmann S. Revisited physicochemical and transport properties of respiratory mucus in genotyped cystic fibrosis patients. Am J Respir Crit Care Med. 1997;156(1):166-172.

108. Albers GM, Tomkiewicz RP, May MK, Ramirez OE, Rubin BK. Ring distraction technique for measuring surface tension of sputum: Relationship to sputum clearability. J Appl Physiol. 1996;81(6):2690-2695.

109. Macy R. Surface tension by the ring method. J Chem Educ. 1935;12(12):573-576.

110. Boat TF, Matthews LW. Chemical composition of human tracheobronchial secretions. In: Fundamentals and Clinical Pathology. 1st edition. Charles C Thomas; 1973:pp 243-274.Sprigfield, IL.

111. Khubchandani KR, Snyder JM. Surfactant protein A (SP-A): The alveolus and beyond. FASEB J. 2001;15(1):59-69.

112. Naumann CA, Brooks CF, Fuller GG, Knoll W, Frank CW. Viscoelastic properties of lipopolymers at the air-water interface: A combined interfacial stress rheometer and film balance study. Langmuir. 1999;15:7752-7761.

113. Krägel J, Kretzschmar G, Li JB, Loglio G, Miller R, Möhwald H. Surface rheology of monolayers. Thin Solid Films. 1996;284-285:361-364.

114. Roberts SA, Kellaway IW, Taylor KM, Warburton B, Peters K. Combined surface pressure-interfacial shear rheology studies of the interaction of proteins with spread phospholipid monolayers at the air-water interface. Int J Pharm. 2005;300(1-2):48-55.

115. Nishimura SY, Magana GM, Ketelson HA, Fuller GG. Effect of lysozyme adsorption on the interfacial rheology of DPPC and cholesteryl myristate films. Langmuir. 2008;24(20):11728-11733.

116. Kaneko D, Gong JP, Zrínyi M, Osada Y. Kinetics of fluid spreading on viscoelastic substrates. J Polym Sci Part B. 2005;43(5):562-572.

117. Daniels KE, Mukhopadhyay S, Behringer RP. Starbursts and wispy drops: Surfactants spreading on gels. Chaos. 2005;15(4):041107.

118. Rasband WS. Image J. U. S. National Institutes of Health, Bethesda, Maryland:1997-2009. Available from: http://rsb.info.nih.gov.proxy.lib.uiowa.edu/ij/.

119. Brooks CF. An interfacial stress rheometer to study the shear rheology of Langmuir monolayers. [Ph.D thesis]. Stanford University; 1999.

120. Notter RH. Introduction to surface tension and surfactants. In: Lung Surfactants: Basic Science and Clinical Applications. Vol 149. New York: Marcel Dekker, Inc.; 2000: pp 7-43.

121. Mohwald H. Phospholipid and phospholipid-protein monolayers at the air/water interface. Annu Rev Phys Chem. 1990;41:441-476.

122. McConlogue CW, Vanderlick TK. Molecular determinants of lipid domain shape. Langmuir. 1999;15:234-237.

123. Nakamura S, Nakahara H, Krafft MP, Shibata O. Two-component Langmuir monolayers of single-chain partially fluorinated amphiphiles with dipalmitoylphosphatidylcholine (DPPC). Langmuir. 2007;23:12634-12644.

124. Banaha M, Daerr A, Limat L. Spreading of liquid drops on agar gels. Eur Phys J. Special Topics. 2009;166:185-188.

125. Daniels KE, Mukhopadhyay S, Houseworth PJ, Behringer RP. Instabilities in droplets spreading on gels. Phys Rev Lett. 2007;99(12):124501.

126. Fester T, Berg RH, Taylor CG. An easy method using glutaraldehyde-introduced fluorescence for the microscopic analysis of plant biotrophic interactions. J Microsc. 2008;231(2):342-348.

127. Gerber F, Krafft MP, Vandamme TF. The detrimental effect of serum albumin on the re-spreading of a dipalmitoylphosphatidylcholine Langmuir monolayer is counteracted by a fluorocarbon gas. BBA - Biomembranes. 2007;1768(3):490-494.

128. Zasadzinski JA, Stenger PC, Shieh I, Dhar P. Overcoming rapid inactivation of lung surfactant: Analogies between competitive adsorption and colloid stability. BBA - Biomembranes. 2010;1798(4):801-828.

129. Zayas G, Valle JC, Alonso M, et al. A new paradigm in respiratory hygiene: Modulating respiratory secretions to contain cough bioaerosol without affecting mucus clearance. BMC Pulm Med. 2007;7:11.

130. Erni P, Windhab EJ, Gunde R, et al. Interfacial rheology of surface-active biopolymers: Acacia senegal gum versus hydrophobically modified starch. Biomacromolecules. 2007;8(11):3458-3466.

131. Kragel J, Derkatch SR, Miller R. Interfacial shear rheology of protein-surfactant layers. Adv Colloid Interface Sci. 2008;144(1-2):38-53.

132. Erni P, Fischer P, Windhab EJ. Sorbitan tristearate layers at the air/water interface studied by shear and dilatational interfacial rheology. Langmuir. 2005;21(23):10555-10563.

133. Khoor A, Stahlman MT, Gray ME, Whitsett JA. Temporal-spatial distribution of SP-B and SP-C proteins and mRNAs in developing respiratory epithelium of human lung. J Histochem Cytochem. 1994;42(9):1187-1199.

134. Madsen J, Kliem A, Tornoe I, Skjodt K, Koch C, Holmskov U. Localization of lung surfactant protein D on mucosal surfaces in human tissues. J Immunol. 2000;164(11):5866-5870.

135. Auten RL, Watkins RH, Shapiro DL, Horowitz S. Surfactant apoprotein A (SP-A) is synthesized in airway cells. Am J Respir Cell Mol Biol. 1990;3(5):491-496.

136. Notter RH, Wang Z, Egan EA, Holm BA. Component-specific surface and physiological activity in bovine-derived lung surfactants. Chem Phys Lipids. 2002;114(1):21-34.

137. Bernhard W, Mottaghian J, Gebert A, Rau GA, von Der HARDT H, Poets CF. Commercial versus native surfactants. surface activity, molecular components, and the effect of calcium. Am J Respir Crit Care Med. 2000;162(4 Pt 1):1524-1533.

138. Antonova N, Todorov R, Exerowa D. Rheological behavior and parameters of the in vitro model of lung surfactant systems: The role of the main phospholipid component. Biorheology. 2003;40(5):531-543.

139. Willson D. Calfactant. Expert Opin Pharmacother. 2001;2(9):1479-1493.

140. Anseth JW, Goffin AJ, Fuller GG, Ghio AJ, Kao PN, Upadhyay D. Lung surfactant gelation induced by epithelial cells exposed to air pollution or oxidative stress. Am J Respir Cell Mol Biol. 2005;33(2):161-168.

141. Alonso C, Bringezu F, Brezesinski G, Waring AJ, Zasadzinski JA. Modifying calf lung surfactant by hexadecanol. Langmuir. 2005;21(3):1028-1035.

142. Hall SB, Venkitaraman AR, Whitsett JA, Holm BA, Notter RH. Importance of hydrophobic apoproteins as constituents of clinical exogenous surfactants. Am Rev Respir Dis. 1992;145(1):24-30.

143. Seurynck SL, Brown NJ, Wu CW, Germino KW, Kohlmeir EK, Ingenito EP, Glucksberg MR, Barron AE, Johnson M. Optical monitoring of bubble size and shape in a pulsating bubble surfactometer. J Appl Physiol. 2005;99(2):624-633.

144. Notter RH, Finkelstein JN. Pulmonary surfactant: An interdisciplinary approach. J Appl Physiol. 1984;57(6):1613-1624.

145. Hawco MW, Davis PJ, Keough KM. Lipid fluidity in lung surfactant: Monolayers of saturated and unsaturated lecithins. J Appl Physiol. 1981;51(2):509-515.

146. Burgess DJ, Sahin NO. Interfacial rheological and tension properties of protein films. J Colloid Interf Sci. 1997;189(1):74-82.

147. King M, Zahm JM, Pierrot D, Vaquez-Girod S, Puchelle E. The role of mucus gel viscosity, spinnability, and adhesive properties in clearance by simulated cough. Biorheology. 1989;26(4):737-745.

148. McRae RD, Jones AS, Young P, Hamilton J. Resistance, humidity and temperature of the tracheal airway. Clin Otolaryngol Allied Sci. 1995;20(4):355-356.

149. Nicas M, Nazaroff WW, Hubbard A. Toward understanding the risk of secondary airborne infection: Emission of respirable pathogens. J Occup Environ Hyg. 2005;2(3):143-154.

150. Well WF. On air-borne infections. study II. droplets and droplet nuclei. Am J Hyg. 1934;20:611-618.

151. MacDonald P, Green P. User's guide to program MIX: An interactive program for fitting mixtures of distributions (Mixdist package, R-software Version 2.12.1). 1988.

152. Casillas-Ituarte NN, Chen X, Castada H, Allen HC. Na(+) and ca(2+) effect on the hydration and orientation of the phosphate group of DPPC at air-water and air-hydrated silica interfaces. J Phys Chem B. 2010;114(29):9485-9495.

153. Annis I, Hargittai B, Barany G. Disulfide bond formation in peptides. Methods Enzymol. 1997;289:198-221.